Diploma Thesis

Calibration of the hydrological model using satellite data of soil moisture

submitted in satisfaction of the requirements for the degree
Diplom-Ingenieur
of the TU Wien, Faculty of Civil and Environmental Engineering

---

Diplomarbeit

Kalibrierung des hydrologischen Modells mithilfe von Satellitendaten zur Bodenfeuchte

ausgeführt zum Zwecke der Erlangung des akademischen Grads
Diplom-Ingenieur
eingereicht an der TU Wien, Fakultät für Bau- und Umweltingenieurwesen

Aryan Eftekhari, BSc

Matr.Nr.: 01228480

Betreuung: Privatdoz. PhD **Juraj Parajka**
Institut für Wasserbau und Ingenieurhydrologie
Forschungsbereich Ingenieurhydrologie und Wassermengenwirtschaf
Technische Universität Wien
Karlsplatz 13/222, 1040 Wien, Österreich

Wien, im December 2023

Acknowledgment

The present master thesis was accomplished at the Institute of Hydraulic Engineering and Water Resources Management, Vienna University of Technology. I would like to express my gratitude to Professor Juraj Parajka, PhD, who provided dedicated and professional guidance throughout the entire project. His expertise, valuable advice, and motivation enabled me to enhance my skills in programming, data analysis, hydrological modeling, and remote sensing.

I am also thankful to my fellow students for their mutual support, assistance, and motivation during our civil engineering studies. Additionally, I extend my appreciation to the Vienna University of Technology for providing the academic environment that facilitated my learning and research.

Special thanks go to my girlfriend for her support and understanding. Lastly, I would like to thank my parents, whose unwavering support made my studies and this achievement possible.

Abstract

Recent advancements in soil moisture remote sensing have led to the development of satellite data sets with enhanced capability to map soil moisture beneath vegetation, as well as higher spatial and temporal resolutions. This master's thesis investigates the effects of using different soil moisture products derived from the merged Sentinel-1 and ASCAT datasets (S1ASCAT), as well as the Scatterometer Synthetic Aperture Radar (SCATSAR) on multiple objective calibration of the dual-layer, conceptual, semi-distributed hydrological model with 18 parameters developed at Technical University of Vienna (TUW_dual model). The study compares this approach to the traditional calibration based only on runoff. The calibration of the hydrological model incorporates root zone soil moisture data from S1ASCAT and SCATSAR retrievals and was carried out for the period September 2014 to December 2020. The model was subsequently validated for the period September 2009 to August 2014. The analysis covered 196 catchments located in diverse climatic and geographical regions of Austria. Following this, the catchments were categorized into 131 Lowland and 65 Alpine catchments.

The findings indicate that the assimilation of S1ASCAT data into the calibration, as opposed to relying only on runoff calibration, resulted in a significant increase in soil moisture efficiency, with the model demonstrating higher efficiency in simulating soil moisture in Lowlands than in Alpine. Specifically, improvements were observed in 98.4% of the Lowland and 94.6% of the Alpine catchments, compared to the runoff only calibration variant. In contrast, the performance of SCATSAR data variants was substantially lower during the calibration period, with improvements noted only in 20.6% to 27.8 % of the Lowland and 47.7% to 54.5% of the Alpine catchments. In the validation process, S1ASCAT demonstrated consistent performance in soil moisture simulation, showing improvements in 91.3% of the Lowland and 87.5% of the Alpine catchments, compared to the runoff only calibration variant. However, SCATSAR data variants once again showed notably lower efficiency, with improvements only in 3.7% to 9.3% of the Lowland and in 13.6% to 20.5% of the Alpine catchments.

In general, the model demonstrated higher efficiency in simulating runoff in Alpine catchments than in Lowland catchments. However, this thesis concludes that the model calibration, incorporating S1ASCAT and SCATSAR satellite soil moisture data, resulted in either no significant change or a slight decline in runoff model efficiency in both Lowland and Alpine catchments.

Kurzfassung

Aktuelle Fortschritte in der Fernerkundung von Bodenfeuchte haben zur Entwicklung von Satellitendaten geführt, die eine verbesserte Fähigkeit zur Kartierung von Bodenfeuchte unter Vegetation sowie höhere räumliche und zeitliche Auflösungen bieten. Diese Masterarbeit untersucht die Auswirkungen der Verwendung verschiedener Bodenfeuchteprodukte, die aus den kombinierten Sentinel-1- und ASCAT-Datensätzen (S1ASCAT) sowie dem Scatterometer Synthetic Aperture Radar (SCATSAR) abgeleitet sind, auf die mehrfache objektive Kalibrierung des Dual-Layer-, konzeptuellen, halbverteilten hydrologischen Modells mit 18 Parametern, das an der Technischen Universität Wien entwickelt wurde (TUW_dual-Modell). Die Studie vergleicht diesen Ansatz mit der traditionellen Kalibrierung, die nur auf Abfluss basiert. Die Kalibrierung des hydrologischen Modells bezieht Wurzelzonen-Bodenfeuchtedaten aus S1ASCAT- und SCATSAR ein und wurde für den Zeitraum von September 2014 bis Dezember 2020 durchgeführt. Das Modell wurde anschließend für den Zeitraum von September 2009 bis August 2014 validiert. Die Analyse umfasste 196 Einzugsgebiete in verschiedenen klimatischen und geografischen Regionen Österreichs. Im Anschluss wurden die Einzugsgebiete in 131 Tiefland- und 65 Alpeneinzugsgebiete kategorisiert.

Die Ergebnisse deuten darauf hin, dass die Assimilation von S1ASCAT-Daten in die Kalibrierung im Vergleich zur ausschließlichen Kalibrierung auf Basis von Abfluss zu einer signifikanten Steigerung der Bodenfeuchteeffizienz führte, wobei das Modell eine höhere Effizienz bei der Simulation von Bodenfeuchte in Tieflandgebieten als in alpinen Gebieten zeigte. Konkret wurden Verbesserungen in 98,4% der Tiefland- und 94,6% der Alpeneinzugsgebiete im Vergleich zur ausschließlichen Abflusskalibrierungsvariante beobachtet. Im Gegensatz dazu war die Leistung der SCATSAR-Datenvarianten während des Kalibrierungszeitraums deutlich niedriger, wobei Verbesserungen nur in 20,6% bis 27,8% der Tiefland- und 47,7% bis 54,5% der Alpeneinzugsgebiete festgestellt wurden.

Im Validierungsprozess zeigte S1ASCAT eine konsistente Leistung in der Simulation von Bodenfeuchte, mit Verbesserungen in 91,3% der Tiefland- und 87,5% der Alpeneinzugsgebiete im Vergleich zur ausschließlichen Abflusskalibrierungsvariante. Die SCATSAR-Datenvarianten zeigten jedoch erneut eine bemerkenswert geringere Effizienz, mit Verbesserungen nur in 3,7% bis 9,3% der Tiefland- und in 13,6% bis 20,5% der Alpeneinzugsgebiete.

Generell zeigte das Modell eine höhere Effizienz bei der Simulation von Abfluss in alpinen Einzugsgebieten als in Tieflandeinzugsgebieten. Diese Arbeit kommt jedoch zu dem Schluss, dass die Kalibrierung des Modells, unter Einbeziehung von S1ASCAT- und SCATSAR-Satelliten-Bodenfeuchtedaten, entweder zu keiner signifikanten Veränderung oder zu einem leichten Rückgang der Effizienz des Abflussmodells sowohl in Tiefland- als auch in Alpeneinzugsgebieten führte

Contents

Acronyms

AMSR-E Advanced Microwave Scanning Radiometer for the Earth Observing System

ASCAT Advanced Scatterometer Satellite Remote Sensing

CDFs cumulative distribution functions

DE Differential Evolution

DEoptim the automatic global optimization algorithm developed by Mullen et al. (2011)

ECMWF European Centre for Medium- Range Weather Forecasts

ERS European Remote Sensing

HBV Hydrologiska Byråns Vattenbalansavdelning model

m.a.s.l. meters above sea level

MetOp Meteorological Operational Satellite

MODIS Moderate Resolution Imaging Spectroradiometer

OF objective functions

OF$_{Q+SR}$ Objective function based on runoff and soil moisture in the root-zone layer

OF$_{Q}$ Objective function based on runoff only

Q runoff only

Q+SR runoff and soil moisture in the root-zone layer

Q+SR+SS runoff and soil moisture both in the root-zone and surface layers

Q+SS runoff and soil moisture in the surface layer

RCDFs relative cumulative distribution functions

S1ASCAT merged Sentinel-1 and ASCAT datasets

SAC-SMA SACramento Soil Moisture Accounting model

SAR Synthetic Aperture Radar

SCATSAR Scatterometer Synthetic Aperture Radar

SSM Surface Soil Moisture

SWI Soil Water Index

SWI$_{root}$ soil moisture in the root-zone layer

T characteristic time length

TUW model semi-distributed hydrological model with 15 parameters developed at the Technical University of Vienna

TUW_dual model dual-layer, conceptual, semi-distributed hydrological model with 18 parameters developed at Technical University of Vienna

UH Unit Hydrograph

ZAMG Zentralanstalt für Meteorologie und Geodynamik

List of Symbols and Notations

A	area [km^2]
AET	actual evaporation [mm/day]
AET_{main}	evaporation from the root-zone soil layer [mm/day]
AET_{skin}	evaporation from the surface soil layer [mm/day]
α	measure of the flow variability error [-]
α	non-linearity coefficient of runoff generation [-]
α_m	transfer parameter
AP	agriculture percentage [%]
β	bias term [-]
β	parameter governing runoff generation [-]
B_Q	base of the transfer triangular function [days]
B_{max}	maximum base at low flows [days]
C_{perc}	constant percolation rate [mm/day]
C_{route}	free scaling parameter [days^2/mm]
cov	covariance between observation and simulation
DDF	degree day factor for snowmelt [mm/°C/day]
ΔS_{UZ}	excess rainfall
Δm	vertical soil moisture gradient
Δt	time step of 1 day [day]
ER	elevation range m
EP	potential evapotranspiration [mm/day]
FC	maximum soil moisture storage index, field capacity [mm]
FP	forest percentage [%]
fc_{skin}	Field capacity, i.e., maximum soil moisture storage of the surface layer [mm]
KGE	Kling-Gupta efficiency coefficient [-]
K_0	storage coefficient governing very fast runoff response [days]
K_1	storage coefficient governing fast runoff response [days]
K_2	storage coefficient governing slow runoff response [days]
L_p	parameter limiting potential evaporation [-]
L_{skin}	capacity of the surface soil reservoir
L_s	capacity of the root soil reservoir
LS_{uz}	storage state
MAP	mean annual precipitation [mm]
M	amount of melt water per time step [mm]
MAT	mean air temperature [°C]
MELE	mean elevation [m.a.s.l.]
μ_{obs}	mean observed values [m^3/s]
μ_{sim}	mean simulated values [m^3/s]
MRI	roughness index [-]
NSE	Nash-Sutcliffe efficiency coefficient [-]
NSE_{log}	logarithmic transformation of Nash-Sutcliffe efficiency [-]

P	mean daily precipitation [mm]
P_r	mean daily precipitation in the form of rain [mm]
P_s	mean daily precipitation in the form of snow [mm]
$\overline{Q}_{obs}$	averaged observed daily runoff over the calibration period of n days [m³/s]
Q_{obs}	observed runoff [m³/s]
$Q_{obs,i}$	observed daily runoff of day i [m³/s]
Q_{sim}	simulated runoff [m³/s]
$Q_{sim,i}$	simulated daily runoff of day i [m³/s]
Q_G	outflow from both reservoirs [mm/d]
Q_m	bidirectional moisture flux
r	Pearson correlation coefficient between observations and simulations [-]
$\mathrm{r_{SR}}$	correlation coefficient between observed and simulated soil moisture [-]
σ_{obs}	observed standard deviation [m³/s]
σ_{sim}	simulated standard deviation [m³/s]
SCF	snow correction factor [-]
SD	potential duration of sunshine during the day [hours]
S_{skin}	surface soil moisture
S_s	moisture state of the root soil reservoir
SL	mean slope [%]
S_{LZ}	lower soil reservoir
S_{UZ}	upper soil reservoir
Sy	mean annual sum of the potential duration of sunshine [hours]
$\frac{SD}{Sy}$	sunshine index [-]
φ	parameter for the fraction of the actual evaporation [-]
T	mean daily temperature of the catchments [°C]
T_A	mean daily air temperature [°C]
T_m	temperature threshold, above which snowmelt occurs [°C]
T_r	upper threshold temperature for snow [°C]
T_s	lower threshold temperature for rain [°C]
t_i	observation times of the previous measurements [days]
t_n	observation time of the current measurement [days]
T	time length [days]
$\theta_{obs,i}$	measured soil moisture by the scatterometer on day i [%]
$\theta_{sim,i}$	relative root zone soil moisture simulated by the model on day i [%]
$\overline{\theta}_{obs}$	average of observed soil moisture over the period of n days without snow days [%]
$\overline{\theta}_{sim}$	average of simulated soil moisture over the period of n days without snow days [%]
$w(t_i)$	weight for SSM [-]
w_Q	weight related to runoff objective OF_Q [-]
w_{SR}	weight related to soil moisture objective OF_{SR} [-]

Chapter 1

Introduction

1.1 Background and Context

Recent advances in remote sensing of soil moisture have led to the development of satellite datasets with higher spatial and temporal resolutions and better assessment of soil moisture within vegetated areas (Tong et al. 2021). Numerous studies have recently assessed the hydrological implications of utilizing satellite soil moisture information. Remarkable uses for satellite soil moisture data include numerical weather predictions, runoff modeling, flood forecasting, assessments of land surface and climate models, and drought monitoring (Kubáň et al. 2021). Soil moisture plays a crucial role in the response of catchments to runoff. It regulates the distribution of rainfall between runoff and infiltration. Various runoff mechanisms, such as saturation excess runoff, infiltration excess runoff, and subsurface storm flow, exhibit a considerable increase in runoff with higher antecedent soil moisture levels under a given rainfall intensity. The influence of antecedent soil moisture on runoff varies depending on the specific runoff mechanism (Wagner, Blöschl, et al. 2007). The flood event that occurred in Austria in 2002 (Figure 1.1a) serves as an illustration of the importance of antecedent soil moisture (Gutknecht et al. 2002), as heavy rainfall was experienced in the northern regions of Austria during the periods of August 7-9 and August 11-13. These two consecutive rainfall events resulted in two separate instances of flooding (Wagner, Blöschl, et al. 2007). Over the course of three days, the estimated flood volume amounted to 70 million m^3. This is approximately half of the average annual runoff volume of 180 million m^3 for the affected regions. The peak flows observed during this event were suggested to have a return period ranging from 2000 to 10,000 years (Gutknecht et al. 2002). Due to the elevated soil moisture levels from the initial event, the flood peak of the subsequent event was larger in many catchments, despite the second event having a lower amount of rainfall. Therefore, a critical factor in many hydrological applications is soil moisture (Wagner, Blöschl, et al. 2007).

Austria, in particular, is prone to flooding due to its topography and geographical location. Figure 1.1b and Figure 1.1c display additional instances of severe floods that have occurred in Austria in the past. Therefore, accurate forecasts are essential for mitigating the risks associated with extreme flood events, which endanger human lives and have the potential to cause significant damage to infrastructure.

Hydrologic models are commonly employed to estimate runoff generation. They utilize various model types and methods to determine model parameters. However, it is important to acknowledge that the resulting simulations of water balance components are susceptible to uncertainties arising from model inputs, parameter estimations, and model structure (Parajka, Merz, et al. 2007; Kavetski et al. 2006; Wagener and Montanari 2011). It is crucial to estimate the spatial and temporal variations in the components of water balance at the regional scale to effectively address practical concerns in water resource management and planning, as well as to comprehend catchment dynamics by examining the interplay of runoff-generation processes that contribute to catchment response (Tong et al. 2021).

Various studies have shown that multiple objective calibration assists in constraining hydrologic models, resulting in lower uncertainty and improved predictions in hydrological modeling (e.g., Efstratiadis and Koutsoyiannis (2010)). In most of these research studies, calibrating hydrological models to runoff and additional variable such as soil moisture (e.g., Parajka, Naeimi, Blöschl, and Komma (2009); Y. Li et al. (2018); Kundu et al. (2017)), evaporation (e.g., Immerzeel and Droogers (2008)), snow cover (e.g., Parajka and Blöschl (2008)), etc., was investigated. In conclusion, these studies have indicated the spatial and temporal characteristics of a catchment's states and flows are often improved by the incorporation of more hydrological variables. However, the efficiency of runoff simulations did not necessarily increased. In fact, the majority of these studies found a slight decline in runoff model efficiency, while the models' internal consistency (i.e., parameter certainty) increased. A few studies investigated the inclusion of additional variables in multiple objective calibration (e.g., Milzow et al. (2011); Kunnath-Poovakka et al. (2016); Nijzink et al. (2018)) and concluded that doing so often reduced parameter uncertainty, particularly in areas with a lack of data. For instance, Nijzink et al. (2018) found that hydrological models benefit from combinations of soil moisture products, especially from Advanced Scatterometer Satellite Remote Sensing (ASCAT) and Advanced Microwave Scanning Radiometer for the Earth Observing System (AMSR-E)[1]. This combination leads to improved performance in identifying soil parameters, particularly in cases where runoff observations are unavailable.

Parajka, Naeimi, Blöschl, Wagner, et al. (2006) compared the soil moisture data simulated by semi-distributed hydrological model with 15 parameters developed at the Technical University of Vienna (TUW model) in 320 Austrian catchments with the soil moisture data obtained from the satellite data and concluded that calibrating the model using runoff and root-zone soil moisture satellite data in alpine areas exhibited lower soil moisture efficiency when compared to lowland areas, potentially due to issues with the satellite data retrieval method in alpine regions. Additionally, they reported a negligible decrease in runoff model efficiency. Subsequently, Parajka, Naeimi, Blöschl, and Komma (2009) used the TUW_dual-layer conceptual hydrologic model with 18 parameters to simulate surface soil moisture for 148 Austrian catchments and found that the simulations of surface soil moisture are more consistently aligned with scatterometer values in comparison to those of the single-layer model's (TUW 15-parameter model) fit to root-zone scatterometer estimations. Furthermore, they noted that the assimilation of the soil moisture data into the hydrologic model did not degrade the runoff model performance in the calibration process.

Tong et al. (2021) tested a new S1ASCAT Soil Water Index (SWI)[2] data product of the root-zone soil moisture along with runoff data and Moderate Resolution Imaging Spectroradiometer (MODIS) snow cover data for multiple objective calibration of the TUW model with 15 parameters in 213 catchments in Austria. The results indicate that soil moisture simulations are primarily improved by including soil moisture data in the calibration process, and the soil-related parameters are influenced only by the soil moisture data inclusion. Moreover, they concluded that runoff and soil moisture model efficiency improved in low elevation and agricultural catchments more than in alpine regions. Kubáň et al. (2021) utilized the S1ASCAT SWI root-zone and S1ASCAT SWI soil surface moisture product at finer spatial resolutions for the multiple objective calibration of the TUW_dual-layer model with 18 parameters in 209 Austrian catchments. The findings demonstrate that multiple objective calibrations significantly enhance the constraint on model parameters. Utilizing both soil moisture and runoff data in the calibration process improved the simulation of soil moisture in many catchments, except for those with higher percentages of forest cover. Furthermore, the runoff model efficiency increased in some lowland catchments

[1] AMSR-E: For more information, see, Owe et al. (2008)

[2] SWI: The Soil Water Index measures soil moisture content at various depths, primarily influenced by precipitation through the infiltration process. (*Copernicus Global Land Service - Soil Water Index* 2023)

(a) Severe flood event of August 2002 (Habersack et al. 2005)

(b) Municipality of Ottensheim during the flood of 2013 (BMK 2013)

(c) Municipality of Mittersill's (Pinzgau) flood of 2021 (Salzburg24 2021)

Fig. 1.1: Extreme flood events in Austria in the years 2002, 2013 and 2021.

characterized by a higher percentage of agricultural land use, as well as in the Alpine catchments where snowmelt and glacier runoff had little to no substantial impact on the runoff.

1.2 Literature Review

1.2.1 History of Hydrological Modelling

The beginnings of the development of the mathematical-physical foundations for later hydrological modeling go back to antiquity. Ancient civilizations like the Sumerians and Egyptians made observations and predictions about rainfall and water levels. The Egyptians had a high-water warning system along the Nile. In China, the first precipitation observations began around 1200 B.C., while systematic measurements of precipitation took place around 200 B.C.. Greek philosophers like Anaximander, Anaxagoras, and Aristotle made significant contributions to our understanding of hydrological processes. Without a thorough understanding of science, the Romans constructed impressive water management systems. The foundation for these engineering solutions in the past was experience and craftsmanship. (Liebscher and Mendel 2010)

In the Middle Ages (500 – 1500), natural sciences, including hydrology, made no progress in the West compared to ancient knowledge. Interest in the water cycle and hydrology was lost and there was no further development in this field in Europe. (Liebscher and Mendel 2010)

During the Renaissance (1500-1700), Leonardo da Vinci studied flood risk, water scarcity, and other hydrological phenomena, providing valuable insights into hydrology. In the 16th century, Palissy described the water cycle in detail and clarified its connections. China recorded long periods of precipitation and in 1573 established a flood service along the Hoang Ho to warn of flood waves. Castelli discovered and formulated the law of continuity for fluid flow in the 17th century. Perrault, Mariotte, and Halley introduced quantitative approaches to hydrology, leading to the scientific development of the field. (Liebscher and Mendel 2010)

From 1700 to 1800, other significant mathematical, physical, and chemical foundations were established. This includes, for example, the formulation of physical connections between speed and pressure, and the law of conservation of energy (Bernoulli's principle), as well as the development of mathematical foundations for various numerical solution methods for partial differential equations by Euler (Biswas 1970). Moreover, gauges and measuring instruments were developed to determine the discharge. In the 18th century, flood notification systems began to be established along some rivers (Liebscher and Mendel 2010).

The time period from 1850 to 1960 marked the transition from the rational method to conceptual models. The Rational Method, proposed by Mulvany in 1850, was the first widely recognized hydrological model, created to design sewers and dam spillways in small impervious catchments. It predicts the peak flow in urban or mountain catchments using the concept of time of concentration. Furthermore, the Unit Hydrograph (UH) was developed by Sherman in 1932 to address the need for estimating not only the peak flow but also the shape and volume of the flood wave. Its purpose was to improve reservoir design and flood protection. Later, "conceptual models" began to emerge with the development and increased accessibility of digital computers, aiming to model the complex interactions of soil-surface runoff generating mechanisms. (Todini 2011)

At the end of the 1970s, the concept that the dynamics of saturated areas primarily control the rainfall-runoff process led to the development of a new type of lumped model known as variable contributing area models. These models relate soil moisture storage to a straightforward monotone function. The assumption commonly used in these models was that all precipitation reaches the soil, and surface runoff occurs when the upper soil layer becomes saturated. (Todini 2011)

Since 1965, distributed process models have been under development. Several studies aimed to improve the physical representation of the rainfall-runoff mechanism as an alternative to conceptual models. For instance, mathematical models based on distributed understanding of surface and subsurface processes were proposed, along with kinematic models for analyzing small urban basins. Recently, a greater amount of distributed information has become available, including data on soil types, land use, and radar rainfall. This availability has assisted in the development of simpler, physically relevant distributed hydrological models. (Todini 2011)

The majority of hydrologic models used today are based on conceptual frameworks that simplify the complex internal state variables within a watershed into relatively simple mathematical equations. Examples of such conceptual models include the SACramento Soil Moisture Accounting model (SAC-SMA) and the Hydrologiska Byråns Vattenbalansavdelning model (HBV). (Yilmaz et al. 2010)

According to Beven (2012), there is no doubt that distributed hydrological models will become more detailed as a result of advancements in computer science. However, it is uncertain whether this kind of improvement would lead to more accurate hydrological predictions. Increased complexity leads to more parameters, which in turn leads to more calibration issues, often resulting in greater prediction uncertainty. Furthermore, the deficiency of data for model inputs, boundary conditions, and parameter values still greatly constrains the development, testing, and utilization of rainfall-runoff models.

1.2.2 Model Theory and Model Classification

All branches of science employ models in their studies. These models naturally differ in terms of their content, style, and functionality. Despite variations among different models, all models share certain general features. (Valk et al. 2007)

The first two fundamental features of scientific models describe a model's structure and function.

1. *A model is always related to a target* (Duit and Glynn 1996; S. W. Gilbert 1991; J. K. Gilbert and Boulter 1997) *and is designed for a specific purpose* (Bullock and Trombley 1999). *The target may be an object, a phenomenon, an event, a process, a system, or an idea. A model is always a representation of the target* (Valk et al. 2007).

2. *A model serves as a research tool that is used to obtain information about the target which itself cannot be easily observed or measured directly.* (Mayer 1992)

   The next two features outline the criteria that a model must fulfill:

3. *A model bears some analogies to the target* (Hempel 1965). *These analogies enable the researcher to reach the purpose of the model; in particular to derive hypotheses from the model or to make predictions, which may be tested while studying the target* (Hesse 1965).

4. *A model differs in certain respects from the target. The differences make the model more accessible for research than the target.* (Woody 1995)

Accordingly, a model can be described as a simplified representation of a part of reality. Each model is comprised of three main components: model input variables, model output variables, and model parameters. (Zellinger 2019)

A rainfall-runoff model simulates the physical processes that lead to the transformation of rainfall into stream runoff in a catchment. This transition is complex because it depends on the characteristics of the land surface, vegetation, stream channel, and human-made infrastructure (dams, highways, etc.). Additionally, this process is non-linear, scale-dependent, and specific to the site (S. Gupta 2011), therefore, it is useful to classify hydrological models. According to Becker and Serban (1990), the most appropriate classification of hydrological models, in terms of problem-related and user-oriented perspectives, is as follows:

1. Purpose of model application:

   Mathematical models have increasingly demonstrated practical applications in the following main categories of problems in terms of operational hydrology and water resources planning and management:

   a) Real-time forecasting and control

      Real-time problems are always tied to the current situation, the present system framework, and the initial conditions. They also involve predictions for a few hours up to a few years (short-term). (Becker and Serban 1990)

   b) Prediction, planning, and design

      Planning and design studies are primarily long-term, necessitating predictions of hydrological conditions and availability of water resources spanning time spans of 10 to 100 years. (Becker and Serban 1990)

c) Research, process studies, model calibration, etc.

One of the main focuses of this category is to use hydrological models, specifically to improve our understanding of processes, enhance our modeling abilities, and estimate model parameters. (Becker and Serban 1990)

2. Type of system to be modelled:

There is a difference between elementary systems and complex or coupled systems. Elementary systems consist of small or medium-sized land surface areas, aquifers (groundwater systems), river reaches or channel reaches, and reservoirs or lakes. Complex (coupled) systems consist of several river reaches, potentially with lakes or reservoirs, as well as river basins or other larger land surface units. (Becker and Serban 1990)

3. Hydrological processes:

Hydrological processes or related variables to be considered include, for example: (Becker and Serban 1990)

- Soil moisture and evapotranspiration (including other related variables).
- Groundwater storage, level, and discharge.
- River discharge and water level.
- Water temperature and ice conditions.
- Sediment yield and related variables.

4. Degree of causality:

Cause-and-effect relationships are the means by which causality is expressed. They function most effectively in *deterministic* models (Figure 1.2) that link a set of independent factors x (causes, inputs or otherstate variables of the system such as initial and boundary conditions) to a set of dependent variables y (effects, outputs or dependent state variables of the system):

$$y = f(x, a)$$

where a are coefficients or parameters that describe the behavior of the system. (Becker and Serban 1990)

The three main types of deterministic models are introduced as follows (Figure 1.2):

a) *Metric* models, also called *black box* models, are empirical, data-based models that solely derive their model structure and associated parameter values from the available time-series data. Consequently, they depend entirely on the content of the data and do not include any prior knowledge about catchment behavior or flow processes. (Wagener, Wheater, et al. 2004)

b) *Mechanistic* models, also called *white box* or *physically based*, are idealized mathematical representation of an actual phenomenon, based on the fundamentals of physical rules. they employ measurable state variables that function in both time and space. However, these models do not necessarily require extensive hydrological and meteorological data for calibration. Instead, this method necessitates substantial information, such as soil moisture content, initial water depth, geography, topology, and more. Due to their complexity, they demand human skills and computing power. they can provide significant amounts of information even beyond the boundary, and they are applicable in various kinds of situations. (Devia et al. 2015)

c) *Parametric* models, also called *grey box* or *conceptual*, involve some degree of empiricism and reflect fundamental rules of physics in a simplified form. In other words, in gray box models, elements of both white box (physically based) and black box (data-based) approaches are combined. (Wagener, Wheater, et al. 2004; Becker and Serban 1990)

The model parameters are assessed with both field data and calibration. Interpreting these parameters is challenging due to the curve fitting required during the calibration process. HBV model is an example. (Devia et al. 2015)

These models consider the catchment as a single homogeneous unit or as smaller sub-catchments, using a so-called semi-distributed approach. (Wagener, Wheater, et al. 2004)

Stochastic models (refer to Figure 1.2) are the other major category of hydrological models that essentially disregard the causality principle (Becker and Serban 1990). In such models, a certain level of uncertainty, associated with both the model parameters and the stochastic inputs, will persist after the modeling has been completed (Mulligan and Wainwright 2013).

The so-called *probabilistic* models, a subcategory of these models, are characterized by the use of probability distribution functions of the relevant hydrological variables, such as maximum and lowest discharges (flood peak flows, low flows, etc.) and water levels or storage volumes. (Becker and Serban 1990)

Time series generation models, the second subcategory of stochastic models, can be used to extrapolate in time a series of observed variables or events while maintaining their statistical properties. (Becker and Serban 1990)

Deterministic and stochastic components are always present in hydrological processes (coupled deterministic-stochastic models are depicted at the top of Figure 1.2). This is valid for both real-time forecasting models as well as prediction, planning, and design models. (Becker and Serban 1990)

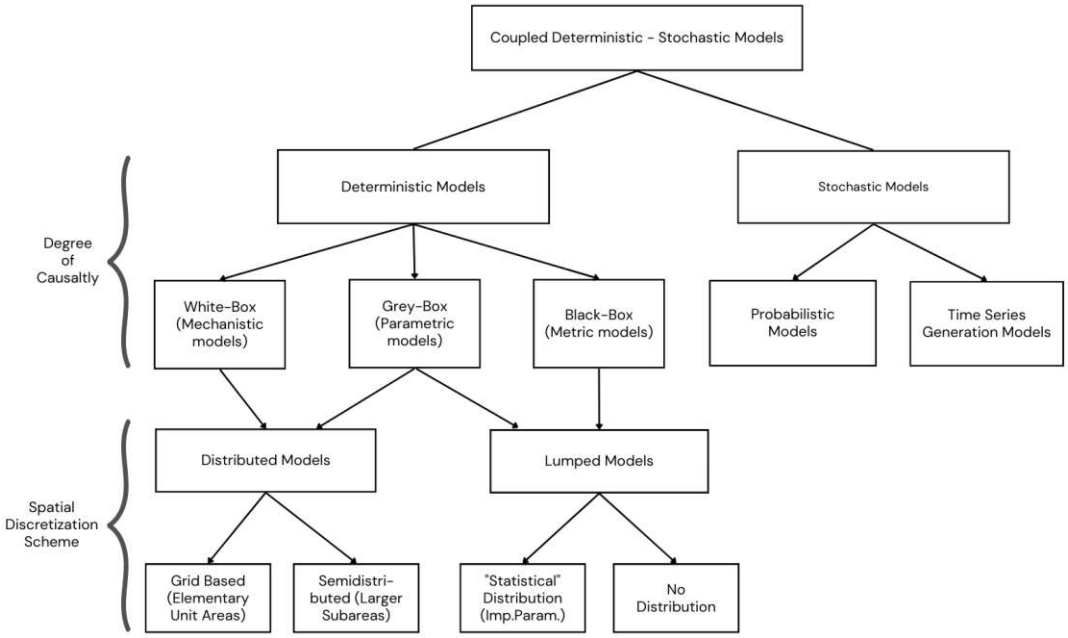

Fig. 1.2: Classification of hydrological models based on application, degree of causality and spatial discretization. (Becker and Serban 1990)

5. Spatial discretization in hydrological modelling:

   The spatial structure of catchment processes in rainfall-runoff models can be categorized as (see Figure 1.3):

   a) *Lumped* models consider the entire catchment as a single entity, and the model inputs are averaged (Beven 2012). The simulations are carried out for the whole catchment, often leading to issues of over- or under-parameterization, which can result in faster computational times (Sitterson et al. 2018).

   b) *Semi-distributed* models are variations of lumped models that include characteristics of distributed models. The modeling process divides the catchment into smaller sections (sub-catchments), each with its own set of parameters. The model inputs are both averaged and specific for each sub-catchment and the simulations are carried out for each sub-catchment. (Sitterson et al. 2018)

   c) *Distributed* models discretize the catchment into a large number of elements or grid squares. Model inputs are averaged and associated with every grid square, and the simulations are carried out for each grid cell. Parameter values are specified for every element in a distributed model. (Beven 2012)

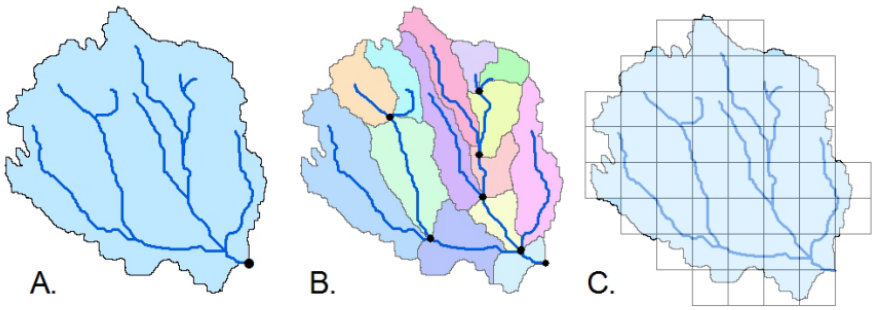

Fig. 1.3: Visual representation of the spatial structure in runoff models. A: Lumped model, B: Semi-Distributed model by sub-catchment, C: Distributed model by grid cell. (Sitterson et al. 2018)

6. Time discretization in hydrological modelling:

   Based on the time factor, there is another classification between *static* and *dynamic* models. Dynamic models involve time, whereas static models do not. (Devia et al. 2015)

   Wheater et al. (2008) divided the models into two categories: *event-based* models and *continuous* models. While the latter create a constant output, the former only produce output for a limited amount of time.

1.2.3 The Hydrological Modeling Process

Hydrologic models are essential instruments for comprehending the functioning of watersheds. These models are constructed using a mathematical framework that represents the coupling of major hydrologic processes. The primary purpose of these models is to simulate the hydrologic behavior of a watershed by estimating certain unknown coefficients, referred to as "parameters". These parameters cannot be directly determined in the field but must be inferred through a process of calibration, which involves matching model outputs to observed input-output records of the watershed's response. (Yilmaz et al. 2010)

In hydrological modeling, a specific purpose is defined first. Next, the processes and equations to be used are determined, and a suitable model code is developed. The model is then created, and efficiency criteria are applied to assess the quality of its fit. Following this, the model calibration process is carried out to estimate the best parameter values. Subsequently, the model is validated by comparing the simulated data with observed data. Finally, the results are evaluated for acceptability. If the results are not acceptable, a revision of the parameter values may be necessary, leading to a reassessment of the conceptual model. (Beven 2012) (see also Figure 1.4)

1.2.4 Model Calibration

Model calibration aims to determine the best possible parameters for the model in order to ensure that the behavior of the model accurately and consistently resembles the observed response of the system (Yilmaz et al. 2010). This process can be divided into the following work steps as outlined by Yapo et al. (1996) and Wagener, Wheater, et al. (2004):

- Collecting the calibration data set.
- Defining objective functions for measuring 'goodness-of-fit.'

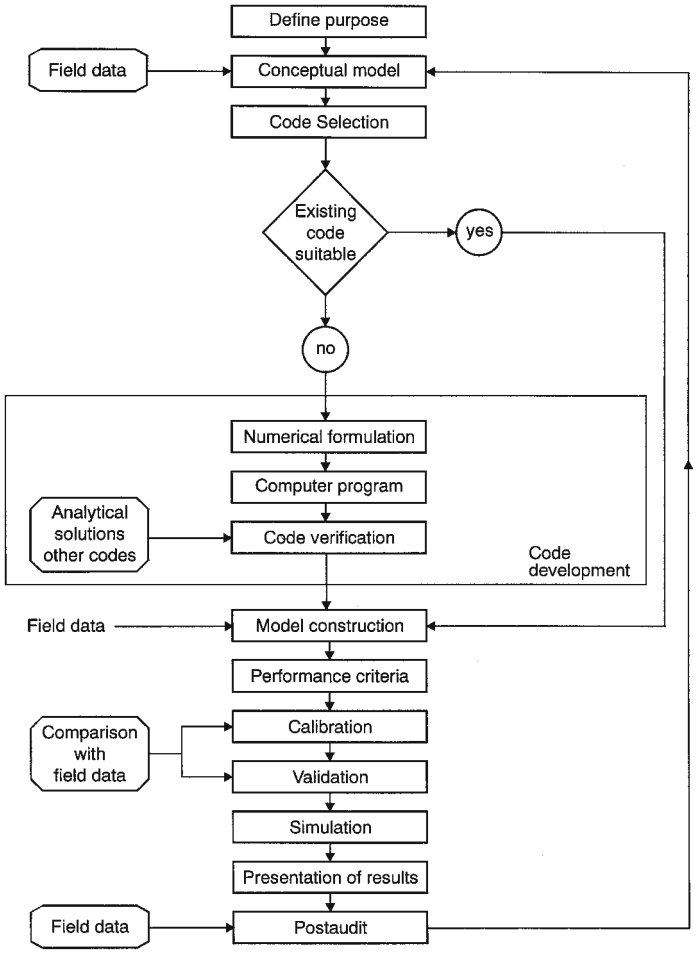

Fig. 1.4: A schematic outline of the steps in the modelling process. (Refsgaard 1997)

- Selecting an automatic parameter search procedure (optimization algorithm).
- Defining permissible maximum and minimum values for each parameter.
- Termination criteria.

1.2.4.1 Calibration Data Set

There are differing opinions regarding the length of the calibration period. According to Sorooshian, V. K. Gupta, et al. (1983), both the quality and quantity of the data used have a significant impact on the effectiveness of the calibration methods. In an effort to meet this condition, some studies have used the longest possible duration of calibration data, However, it's not the length of the data used but the quality of the information it contains that is important, and using more data than necessary would only slightly enhance parameter estimations. Also, the data should be a good representation of the hydrological or environmental characteristics of the watershed. It is possible to obtain reliable parameter estimates with only a 1-year calibration, however, it is advisable to use variable data records, including wet, average, and dry periods, and not to use less than one year of data.

C.-z. Li et al. (2010) and Yapo et al. (1996) suggest that approximately 8 years of calibration data are sufficient to obtain reliable model parameters. Additionally, there may not be much value in utilizing calibration data older than eight years.

Franchini and Pacciani (1991) suggested that there is a direct correlation between the number of parameters that need to be optimized and the length of the calibration data.

1.2.4.2 Objective Functions

The purpose of calibration is to determine parameter values for the model in such a way that it minimizes the variation between model predictions and observations. This is achieved by utilizing an 'objective function' (Yilmaz et al. 2010). The objective function serves as a measure of how well the residuals fit (Beven 2012).

Practical experience with model calibration indicates that relying on a single-objective function may not be adequate to ensure that the model accurately represents the most crucial characteristics of the observed data. This often necessitates the adoption of a more effective and efficient 'multi-objective' calibration procedure. (Yapo et al. 1996; H. V. Gupta, Sorooshian, et al. 1998)

Houghton-Carr (1999) concluded that quantitative measures alone are uncommonly sufficient to assess a model's performance quality. Typically, some qualitative evidence of goodness-of-fit, such as the quality of the synthetic daily flow hydrograph, is required.

1.2.4.3 Optimization Algorithm

Model calibration can be performed either manually or automatically. In the manual approach, model parameters are estimated through a trial-and-error process, which requires a good understanding of the model, the use of multiple objective functions, visualizations, and human assessment (Duan 2003). The time-consuming nature of manual trial-and-error calibration led to the development of automated (computer-based) calibration methods. By selecting an appropriate automatic optimization algorithm, it is possible to determine parameter values that minimize the discrepancy between the simulated and the observed data (Yapo et al. 1998).

In this context, a distinction is made between local and global optimization methods. Local optimization methods can be unreliable because the parameter estimations they provide often heavily depend on the starting position. The objective function response spectrum frequently contains many local optima, therefore any optimization approach must navigate through numerous local solutions to reach the global optimum (Yapo et al. 1996). Multiple local optima, discontinuous derivatives, insensitivity, and parameter interdependency are among the deficiencies of local optimization methods. These weaknesses have led to the development of global optimization methods capable of dealing these difficulties (Duan 2003).

An example of a global optimization method is the DEoptim implementation developed by Mullen et al. (2011) which is based on an evolution strategy presented by Storn and Price (1997) called Differential Evolution (DE). DEoptim is available as a global optimization algorithm in the R language and environment for statistical computing. The R language's DEoptim function is used to determine the minimum of the objective function within the specified upper and lower limits for each parameter that needs to be optimized.

1.2.4.4 Permissible Maximum and Minimum Values for each Parameter

The permissible maximum and minimum values are usually defined as upper and lower bounds for each parameter. (Duan et al. 1992)

A priori estimation of model parameters for conceptual models is not possible since they are not directly measurable. Nevertheless, valuable empirical relations have been identified. (Parajka, Andréassian, et al. 2013)

Model parameters in gauged catchments are typically calibrated to observed runoff in order to minimize bias in the prediction of runoff. (Parajka, Andréassian, et al. 2013)

1.2.4.5 Termination Criteria

As an integral part of the automatic calibration process, the optimization algorithm operates as an iterative procedure and is terminated based on multiple objective criteria. According to Sorooshian and H. V. Gupta (1995), these criteria are as follows:

- *Function convergence*: When the objective function's improvement falls below a user-selected threshold value after a number of iteration steps, the calibration is stopped.
- *Parameter convergence*: It determines if the best parameter estimate stays within a fraction of its plausible range; if all of the parameters stay within this fraction after a certain number of iterations, the search is terminated.
- *Maximum number of iterations*: This criterion is set to prevent excessive model runs in case the other two convergence criteria are not met.

Sorooshian, Duan, et al. (1993) proposed that the best termination criterion is parameter convergence.

1.2.5 Model Validation

Model validation evaluates the model's efficiency using calibrated parameters on a data set that is independent from the calibration data, and ensures whether the model's results are feasible. Furthermore, the use of a hydrological simulation model is considered valuable when it accurately synthesize hydrological data that are not accessible or available through direct observation. (Klemeš 1986)

Klemeš (1986) proposed different model validation methods, such as the *split-sample* test, where the available dataset is divided into two independent segments: one for calibration and the other for validation.

1.2.6 Model Uncertainties in Hydrological Modeling

Uncertainty is an inherent part of every hydrological modeling; therefore, it is important to analyze its effects on the predictions . There are several sources of uncertainty, with the following being the most significant according to Beven (2012) and Wagener, Wheater, et al. (2004):

- *Uncertainties in model inputs*, i.e., errors in measurement or data pre-processing.
- *Uncertainties in initial and boundary conditions*, i.e., the unknown state of the model at the begining of the calibration.
- *Uncertainties in the model structure*, i.e., model simplifications, and model deficiencies which leads to different parameter sets, fitting only one mode of system response and make the other response modes inaccurate.
- *Uncertainties in the model parameter estimates*, i.e., data and model uncertainties result in calibrated model parameters.

- *Uncertainties that have been overlooked*

Various methods have been proposed to propagate the uncertainty inherent in the modeling process to improve the accuracy of mode predictions. For example, first order analysis, which involves estimating the mean and variance of the predicted variable by carrying forward the mean and variance of the input data or model parameters through the model itself (Melching 1995). Many researchers later developed methods that are based on Monte Carlo sampling for more complex models (Wagener, Wheater, et al. 2004).

Yapo et al. (1996) recommended explicitly addressing uncertainties that arise from model structural inadequacies and errors, which are currently the primary factor limiting model performance.

1.2.7 Selected "Goodness-of-Fit" Criteria for Assessing Model Efficiency

Having trustworthy criteria is an essential component of the modeling procedure. A goodness-of-fit statistic is intended to represent a portion of the calibrated model's prediction accuracy. Therefore, careful selection of a statistic is crucial to ensure its accuracy in reflecting the intended characteristic. (McCuen et al. 2006)

1.2.7.1 Nash-Sutcliffe Efficiency Coefficient

Nash-Sutcliffe efficiency coefficient (NSE) was defined by Nash and Sutcliffe (1970) and is widely used statistic for assessing the goodness-of-fit of hydrologic models. It compares the residual variance (also known as 'noise') with the measured data variance (also known as 'information'). NSE is computed as shown in Equations (1.1) and (1.2).

$$\mathrm{NSE} = 1 - \frac{\sum_{i=1}^{n} (Q_{obs,i} - Q_{sim,i})^2}{\sum_{i=1}^{n} (Q_{obs,i} - \overline{Q}_{obs})^2} \tag{1.1}$$

$$\overline{Q}_{obs} = \frac{1}{n} \cdot \sum_{i=1}^{n} Q_{obs,i} \tag{1.2}$$

where:

NSE ... is the Nash-Sutcliffe efficiency coefficient [-],
$Q_{obs,i}$ ... is the observed daily runoff of day i [m³/s],
$Q_{sim,i}$ ... is the simulated daily runoff of day i [m³/s],
$\overline{Q}_{obs}$ ... is the average of observed daily runoff over the calibration (or verification) period of n days [m³/s].

The NSE is dimensionless and ranges from $-\infty$ to 1.0 (1 inclusive), where NSE = 1 is the best possible value. Values less than 0.0 suggest that the mean observed value is more accurate than the simulated value, indicating inadequate accuracy (Moriasi et al. 2007). Although determining limits of acceptability for model predictions is subjective and depends on the specific model application (Beven 2006), four model performance classes, labeled as Unsatisfactory, Acceptable, Good, and Very Good, are introduced in Table 1.1 as a reference guide. These NSE ranges are based on the study by Moriasi et al. (2007). The threshold value for an Acceptable model efficiency proposed by Moriasi et al. (2007) was NSE $\geq$ 0.5, while Ritter and Muñoz-Carpena (2013) suggested a value of NSE $\geq$ 0.65.

The NSE's versatility in its application to various mathematical models makes it a commonly used indicator in the field of hydrology. It can be calculated independently for different catchments (Madsen 2003), various types of observations (e.g., runoff and snow observations) (Bergström et al. 2002), and specific subsets of a single observation (Boyle et al. 2000). However, biased model predictions and the presence of unusually high or low data values in the dataset can have a disproportionate impact on the NSE value (McCuen et al. 2006). In order to tackle these issues, several authors proposed modified NSE, which are based on transforming observations and model estimates (log, using root squared, or inverse-transformed series) (Oudin et al. 2006; Le Moine 2008).

The NSE and the logarithmic NSE will be used in this thesis to calculate the objective functions. (see Chapter 2.1.4). The logarithmic Nash-Sutcliffe efficiency (NSE_{Log}) is calculated as demonstrated in Equation (1.3):

$$NSE_{log} = 1 - \frac{\sum_{i=1}^{n} (logQ_{obs,i} - logQ_{sim,i})^2}{\sum_{i=1}^{n} (logQ_{obs,i} - log\overline{Q}_{obs})^2} \tag{1.3}$$

Tab. 1.1: Performance Rating for NSE according to Moriasi et al. (2007)

Performance Rating	NSE Value Range
Very Good	$0.75 < NSE \leq 1.0$
Good	$0.65 < NSE \leq 0.75$
Acceptable	$0.5 < NSE \leq 0.65$
Unsatisfactory	$NSE \leq 0.5$

1.2.7.2 Kling-Gupta Efficiency

The Kling-Gupta Efficiency (KGE) was proposed by H. V. Gupta, Kling, et al. (2009) as an alternative criterion to Nash-Sutcliffe efficiency (NSE). H. V. Gupta, Kling, et al. (2009) decomposed NSE into three components: a) linear correlation between observations and simulations, b) bias, and c) a measure of the flow variability error. KGE is computed as shown in Equations (1.4), (1.5), (1.6) and (1.7):

$$KGE = 1 - \sqrt{(r-1)^2 + (\alpha - 1)^2 + (\beta - 1)^2} \tag{1.4}$$

$$r = \frac{\mathrm{cov}(Q_{obs}, Q_{sim})}{\sigma_{obs}^2 \sigma_{sim}^2} \tag{1.5}$$

$$\alpha = \frac{\sigma_{sim}}{\sigma_{obs}} \tag{1.6}$$

$$\beta = \frac{\mu_{sim}}{\mu_{obs}} \tag{1.7}$$

where:

KGE ... is the Kling-Gupta efficiency coefficient [-],
r ... is the the Pearson correlation coefficient between observations and simulations [-],
α ... is the measure of the flow variability error [-],
β ... is the bias term [-],
Q_{obs} ... is the observed runoff [m³/s],
Q_{sim} ... is the simulated runoff [m³/s],
σ_{obs} ... is the observed standard deviation [m³/s],
σ_{sim} ... is the simulated standard deviation [m³/s],
μ_{obs} ... is the mean observed values [m³/s],
μ_{sim} ... is the mean simulated values [m³/s],
cov ... is the covariance between observation and simulation.

The decomposition makes it easier to analyze the relative significance of these components in relation to hydrological modeling and illustrates how interactions between them might lead to issues with model calibration. While avoiding the NSE-related issues, the use of this alternate criterion also introduces new issues. For instance, Santos et al. (2018) showed that assessing KGE performance on low flows using log-transformed discharges may lead to numerical problems and bias in the model's performance.

Similar to NSE, The KGE is dimensionless and ranges from $-\infty$ to 1.0 (1 inclusive), where KGE = 1 is the best possible value. Values less than 0.0 suggest that the mean observed value is more accurate than the simulated value, indicating inadequate accuracy (Castaneda-Gonzalez 2019; Koskinen et al. 2017). Knoben et al. (2019) stated that the relationship between NSE and KGE values is not unique and partly dependent on the coefficient of variation of the observed time series, therefore, it is not possible to compare them directly. Although various performance indicators have been proposed by different studies, in this thesis, we employ the three model performance classes introduced by Rogelis et al. (2016), which are labeled as Poor, Intermediate, and Good. These classes are presented in Table 1.2, with the omission of negative KGE values.

Tab. 1.2: Performance Rating for KGE according to Rogelis et al. (2016)

Performance Rating	KGE Value Range
Very Good	$0.75 < \text{KGE} \leq 1.0$
Good	$0.5 < \text{KGE} \leq 0.75$
Poor	$0.0 < \text{KGE} \leq 0.5$

1.2.7.3 Correlation Coefficient

The Correlation Coefficient (r_{SR}) was adopted from the studies conducted by Tong et al. (2021) and Parajka, Naeimi, Blöschl, and Komma (2009), expressing the correlation between the simulated soil moisture's relative values in the root-zone by the hydrologic model and the measured values of the Soil Water Index (SWI) in the root-zone from the S1ASCAT and SCATSAR data. The correlation coefficient was only calculated on days without snow cover in

order to mitigate the influence of snow cover on the scatterometer soil moisture accuracy. It is estimated by the following Equation (1.8):

$$r_{SR} = \frac{\sum_{i=1}^{n}(\theta_{sim,i} - \overline{\theta}_{sim})(\theta_{obs,i} - \overline{\theta}_{obs})}{\sqrt{\sum_{i=1}^{n}((\theta_{sim,i} - \overline{\theta}_{sim})^2(\theta_{obs,i} - \overline{\theta}_{obs})^2)}} \tag{1.8}$$

where:

r_{SR} ... is the correlation coefficient between observed and simulated soil moisture [-],
$\theta_{sim,i}$ ... the relative root zone soil moisture simulated by the model on day i [%],
$\theta_{obs,i}$ ... is the measured soil moisture by the scatterometer on day i [%],
$\overline{\theta}_{sim}$ ... is the average of simulated soil moisture over the period of n days without snow days [%],
$\overline{\theta}_{obs}$ ... is the average of observed soil moisture over the period of n days [%] without snow days [%].

The correlation coefficient facilitates the comparison of how observed and simulated soil moisture vary over time, regardless of the respective magnitudes and possible intercepts in the interaction between simulated and observed soil moisture. (Tong et al. 2021)

The r_{SR} is dimensionless and ranges from -1.0 to 1.0, where $r_{SR} = 1$ means perfect positive correlation, $r_{SR} = -1$ means perfect negative correlation, and $r_{SR} = 0$ indicates no linear relationship between the variables (Huang 2010). Furthermore, in this thesis, the r_{SR} will be designated as Not-Available (N/A) if the observed soil moisture data for a specific catchment is unavailable for comparison with the simulated soil moisture.

1.2.8 Hydrological Models and Satellite Data for Soil Moisture Estimation

There are two approaches for estimating the dynamics of soil moisture in large regions. The first method consists of the use of hydrological models to estimate soil moisture content. The second method uses satellite measurements to calculate soil moisture. The main benefit of employing hydrological models to estimate soil moisture lies in their specific representation of areal averages across catchments and the input data are typically available over vast areas. Additionally, the soil moisture simulated by these models represents the entire root zone, which is the most critical zone for runoff generation in hydrology (Parajka, Naeimi, Blöschl, Wagner, et al. 2006). The main disadvantage of such models is the inevitable need for calibration to accurately depict hydrological processes in specific cases (Blöschl and Grayson 2002).

The advantage of estimating soil moisture using satellite data is that they generate an integral value over an area rather than point values and the data sources are accessible on a global scale, making them well-suited for ungauged catchments problems. The primary limitation of this approach is the restricted penetration depth of microwaves, which only sense the top few centimeters of soil or less. Considering the significance of soil moisture in deeper layers for hydrological predictions, it is essential to carefully consider the implications of this limited penetration depth when utilizing such data for hydrological purposes. (Parajka, Naeimi, Blöschl, Wagner, et al. 2006)

It appears that combining the two approaches of soil moisture estimation benefits from the advantages of both methods, despite their obvious limitations and high levels of uncertainty. The

hypothesis is that their combination should contribute to minimizing the uncertainty associated with the estimates. (Parajka, Naeimi, Blöschl, Wagner, et al. 2006)

1.2.9 Model Calibration Using Satellite Data of Soil Moisture

Recent developments in remote sensing technologies for soil moisture, along with advancements in data retrieval and mapping, have led to a growing interest in the assimilation of soil moisture data into the calibration of hydrological models, as demonstrated by studies such as Y. Li et al. (2018), Parajka, Naeimi, Blöschl, and Komma (2009), Parajka, Naeimi, Blöschl, Wagner, et al. (2006), Rajib et al. (2016), Sutanudjaja et al. (2014), and Wanders et al. (2014). According to Tong et al. (2021), most of these studies reported a slight degradation in runoff model efficiency, although the internal consistency of the models improved. In contrast, there was an observed increase in soil moisture model efficiency.

1.3 Problem Statement

This master's thesis follows previous studies which assimilated different satellite soil moisture products into calibration of conceptual hydrological models (e.g. Parajka, Naeimi, Blöschl, and Komma (2009), Tong et al. (2021), or Kubáň et al. (2021)). The first attempts analysed the value of the ERS scatterometer into multiple-objective calibration and hydrological predictions in ungauged sites (Parajka, Naeimi, Blöschl, and Komma 2009). The results showed, however, that the ERS products have a very coarse spatial (25km) resolution, which does not allow a significant improvement of hydrological simulations in small and medium-sized catchments. The coarse spatial resolution was also a primary limiting factor in describing the soil moisture variability in alpine regions. The recent advance in remote sensing opens new possibilities for advancing hydrological predictions. Numerous new soil moisture products merge different sources of information and have thus improved spatial and temporal resolutions. One of these new experimental products (merged ASCAT and Sentinel-1 datasets - S1ASCAT) has been successfully tested by Tong et al. (2021) and Kubáň et al. (2021). Their results showed that using the merged Sentinel-1 and ASCAT soil moisture satellite data can improve runoff simulations at the regional scale. Still, there are some other soil moisture products that can be compared and evaluated for hydrological modelling. Comparing their application for the multiple-objective calibration of hydrologic models can shed additional new knowledge about the impact of different spatial and temporal resolutions and mapping algorithms on the performance and efficiency of hydrological models. This thesis aims to examine and compare the performance of Scatterometer Synthetic Aperture Radar (SCATSAR) and S1ASCAT datasets. The specific goals are:

- To process SCATSAR satellite data and identify the availability and frequency of observations for 196 catchments used in previous model evaluations;
- To assess the value of three variants of SCATSAR data for calibrating conceptual hydrologic models and to compare the model performance with respect to traditional runoff only and multiple objective calibrations to runoff and S1ASCAT data;
- To examine the factors that control the model efficiency in Austria

1.4 Approach and Overview

The following procedure is chosen in order to achieve the goal of this thesis:

1. Retrieving the following datasets for the 196 catchment areas as calibration input for TUW_dual model:
   - Precipitation
   - Air temperature
   - Evapotranspiration
   - Soil moisture
   - Measured discharge
   - Catchment elevation zones

   Additionally, the geographic characteristics of each catchment are obtained for the potential subsequent analyses and comparisons. These characteristics include coordinates, area, mean elevation, mean slope, elevation range, roughness index, forest land cover, and agricultural land cover.

2. Calibration of the TUW_dual-laye conceptual hydrological model (with 18 parameters) was performed for the period from September 2014 to December 2020 using the `R` programming language[3] with input data from 196 Austrian catchments.

   The model calibration involves determining the parameters of the TUW_dual model for each catchment area. This process utilizes an automatic optimization algorithm (DEoptim) and two different objective functions. The first objective function is based on both runoff and soil moisture in the root-zone layer (Q+SR), while the second is based only on runoff (Q).

3. Validation of the TUW_dual model for the period from September 2009 to August 2014 using the best parameters retrieved from the calibration period. comparing its results with the observed discharge values.

4. Assessing the runoff simulation results and evaluating the performance of the S1ASCAT and SCATSAR soil moisture products compared to the simulated runoff by the model.

5. Assessing the soil moisture simulation results and evaluating the performance of the S1ASCAT and SCATSAR soil moisture products compared to the simulated soil moisture by the model.

In summary, providing an overview of this thesis, Chapter 1 provides an introduction and an overview of scientific findings in the area of hydrological modeling process. Following this, Chapter 2 details the TUW_dual model structure and parameters, objective functions used for model calibration and validation, criteria for assessing model efficiency, and the chosen optimization algorithm.

Chapter 3 provides a description of the study area and Austrian regional characteristics. Additionally, it presents the hydrological, meteorological, and satellite data upon which the results are based.

Chapter 4 offers a comprehensive presentation of all evaluations and results from the current work. Given the extensive volume of data, the tabular overviews and graphics in the appendix are intended to be supplementary to the content presented in Chapter 4.

Chapter 5 provides an interpretation and discussion of the results. Finally, Chapter 6 reviews the essential work steps and findings, providing a summary and an outlook on potential future research subjects.

[3] `R` programming language: `https://www.r-project.org/`

Chapter 2

Methods

2.1 Conceptual Dual-Layer Hydrological Model

2.1.1 Model Structure

This thesis utilizes the TUW_dual conceptual dual-layer hydrological model, developed at the Vienna University of Technology by Parajka, Naeimi, Blöschl, and Komma (2009), as a semi-distributed conceptual rainfall-runoff model based on the structure of the HBV (Hydrologiska Byråns Vattenbalansavdelning) model introduced by Bergström (1976). The model includes a soil moisture routine, a runoff routing routine, and a snow routine, and it operates on a daily time step (Merz and Blöschl 2004).

Soil Moisture Routine

This subroutine calculates the extent to which rain and meltwater increase soil moisture or contribute to runoff. (Blöschl, Komma, et al. 2017)

In the TUW_dual hydrological model, the soil layer is segmented into two sections: the root zone soil layer and the surface soil layer. A thin layer of surface soil (dQ_{skin} in Figure 2.1), resting on top of the root soil reservoir, serves as a representation of the soil storage. The surface soil reservoir is filled with melted snow and rainwater. The dQ_{skin} flow is divided into two sections When the L_{skin} capacity is exceeded. the dQ fraction becomes direct runoff and dS_{s} fraction increases the root soil moisture S_{s}. The skin soil reservoir's soil moisture content is decreased by a proportion of the actual evaporation as shown in Equation (2.1), where AET represents the actual evaporation and the parameter φ splits it into evaporation from the root-zone AET_{main} (see Equation (2.2)) and the surface soil layer AET_{skin}. (Parajka, Naeimi, Blöschl, and Komma 2009)

$$AET_{\text{skin}} = (1 - \varphi) \cdot AET \tag{2.1}$$

$$AET_{\text{main}} = \varphi \cdot AET \tag{2.2}$$

where:

AET ... is the actual evaporation [mm/day],
AET_{skin} ... is the evaporation from the surface soil layer [mm/day],
AET_{main} ... is the evaporation from the root-zone soil layer [mm/day],
φ ... is the parameter for the fraction of the actual evaporation [-],

The bidirectional moisture flux Q_m, which is considered to be a linear function of the vertical soil moisture gradient Δm, connects the skin soil reservoir and the main soil reservoir and is represented in Equation (2.3). (Parajka, Naeimi, Blöschl, and Komma 2009)

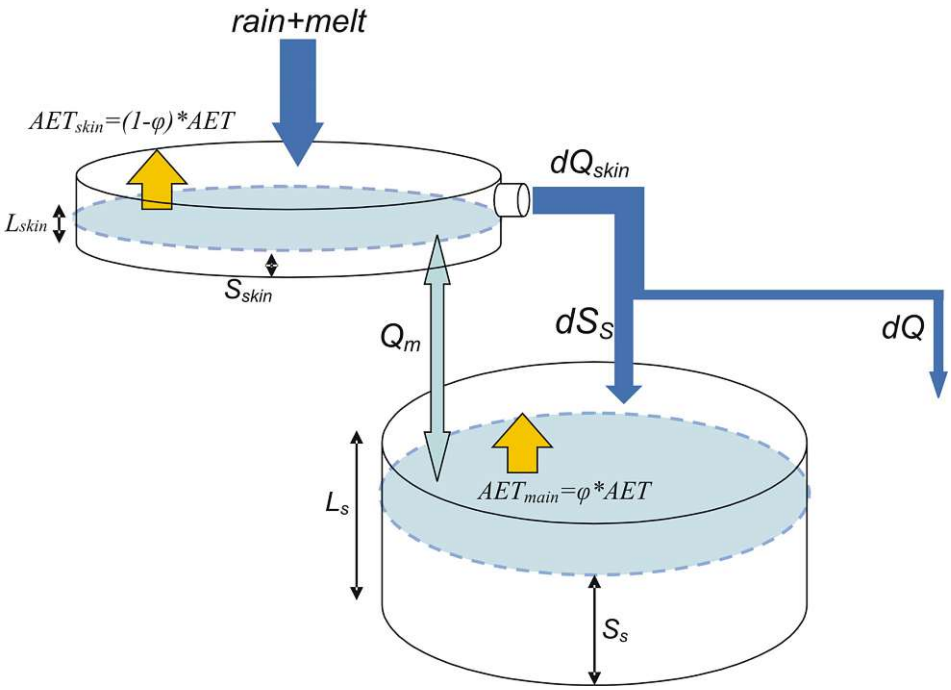

Fig. 2.1: The schematic structure of the dual layer soil moisture accounting approach introduced in the TUW_dual model. (Parajka, Naeimi, Blöschl, and Komma 2009)

$$Q_m = \Delta m \cdot \alpha_m, \tag{2.3}$$

where:

Q_m ... is the bidirectional moisture flux,
Δm ... is the vertical soil moisture gradient,
α_m ... is a transfer parameter,

Percolation from the skin to the main soil layer happens if the skin soil moisture is higher than the main layer's soil moisture ($Q_m > 0$). Capillary rise from the main to the skin soil layer occurs if the moisture content of the skin soil is lower than that of the main layer ($Q_m < 0$). The difference between the relative soil moisture in the skin soil reservoir and the main soil reservoir is known as the vertical soil moisture gradient Δm and is computed as shown in Equation (2.4):

$$\Delta m = \frac{S_{\text{skin}}}{L_{\text{skin}}} - \frac{S_s}{L_s} \tag{2.4}$$

where:

Δm ... is the vertical soil moisture gradient,
S_{skin} ... is the surface soil moisture,
L_{skin} ... is the capacity of the surface soil reservoir,
S_s ... is the moisture state of the root soil reservoir,
L_s ... is the capacity of the root soil reservoir.

The dual-layer soil moisture accounting system incorporates the following parameters for the surface soil layer:

- Field capacity fc_{skin}, i.e., the maximum soil moisture storage of the surface skin layer.
- The transfer parameter α.
- the parameter φ, which proportionates the actual evapotranspiration.

The root zone soil layer includes the following parameters:

- The field water capacity FC, which determines the maximum soil moisture achievable in the catchment area. If this value is reached, the soil becomes saturated, and no more water can be stored. Therefore, rain or meltwater turns into runoff.
- The parameter β, which is the measure of the nonlinearity of runoff formation.
- The parameter L_p, which represents the limit for potential evaporation.

The summary of TUW_dual Model parameters along with their respective ranges and units can be found in Table 2.1 according to Parajka, Naeimi, Blöschl, and Komma (2009).

Runoff Routing Routine

Runoff routing on hillslopes is represented by the movement of water through an upper and a lower soil reservoir, which are labeled as S_{UZ} and S_{LZ}, respectively. Excess rainfall ΔS_{UZ} infiltrates the upper zone reservoir and exits through three separate pathways: outflow from the reservoir through a fast storage coefficient K_0; percolation to the lower zone with a constant percolation rate C_{perc}; and, if the storage state LS_{uz} threshold is exceeded, through an additional outlet based on a fast storage coefficient K_1. Water within the lower zone reservoir is released using a slow storage coefficient, represented as K_2. Subsequently, the outflow from both reservoirs Q_G is directed by a triangular transfer function (see Figure 2.2) that characterizes the runoff routing within the stream network. The base of the transfer triangular function can be calculated by the Equation (2.5) (Parajka, Merz, et al. 2007):

$$B_Q = \begin{cases} B_{max} - C_{route} Q_G & \text{if } B_{max} - C_{route} Q_G \geq 1.0 \\ 1 & \text{otherwise} \end{cases} \tag{2.5}$$

where:

B_Q ... is the base of the transfer triangular function [days],
B_{max} ... is the maximum base at low flows [days],
C_{route} ... is a free scaling parameter [days²/mm],
Q_G ... is the outflow from both reservoirs [mm/days].

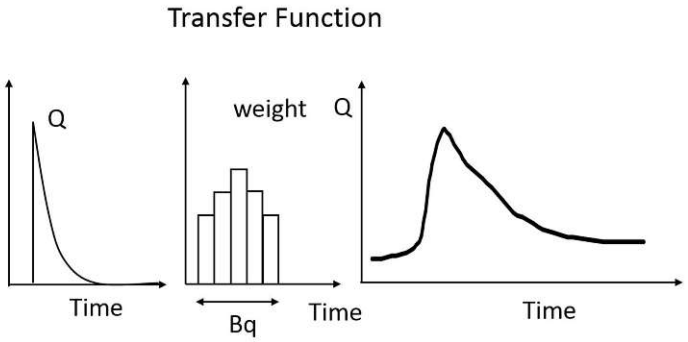

Fig. 2.2: The transfer funktion according to Parajka, Merz, et al. (2005)

Snow Routine

The snow routine employs a fundamental degree-day concept to represent snow accumulation and melting. Based on the mean daily air temperature T_A, the mean daily precipitation P in an elevation zone is divided into rain P_r and snow P_s. These are computed in Equations (2.6) and (2.7) (Parajka, Merz, et al. 2007):

$$P_r = \begin{cases} P & \text{if } T_A \geq T_r \\ P \cdot \frac{T_A - T_s}{T_r - T_s} & \text{if } T_s < T_A < T_r \\ 0 & \text{if } T_A < T_s \end{cases} \tag{2.6}$$

$$P_s = P - P_r, \tag{2.7}$$

where:

P ... is the mean daily precipitation [mm],
P_r ... is the mean daily precipitation in the form of rain[mm],
P_s ... is the mean daily precipitation in the form of snow [mm],
T_A ... is the mean daily air temperature [°C].
T_r ... is the upper threshold temperature for snow [°C].
T_s ... is the lower threshold temperature for rain [°C].

If the temperature falls below the limit T_s, all precipitation falls as snow, whereas when the limit temperature T_r is exceeded, all precipitation consists of rain.

Melting begins at air temperatures that exceed the threshold T_m, as demonstrated in Equations (2.8). A snow correction factor SCF is used to adjust the catch deficit of the precipitation gauges during snowfall. Fluctuations in the snow water equivalent (SWE) from days $i-1$ to i are explained by the Equation (2.9) (Parajka, Merz, et al. 2005):

$$M = \begin{cases} (T_A - T_m) \cdot DDF & \text{if } T_A > T_m \text{ and } SWE > 0 \\ 0 & \text{otherwise} \end{cases} \tag{2.8}$$

$$SWE_i = SWE_{i-1} + (SCF \cdot P_s - M) \cdot \Delta t \tag{2.9}$$

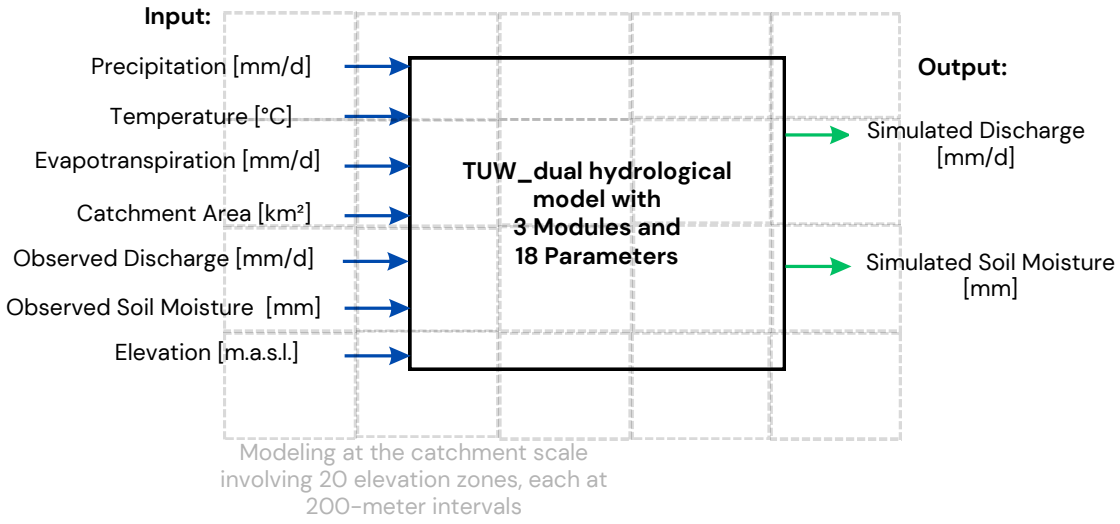

Fig. 2.3: Schematic representation of the TUW_dual hydrological mode

where:

M ... is the amount of melt water per time step [mm],
T_m ... is the temperature threshold, above which snowmelt occurs [°C],
DDF ... is the degree day factor for snowmelt [mm/°C/day],
SWE ... is the snow water equivalent [mm],
SCF ... is the snow correction factor [-],
Δt ... is the time step of 1 day [day].

2.1.2 Model Scheme

In the present work, the TUW_dual model is used as a semi-distributed model, whereby each considered catchment is spatially subdivided into 20 hypsometrical elevation zones with a range of 200 meters in altitude. The time step of the simulation is set to one day. The schematic structure of the TUW_dual model is shown in Figure 2.3.

2.1.3 Model Parameters

The TUW_dual hydrological model consists of a total of 18 model parameters. Among them, five parameters, namely, SCF, DDF, T_r, T_s, and T_m, are specifically assigned to the snow module. The soil moisture module is characterized by three model parameters: L_p, FC, and β for the root zone layer, and three model parameters for the surface layer: fc_{skin}, α, and φ. The remaining seven model parameters (K_0, K_1, K_2, LS_{uz}, C_{perc}, B_{max}, and C_{route}) are associated with the runoff module.

Model parameters in gauged catchments are typically calibrated to observed runoff in order to minimize bias in the prediction of runoff (Parajka, Andréassian, et al. 2013). The model parameters used in this thesis are adopted from the study by Parajka, Naeimi, Blöschl, and Komma (2009) and Kubáň et al. (2021). They are determined through automatic model calibration, and the same set of parameters is applied to each elevation zone within the catchment. They are presented in Table 2.1.

2.1.4 Model Calibration and Validation

The TUW_dual conceptual dual-layer hydrological model, implemented as an `R` package (version 4.2.2), was employed for rainfall-runoff modeling in 196 Austrian catchments. For the model calibration, the automatic global optimization algorithm developed by Mullen et al. (2011) (DEoptim) was chosen.

The iterative Termination Criteria is concluded based on multiple objective criteria, as follows:

- When the improvement in the objective function falls below the relative tolerance of convergence of 10^{-4} after 50 iteration steps, the calibration is stopped.
- The maximum number of iterations steps is set to 700, after which the search is terminated.

The model validation employs the *split-sample* test as described by Klemeš (1986), in which the model calibration is carried out for the period September 2014 to December 2020, and the model validation for the period September 2009 to August 2014.

The model warm-up is a procedure that optimizes the model to achieve a realistic and steady state, resulting in a better match between simulated and observed data (Kim et al. 2018). For this purpose, the model warm-up period were set to 365 days.

As discussed in 1.2.7.3, The correlation coefficient (r_{SR}) is defined as Not-Available (N/A) by the model when satellite soil moisture data for a specific catchment is missing for comparison with its corresponding simulated soil moisture data.

The Appendix provides an overview of the calibration and validation of the TUW_dual model.

2.1.4.1 Utilized Objective Functions

In this study, for the multi-objective calibration of the TUW_dual model, we utilized the following objective functions (OF):

- Objective function based on runoff only (OF_Q)
- Objective function based on runoff and soil moisture in the root-zone layer (OF_{Q+SR})

To calculate the individual objective functions OF_Q, a combination of the Nash-Sutcliffe efficiency (NSE) and the logarithmic Nash-Sutcliffe efficiency coefficient (NSE_{Log}) (refer to (1.1) and (1.3)), following the approach outlined by Tong et al. (2021) and Kubáň et al. (2021), as shown in Equation (2.10), was employed:

$$OF_Q = \frac{NSE + NSE_{Log}}{2} \tag{2.10}$$

In the objective functions OF_Q, the simulated values of runoff (Q_{sim}) were compared with observed runoff (Q_{obs}).

Adopting the approach by Tong et al. (2021) and Parajka, Naeimi, Blöschl, and Komma (2009), the individual objective functions OF_{SR} is defined through the correlation coefficient (r_{SR}) discussed in 1.2.7.3, and is computed as demonstrated in Equation (2.11):

$$OF_{SR} = r_{SR} = \frac{\sum_{i=1}^{n}(\theta_{sim,i} - \overline{\theta}_{sim})(\theta_{obs,i} - \overline{\theta}_{obs})}{\sqrt{\sum_{i=1}^{n}((\theta_{sim,i} - \overline{\theta}_{sim})^2(\theta_{obs,i} - \overline{\theta}_{obs})^2)}} \tag{2.11}$$

where:

r_{SR} ... is the correlation coefficient between observed and simulated soil moisture [-],
$\theta_{sim,i}$ ... the relative root zone soil moisture simulated by the model on day i [%],
$\theta_{obs,i}$ ... is the measured soil moisture by the scatterometer on day i [%],
$\overline{\theta}_{sim}$ ... is the average of simulated soil moisture over the period of n days without snow days [%],
$\overline{\theta}_{obs}$ ... is the average of observed soil moisture over the period of n days [%] without snow days [%].

In the objective functions OF_{Q+SR}, the simulated values of runoff (Q_{sim}) and soil moisture in the root-zone layer (θ_{sim}) were contrasted respectively with observed runoff (Q_{obs}) and soil moisture in the root-zone layer (SWI_{root}) obtained from S1ASCAT and SCATSAR data, with different weights for the individual objectives regarding runoff OF_Q and soil moisture OF_{SR}, as shown in Equation (2.12):

$$OF_{Q+SR} = OF_Q \cdot w_Q + OF_{SR} \cdot w_{SR} \tag{2.12}$$

where:

w_Q ... is the weight related to runoff objective OF_Q [-],
w_{SR} ... is the weight related to soil moisture objective OF_{SR} [-]

As suggested in the study by Tong et al. (2021), the weights w_Q and w_{SR} were defined with a value of 1/2, which has been demonstrated to contribute to more reliable calibration.

2.1.5 Criteria for Assessing Model Efficiency

The following efficiency criteria were applied in this work in order to assess the runoff model efficiency for the calibration and validation:

- Nash-Sutcliffe Efficiency Coefficient (NSE)
- Kling-Gupta Efficiency (KGE)

Additionally, the following criterion was used to evaluate the model's efficiency in simulating soil moisture:

- Correlation Coefficient (r_{SR})

For further details, please refer to Subsection 1.2.7, where Equations (1.1) to (1.8) provide a mathematical explanation of the efficiency criteria.

Tab. 2.1: Description of TUW_dual model parameters and parameter ranges for the 196 Austrian catchments (Parajka, Naeimi, Blöschl, and Komma 2009).

Abbreviation	Description of the Model Parameters	Model Part	Parameter Range
1. SCF	Snow correction factor	Snow	0.9–1.5 (-)
2. DDF	Degree day factor for snowmelt	Snow	0.0–5.0 (mm/°C/day)
3. T_r	Temperature threshold, above which precipitation is considered liquid	Snow	1.0–3.0 (°C)
4. T_s	Temperature threshold, below which precipitation is considered solid	Snow	-3.0–1.0 (°C)
5. T_m	Temperature threshold, above which snowmelt occurs	Snow	-2.0–2.0 (°C)
6. L_p	Parameter limiting potential evaporation	Soil (root zone)	0.0–1.0 (-)
7. FC	Maximum soil moisture storage index, field capacity	Soil (root zone)	0–600 (mm)
8. β	Parameter governing runoff generation	Soil (root zone)	0.0–20.0 (-)
9. K_0	Storage coefficient governing very fast runoff response	Runoff	0.0–2.0 (days)
10. K_1	Storage coefficient governing fast runoff response	Runoff	2.0–30.0 (days)
11. K_2	Storage coefficient governing slow runoff response	Runoff	30.0–250 (days)
12. LS_{uz}	Threshold parameter storage state for initiation of the very fast runoff response	Runoff	1.0–100 (mm)
13. C_{perc}	Constant percolation rate	Runoff	0.0–8.0 (mm/day)
14. B_{max}	Maximum base at low flows	Runoff	0.0–30.0 (days)
15. C_{route}	Free scaling parameter for routing	Runoff	0.0–50.0 (days²/mm)
16. fc_{skin}	Field capacity, i.e., maximum soil moisture storage of the surface layer	Soil (surface)	0.1–10 (mm)
17. α	Non-linearity coefficient of runoff generation	Soil (surface)	0.7–0.95 (-)
18. φ	Parameter for the fraction of the actual evaporation	Soil (surface)	5–15 (-)

Chapter 3

Study Area and Data Basis

3.1 Study Area

The study area includes 196 catchments in Austria based on the previous studies by Kubáň et al. (2021) and Tong et al. (2021). The diversity of geographic, landscape, climate, and hydrologic characteristics serves as the criteria for selecting these catchments (Tong et al., 2021). The catchment areas vary from 14.2 km² (Spöttling-Taurer) to 6214 km² (Bruck an der Mur unter Mürz, Mur River) with a median of 170.15 km². The mean elevation ranges from 353 to 2710 meters above sea level (m.a.s.l.), with a median of 1002 m a.s.l. Mean daily air temperatures range from -1.5 degrees Celsius in the Alpine catchments to +10.3 degrees Celsius in the Lowland catchments. The percentage of forest cover ranges from 0% to 94.6%, while agricultural soil cover ranges from 0% up to 92.9%. Figure 3.1 illustrates both the geographical area and the specific locations of the selected catchments, along with the Austria's elevation map. To facilitate the comparison of results among catchments with distinct topographic and climatic characteristics, and due the fact that it is difficult to derive soil moisture data from alpine regions, they were categorized into Lowland and Alpine catchments, as per the study by Kubáň et al. (2021). These categories are depicted in Figure 3.2. According to Xu et al. (2014) and Brocca et al. (2012), the quality of soil moisture products decrease with higher forest cover percentages, therefore, in order to add more spatial details to the physical coverage of the studied catchments, land use characteristics, i.e., forest land cover and agricultural land cover within the Austrian boundary for the year 2019 are visualized through the Figure 3.3. For more information about the catchments characteristics refer to 7.1 in Appendix.

3.2 Data Basis

The input data for calibrating and validating the hydrological model in this section of the thesis were collected primarily from the studies by Kubáň et al. (2021) and Tong et al. (2021).

In order to calculate mean daily potential solar radiation and morphological characteristics, including elevations, roughness index, and slopes, a digital elevation model of Austria was employed. The 'R.sun' function in GIS-GRASS was utilized to estimate the sunlight index for a 1x1 km² raster. Land use data for the year 2006 was sourced from the Copernicus Land Monitoring Service and the CORINE land cover databases. The High-Resolution Global Map of Soil Hydraulic Properties dataset offers global maps depicting mean values and standard deviations of soil hydraulic parameters utilizing the Kosugi water retention model at a 1 km resolution for surface soil (0–5 cm). From this dataset, soil-related data were extracted , including field capacity and saturated hydraulic conductivity. These parameters were approximated for the surface soil using the Kosugi K3 pedotransfer function model, with inputs consisting of sand, silt, clay, and bulk density percentages. All these parameters were interpolated into 200-meter elevation intervals, starting from sea level (0 meters) to 200 meters above sea level. The selected catchment characteristics are listed in Table 3.1.

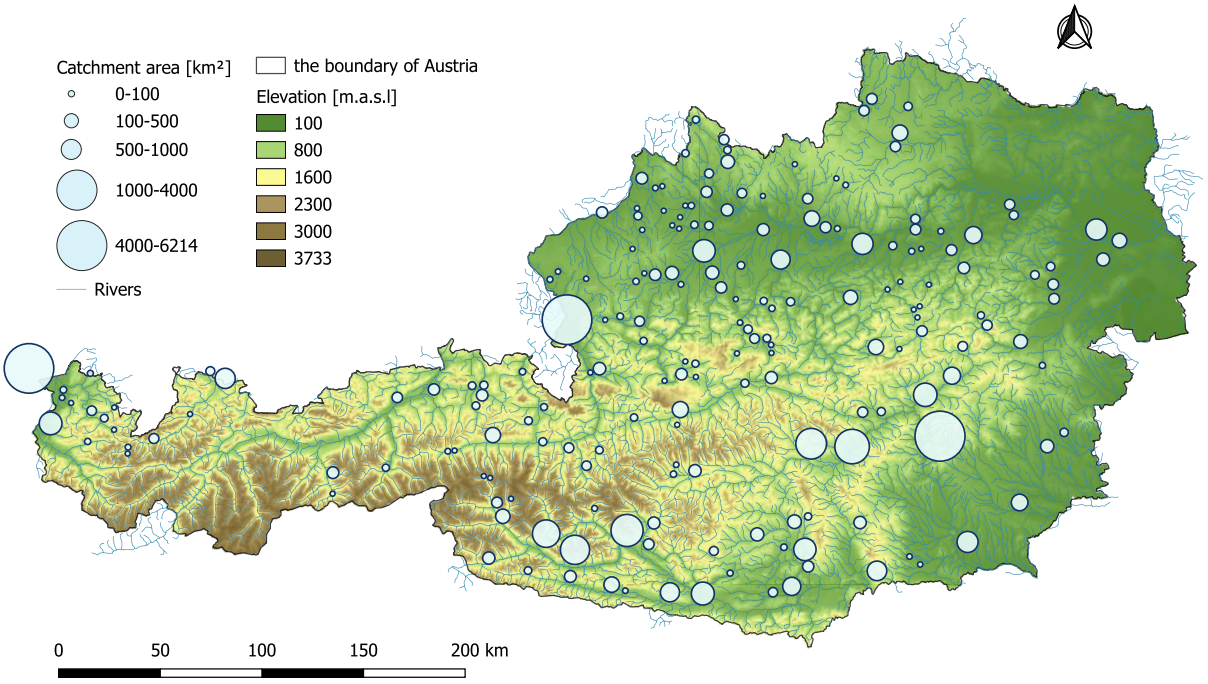

Fig. 3.1: The sizes of the 196 selected catchment areas and Austria's elevation map.

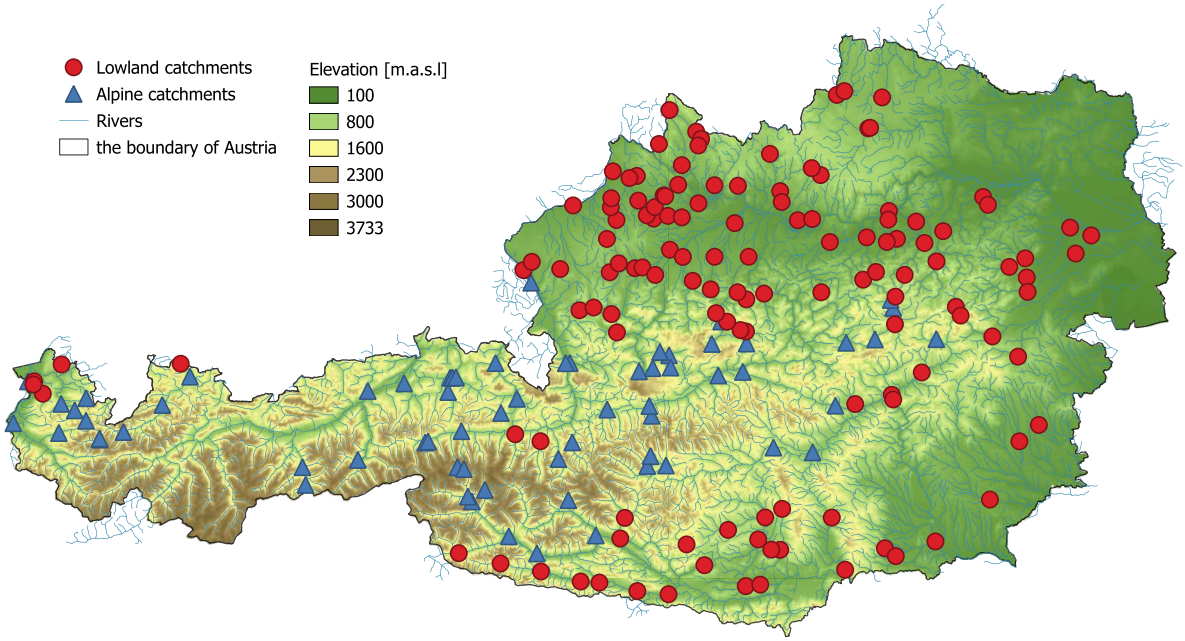

Fig. 3.2: Geographic location of the 131 Lowland and 65 Alpine catchments. The red circles represent the Lowland catchments, and the blue triangles the Alpine catchments.

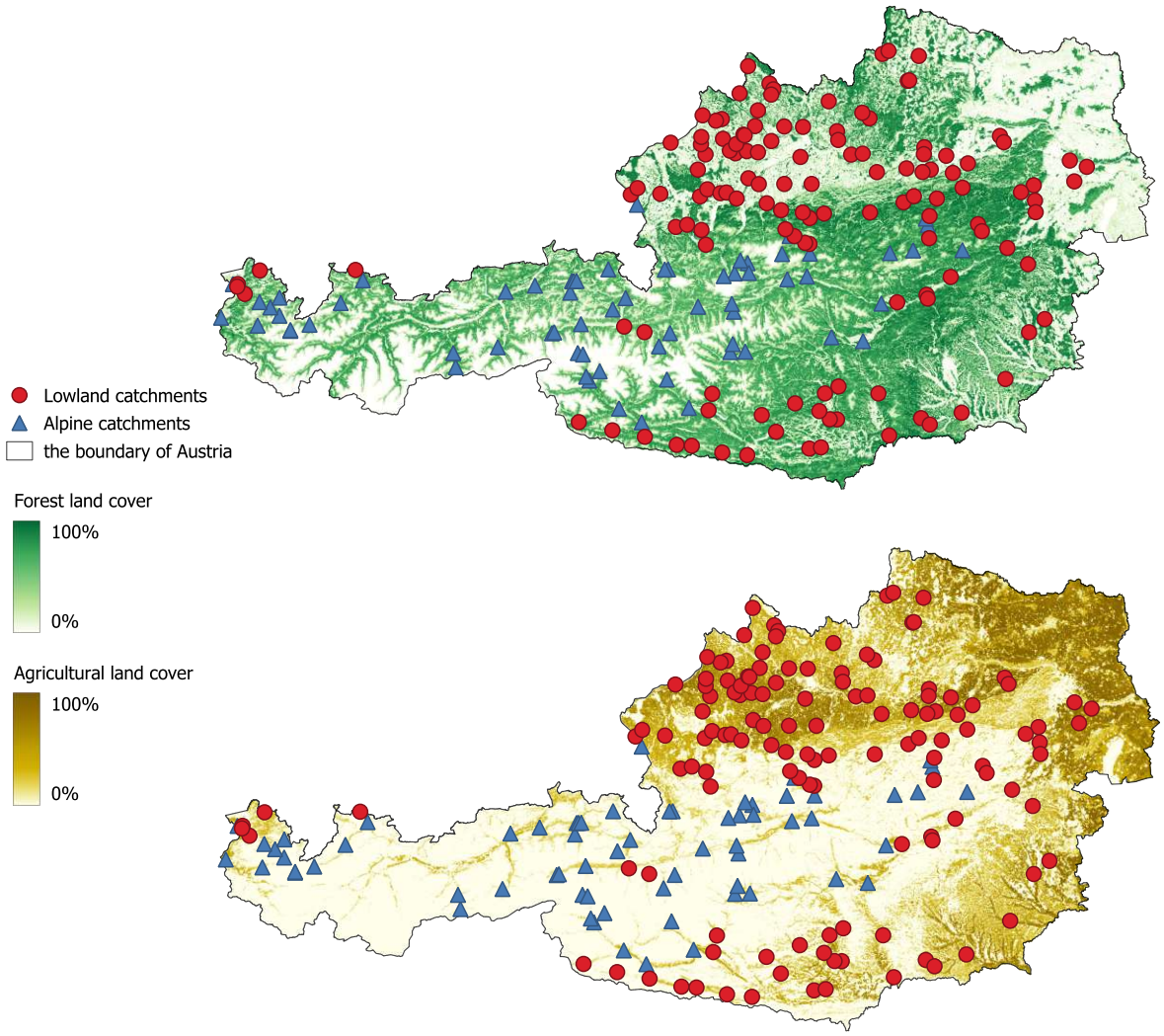

Fig. 3.3: Forest and agricultural soil cover in Austria for the year 2019. (*Copernicus Land Monitoring Service - Land Cover* 2023)

Tab. 3.1: Basic characteristics of the 196 catchments, including abbreviations, units, minimums, maximums, and medians.

Information	Attribute	Abbrev.	Unit	Min.	Max.	Median
Area	Area	A	km²	14.2	6214	170.15
Elevation	Mean elevation	MELE	m.a.s.l.	353	2710	1002
	Mean slope	SL	%	1.7	43.9	18.8
	Elevation range	ER	m	80	3072	1286
	Roughness index	MRI	-	0.15	0.65	0.38
Land cover	Forest percentage	FP	%	0.0	94.6	46.6
	Agriculture percentage	AP	%	0.0	92.9	16.3
Climate	Mean annual precipitation	MAP	mm	728	2302	1285
	Mean air temperature	MAT	°C	-1.5	10.3	7.4

3.2.1 Hydrological Data

Daily discharge measurements for the calibration period from September 2014 to December 2020 and the validation period from September 2009 to August 2014 were obtained from the 196 gauging stations. These data are available at the Central Hydrographical Bureau (HZB; `https://ehyd.gv.at/`).

3.2.2 Meteorological Data

Precipitation & Temperature

Mean daily precipitation and air temperature data for both the calibration and the validation periods were derived from the gridded SPARTACUS dataset provided by Zentralanstalt für Meteorologie und Geodynamik (ZAMG). This dataset provides minimum and maximum air temperatures, as well as precipitation sums, at a spatial resolution of 1 km and a daily temporal resolution over the entire country of Austria. It has been operational since 1961 and is continuously interpolated into 200-meter elevation zones.

The dataset of daily precipitation is constructed using the traditional two-tier methodology, which involves independent interpolations for daily relative anomalies and mean monthly precipitation. The interpolation for daily relative anomalies is based on data from 1,249 stations and employs kriging with topography predictors as external drift. The interpolation for mean monthly precipitation utilizes data from 523 stations and relies on angular distance weighting. (Hiebl and Frei 2018)

To address the complex and highly variable temperature patterns in the high-mountain region, as well as the geographical representatives of station measurements, Hiebl and Frei (2016) developed an interpolation approach. This method interpolates the data into 200-meter hypsometrical elevation zones, enabling the estimation of nonlinear temperature profiles with altitude. The spatial analysis was based on 150 station series, which were homogenized where possible in and around Austria, all covering the entire study period without any gaps.

Evapotranspiration

The potential evapotranspiration (EP) is determined using the modified Blaney-Criddle equation introduced by Parajka, Merz, et al. (2003) (see Equation (3.1)) with data from gridded maps of mean daily air temperature and potential sunshine duration index:

$$EP = -1.55 + 0.96 \cdot (8.128 + 0.457 \cdot T) \cdot \frac{SD}{Sy} \cdot 100 \tag{3.1}$$

where:

EP ... is the potential evapotranspiration [mm/day],

T ... is the mean daily temperature of the catchments [°C],

SD ... is the potential duration of sunshine during the day [hours],

Sy ... is the mean annual sum of the potential duration of sunshine [hours],

$\frac{SD}{Sy}$ ... is the sunshine index [-].

The SD and Sy values were obtained using the 'R.sun' function on a 1 x 1 km grid from a digital relief model in GIS-GRASS.

3.2.3 Satellite Data

Soil moisture data can be obtained using either in situ or airborne/satellite methods. In situ observations offer benefits such as temporal resolution and the ability to measure at various observation depths in the ground. However, remote sensing devices can provide unparalleled spatial coverage, ranging from a few square meters to thousands of square kilometers. The majority of satellite technologies for estimating soil moisture employ microwave frequencies and can be divided into passive (e.g. AMSR-E) and active instruments (e.g. ASCAT and SAR) (Paulik et al. 2014). Active microwave sensors transmit an electromagnetic pulse, which is then used to detect the energy reflected back from the Earth's surface. Passive sensors (radiometers) gauge the level of emissions from the Earth's surface. Therefore, they are able to capture images unrestricted during day and night, but they are unable to do so when the Earth is frozen or covered in snow (Wagner, Blöschl, et al. 2007).

In this thesis, we employed the merged ASCAT and Sentine-l datasets (S1ASCAT) Soil Water Index (SWI) with characteristic time length of 40 days (T=40) and Scatterometer Synthetic Aperture Radar Soil Water Index (SCATSAR SWI) products with three different characteristic time lengths of 20, 40, and 100 days (T=20, T=40, T=100), distributed by the Copernicus Global Land Service.

3.2.3.1 S1ASCAT Soil Water Index Product

Following the approach outlined in Tong et al. (2021), to enhance the soil component response of the catchments, the new Meteorological Operational Satellite (MetOp) ASCAT Surface Soil Moisture (SSM)[1] product combined with Sentinel-1 backscatter was employed in this thesis. The novelty in this approach lies in the inclusion of a parametrization for vegetation correction, as developed by Hahn et al. (2021), and the application of a new method for disaggregating ASCAT soil moisture retrievals into a finer grid. For retrieving the S1ASCAT SWI dataset, the primary processing steps include:

- Using the TU Wien Change Detection Algorithm by Naeimi et al. (2009) to recover surface soil moisture from ASCAT backscatter time series, which is distributed by the Copernicus Global Land Service.

[1] SSM: Surface Soil Moisture refers to the relative water content in the top few centimeters of soil, expressed as a percentage of saturation. (*Copernicus Global Land Service - Surface Soil Moisture* 2023)

- Disaggregating the initial ASCAT dataset for surface soil moisture, which has a spatial resolution of 12.5 km, into a 500x500 m grid. The method involves targeted resampling, which connects backscatter data from the Sentinel-1 Synthetic Aperture Radar (SAR) at regional (12.5 km) and local (0.5 km) scales, preserving soil moisture patterns that remain temporally stable.
- Determining the SWI using an exponential filter introduced by Wagner, Lemoine, et al. (1999), with the characteristic time length (T). (see Equation (3.2))

$$SWI_T(t_n) = \frac{\sum_{i}^{n} SSM(t_i) \cdot e^{\frac{-(t_n - t_i)}{T}}}{\sum_{i}^{n} e^{\frac{-(t_n - t_i)}{T}}} \qquad \text{for } t_i \leqslant t_n \tag{3.2}$$

where:

SSM ... is the surface soil moisture estimate in [%] from the Scatterometer at time t_i,
t_n ... is the observation time of the current measurement [days],
t_i ... are the observation times of the previous measurements [days],
T ... is the time length [days].

The formula defines the conversion process for SSM observations into the SWI. The so-called time length (T, also T-value) is a local, soil-dependent indicator of the infiltration time, increasing with soil depth (Bauer-Marschallinger, Paulik, Hochstöger, et al. 2018). Careful consideration of T is necessary to avoid losing information about short-term conditions due to the presence of soil moisture dynamics in deeper soil layers (Kubáň et al. 2021). Since an increased T value represents a deeper soil layer, a value of T = 40 days was selected in this thesis to account for soil moisture in the root-zone.

To eliminate invalid S1ASCAT observations related to snow and frozen ground, soil moisture was masked based on soil temperature and snow cover data from the European Centre for Medium-Range Weather Forecasts (ECMWF) Copernicus Climate Service ERA5-Land dataset. This masking occurred when the snow cover exceeded 30% of the pixel area or when soil temperatures at a depth of 0-7 cm fell below 1°C. (Tong et al. 2021)

The S1ASCAT product used in this thesis includes daily data for the root-zone soil layer for the years 2014 to 2020 and was interpolated from a 500x500 m grid to match the 200-meter hypsometrical elevation zones elevation zones. The naming convention 'S1ASCAT' will be further used in the upcoming chapters to refer to the Advanced Scatterometer Satellite Remote Sensing product for soil water index in the root-zone layer with a 40-day time value.

3.2.3.2 SCATSAR Soil Water Index Product

The Scatterometer Synthetic Aperture Radar Soil Water Index (SCATSAR SWI) is created by merging coarse-scale surface soil moisture (SSM) data from Metop ASCAT (scatterometer, 25 km resolution) with fine-scale SSM data from Sentinel-1 Synthetic Aperture Radar (SAR, 1 km resolution). This fusion resulted in daily kilometer-scale observational data suitable for operational use, characterized by high temporal and spatial resolution. For both ASCAT SSM and Sentinel-1 SSM data the TU Wien Change Detection Algorithm were employed, However, the input SSM data quality from ASCAT and SAR is not always the same and can change over time. To adjust the influence of the input quality on the SCATSAR SWI, weights for ASCAT

($w_{ASCAT}(t_p)$) and SAR ($w_{SAR}(t_p)$) were introduced, which determine the weight of the individual SSM values in the SSM history. (see Equation (3.3)) (Bauer-Marschallinger, Paulik, Hochstöger, et al. 2018)

$$SWI_T^w(t_n) = \frac{n \cdot \sum_{i=1}^{n} w(t_i) \cdot SSM(t_i) \cdot e^{\frac{-(t_n - t_i)}{T}}}{\sum_{i=1}^{n} w(t_i) \cdot \sum_{i=1}^{n} e^{\frac{-(t_n - t_i)}{T}}} \qquad \text{for } t_i \leqslant t_n \tag{3.3}$$

where:

SSM ... is the surface soil moisture estimate in [%] from the Scatterometer at time t_i,
t_n ... is the observation time of the current measurement [days],
t_i ... are the observation times of the previous measurements [days],
T ... is the time length [days].
$w(t_i)$ ... is the weight for SSM [-].

There are some limitations to SCATSAR SWI products. First, soil texture, which establishes the relationship between the T-value and soil depth, is not considered by the SWI retrieval method. To provide users with more options for selecting the best-matching data, eight T-values (2, 5, 10, 15, 20, 40, 60, 100) are provided for each product. Second, evapotranspiration is not accounted for when precipitation occurs simultaneously with satellite observations, potentially resulting in an excessively high SWI calculation of soil moisture in the root-zone. Lastly, frozen- and snow-conditions, high-altitude permafrost areas, glaciers, dense forests, and deserts are unsuitable environments for the SWI algorithm (Bauer-Marschallinger, Paulik, and Jacobs 2022). The figure 3.4 illustrates the SCATSAR SWI observations within the Austrian boundary from January 1, 2020, to December 1, 2020, at monthly intervals. The masked SWI data (depicted as white areas) are a result of invalid soil moisture data caused by snow cover and frozen ground. Comparing Figure 3.2 with Figure 3.4 reveals a deficiency in soil moisture data for the majority of the selected Alpine catchments.

The SCATSAR product used in this thesis includes daily data for the root-zone soil layer for the years 2014 to 2020 and was interpolated from a 1x1 km grid to match the 200-meter hypsometrical elevation zones. The naming convention 'SCATSAR 020,' 'SCATSAR 040,' and 'SCATSAR 100' will be used in the upcoming chapters to refer to the Scatterometer Synthetic Aperture Radar product for soil water index in the root-zone layer with 20-day, 40-day, and 100-day time values, respectively.

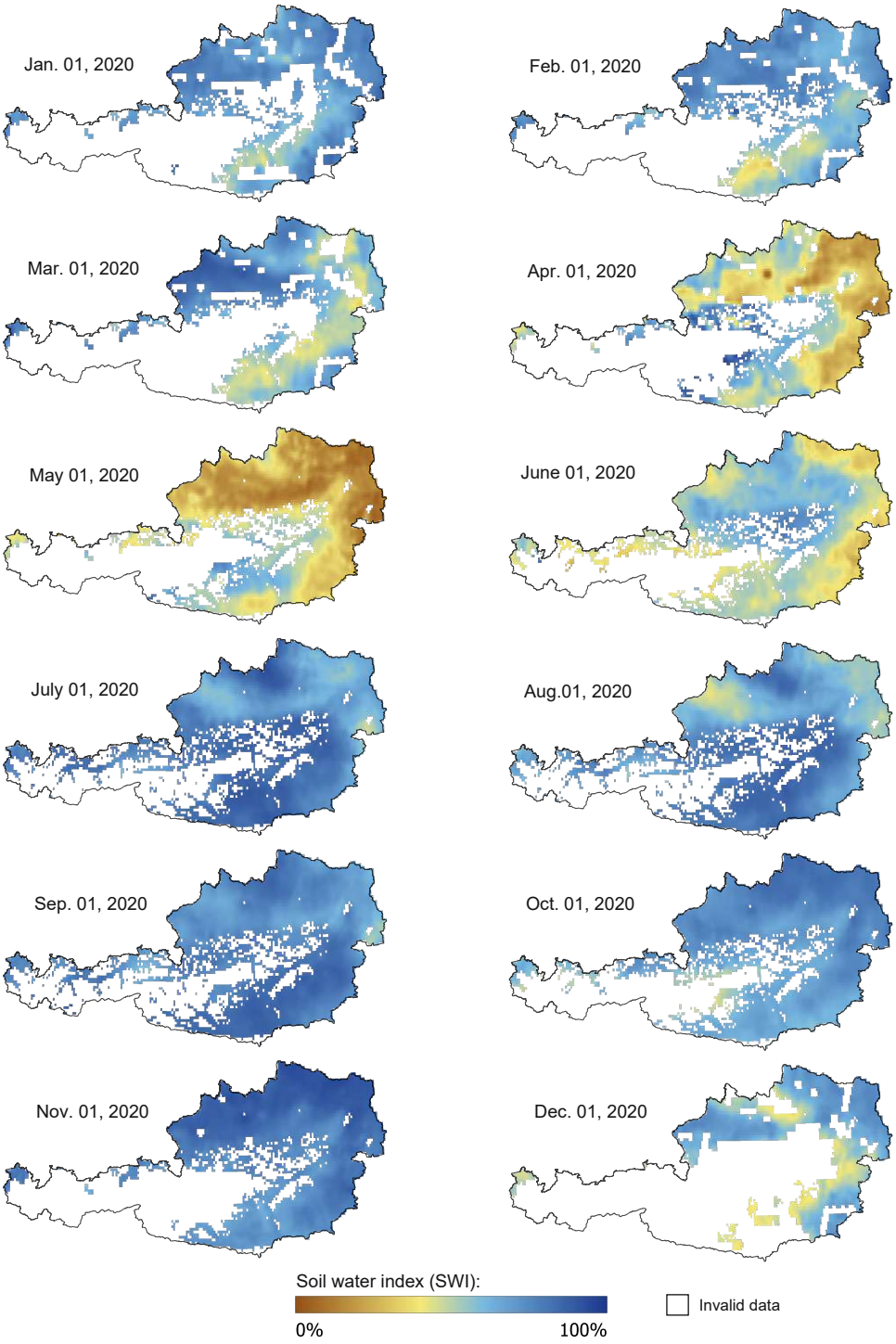

Fig. 3.4: SCATSAR Soil Water Index (SWI) for Austria, from January 1, 2020, to December 1, 2020. White areas within the boundaries of Austria indicate invalid soil moisture data. (*Copernicus Global Land Service - Soil Water Index* 2023)

Chapter 4

Results

4.1 Model Performance Comparison: S1ASCAT and SCATSAR Variants during Calibration

The TUW_dual was calibrated for a total of 196 catchments, comprising 131 Lowland catchments and 65 Alpine catchments. The calibration process was initially conducted for runoff and soil moisture in the root-zone layer (Q+SR), utilizing four different satellite products (S1ASCAT, SCATSAR 020, SCATSAR 040, and SCATSAR 100). Subsequently, the model was calibrated only to runoff (Q). For both calibration variants, the best possible model parameters were applied, and the calibration was carried out over the period from September 2014 to December 2020.

The relative cumulative distribution functions (RCDFs) of the Nash-Sutcliffe Efficiency (NSE) and the Kling-Gupta Efficiency (KGE) are compared in Figure 4.1 and 4.2, respectively.

The cumulative distribution functions (CDFs) of the correlation coefficient (r_{SR}) are depicted in Figure 4.3. Some catchments had unavailable r_{SR} values; therefore, the x-axis of the CDFs does not represent relative frequency, which could led to misleading visualizations. Instead, the number of catchments was used to provide a more precise representation. The r_{SR} values, including the unavailable values, are illustrated in Figure 4.4, along with their corresponding geographic catchment locations. Additionally, a detailed listing of these missing values can be found in the Appendix, from Table 7.21 to Table 7.25.

The medians of the Nash-Sutcliffe Efficiency (NSE), the Kling-Gupta Efficiency (KGE), and the correlation coefficient (r_{SR}) values are summed up in Table 4.1.

Nash-Sutcliffe Efficiency (NSE)

From RCDFs in Figure 4.1, it is evident that the calibration to runoff and soil moisture in the root-zone layer (Q+SR) generally results in a slight decline in NSE medians for the Lowland and a more pronounced decrease in NSE medians for the Alpine catchments compared to calibration to runoff only (Q). Table 4.1 confirms these observations, indicating a median drop in NSE values from 0.74 to 0.73 for S1ASCAT and 0.74 to 0.71 for SCATSAR 020, SCATSAR 040, and SCATSAR 100 in the case of Lowland catchments. In the case of Alpine catchments, the median reduction in NSE values ranges from 0.81 to 0.77 for S1ASCAT, 0.81 to 0.79 for SCATSAR 020, 0.81 to 0.77 SCATSAR 040, and 0.81 to 0.78 for SCATSAR 100.

Comparing the results in Figure 4.1 and Table 4.1, indicates that assimilating the S1ASCAT soil moisture data in the calibration performs better to some extent in retrieving NSE values for Lowland catchments, while SCATSAR 020/040/100 soil moisture data perform slightly better in Alpine catchments.

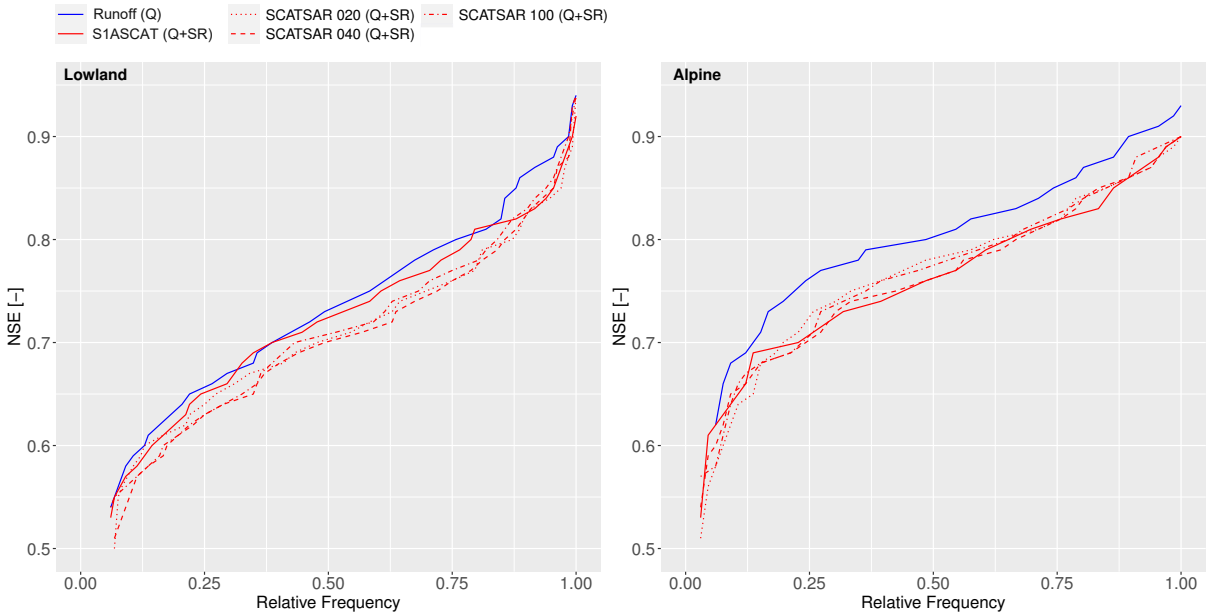

Fig. 4.1: Relative cumulative distribution functions of the Nash-Sutcliffe Efficiency (NSE) values, comparing the three SCATSAR variants with S1ASCAT and runoff only (Q) calibration variant in the 131 Lowland (left) and 65 Alpine (right) catchments during the calibration period from September 2014 to December 2020.

Kling-Gupta Efficiency (KGE)

From RCDFs in Figure 4.2, it can be seen that the calibration to runoff and soil moisture in the root-zone layer (Q+SR) using S1ASCAT product leads to no improvement nor decline in KGE values compared to calibration to runoff only (Q) for the Lowland catchments. In contrast, for SCATSAR 020/040/100, a decrease in KGE values is evident. Table 4.1 indicates median KGE values of 0.81 for both S1 (Q) and S1ASCAT (Q+SR) for the Lowland catchments, while it also shows a median decrease in KGE values from 0.81 to 0.79 for SCATSAR 020/040/100.

In the case of Alpine catchments, it can be inferred from Figure 4.2 that the calibration to runoff and soil moisture in the root-zone layer (Q+SR) generally causes a slight decline in KGE values in comparison to calibration to runoff only (Q). The median reductions in KGE varies from 0.85 to 0.82 for S1ASCAT, 0.85 to 0.81 for SCATSAR 020, 0.85 to 0.80 for SCATSAR 040, and 0.85 to 0.80 for SCATSAR 100 in the Alpine catchments, as listed in Table 4.1.

The results in Figure 4.2 and Table 4.1 reveal that assimilating S1ASCAT soil moisture data in the calibration slightly outperforms SCATSAR 020/040/100 in the retrieval of KGE values for both Lowland and Alpine catchments.

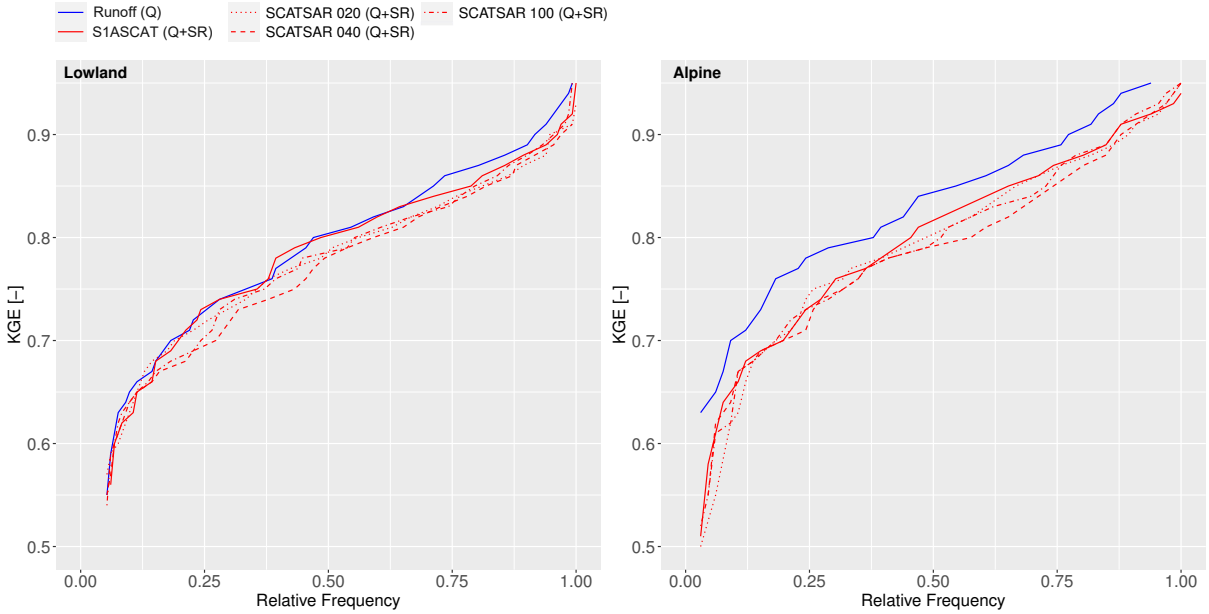

Fig. 4.2: Relative cumulative distribution functions of the Kling-Gupta Efficiency (KGE) values, comparing the three SCATSAR variants with S1ASCAT and runoff only (Q) calibration variant in the 131 Lowland (left) and 65 Alpine (right) catchments during the calibration period from September 2014 to December 2020.

Correlation Coefficient (r_{SR})

The CDFs in Figure 4.3 indicate that calibration to runoff and soil moisture in the root-zone layer (Q+SR) using S1ASCAT product significantly increases the values of the correlation coefficient (r_{SR}) between the simulated and measured soil moisture in root-zone both in Lowland and Alpine catchments, as compared to calibration to runoff only (Q). The SCATSAR 020/040/100 products exhibit an underwhelming performance in Lowland catchments, adversely affecting the calibration with a substantial reduction in r_{SR} values in comparison to runoff only (Q). However, in Alpine catchments, the SCATSAR products impact the calibration positively, resulting in increased r_{SR} values compared to runoff only (Q). Figure 4.4 provides a visual representation of these findings. Additionally, by comparing the r_{SR} values in Figure 4.4 with the forest and agricultural land cover percentage in Figure 3.3, it can be deducted that in the regions with extensive forest land cover, the r_{SR} values are lower, which may be attributed to the difficulties in retrieving satellite data in dense vegetation. In contrast, in high agricultural regions the r_{SR} show higher values.

In Lowland catchments, the median of the correlation coefficient (r_{SR}) increases from 0.58 to 0.69 for S1ASCAT. Contrary to this, the medians decrease from 0.58 to 0.32, 0.58 to 0.36, and 0.58 to 0.38 for SCATSAR 020, SCATSAR 040, and SCATSAR 100, respectively.

In Alpine catchments, the r_{SR} medians rise from 0.12 to 0.38, 0.12 to 0.24, 0.12 to 0.22, and 0.12 to 0.21 for S1ASCAT, SCATSAR 020, SCATSAR 040, and SCATSAR 100, respectively.

By comparing the findings in Figure 4.3, 4.4, and Table 4.1, it can be concluded that utilizing S1ASCAT soil moisture data in model calibration (Q+SR) overall provides much better r_{SR} values than SCATSAR 020/040/100 in the majority of Lowland and Alpine catchments.

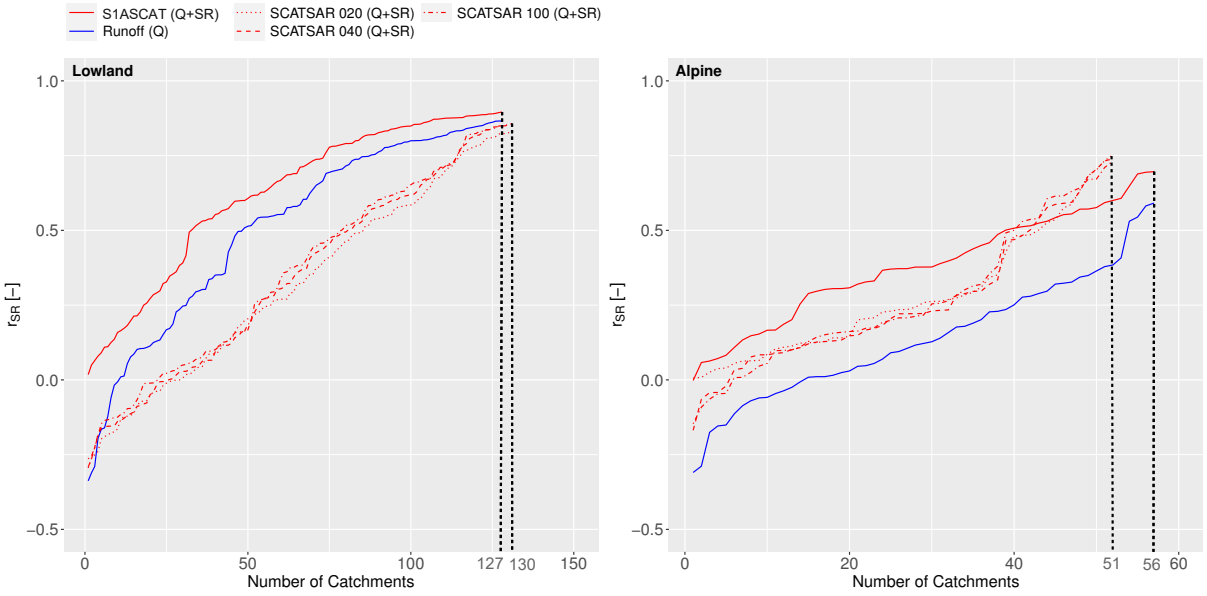

Fig. 4.3: Cumulative distribution functions of the correlation coefficients (r_{SR}) between the simulated and measured root soil moisture, comparing the three SCATSAR variants with S1ASCAT and runoff only (Q) calibration variant in the 131 Lowland (left) and 65 Alpine (right) catchments during the calibration period from September 2014 to December 2020. Missing r_{SR} values are excluded, but can be obtained from Table 7.21 to Table 7.25 in the Appendix.

Tab. 4.1: Medians of the values of the Nash-Sutcliffe Efficiency (NSE), the Kling-Gupta Efficiency (KGE), and the correlation coefficients (r_{SR}), comparing the three SCATSAR variants with S1ASCAT and runoff only (Q) calibration variant in the two groups of catchments (131 Lowland and 65 Alpine catchments) during the calibration period from September 2014 to December 2020.

Satellite Products	**NSE**		**KGE**		**r_{SR}**	
and Calibration Variant	**Low.**	**Alp.**	**Low.**	**Alp.**	**Low.**	**Alp.**
S1ASCAT (Q+SR)	0.73	0.77	0.81	0.82	0.69	0.38
SCATSAR 020 (Q+SR)	0.71	0.79	0.79	0.81	0.32	0.24
SCATSAR 040 (Q+SR)	0.71	0.77	0.79	0.80	0.36	0.22
SCATSAR 100 (Q+SR)	0.71	0.78	0.79	0.80	0.38	0.21
Runoff (Q)	0.74	0.81	0.81	0.85	0.58	0.12

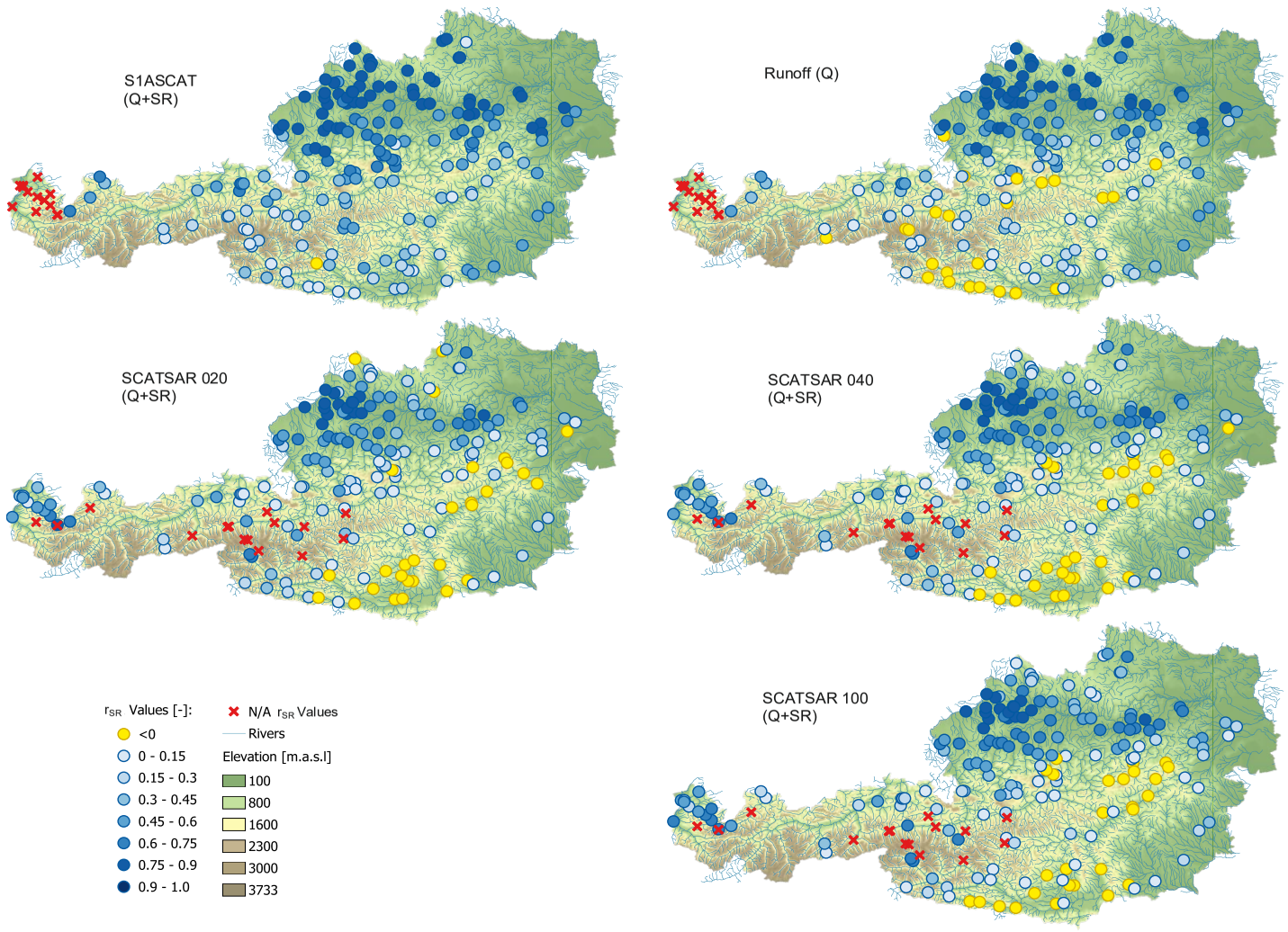

Fig. 4.4: Spatial analysis of the correlation coefficient (r_{SR}) values, comparing the three SCATSAR variants with S1ASCAT and runoff only (Q) calibration variant in the 196 catchments using the four different satellite products during the calibration period from September 2014 to December 2020.

4.2 Model Performance Comparison: S1ASCAT and SCATSAR Variants during Validation

In the validation process, the model was validated for the 196 catchments, consisting 131 Lowland catchments and 65 Alpine catchments. The validation process was conducted for runoff and soil moisture in the root-zone layer (Q+SR), utilizing four different satellite products (S1ASCAT, SCATSAR 020, SCATSAR 040, and SCATSAR 100) and the runoff only (Q). For both calibration variants, the best possible model parameters from the calibration period were applied, and the validation was carried out over the period from September 2009 to August 2014.

The relative cumulative distribution functions (RCDFs) of the Nash-Sutcliffe Efficiency (NSE) and the Kling-Gupta Efficiency (KGE) are compared in Figure 4.5 and 4.6, respectively.

The cumulative distribution functions (CDFs) of the correlation coefficient (r_{SR}) are depicted in Figure 4.3. Similar to 4.1, instead of relative frequency, the number of catchments was used on the x-axis of the CDFs to provide a more precise representation. The r_{SR} values, including the unavailable values, are illustrated in Figure 4.8, along with their corresponding geographic catchment locations. Additionally, a detailed listing of these missing values can be found in the Appendix, from Table 7.36 to Table 7.40.

The medians of the Nash-Sutcliffe Efficiency (NSE), the Kling-Gupta Efficiency (KGE), and the correlation coefficient (r_{SR}) values are summed up in Table 4.2.

Nash-Sutcliffe Efficiency (NSE)

Examining the RCDFs in Figure 4.5, the NSE values in model validation display a identical relation as in calibration, both in Lowland and Alpine catchments. This verifies the adequate efficiency of the model in simulating runoff. However, contrary to calibration, the NSE validation median values using S1ASCAT and SCATSAR 100 remain constant compared to runoff only (Q) in Lowland catchments. Moreover, SCATSAR 020 and SCATSAR 040 show minor improvement in NSE values. In Alpine catchments, all the satellite products result in slight median decreases.

Table 4.2 confirms these observations, indicating unchanged NSE medians of 0.67 for S1ASCAT and SCATSAR 100, and minor median increases from 0.67 to 0.68 for SCATSAR 020 and SCATSAR 040 in the case of Lowland catchments. In the case of Alpine catchments, the median reductions in NSE ranges from 0.77 to 0.76 for S1ASCAT and from 0.77 to 0.75 for SCATSAR 020, SCATSAR 040, and SCATSAR 100.

A comparison of the results in Figure 4.5 and Table 4.2, indicates that S1ASCAT and SCATSAR 020/040/100 perform nearly equal in model validation, retrieving NSE values for both Lowland and Alpine catchments.

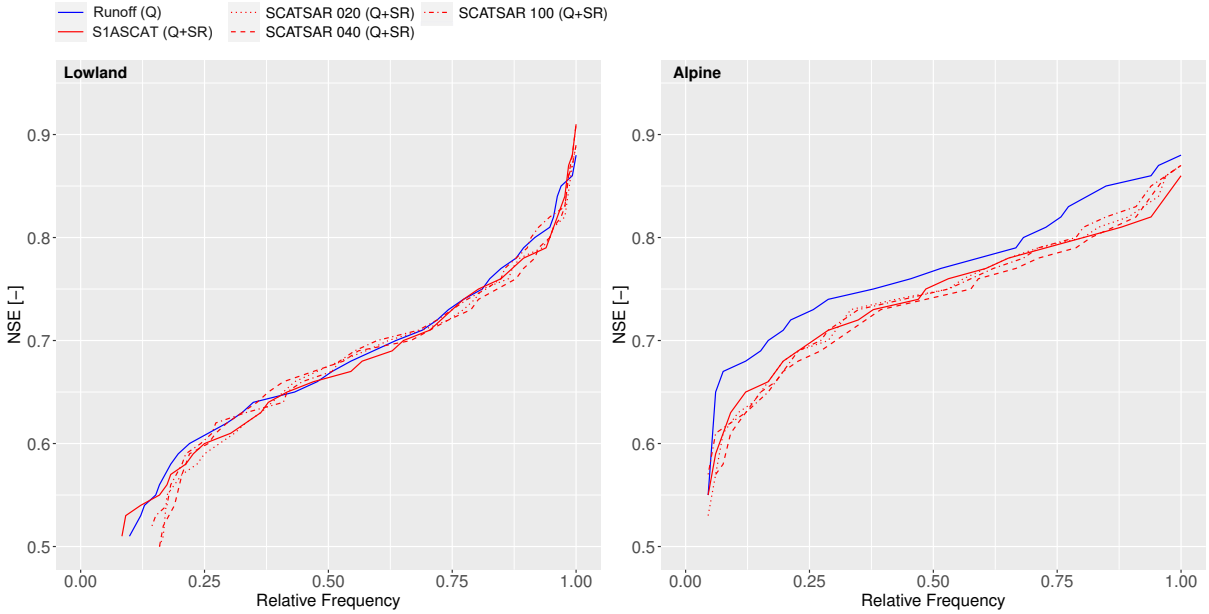

Fig. 4.5: Cumulative distribution functions of the Nash-Sutcliffe Efficiency (NSE) values, comparing the three SCATSAR variants with S1ASCAT and runoff only (Q) calibration variant in the the 131 Lowland (left) and 65 Alpine (right) catchments during the validation period from September 2009 to August 2014.

Kling-Gupta Efficiency (KGE)

Examining the RCDFs in Figure 4.6, the validated KGE values exhibit a similar behavior to calibration in both Lowland and Alpine catchments, supporting the conclusion regarding the model's efficiency in simulating runoff. However, the KGE values in the validation of the model using S1ASCAT and SCATSAR 100 show slight median increases in Lowland catchments, while SCATSAR 020 and SCATSAR 040 have slightly decreased KGE medians compared to runoff only (Q). In Alpine catchments, a slight decline in KGE medians in comparison to calibration to runoff only (Q) can be witnessed for all of the satellite products, with an exception of SCATSAR 020, which remains constant.

These finding are supported by Table 4.2, which shows a minor increase in KGE medians from of 0.77 to 0.78 for S1ASCAT and SCATSAR 100, and a minor decrease in KGE medians from 0.77 to 0.76 for SCATSAR 020 and SCATSAR 040 in the Lowland catchments. In the case of Alpine catchments, the reduction in KGE medians ranges from 0.81 to 0.79 for S1ASCAT and SCATSAR 100, from 0.81 to 0.78 for SCATSAR 040, and for SCATSAR 020, the median remains constant at 0.81, as presented in Table 4.2.

The results in Figure 4.6 and Table 4.2 demonstrate that S1ASCAT and SCATSAR 020/040/100 perform similarly in model validation, retrieving KGE values for both Lowland and Alpine catchments.

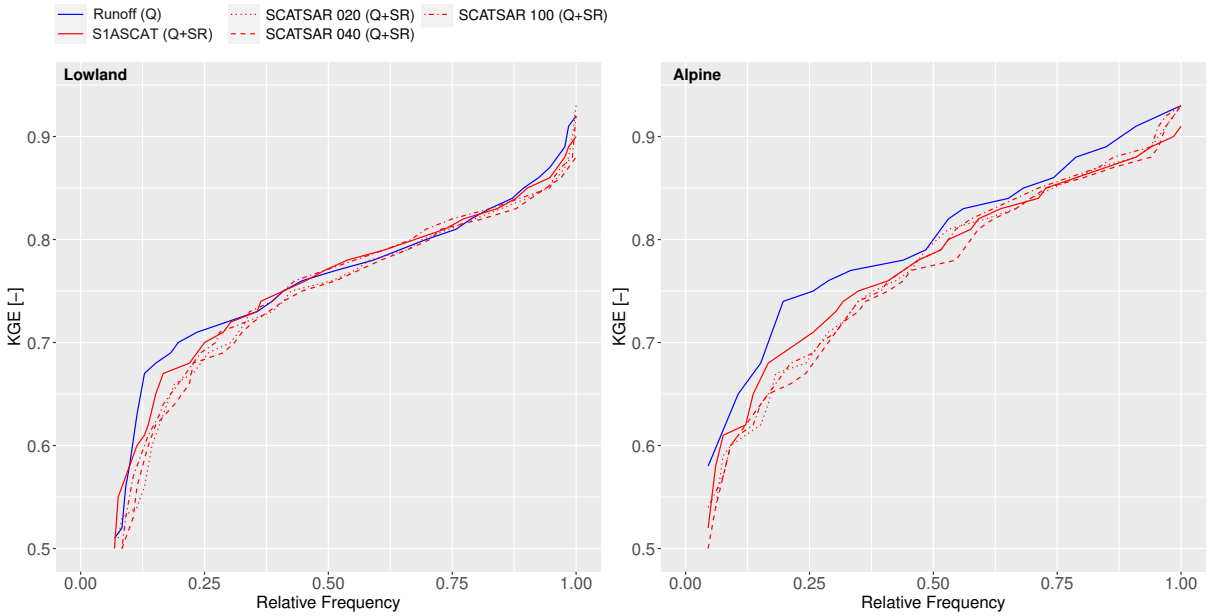

Fig. 4.6: Cumulative distribution functions of the Kling-Gupta Efficiency (KGE) values, comparing the three SCATSAR variants with S1ASCAT and runoff only (Q) calibration variant in the 131 Lowland (left) and 65 Alpine (right) catchments during the validation period from September 2009 to August 2014.

Correlation Coefficient (r_{SR})

The CDFs in Figure 4.7 demonstrate that similar to model calibration, the validation of the model with parameters calibrated to runoff and soil moisture in the root-zone layer (Q+SR) using S1ASCAT product significantly increases the values of the correlation coefficient (r_{SR}) both in Lowland and Alpine catchments, as compared to calibration to runoff only (Q). This confirms the model's efficiency in simulating soil moisture. Identical to calibration, the SCATSAR 020/040/100 products exhibit an underwhelming performance in Lowland catchments, negatively impacting the validation with a substantial reduction in r_{SR} values. Contrary to calibration, in Alpine catchments, The SCATSAR products negatively impact the validation, resulting in decreased r_{SR} values compared to runoff only (Q). Figure 4.8 visually illustrates these findings. Additionally, by comparing the r_{SR} values in Figure 4.8 with the forest and agricultural land cover percentage in Figure 3.3, it can be deducted that in the regions with extensive forest land cover, the r_{SR} values for S1ASCAT are lower, which may be attributed to the difficulties in retrieving satellite data in dense vegetation, while, in contrast, in high agricultural regions the r_{SR} show higher values. For SCATSAR products, it can be seen that most catchments have either negative, low, or N/A r_{SR} values. This might be due to the lower quality and unavailability of SCATSAR soil moisture data retrievals in the corresponding catchments. Therefore, it's advisable to closely examine the influence of SCATSAR products on calibrating and validating hydrological models for simulating soil moisture in further studies.

In Lowland catchments, the median of the correlation coefficient (r_{SR}) increases from 0.61 to 0.68 for S1ASCAT. Contrary to this, the medians decrease from 0.61 to -0.22, 0.61 to -0.21, and 0.61 to -0.21 for SCATSAR 020, SCATSAR 040, and SCATSAR 100, respectively.

In Alpine catchments, the r_{SR} median increases from 0.30 to 0.46 for S1ASCAT, while the medians decrease from 0.30 to 0.0, 0.30 to -0.06, and 0.30 to -0.03 for SCATSAR 020, SCATSAR 040, and SCATSAR 100, respectively.

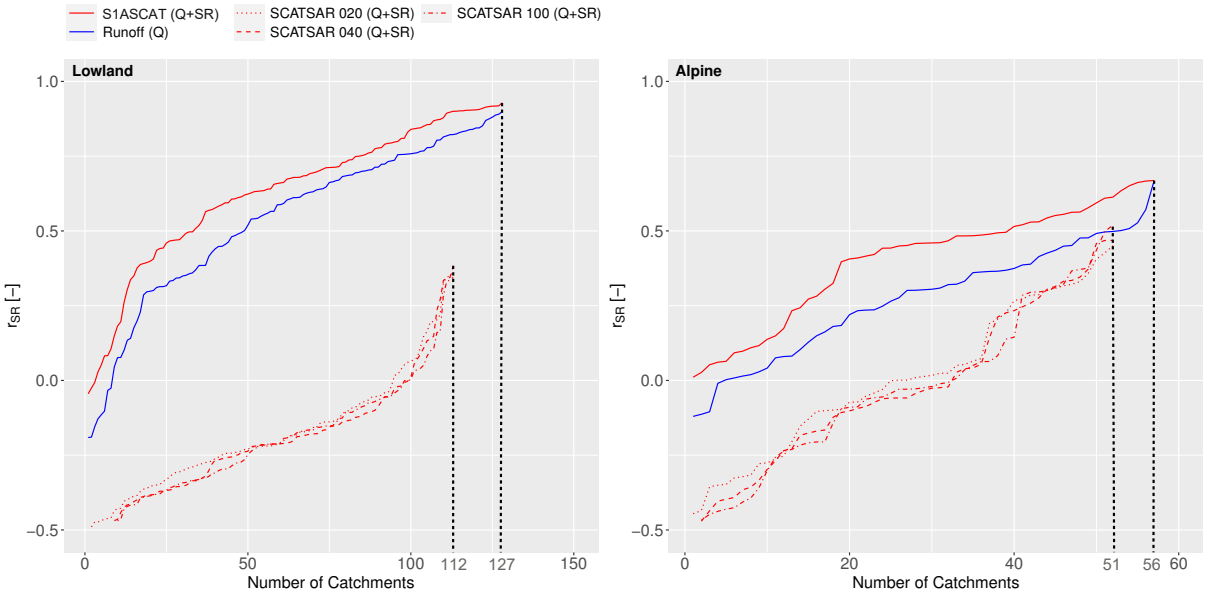

Fig. 4.7: Cumulative distribution functions of Correlation Coefficients (r_{SR}) between the simulated and measured root soil moisture, comparing the three SCATSAR variants with S1ASCAT and runoff only (Q) calibration variant in the 131 Lowland (left) and 65 Alpine (right) catchments during the validation period from September 2009 to August 2014.

Comparing the results in Figure 4.7 and Table 4.2 leads to the conclusion that utilizing S1ASCAT soil moisture data in model validation (Q+SR) generally provides significantly improved r_{SR} values than SCATSAR 020/040/100 in the majority of Lowland and Alpine catchments.

Tab. 4.2: Medians of the values of the Nash-Sutcliffe Efficiency (NSE), the Kling-Gupta Efficiency (KGE), and the correlation coefficients (r_{SR}), comparing the three SCATSAR variants with S1ASCAT and runoff only (Q) calibration variant in the two groups of catchments (131 Lowland and 65 Alpine catchments) during the validation period from September 2009 to August 2014.

Satellite Products	**NSE**		**KGE**		**r_{SR}**	
and Calibration Variant	**Low.**	**Alp.**	**Low.**	**Alp.**	**Low.**	**Alp.**
S1ASCAT (Q+SR)	0.67	0.76	0.78	0.79	0.68	0.46
SCATSAR 020 (Q+SR)	0.68	0.75	0.76	0.81	-0.22	0.0
SCATSAR 040 (Q+SR)	0.68	0.75	0.76	0.78	-0.21	-0.06
SCATSAR 100 (Q+SR)	0.67	0.75	0.78	0.79	-0.21	-0.03
Runoff (Q)	0.67	0.77	0.77	0.81	0.61	0.30

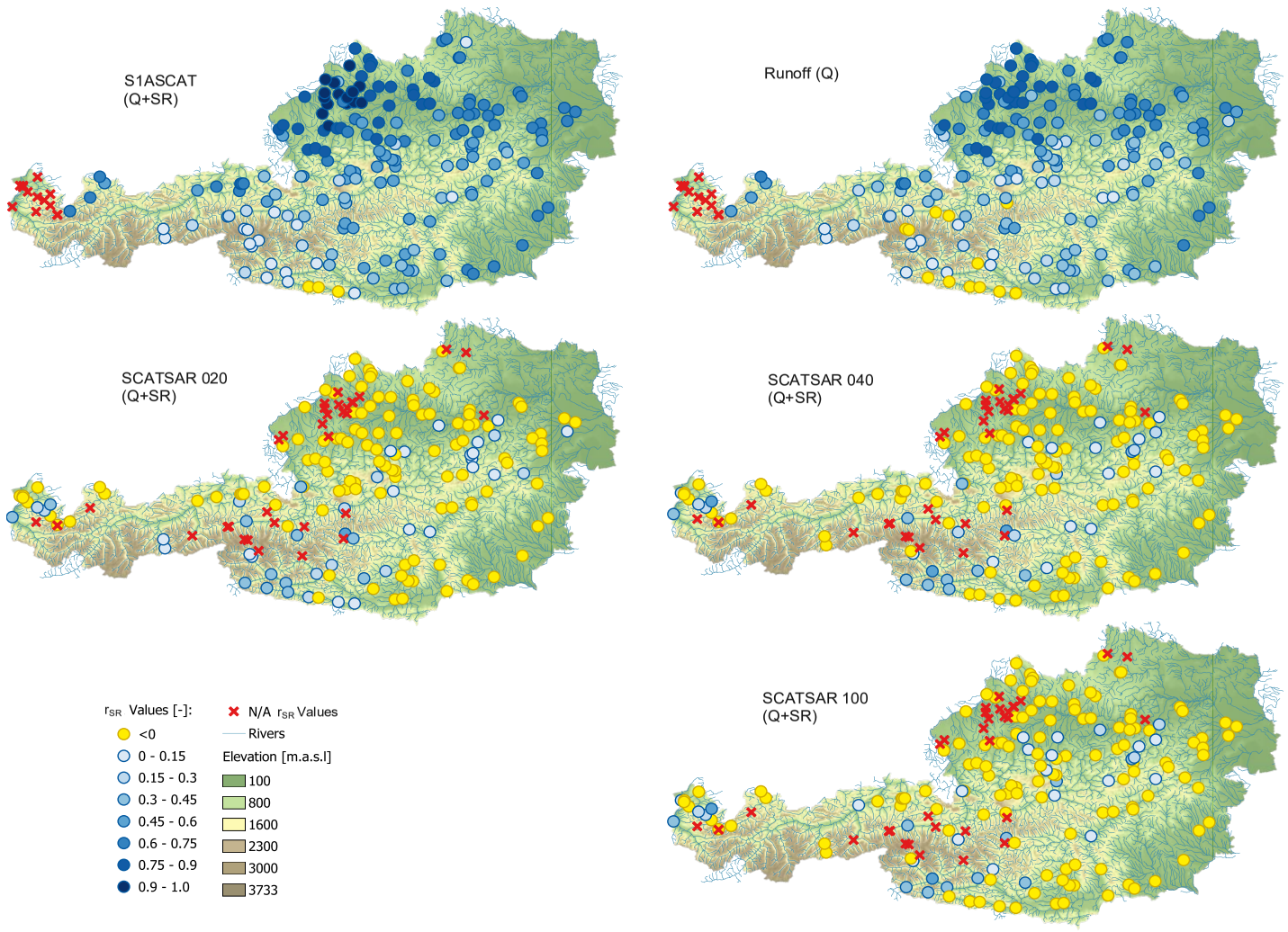

Fig. 4.8: Spatial analysis of the correlation coefficient (r_{SR}) values, comparing the three SCATSAR variants with S1ASCAT and runoff only (Q) calibration variant in the 196 catchments using the four different satellite products during the validation period from September 2009 to August 2014.

Tab. 4.3: The number and percentage of the 131 Lowland and 65 Alpine catchments that have shown improvement in correlation coefficient r_{SR} using the three SCATSAR variants and S1ASCAT soil moisture data versus the runoff only (Q) calibration variant during the calibration period. The number of catchments with Not-Available data are also listed. These were omitted from the statistics.

Satellite Products	r_{SR}					
	Lowland			Alpine		
	Num.	%	N/A	Num.	%	N/A
S1ASCAT (Q+SR)	125	98.4	4	53	94.6	9
SCATSAR 020 (Q+SR)	26	20.6	5	24	54.5	21
SCATSAR 040 (Q+SR)	29	23.0	5	22	50.0	21
SCATSAR 100 (Q+SR)	35	27.8	4	21	47.7	21

4.3 Improvement of Multiple-Objective Calibrations to Calibration Using Runoff Only

4.3.1 Improvement of the Soil Moisture Model Efficiency in Calibration

As discussed in Section 4.1, assimilating S1ASCAT soil moisture data in model calibration generally indicated enhanced correlation coefficient (r_{SR}) values, compared to the simulated soil moisture by the model calibrated to runoff only (Q), while SCATSAR products negatively impacted the calibration in most of the cases. Therefore, Table 4.3 were provided to establish a comparison between the improved r_{SR} values calibrated to runoff and root-zone soil moisture (Q+SR) using S1ASCAT and SCATSAR products compared to runoff only (Q) for both Lowland and Alpine catchments. Improvements were observed in 125 (98.4%), 26 (20.6%), 29 (23.0%), and 35 (27.8%), out of 131 Lowland catchments (catchments with N/A values were excluded from the statistics) for S1ASCAT, SCATSAR 020, SCATSAR 040, and SCATSAR 100, respectively, compared to runoff only (Q) calibration variant. In Alpine catchments, enhancements were observed in 53 (94.6%), 24 (54.5%), 22 (50.0%), and 21 (47.7%) out of a total of 65 Alpine catchments (catchments with N/A values were excluded from the statistics) for S1ASCAT, SCATSAR 020, SCATSAR 040, and SCATSAR 100, respectively, compared to runoff only (Q) calibration variant. Assessing the results brings up the conclusion that the S1ASCAT product led to slightly better improvements in Lowland catchments than in Alpine catchments. In the case of SCATSAR, a large number of Alpine catchments exhibit Not-Available (N/A) r_{SR} values, making it challenging to make an exact statement, however, considering only the available data indicates better improvements in Alpine catchments than in Lowland catchments.

As mentioned in in Section 4.1, the S1ASCAT soil moisture data demonstrated greater effectiveness in model calibration for simulating soil moisture, compared to the SCATSAR products and the simulated soil moisture by the model calibrated to runoff only (Q). Therefore, the correlation coefficient (r_{SR}) values of S1ASCAT have been plotted against SCATSAR 020, SCATSAR 040, SCATSAR 100, and runoff only (Q) in Figure 4.9 to assess the calibration improvement using the S1ASCAT product compared to the other variations. In the scatter charts, Figures 4.9a and 4.9b, if the black dots are positioned below the 1:1 red dashed lines, it signifies an improvement in the corresponding catchments using S1ASCAT in the calibration process in relation to the other variants.

Tab. 4.4: The number and percentage of the 131 Lowland and 65 Alpine catchments that have shown improvement in correlation coefficient (r_{SR}) values using S1ASCAT soil moisture data versus the three SCATSAR variants and the runoff only (Q) calibration variant during the calibration period. The number of catchments with Not-Available data are also listed. These were omitted from the statistics.

Satellite Products	**S1ASCAT (Q+SR)**					
	Lowland			**Alpine**		
and Calibration Variant	**Num.**	**%**	**N/A**	**Num.**	**%**	**N/A**
SCATSAR 020 (Q+SR)	119	94.4	5	34	77.3	21
SCATSAR 040 (Q+SR)	120	95.2	5	41	93.2	21
SCATSAR 100 (Q+SR)	121	96	5	41	93.2	21
Runoff (Q)	125	98.4	4	53	94.6	9

Based on the results presented in Figure 4.9a and Table 4.4 can be inferred that a significant percentage of Lowland catchments benefited from using S1ASCAT product in retrieving the correlation coefficients (r_{SR}). Improvements was observed in 119 (94.4%), 120 (95.2%), 121 (96%), and 125 (98.4%), out of 131 Lowland catchments (excluding catchments with N/A values) when compared to SCATSAR 020, SCATSAR 040, SCATSAR 100, and runoff only (Q) calibration variant, respectively.

According to Figure 4.9b and Table 4.4 can be concluded that, Similar to Lowland, but to a lesser extend, 34 (77.3%), 41 (93.2%), 41 (93.2%), and 53 (94.6%) out of 65 Alpine catchments (excluding catchments with N/A values) benefited from S1ASCAT in comparison to SCATSAR 020, SCATSAR 040, SCATSAR 100, and runoff only (Q), respectively.

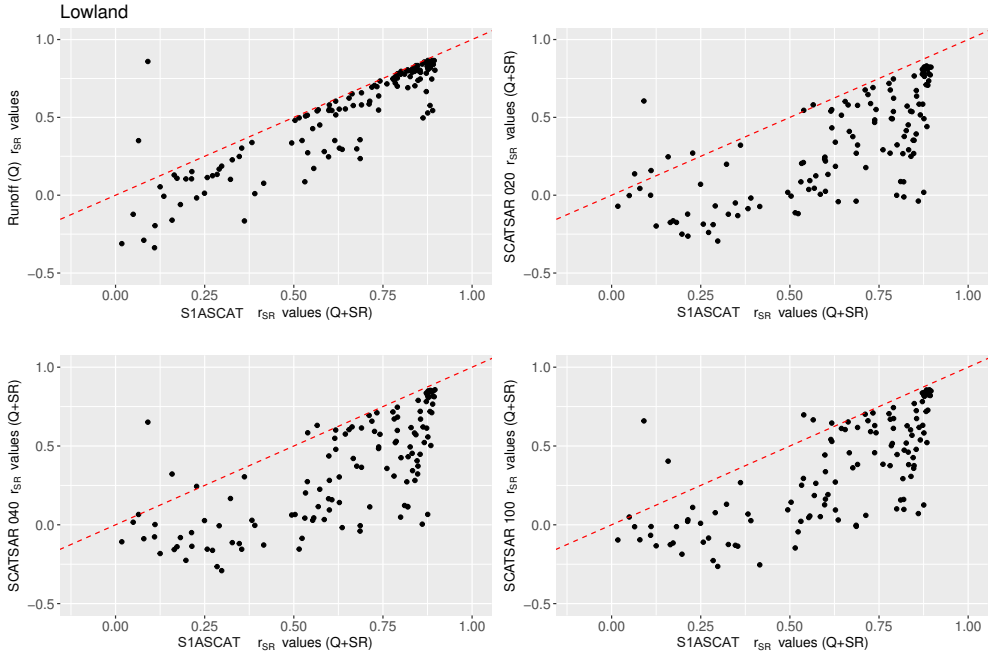

(a) The correlation coefficients (r_{SR}) of the runoff and soil moisture in the root-zone layer (Q+SR) calibration variant, using S1ASCAT product on the x-axis and SCATSAR 020, SCATSAR 040, SCATSAR 100, and the simulated soil moisture for the root-zone calibrated to runoff only (Q) on the y-axis, in the 131 Lowland catchments during the calibration period from September 2014 to December 2020.

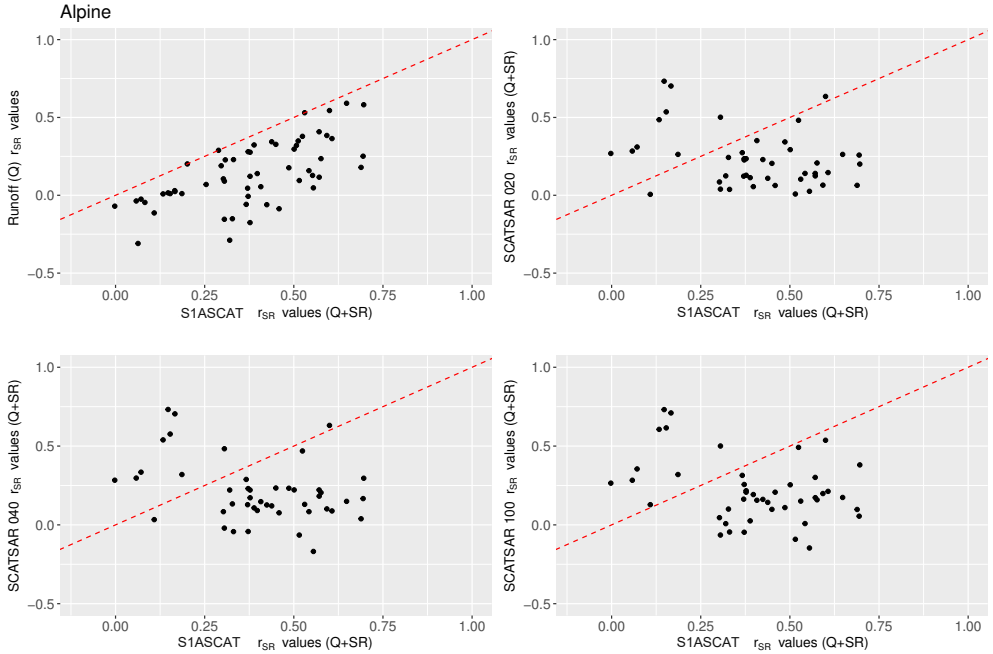

(b) The correlation coefficients (r_{SR}) of the runoff and soil moisture in the root-zone layer (Q+SR) calibration variant, using S1ASCAT product on the x-axis and SCATSAR 020, SCATSAR 040, SCATSAR 100, and the simulated soil moisture for the root-zone calibrated to runoff only (Q) on the y-axis, in the 65 Alpine catchments during the calibration period from September 2014 to December 2020.

Fig. 4.9: The correlation coefficients (r_{SR}) scatter charts for the calibration period.

Tab. 4.5: The number and percentage of the 131 Lowland and 65 Alpine catchments that have shown improvement in NSE and KGE values using the three SCATSAR variants and S1ASCAT soil moisture data versus the runoff only (Q) calibration variant during the validation period.

Satellite Products	NSE				KGE			
	Lowland		Alpine		Lowland		Alpine	
	Num.	%	Num.	%	Num.	%	Num.	%
S1ASCAT (Q+SR)	47	35.9	13	20.0	51	38.9	17	26.2
SCATSAR 020 (Q+SR)	45	34.4	14	21.5	42	32.1	14	21.5
SCATSAR 040 (Q+SR)	53	40.5	13	20.0	43	32.8	16	24.6
SCATSAR 100 (Q+SR)	58	44.3	16	24.6	52	39.7	15	23.1

4.3.2 Improvement of the Runoff Model Efficiency in Validation

As mentioned in Section 4.2, the medians of the NSE and KGE values did not generally improve with the parameters calibrated to runoff and soil moisture in the root zone (Q+SR). However, in Lowland catchments, minor enhancements were observed in a few cases. Table 4.5 provides more detail regarding the individual catchments that indicated improvements in NSE and KGE values during the validation period.

The NSE values increased in 47 (35.9%), 45 (34.4%), 53 (40.5%), and 58 (44.3%) out of 131 Lowland catchments for S1ASCAT, SCATSAR 020, SCATSAR 040, and SCATSAR 100, respectively, compared to runoff only (Q) calibration variant. In Alpine catchments, enhancements were observed in 13 (20.0%), 14 (21.5%), 13 (20.0%), and 16 (24.6%) out of a total of 65 Alpine catchments for S1ASCAT, SCATSAR 020, SCATSAR 040, and SCATSAR 100, respectively.

The KGE values increased in 51 (38.9%), 42 (32.1%), 43 (32.8%), and 52 (39.7%) out of 131 Lowland catchments for S1ASCAT, SCATSAR 020, SCATSAR 040, and SCATSAR 100, respectively, compared to runoff only (Q) calibration variant. In Alpine catchments, enhancements were observed in 17 (26.2%), 14 (21.5%), 16 (24.6%), and 15 (23.1%) out of a total of 65 Alpine catchments for S1ASCAT, SCATSAR 020, SCATSAR 040, and SCATSAR 100, respectively.

4.3.3 Improvement of the Soil Moisture Model Efficiency in Validation

As discussed in Section 4.2, validating the model using parameters calibrated to S1ASCAT soil moisture data commonly indicated enhanced model efficiency in simulating soil moisture, compared to the simulated soil moisture by the model calibrated to runoff only (Q), while SCATSAR products adversely affected the validation in most of the cases. Therefore, Table 4.6 were provided to establish a comparison between the improved r_{SR} values calibrated to runoff and root-zone soil moisture (Q+SR) using S1ASCAT and SCATSAR products compared runoff only (Q) for both Lowland and Alpine catchments. Improvements were observed in 119 (91.3%), 10 (9.3%), 5 (4.6%), and 4 (3.7%) out of 131 Lowland catchments (catchments with N/A values were excluded from the statistics) for S1ASCAT, SCATSAR 020, SCATSAR 040, and SCATSAR 100, respectively, compared to runoff only (Q) calibration variant. In Alpine catchments, enhancements were observed in 49 (87.5%), 9 (20.5%), 6 (13.6%), and 6 (13.6%) out of a total of 65 Alpine catchments (catchments with N/A values were excluded from the statistics) for S1ASCAT, SCATSAR 020, SCATSAR 040, and SCATSAR 100, respectively, compared to runoff only (Q) calibration variant. Similar to calibration, validation results shows that the

Tab. 4.6: The number and percentage of the 131 Lowland and 65 Alpine catchments that have shown improvement in correlation coefficient r_{SR} values using the three SCATSAR variants and S1ASCAT versus the runoff only (Q) calibration variant during the validation period. The number of catchments with Not-Available data are also listed. These were omitted from the statistics.

Satellite Products	r_{SR}					
	Lowland			Alpine		
	Num.	%	N/A	Num.	%	N/A
S1ASCAT (Q+SR)	116	91.3	4	49	87.5	9
SCATSAR 020 (Q+SR)	10	9.3	23	9	20.5	21
SCATSAR 040 (Q+SR)	5	4.6	23	6	13.6	21
SCATSAR 100 (Q+SR)	4	3.7	23	6	13.6	21

S1ASCAT product again led to slightly better improvements in Lowland catchments than in Alpine catchments. In the case of SCATSAR, similar to calibration, a significant number of Alpine catchments exhibit Not-Available (N/A) r_{SR} values, making it challenging to make a precise statement. Nonetheless, focusing on the available data indicates better improvements in Alpine catchments compared to Lowland catchments.

As also mentioned in Section 4.2, the S1ASCAT soil moisture data proved to be more effective in model validation for simulating soil moisture, compared to the SCATSAR products and the simulated soil moisture by the model calibrated to runoff only (Q). Similar to calibration, for the validation period, the correlation coefficient (r_{SR}) values of S1ASCAT have been plotted against SCATSAR 020, SCATSAR 040, SCATSAR 100, and runoff only (Q) in Figure 4.10 to assess the validation improvement using the S1ASCAT product compared to the other variations. In the scatter charts, Figures 4.10a and 4.10b, if the black dots are positioned below the 1:1 red dashed lines, it signifies an improvement in the corresponding catchments using S1ASCAT in the validation process in relation to the other variants.

Based on the results presented in Figure 4.10a and Table 4.7, it can be deduced that a substantial percentage of Lowland catchments benefited from using S1ASCAT product in retrieving the correlation coefficients (r_{SR}). The improvement was observed in 102 (94.4%), 105 (97.2%), 106 (98.2%), and 116 (91.3%), out of 131 Lowland catchments (excluding catchments with N/A values) when compared to SCATSAR 020, SCATSAR 040, SCATSAR 100, and runoff only (Q), respectively.

According to the results presented in Figure 4.10b and Table 4.7, 38 (86.4%), 39 (88.6%), 40 (90.9%), and 49 (87.5%) out of 65 Alpine catchments (excluding catchments with N/A values) benefited from S1ASCAT in comparison to SCATSAR 020, SCATSAR 040, SCATSAR 100, and runoff only (Q), respectively.

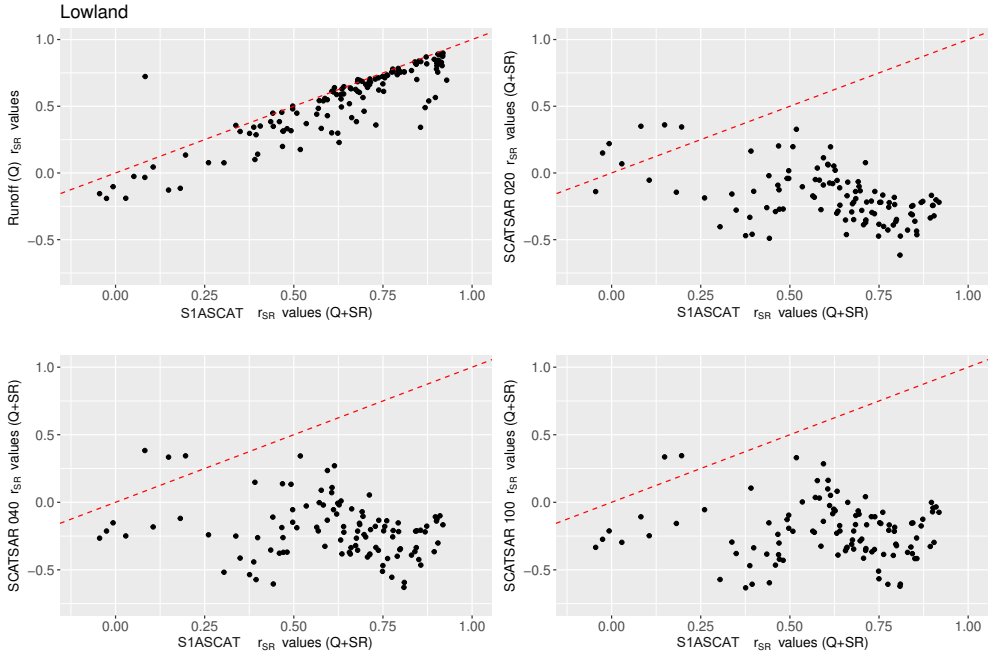

(a) The correlation coefficients (r_{SR}) of the runoff and soil moisture in the root-zone layer (Q+SR) calibration variant, using S1ASCAT product on the x-axis and SCATSAR 020, SCATSAR 040, SCATSAR 100, and the simulated soil moisture for the root-zone calibrated to runoff only (Q) on the y-axis, in the 131 Lowland catchments during the validation period from September 2009 to August 2014.

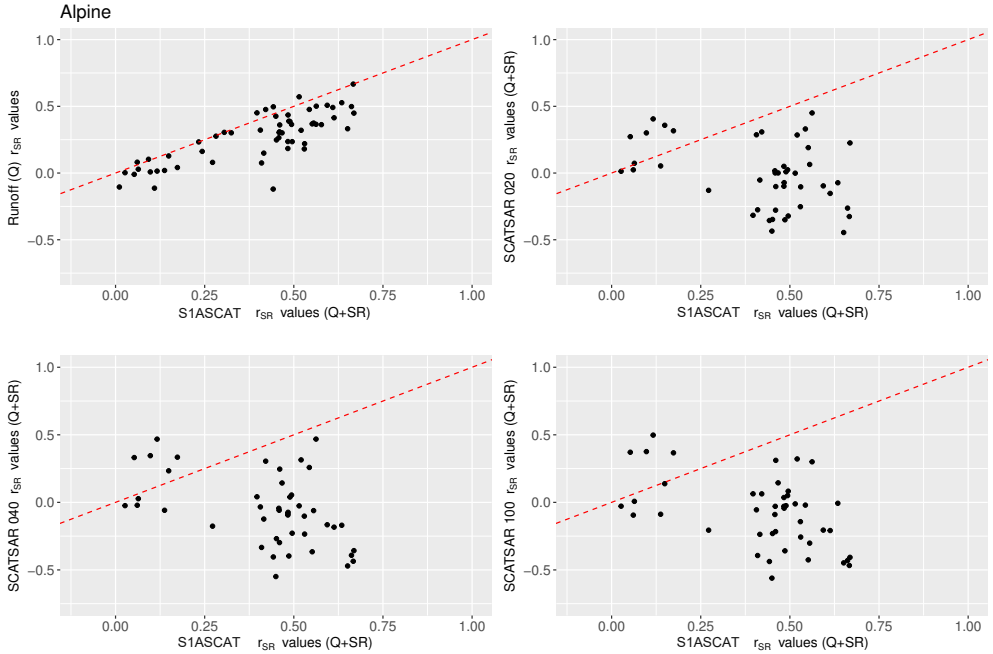

(b) The correlation coefficients (r_{SR}) of the runoff and soil moisture in the root-zone layer (Q+SR) calibration variant, using S1ASCAT product on the x-axis and SCATSAR 020, SCATSAR 040, SCATSAR 100, and the simulated soil moisture for the root-zone calibrated to runoff only (Q) on the y-axis, in the 65 Alpine catchments during the validation period from September 2009 to August 2014.

Fig. 4.10: The correlation coefficients (r_{SR}) scatter charts for the validation period.

Tab. 4.7: The number and percentage of the 131 Lowland and 65 Alpine catchments that have shown improvement in correlation coefficient (r_{SR}) values using S1ASCAT soil moisture data versus the three SCATSAR variants and the runoff only (Q) calibration variant during the validation period. The number of catchments with Not-Available data are also listed. These were omitted from the statistics.

Satellite Products	**S1ASCAT (Q+SR)**					
	Lowland			**Alpine**		
and Calibration Variant	**Num.**	**%**	**N/A**	**Num.**	**%**	**N/A**
SCATSAR 020 (Q+SR)	102	94.4	23	38	86.4	21
SCATSAR 040 (Q+SR)	105	97.2	23	39	88.6	21
SCATSAR 100 (Q+SR)	106	98.2	23	40	90.9	21
Runoff (Q)	116	91.3	4	49	87.5	9

Chapter 5

Discussion

5.1 Runoff Model Performance of Different Satellite Soil Moisture Products

In the calibration, evaluating the runoff efficiency criteria, i.e., the Nash-Sutcliffe Efficiency Coefficient (NSE) and Kling-Gupta Efficiency (KGE) values, both the calibration for runoff and soil moisture in the root-zone layer (Q+SR) and runoff-only (Q) demonstrated better results for Alpine catchments compared to Lowland catchments. This conclusion was also conveyed by Kubáň et al. (2021); however, they employed a combination of the Nash–Sutcliffe efficiency coefficient (NSE) and the logarithmic NSE for the estimation of the runoff model efficiency, defined as $RME = (NSE + logNSE)/2$. Additionally, they assumed that the discrepancy in the runoff model efficiency between Alpine and Lowland catchments may be attributed to the better functionality of the TUW_dual model in catchments with higher altitudes and higher surface and subsurface flow patterns.

Generally, the assimilation of satellite soil moisture data into the model calibration led to an overall slight decline in simulating runoff in both Alpine and Lowland catchments. These findings are consistent with studies conducted by Parajka, Naeimi, Blöschl, Wagner, et al. (2006) and Kubáň et al. (2021). However, Parajka, Naeimi, Blöschl, Wagner, et al. (2006) utilized European Remote Sensing (ERS) products, while Kubáň et al. (2021) used S1ASCAT in their calibrations. In this thesis, S1ASCAT and SCATSAR products were employed, with the former causing less degradation in the calibration compared to the latter.

In the model validation, again the NSE and KGE values for both calibration variants (Q+SR and Q) displayed better results for Alpine catchments compared to Lowland catchments, consistent with the findings of Kubáň et al. (2021). This confirms the adequate efficiency of the model in simulating runoff. However, contrary to calibration, in the validation process, SCATSAR 020 and SCATSAR 040 products resulted in a minor NSE median increase from 0.67 to 0.68, while S1ASCAT and SCATSAR 100 did not show significant changes in the NSE values compared to runoff only (Q) in Lowland catchments. In Alpine catchments, similar to calibration, the median NSE values for S1ASCAT and SCATSAR products slightly declined, juxtaposed with the values for runoff only (Q). According to Table 4.5, in the validation period, 45 (34.4%) to 58 (44.3%) out of the 131 Lowland catchments, and 13 (34.4%) to 16 (44.3%) out of the 65 Alpine catchments indicated improved NSE values . The KGE values in the validation of the model using S1ASCAT and SCATSAR 100 showed slight median increases in Lowland catchments, while SCATSAR 020 and SCATSAR 040 caused a minor decline compared to runoff only (Q) in Lowland catchments. In Alpine catchments, all satellite products showed a slight decline in KGE medians compared to the calibration with runoff only (Q), except for SCATSAR 020, which remained constant. According to Table 4.5, in the validation period, 42 (32.1%) to 52 (39.7%) out of the 131 Lowland catchments, and 14 (21.5%) to 17 (26.2%) out of the 65 Alpine catchments indicated improved NSE values .

In general, it can be concluded that model validation with parameters calibrated to runoff and soil moisture in the root-zone layer (Q+SR) results in either minor or no changes in runoff model efficiency compared to runoff only (Q), as indicated in studies by Y. Li et al. (2018) and Kubáň et al. (2021). Hence, it is recommended to conduct further investigations into the effectiveness of S1ASCAT and SCATSAR soil moisture data in the calibration and validation of hydrological models in simulating runoff, given its significant implications for water resources management.

5.2 Soil Moisture Performance of Different Satellite Soil Moisture Products

In the calibration process, the evaluation of soil moisture efficiency revealed notable patterns. The assimilation of S1ASCAT products into the calibration significantly enhanced the correlation coefficient (r_{SR}) values in both Lowland and Alpine catchments compared to runoff only (Q). Conversely, the use of SCATSAR products led to a decline in r_{SR} values in Lowland catchments but an increase in Alpine catchments.

Comparing the calibrations for runoff and soil moisture in the root-zone layer (Q+SR) using S1ASCAT products with runoff only (Q), it became evident that Q+SR demonstrated significantly better results for Lowland catchments compared to Alpine catchments. This could be attributed to the higher accuracy of soil moisture retrievals from S1ASCAT in Lowland areas. These results are in agreement with findings from studies by Tong et al. (2021), Kubáň et al. (2021), and Parajka, Naeimi, Blöschl, and Komma (2009), with the latter using ERS satellite data. For SCATSAR products, the median of r_{SR} values were higher in Lowland than in Alpine catchments, probably due the better quality of SCATSAR satellite data in Lowlands.

Furthermore, by comparing the r_{SR} values (refer Figure 4.4 and 3.3), we came to the conclusion that in regions with a high percentage of forest land cover, the r_{SR} values were lower. This could be attributed to the difficulties in retrieving satellite data in dense vegetation. Conversely, the r_{SR} showed higher values in high agricultural regions. These findings are reported in studies by Tong et al. (2021) and Kubáň et al. (2021) as well.

In the validation process, the assessment of soil moisture efficiency again revealed that S1ASCAT products significantly increased the correlation coefficient (r_{SR}) values in both Lowland and Alpine catchments compared to runoff only (Q). However, the use of SCATSAR products led to a considerable decrease in r_{SR} values in both Lowland and Alpine catchments, provoking the question whether SCATSAR products could be useful for calibrating and validating the TUW_dual model in simulating soil moisture. These findings are confirmed in Figure 4.8.

To provide additional information on the performance of SCATSAR products, the individual catchments which benefited most in soil moisture efficiency during the calibration and validation, respective to the T-value of SCATSAR data, are depicted in Figure 5.1. It can be seen that SCATSAR 020 demonstrated better performance in Alpine catchments, while SCATSAR 100 showed better performance in Lowland catchments during the calibration. In the validation period, not only did SCATSAR 020 indicate better performance in Alpine catchments, but it also exhibited improved results in some Lowland catchments. In contrast, SCATSAR 040 and SCATSAR 100 showed less effectiveness.

The results of this thesis are overall in agreement with those presented in the studies by Kubáň et al. (2021), Tong et al. (2021), and Parajka, Naeimi, Blöschl, and Komma (2009). However in Kubáň et al. (2021), the S1ASCAT Soil Water Index for both root-zone and surface soil layer, incorporating four objective functions (runoff only (Q), runoff and soil moisture in the root-zone layer (Q+SR), runoff and soil moisture in the surface layer (Q+SS), and runoff and soil moisture both in the root-zone and surface layers (Q+SR+SS)) for calibration and validation of the

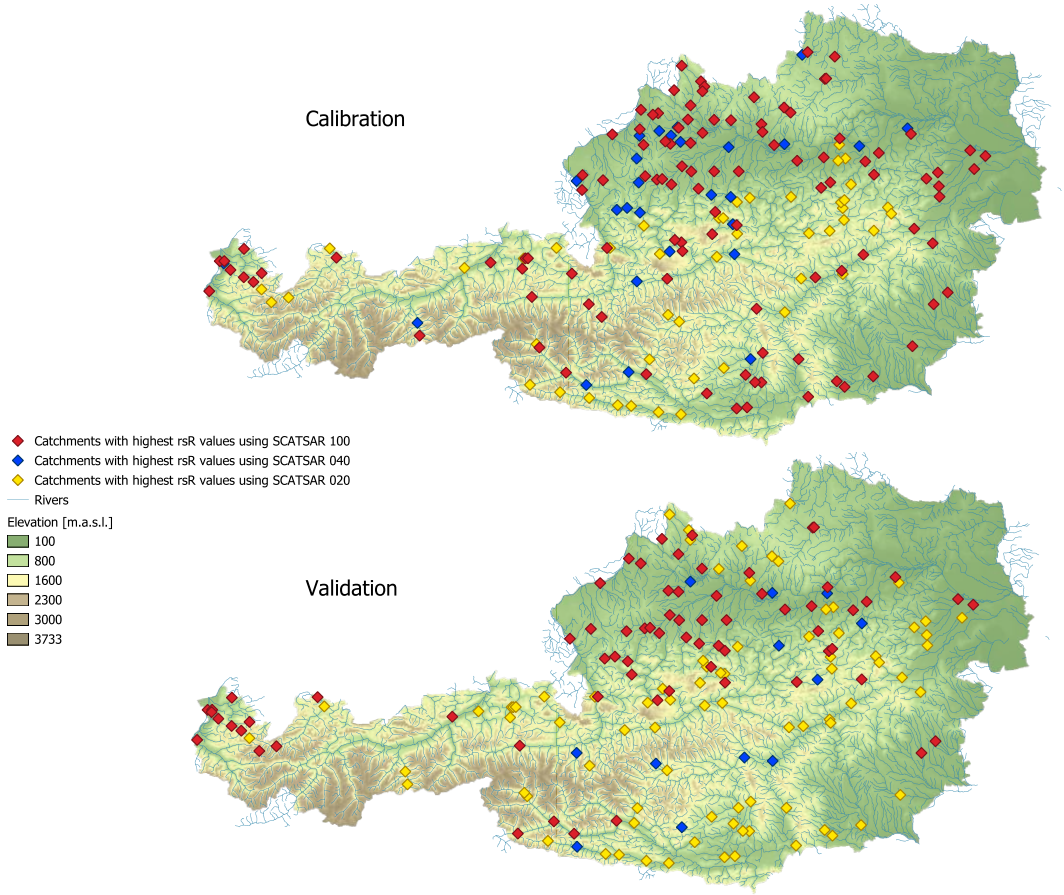

Fig. 5.1: The individual catchments with highest r_{SR} values during the calibration (top) and validation (bottom) period, relative to the T-values of SCATSAR data.

TUW_dual model in 209 Austrian catchments. In Tong et al. (2021), the TUW 15-parameter model was applied in 213 catchments in Austria, utilizing the same S1ASCAT Soil Water Index for the root-zone layer and employing identical objective functions as in this thesis. However, they used different calibration weights to test their influence on the runoff objective during model calibration. In Parajka, Naeimi, Blöschl, and Komma (2009), the TUW_dual model underwent calibration and validation across 148 Austrian catchments, with ERS satellite data employed for the process. The evaluation of runoff model efficiency utilized Nash-Sutcliffe Efficiency (NSE) and the logarithmic NSE, while soil moisture model efficiency was assessed using the correlation coefficient.

Chapter 6

Conclusion

The primary objective of this thesis is to assess the effects of S1ASCAT and SCATSAR satellite soil moisture datasets on the efficiency of the TUW_dual model in simulating runoff and soil moisture, establishing a comprehensive comparison between them. The model was calibrated using a multi-objective approach, incorporating both runoff and soil moisture in the root-zone layer (Q+SR) and runoff only (Q) calibration variants. The DEoptim optimization algorithm was implemented in order to retrieve the best model parameters, which were subsequently employed in model validation process. To assess the runoff model efficiency, Nash-Sutcliffe Efficiency Coefficient (NSE) and Kling-Gupta Efficiency (KGE) were employed, while the correlation coefficient (r_{SR}) was used to evaluate the model's efficiency in simulating soil moisture. The model calibration was carried out for the period September 2014 to December 2020, and the model validation for the period September 2009 to August 2014.

In general, this thesis concludes that the assimilation of S1ASCAT and SCATSAR product variants into both model calibration and validation resulted in either no significant change or a slight decline in runoff model efficiency in both Lowland and Alpine catchments. Nevertheless, the model demonstrated higher efficiency in simulating runoff in Alpine catchments than in Lowland catchments during both calibration and validation.

The soil moisture model efficiency considerably benefited from S1ASCAT products in both Lowland and Alpine catchments, with the model demonstrating higher efficiency in simulating soil moisture in Lowlands either in model calibration and validation. The SCATSAR data variants showed a slight increase in the correlation coefficient (r_{SR}) values between simulated and observed soil moisture in Alpine catchments during the calibration period, while in Lowland catchments, they negatively impacted the results. During the validation process, both Lowland and Alpine catchments experienced adverse impacts on the results from the SCATSAR products. The overall poor performance and result inconsistencies of SCATSAR products make it challenging to provide a precise statement, prompting the need for further examination in this case.

There are several reasons why the runoff and soil moisture efficiency criteria for the calibration period differ significantly from those of the validation period. Factors such as data period discrepancy, hydrological changes, and the spatial and temporal resolution of soil moisture data might contribute to these differences. Therefore, it would be useful to extend this thesis for other studies. For instance, adjusting the data length of the calibration period, incorporating soil moisture data with increased resolution, and enhancing horological and meteorological data, while also considering the addition of more variables and calibration variants. The impact of climate change and global warming on hydrological processes, and eventually on hydrological models, could be valuable subjects for further research. Further investigation into this topic could provide valuable insights that contribute to our understanding of how hydrological dynamics are evolving and the development of more reliable hydrological models. Such advancements have the potential to play a significant role in water resource management and adaptation strategies in the future. Recent advancements in artificial intelligence and data-driven machine learning models may inspire the integration of these technologies into traditional hydrological models,

aiming to further increase simulation accuracy. This could be also as a complex and intriguing study subject.

Bibliography

Bauer-Marschallinger, B., C. Paulik, S. Hochstöger, T. Mistelbauer, S. Modanesi, L. Ciabatta, C. Massari, L. Brocca, and W. Wagner (2018). "Soil Moisture from Fusion of Scatterometer and SAR: Closing the Scale Gap with Temporal Filtering". In: *Remote Sensing* 10.7. ISSN: 2072-4292. DOI: 10.3390/rs10071030. URL: https://www.mdpi.com/2072-4292/10/7/1030.

Bauer-Marschallinger, B., C. Paulik, and T. Jacobs (2022). *Copernicus Global Land Operations 'Vegetation and Energy' Product User Manual Soil Water Index Collection 1km Version 1*. Date Issued: 08.11.2022. URL: https://land.copernicus.eu/global/sites/cgls.vito.be/files/products/CGLOPS1_PUM_SWI1km-V1_I1.40.pdf.

Becker, A. and P. Serban (1990). *Hydrological Models for Water-resources System Design and Operation*. OMM (Collection). Secretariat of the World Meteorological Organization. ISBN: 9789263107404. URL: https://books.google.at/books?id=R7QPAQAAIAAJ.

Bergström, S. (Jan. 1976). *Development and Application of a Conceptual Runoff Model for Scandinavian Catchments*. Vol. 134 pp.

Bergström, S., G. Lindström, and A. Pettersson (Feb. 2002). "Multi-Variable Parameter Estimation to Increase Confidence in Hydrological Modeling". In: *Hydrological Processes* 16, pp. 413–421. DOI: 10.1002/hyp.332.

Beven, K. (2006). "A manifesto for the equifinality thesis". In: *Journal of Hydrology* 320.1. The model parameter estimation experiment, pp. 18–36. ISSN: 0022-1694. DOI: https://doi.org/10.1016/j.jhydrol.2005.07.007. URL: https://www.sciencedirect.com/science/article/pii/S002216940500332X.

– (Feb. 2012). *Rainfall-Runoff Modelling: The Primer*. Vol. 15. ISBN: 9780470714591. DOI: 10.1002/9781119951001.

Biswas, A. (1970). *History of Hydrology*. North-Holland Publishing Company. ISBN: 9780720480184. URL: https://books.google.at/books?id=2-kHAQAAIAAJ.

Blöschl, G. and R. B. Grayson (July 2002). "Advances in Distributed Hydrological Modelling – Towards a New Paradigm". In: *Proceedings of the Third International Conference on Water Resources and Environment Research (ICWRER)*. Vol. Volume I. Dresden, Germany: Dresden University of Technology, pp. 17–25.

Blöschl, G., J. Komma, T. Nester, J. Salinas, R. Tong, and A. Viglione (2017). *Auswirkung Alpiner Retention auf die Hochwasserabflüsse des Inn*. Tech. rep. Institut für Wasserbau und Ingenieurhydrologie, Technische Universität Wien.

BMK (2013). *Hochwasser an der Donau - Ereignisanalyse 2013*. URL: https://www.bmk.gv.at/themen/verkehr/wasser/hochwasserschutz/publikationen/hochwasserdonau2013.html.

Boyle, D. P., H. V. Gupta, and S. Sorooshian (2000). "Toward improved calibration of hydrologic models: Combining the strengths of manual and automatic methods". In: *Water Resources Research* 36.12, pp. 3663–3674.

Brocca, L., T. Moramarco, F. Melone, W. Wagner, S. Hasenauer, and S. Hahn (2012). "Assimilation of Surface- and Root-Zone ASCAT Soil Moisture Products Into Rainfall–Runoff Modeling". In: *IEEE Transactions on Geoscience and Remote Sensing* 50.7, pp. 2542–2555. DOI: 10.1109/TGRS.2011.2177468.

Bullock, A. and S. Trombley (1999). *The New Fontana Dictionary of Modern Thought*. 3rd. London: Harper Collins.

Castaneda-Gonzalez, M. (Nov. 2019). "Impacts of Regional Climate Model Spatial Resolution on Summer Flood Simulation". In: DOI: 10.29007/hd8l.

Copernicus Global Land Service - Soil Water Index (2023). URL: https://land.copernicus.eu/global/products/swi (Date accessed: 09/23/2023).

Copernicus Global Land Service - Surface Soil Moisture (2023). URL: https://land.copernicus.eu/global/products/ssm (Date accessed: 09/23/2023).

Copernicus Land Monitoring Service - Land Cover (2023). URL: https://land.copernicus.eu/global/products/lc (Date accessed: 09/28/2023).

Devia, G. K., B. Ganasri, and G. Dwarakish (2015). "A Review on Hydrological Models". In: *Aquatic Procedia* 4. INTERNATIONAL CONFERENCE ON WATER RESOURCES, COASTAL AND OCEAN ENGINEERING (ICWRCOE'15), pp. 1001–1007. ISSN: 2214-241X. DOI: https://doi.org/10.1016/j.aqpro.2015.02.126. URL: https://www.sciencedirect.com/science/article/pii/S2214241X15001273.

Duan, Q. (2003). "Global Optimization for Watershed Model Calibration". In: *Calibration of Watershed Models*. American Geophysical Union (AGU), pp. 89–104. ISBN: 9781118665671. DOI: https://doi.org/10.1002/9781118665671.ch6. eprint: https://agupubs.onlinelibrary.wiley.com/doi/pdf/10.1002/9781118665671.ch6. URL: https://agupubs.onlinelibrary.wiley.com/doi/abs/10.1002/9781118665671.ch6.

Duan, Q., S. Sorooshian, and V. Gupta (Apr. 1992). "Effective and Efficient Gobal Optimization for Conceptual Rainfall-Runoff Models". In: *Water Resources Research - WATER RESOUR RES* 28, pp. 1015–1031. DOI: 10.1029/91WR02985.

Duit, R. and S. Glynn (1996). "Mental modelling". In: *Research in science education in Europe*, pp. 166–176.

Efstratiadis, A. and D. Koutsoyiannis (2010). "One decade of multi-objective calibration approaches in hydrological modelling: a review". In: *Hydrological Sciences Journal* 55.1, pp. 58–78. DOI: 10.1080/02626660903526292. eprint: https://doi.org/10.1080/02626660903526292. URL: https://doi.org/10.1080/02626660903526292.

Franchini, M. and M. Pacciani (1991). "Comparative analysis of several conceptual rainfall-runoff models". In: *Journal of Hydrology* 122.1, pp. 161–219. ISSN: 0022-1694. DOI: https://doi.org/10.1016/0022-1694(91)90178-K. URL: https://www.sciencedirect.com/science/article/pii/002216949190178K.

Gilbert, J. K. and C. J. Boulter (1997). "Learning Science Through Models and Modelling". In: *The International Handbook of Science Education*. Ed. by B. J. Fraser and K. Tobin. Dordrecht, The Netherlands: Kluwer, pp. 53–66.

Gilbert, S. W. (1991). "Model building and a definition of science". In: *Journal of Research in Science Teaching* 28.1, pp. 73–79. DOI: https://doi.org/10.1002/tea.3660280107. eprint: https://onlinelibrary.wiley.com/doi/pdf/10.1002/tea.3660280107. URL: https://onlinelibrary.wiley.com/doi/abs/10.1002/tea.3660280107.

Gupta, H. V., H. Kling, K. K. Yilmaz, and G. F. Martinez (2009). "Decomposition of the mean squared error and NSE performance criteria: Implications for improving hydrological modelling". In: *Journal of Hydrology* 377.1, pp. 80–91. ISSN: 0022-1694. DOI: https://doi.org/10.1016/j.jhydrol.2009.08.003. URL: https://www.sciencedirect.com/science/article/pii/S0022169409004843.

Gupta, H. V., S. Sorooshian, and P. O. Yapo (1998). "Toward improved calibration of hydrologic models: Multiple and noncommensurable measures of information". In: *Water Resources Research* 34.4, pp. 751–763. DOI: https://doi.org/10.1029/97WR03495. eprint: https:

//agupubs.onlinelibrary.wiley.com/doi/pdf/10.1029/97WR03495. URL: https://agupubs.onlinelibrary.wiley.com/doi/abs/10.1029/97WR03495.

Gupta, S. (2011). *Modern Hydrology and Sustainable Water Development*. Wiley. ISBN: 9781444347722. URL: https://books.google.at/books?id=a_0z7qY65S4C.

Gutknecht, D., C. Reszler, and G. Blöschl (Dec. 2002). "Das Katastrophenhochwasser vom 7. August 2002 am Kamp — Eine erste Einschätzung". In: *e i Elektrotechnik und Informationstechnik* 119, pp. 411–413. DOI: 10.1007/BF03161354.

Habersack, H., H. Stiefelmeyer, A. Petrascheck, et al. (2005). "Analyse der Hochwasserereignisse vom August 2002 — FloodRisk". In: *Österr Wasser- und Abfallw* 57, pp. 88–94. DOI: 10.1007/BF03169029. URL: https://doi.org/10.1007/BF03169029.

Hahn, S., W. Wagner, S. C. Steele-Dunne, M. Vreugdenhil, and T. Melzer (2021). "Improving ASCAT Soil Moisture Retrievals With an Enhanced Spatially Variable Vegetation Parameterization". In: *IEEE Transactions on Geoscience and Remote Sensing* 59.10, pp. 8241–8256. DOI: 10.1109/TGRS.2020.3041340.

Hempel, C. G. (1965). *Aspects of Scientific Explanation and Other Essays in the Philosophy of Science*. New York: The Free Press.

Hesse, M. (1965). "Models and Analogies in Science". In: *British Journal for the Philosophy of Science* 16.62, pp. 161–163.

Hiebl, J. and C. Frei (Feb. 2016). "Daily temperature grids for Austria since 1961—concept, creation and applicability". In: *Theoretical and Applied Climatology* 124, pp. 161–178. DOI: 10.1007/s00704-015-1411-4.

– (Apr. 2018). "Daily precipitation grids for Austria since 1961—development and evaluation of a spatial dataset for hydroclimatic monitoring and modelling". In: *Theoretical and Applied Climatology* 132.1, pp. 327–345. ISSN: 1434-4483. DOI: 10.1007/s00704-017-2093-x. URL: https://doi.org/10.1007/s00704-017-2093-x.

Houghton-Carr, H. (Apr. 1999). "Assessment criteria for simple conceptual daily rainfall-runoff models". In: *HydroIogicalSciences-Journal-des Sciences Hydrologiques* 44. DOI: 10.1080/02626669909492220.

Huang, G.-H. (2010). "Measure of Association". In: *International Encyclopedia of Education (Third Edition)*. Ed. by P. Peterson, E. Baker, and B. McGaw. Third Edition. Oxford: Elsevier, pp. 260–263. ISBN: 978-0-08-044894-7. DOI: https://doi.org/10.1016/B978-0-08-044894-7.01342-7. URL: https://www.sciencedirect.com/science/article/pii/B9780080448947013427.

Immerzeel, W. and P. Droogers (2008). "Calibration of a distributed hydrological model based on satellite evapotranspiration". In: *Journal of Hydrology* 349.3, pp. 411–424. ISSN: 0022-1694. DOI: https://doi.org/10.1016/j.jhydrol.2007.11.017. URL: https://www.sciencedirect.com/science/article/pii/S0022169407006944.

Kavetski, D., G. Kuczera, and S. W. Franks (2006). "Bayesian analysis of input uncertainty in hydrological modeling: 1. Theory". In: *Water Resources Research* 42.3. DOI: https://doi.org/10.1029/2005WR004368. eprint: https://agupubs.onlinelibrary.wiley.com/doi/pdf/10.1029/2005WR004368. URL: https://agupubs.onlinelibrary.wiley.com/doi/abs/10.1029/2005WR004368.

Kim, K. B., H.-H. Kwon, and D. Han (2018). "Exploration of warm-up period in conceptual hydrological modelling". In: *Journal of Hydrology* 556, pp. 194–210. ISSN: 0022-1694. DOI: https://doi.org/10.1016/j.jhydrol.2017.11.015. URL: https://www.sciencedirect.com/science/article/pii/S0022169417307692.

Klemeš, V. (1986). "Operational testing of hydrological simulation models". In: *Hydrological Sciences Journal* 31.1, pp. 13–24. DOI: 10.1080/02626668609491024. eprint: https://doi.org/10.1080/02626668609491024. URL: https://doi.org/10.1080/02626668609491024.

Knoben, W. J. M., J. E. Freer, and R. A. Woods (2019). "Technical note: Inherent benchmark or not? Comparing Nash–Sutcliffe and Kling–Gupta efficiency scores". In: *Hydrology and Earth System Sciences* 23.10, pp. 4323–4331. DOI: 10.5194/hess-23-4323-2019. URL: https://hess.copernicus.org/articles/23/4323/2019/.

Koskinen, M., T. Tahvanainen, S. Sarkkola, M. Menberu, A. Lauren, T. Sallantaus, H. Marttila, A.-K. Ronkanen, M. Parviainen, A. Tolvanen, H. Koivusalo, and M. Nieminen (May 2017). "Restoration of nutrient-rich forestry-drained peatlands poses a risk for high exports of dissolved organic carbon, nitrogen, and phosphorus". English. In: *The Science of the Total Environment* 586, pp. 858–869. ISSN: 0048-9697. DOI: 10.1016/j.scitotenv.2017.02.065.

Kubáň, M., J. Parajka, R. Tong, I. Pfeil, M. Vreugdenhil, P. Sleziak, B. Adam, J. Szolgay, S. Kohnová, and K. Hlavčová (2021). "Incorporating Advanced Scatterometer Surface and Root Zone Soil Moisture Products into the Calibration of a Conceptual Semi-Distributed Hydrological Model". In: *Water* 13.23. ISSN: 2073-4441. DOI: 10.3390/w13233366. URL: https://www.mdpi.com/2073-4441/13/23/3366.

Kundu, D., R. W. Vervoort, and F. F. van Ogtrop (2017). "The value of remotely sensed surface soil moisture for model calibration using SWAT". In: *Hydrological Processes* 31.15, pp. 2764–2780. DOI: https://doi.org/10.1002/hyp.11219. eprint: https://onlinelibrary.wiley.com/doi/pdf/10.1002/hyp.11219. URL: https://onlinelibrary.wiley.com/doi/abs/10.1002/hyp.11219.

Kunnath-Poovakka, A., D. Ryu, L. Renzullo, and B. George (2016). "The efficacy of calibrating hydrologic model using remotely sensed evapotranspiration and soil moisture for streamflow prediction". In: *Journal of Hydrology* 535, pp. 509–524. ISSN: 0022-1694. DOI: https://doi.org/10.1016/j.jhydrol.2016.02.018. URL: https://www.sciencedirect.com/science/article/pii/S0022169416300439.

Le Moine, N. (2008). "Le bassin versant de surface vu par le souterrain : une voie d'amélioration des performances et du réalisme des modèles pluie-débit ?" [Departement_IRSTEA]RE [TR1_IRSTEA]RIE / TRANSFEAU [Encadrant_IRSTEA]Andreassian, V. Theses. Doctorat Géosciences et Ressources Naturelles, Université Pierre et Marie Curie Paris VI, p. 348. URL: https://hal.inrae.fr/tel-02591478.

Li, C.-z., H. Wang, J. Liu, D.-h. Yan, F.-l. Yu, and L. Zhang (2010). "Effect of calibration data series length on performance and optimal parameters of hydrological model". In: *Water Science and Engineering* 3.4, pp. 378–393. ISSN: 1674-2370. DOI: https://doi.org/10.3882/j.issn.1674-2370.2010.04.002. URL: https://www.sciencedirect.com/science/article/pii/S1674237015301289.

Li, Y., S. Grimaldi, V. R. Pauwels, and J. P. Walker (2018). "Hydrologic model calibration using remotely sensed soil moisture and discharge measurements: The impact on predictions at gauged and ungauged locations". In: *Journal of Hydrology* 557, pp. 897–909. ISSN: 0022-1694. DOI: https://doi.org/10.1016/j.jhydrol.2018.01.013. URL: https://www.sciencedirect.com/science/article/pii/S0022169418300131.

Liebscher, H. and H. Mendel (2010). *Vom empirischen Modellansatz zum komplexen hydrologischen Flussgebietsmodell: Rückblick und Perspektiven*. BFG. URL: https://books.google.at/books?id=bAO6XwAACAAJ.

Madsen, H. (2003). "Parameter estimation in distributed hydrological catchment modelling using automatic calibration with multiple objectives". In: *Advances in Water Resources* 26.2, pp. 205–216. ISSN: 0309-1708. DOI: https://doi.org/10.1016/S0309-1708(02)00092-1. URL: https://www.sciencedirect.com/science/article/pii/S0309170802000921.

Mayer, R. E. (1992). "Knowledge and thought: Mental models that support scientific reasoning". In: *Philosophy of science, cognitive psychology, and educational theory and practice*, pp. 226–243.

McCuen, R. H., Z. Knight, and A. G. Cutter (2006). "Evaluation of the Nash–Sutcliffe Efficiency Index". In: *Journal of Hydrologic Engineering* 11.6, pp. 597–602. DOI: 10.1061/(ASCE)1084-0699(2006)11:6(597). eprint: https://ascelibrary.org/doi/pdf/10.1061/%28ASCE%291084-0699%282006%2911%3A6%28597%29. URL: https://ascelibrary.org/doi/abs/10.1061/%28ASCE%291084-0699%282006%2911%3A6%28597%29.

Melching, C. (1995). "Reliability Estimation". In: *Computer Models of Watershed Hydrology*. Ed. by V. Singh. Highlands Ranch, USA: Water Resources Publications, pp. 69–118.

Merz, R. and G. Blöschl (Feb. 2004). "Regionalisation of Catchment Model Parameters". In: *Journal of Hydrology* 287, pp. 95–123. DOI: 10.1016/j.jhydrol.2003.09.028.

Milzow, C., P. E. Krogh, and P. Bauer-Gottwein (2011). "Combining satellite radar altimetry, SAR surface soil moisture and GRACE total storage changes for hydrological model calibration in a large poorly gauged catchment". In: *Hydrology and Earth System Sciences* 15.6, pp. 1729–1743. DOI: 10.5194/hess-15-1729-2011. URL: https://hess.copernicus.org/articles/15/1729/2011/.

Moriasi, D. N., J. G. Arnold, M. Liew, R. L. Bingner, R. D. Harmel, and T. L. Veith (2007). "Model Evaluation Guidelines for Systematic Quantification of Accuracy in Watershed Simulations". In: *Transactions of the ASABE* 50, pp. 885–900. URL: https://api.semanticscholar.org/CorpusID:11186951.

Mullen, K. M., D. Ardia, D. L. Gil, D. Windover, and J. Cline (2011). "DEoptim: An R Package for Global Optimization by Differential Evolution". In: *Journal of Statistical Software* 40.6, pp. 1–26. DOI: 10.18637/jss.v040.i06. URL: https://www.jstatsoft.org/index.php/jss/article/view/v040i06.

Mulligan, M. and J. Wainwright (2013). "Modelling Catchment and Fluvial Processes and their Interactions". In: *Environmental Modelling*. John Wiley Sons, Ltd. Chap. 11, pp. 183–205. ISBN: 9781118351475. DOI: https://doi.org/10.1002/9781118351475.ch11. eprint: https://onlinelibrary.wiley.com/doi/pdf/10.1002/9781118351475.ch11. URL: https://onlinelibrary.wiley.com/doi/abs/10.1002/9781118351475.ch11.

Naeimi, V., K. Scipal, Z. Bartalis, S. Hasenauer, and W. Wagner (2009). "An Improved Soil Moisture Retrieval Algorithm for ERS and METOP Scatterometer Observations". In: *IEEE Transactions on Geoscience and Remote Sensing* 47.7, pp. 1999–2013. DOI: 10.1109/TGRS.2008.2011617.

Nash, J. and J. Sutcliffe (1970). "River flow forecasting through conceptual models part I — A discussion of principles". In: *Journal of Hydrology* 10.3, pp. 282–290. ISSN: 0022-1694. DOI: https://doi.org/10.1016/0022-1694(70)90255-6. URL: https://www.sciencedirect.com/science/article/pii/0022169470902556.

Nijzink, R. C., S. Almeida, I. G. Pechlivanidis, R. Capell, D. Gustafssons, B. Arheimer, J. Parajka, J. Freer, D. Han, T. Wagener, R. R. P. van Nooijen, H. H. G. Savenije, and M. Hrachowitz (2018). "Constraining Conceptual Hydrological Models With Multiple Information Sources". In: *Water Resources Research* 54.10, pp. 8332–8362. DOI: https://doi.org/10.1029/2017WR021895. eprint: https://agupubs.onlinelibrary.wiley.com/doi/pdf/10.1029/2017WR021895. URL: https://agupubs.onlinelibrary.wiley.com/doi/abs/10.1029/2017WR021895.

Oudin, L., V. Andréassian, T. Mathevet, C. Perrin, and C. Michel (2006). "Dynamic averaging of rainfall-runoff model simulations from complementary model parameterizations". In: *Water Resources Research* 42.7. DOI: https://doi.org/10.1029/2005WR004636. eprint: https://agupubs.onlinelibrary.wiley.com/doi/pdf/10.1029/2005WR004636. URL: https://agupubs.onlinelibrary.wiley.com/doi/abs/10.1029/2005WR004636.

Owe, M., R. de Jeu, and T. Holmes (2008). "Multisensor historical climatology of satellite-derived global land surface moisture". In: *Journal of Geophysical Research: Earth Surface* 113.F1. DOI: https://doi.org/10.1029/2007JF000769. eprint: https://agupubs.onlinelibrary.

wiley.com/doi/pdf/10.1029/2007JF000769. URL: https://agupubs.onlinelibrary.wiley.com/doi/abs/10.1029/2007JF000769.

Parajka, J., V. Andréassian, S. A. Archfield, A. Bárdossy, G. Blöschl, F. Chiew, Q. Duan, A. Gelfan, K. Hlavčová, R. Merz, and et al. (2013). "Prediction of runoff hydrographs in ungauged basins". In: *Runoff Prediction in Ungauged Basins: Synthesis across Processes, Places and Scales*. Ed. by G. Blöschl, M. Sivapalan, T. Wagener, A. Viglione, and H. Savenije. Cambridge University Press, pp. 227–269. DOI: 10.1017/CBO9781139235761.013.

Parajka, J. and G. Blöschl (2008). "The value of MODIS snow cover data in validating and calibrating conceptual hydrologic models". In: *Journal of Hydrology* 358.3, pp. 240–258. ISSN: 0022-1694. DOI: https://doi.org/10.1016/j.jhydrol.2008.06.006. URL: https://www.sciencedirect.com/science/article/pii/S0022169408002862.

Parajka, J., R. Merz, and G. Blöschl (Nov. 2003). "Estimation of daily potential evapotranspiration for regional water balance modeling in Austria". In: *11th International Poster Day and Institute of Hydrology Open Day "Transport of Water, Chemicals and Energy in the Soil — Crop Canopy — Atmosphere System"*. Bratislava, Slovakia: Slovak Academy of Sciences, pp. 299–306. ISBN: 80-89139-02-7.

– (2005). "Regionale Wasserbilanzkomponenten für Österreich auf Tagesbasis". In: *Österreichische Wasser- und Abfallwirtschaft* 57.3, pp. 43–56. ISSN: 1613-7566. DOI: 10.1007/BF03165611. URL: https://doi.org/10.1007/BF03165611.

– (2007). "Uncertainty and multiple objective calibration in regional water balance modelling: case study in 320 Austrian catchments". In: *Hydrological Processes* 21.4, pp. 435–446. DOI: https://doi.org/10.1002/hyp.6253. eprint: https://onlinelibrary.wiley.com/doi/pdf/10.1002/hyp.6253. URL: https://onlinelibrary.wiley.com/doi/abs/10.1002/hyp.6253.

Parajka, J., V. Naeimi, G. Blöschl, and J. Komma (2009). "Matching ERS scatterometer based soil moisture patterns with simulations of a conceptual dual layer hydrologic model over Austria". In: *Hydrology and Earth System Sciences* 13.2, pp. 259–271. DOI: 10.5194/hess-13-259-2009. URL: https://hess.copernicus.org/articles/13/259/2009/.

Parajka, J., V. Naeimi, G. Blöschl, W. Wagner, R. Merz, and K. Scipal (2006). "Assimilating scatterometer soil moisture data into conceptual hydrologic models at the regional scale". In: *Hydrology and Earth System Sciences* 10.3, pp. 353–368. DOI: 10.5194/hess-10-353-2006. URL: https://hess.copernicus.org/articles/10/353/2006/.

Paulik, C., W. Dorigo, W. Wagner, and R. Kidd (2014). "Validation of the ASCAT Soil Water Index using in situ data from the International Soil Moisture Network". In: *International Journal of Applied Earth Observation and Geoinformation* 30, pp. 1–8. ISSN: 1569-8432. DOI: 10.1016/j.jag.2014.01.007. URL: https://www.sciencedirect.com/science/article/pii/S0303243414000099.

Rajib, M. A., V. Merwade, and Z. Yu (2016). "Multi-objective calibration of a hydrologic model using spatially distributed remotely sensed/in-situ soil moisture". In: *Journal of Hydrology* 536, pp. 192–207. ISSN: 0022-1694. DOI: https://doi.org/10.1016/j.jhydrol.2016.02.037. URL: https://www.sciencedirect.com/science/article/pii/S0022169416300713.

Refsgaard, J. C. (1997). "Parameterisation, calibration and validation of distributed hydrological models". In: *Journal of Hydrology* 198.1, pp. 69–97. ISSN: 0022-1694. DOI: https://doi.org/10.1016/S0022-1694(96)03329-X. URL: https://www.sciencedirect.com/science/article/pii/S002216949603329X.

Ritter, A. and R. Muñoz-Carpena (2013). "Performance evaluation of hydrological models: Statistical significance for reducing subjectivity in goodness-of-fit assessments". In: *Journal of Hydrology* 480, pp. 33–45. ISSN: 0022-1694. DOI: https://doi.org/10.1016/j.jhydrol.2012.12.004. URL: https://www.sciencedirect.com/science/article/pii/S0022169412010608.

Rogelis, M. C., M. Werner, N. Obregón, and N. Wright (2016). "Hydrological model assessment for flood early warning in a tropical high mountain basin". In: *Hydrology and Earth System Sciences Discussions* 2016, pp. 1–36. DOI: 10.5194/hess-2016-30. URL: https://hess.copernicus.org/preprints/hess-2016-30/.

Salzburg24 (2021). *Hochwasser in Salzburg: Das ganze Land unter Schock*. URL: https://www.salzburg24.at/news/salzburg/hochwasser-in-salzburg-das-ganze-land-unter-schock-106736626.

Santos, L., G. Thirel, and C. Perrin (Aug. 2018). "Technical note: Pitfalls in using log-transformed flows within the KGE criterion". In: *Hydrology and Earth System Sciences* 22, pp. 4583–4591. DOI: 10.5194/hess-22-4583-2018.

Sitterson, J., C. Knightes, R. Parmar, K. Wolfe, B. Avant, and M. Muche (2018). "An overview of rainfall-runoff model types". In.

Sorooshian, S., Q. Duan, and V. K. Gupta (1993). "Calibration of rainfall-runoff models: Application of global optimization to the Sacramento Soil Moisture Accounting Model". In: *Water Resources Research* 29.4, pp. 1185–1194. DOI: https://doi.org/10.1029/92WR02617. eprint: https://agupubs.onlinelibrary.wiley.com/doi/pdf/10.1029/92WR02617. URL: https://agupubs.onlinelibrary.wiley.com/doi/abs/10.1029/92WR02617.

Sorooshian, S. and H. V. Gupta (1995). "Model Calibration". In: *Computer Models of Watershed Hydrology*. Ed. by V. P. Singh. Colorado: Water Resources Publications. ISBN: 0-918334-91-8.

Sorooshian, S., V. K. Gupta, and J. L. Fulton (1983). "Evaluation of Maximum Likelihood Parameter estimation techniques for conceptual rainfall-runoff models: Influence of calibration data variability and length on model credibility". In: *Water Resources Research* 19.1, pp. 251–259. DOI: https://doi.org/10.1029/WR019i001p00251. eprint: https://agupubs.onlinelibrary.wiley.com/doi/pdf/10.1029/WR019i001p00251. URL: https://agupubs.onlinelibrary.wiley.com/doi/abs/10.1029/WR019i001p00251.

Storn, R. and K. Price (Jan. 1997). "Differential Evolution - A Simple and Efficient Heuristic for Global Optimization over Continuous Spaces". In: *Journal of Global Optimization* 11, pp. 341–359. DOI: 10.1023/A:1008202821328.

Sutanudjaja, E., L. Van Beek, S. De Jong, F. Van Geer, and M. Bierkens (2014). "Calibrating a large-extent high-resolution coupled groundwater-land surface model using soil moisture and discharge data". In: *Water Resources Research* 50.1. Cited by: 99; All Open Access, Bronze Open Access, pp. 687–705. DOI: 10.1002/2013WR013807. URL: https://www.scopus.com/inward/record.uri?eid=2-s2.0-84896696983&doi=10.1002%2f2013WR013807&partnerID=40&md5=e586b0f01560bfd3f5e73ef1aa43bbe7.

Todini, E. (Feb. 2011). "History and perspectives of hydrological catchment modelling". In: *Hydrology Research* 42, p. 73. DOI: 10.2166/nh.2011.096.

Tong, R., J. Parajka, A. Salentinig, I. Pfeil, J. Komma, B. Széles, M. Kubáň, P. Valent, M. Vreugdenhil, W. Wagner, and G. Blöschl (2021). "The value of ASCAT soil moisture and MODIS snow cover data for calibrating a conceptual hydrologic model". In: *Hydrology and Earth System Sciences* 25.3, pp. 1389–1410. DOI: 10.5194/hess-25-1389-2021. URL: https://hess.copernicus.org/articles/25/1389/2021/.

Valk, T., J. Driel, and W. Vos (Oct. 2007). "Common Characteristics of Models in Present-day Scientific Practice". In: *Research in Science Education* 37, pp. 469–488. DOI: 10.1007/s11165-006-9036-3.

Wagener, T. and A. Montanari (2011). "Convergence of approaches toward reducing uncertainty in predictions in ungauged basins". In: *Water Resources Research* 47.6. DOI: https://doi.org/10.1029/2010WR009469. eprint: https://agupubs.onlinelibrary.wiley.com/doi/pdf/10.1029/2010WR009469. URL: https://agupubs.onlinelibrary.wiley.com/doi/abs/10.1029/2010WR009469.

Wagener, T., H. Wheater, and H. Gupta (Jan. 2004). *Rainfall-Runoff Modelling In Gauged And Ungauged Catchments*, p. 306. DOI: 10.1142/9781860945397.

Wagner, W., G. Blöschl, P. Pampaloni, J.-C. Calvet, B. Bizzarri, J.-P. Wigneron, and Y. Kerr (Feb. 2007). "Operational readiness of microwave remote sensing of soil moisture for hydrologic applications". In: *Hydrology Research* 38.1, pp. 1–20. ISSN: 0029-1277. DOI: 10.2166/nh.2007.029. eprint: https://iwaponline.com/hr/article-pdf/38/1/1/364787/1.pdf. URL: https://doi.org/10.2166/nh.2007.029.

Wagner, W., G. Lemoine, and H. Rott (1999). "A Method for Estimating Soil Moisture from ERS Scatterometer and Soil Data". In: *Remote Sensing of Environment* 70.2, pp. 191–207. ISSN: 0034-4257. DOI: https://doi.org/10.1016/S0034-4257(99)00036-X. URL: https://www.sciencedirect.com/science/article/pii/S003442579900036X.

Wanders, N., M. F. P. Bierkens, S. M. de Jong, A. de Roo, and D. Karssenberg (2014). "The benefits of using remotely sensed soil moisture in parameter identification of large-scale hydrological models". In: *Water Resources Research* 50.8, pp. 6874–6891. DOI: https://doi.org/10.1002/2013WR014639. eprint: https://agupubs.onlinelibrary.wiley.com/doi/pdf/10.1002/2013WR014639. URL: https://agupubs.onlinelibrary.wiley.com/doi/abs/10.1002/2013WR014639.

Wheater, H. et al. (2008). "Modelling hydrological processes in arid and semi-arid areas: an introduction to the workshop". In: *Hydrol. Model. Arid. Semi-Arid Areas*, pp. 1–20.

Woody, A. (1995). "The Explanatory Power of Our Models: A Philosophical Analysis with Some Implications for Science Education". In: *Proceedings of the Third International History, Philosophy, and Science Teaching Conference*. Ed. by F. Finley, D. Allchin, D. Rhees, and S. Fifield. Vol. 2. Minneapolis, USA: University of Minneapolis, pp. 1295–1304.

Xu, X., J. Li, and B. A. Tolson (2014). "Progress in integrating remote sensing data and hydrologic modeling". In: *Progress in Physical Geography: Earth and Environment* 38.4, pp. 464–498. DOI: 10.1177/0309133314536583. eprint: https://doi.org/10.1177/0309133314536583. URL: https://doi.org/10.1177/0309133314536583.

Yapo, P. O., H. V. Gupta, and S. Sorooshian (1996). "Automatic calibration of conceptual rainfall-runoff models: sensitivity to calibration data". In: *Journal of Hydrology* 181.1, pp. 23–48. ISSN: 0022-1694. DOI: https://doi.org/10.1016/0022-1694(95)02918-4. URL: https://www.sciencedirect.com/science/article/pii/0022169495029184.

Yapo, P. O., H. V. Gupta, and S. Sorooshian (1998). "Multi-objective global optimization for hydrologic models". In: *Journal of Hydrology* 204.1, pp. 83–97. ISSN: 0022-1694. DOI: https://doi.org/10.1016/S0022-1694(97)00107-8. URL: https://www.sciencedirect.com/science/article/pii/S0022169497001078.

Yilmaz, K., J. Vrugt, H. Gupta, and S. Sorooshian (Aug. 2010). "Model calibration in watershed hydrology". In: pp. 53–105. ISBN: 978-981-4307-97-0. DOI: 10.1142/9789814307987_0003.

Zellinger, B. (2019). "Estimation of Regional Floods with Large Return Periods". Master's thesis. TU Wien, Faculty of Civil Engineering.

List of Figures

List of Tables

Chapter 7

Appendix

7.1 Data Basis

The characteristics of the catchments, including X coordinates, Y coordinates, area, mean elevation, mean slope, can be taken from Table 7.1 to Table 7.5, while other features such as forest cover, elevation range, mean precipitation, mean temperature, and mean Q/A can be extracted from Table 7.6 to Table 7.10. Light gray rows depict alpine catchments, while white rows represent lowland catchments. Figure 7.1 displays the gauge numbers associated with the catchments. The categorization of the catchments into Lowland and Alpine is based on the study by Kubáň et al. (2021).

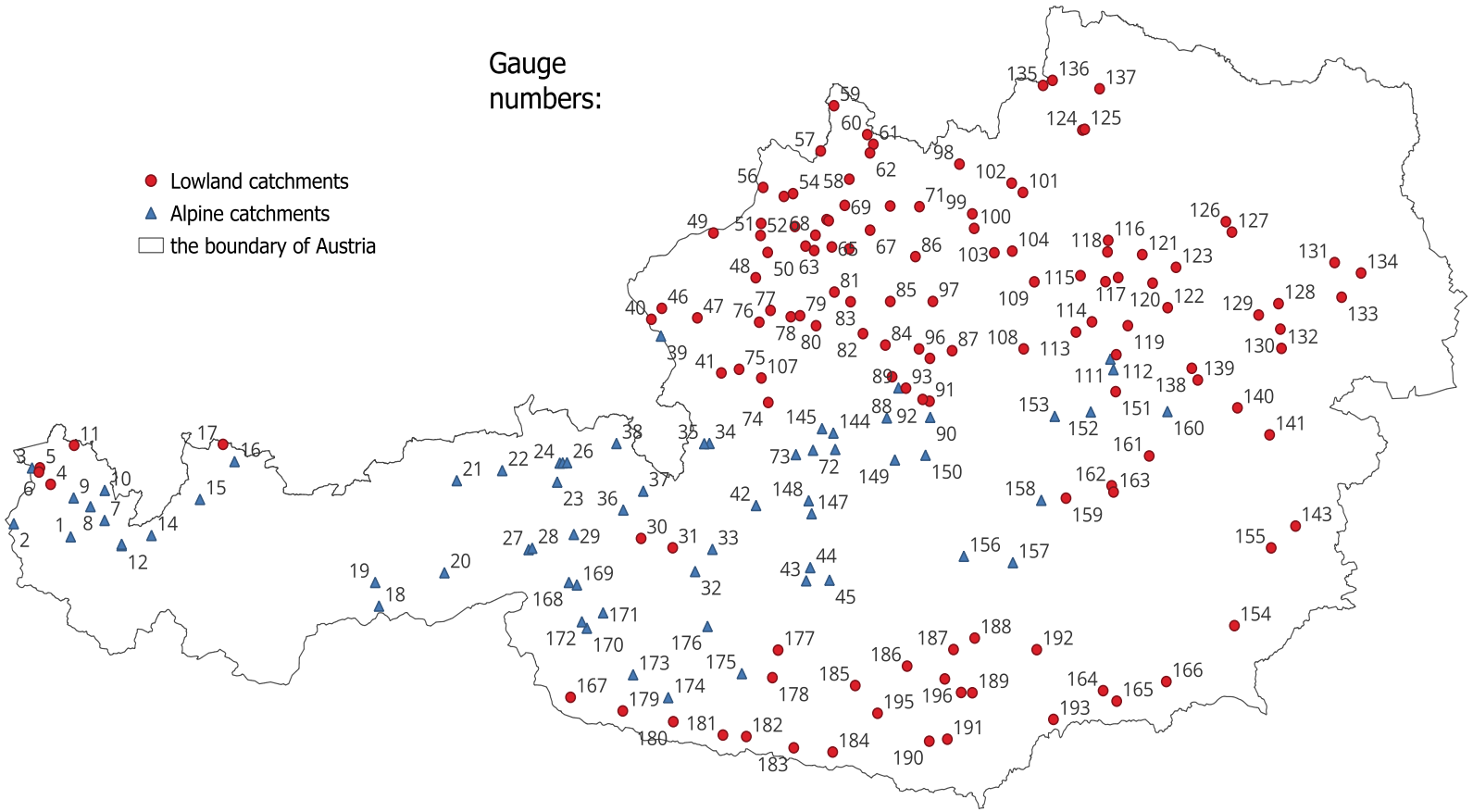

Fig. 7.1: The gauge numbers associated with the catchments.

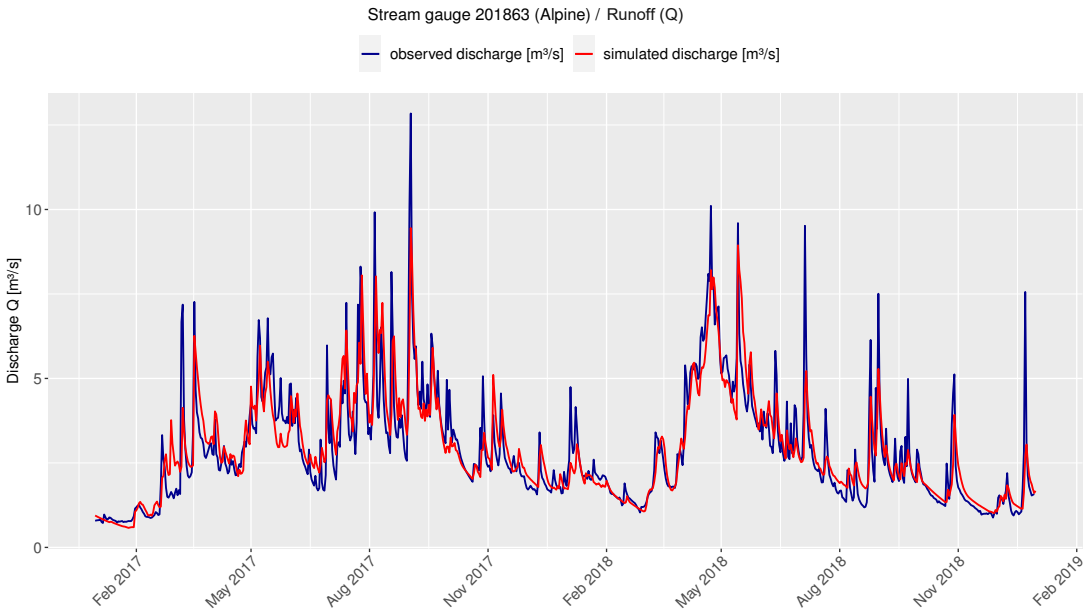

Fig. 7.2: Simulation results of the model calibrated to runoff only (Q) the Alpine catchment of stream gauge 201863, over the period from December 31, 2016, to December 31, 2018.

7.2 Model Efficiency

7.2.1 Calibration Period

7.2.1.1 Runoff Model Efficiency

To visually assess the runoff model efficiency during the calibration period, hydrographs from a selected stream gauge in the Alpine catchment (201863 - Bruckhäusl) and another in the Lowland (205021 - Bad Schallerbach) catchment were chosen for comparison.

Hydrographs - Alpine Stream Gauge 201863
Figures 7.2 to 7.6 depict the simulation results of the model calibration for the stream gauge 201863, situated in Alpine. Observed discharge hydrographs are shown in blue, and simulated discharge hydrographs are shown in red. For better clarity of the hydrographs, a two-year period from December 31, 2016, to December 31, 2018, was selected.

Hydrographs - Lowland Stream Gauge 205021
Figures 7.7 to 7.11 depict the simulation results of the model calibration for the stream gauge 205021, situated in Lowland. Observed discharge hydrographs are shown in blue, and simulated discharge hydrographs are shown in red. For better clarity of the hydrographs, a two-year period from December 31, 2016, to December 31, 2018, was selected.

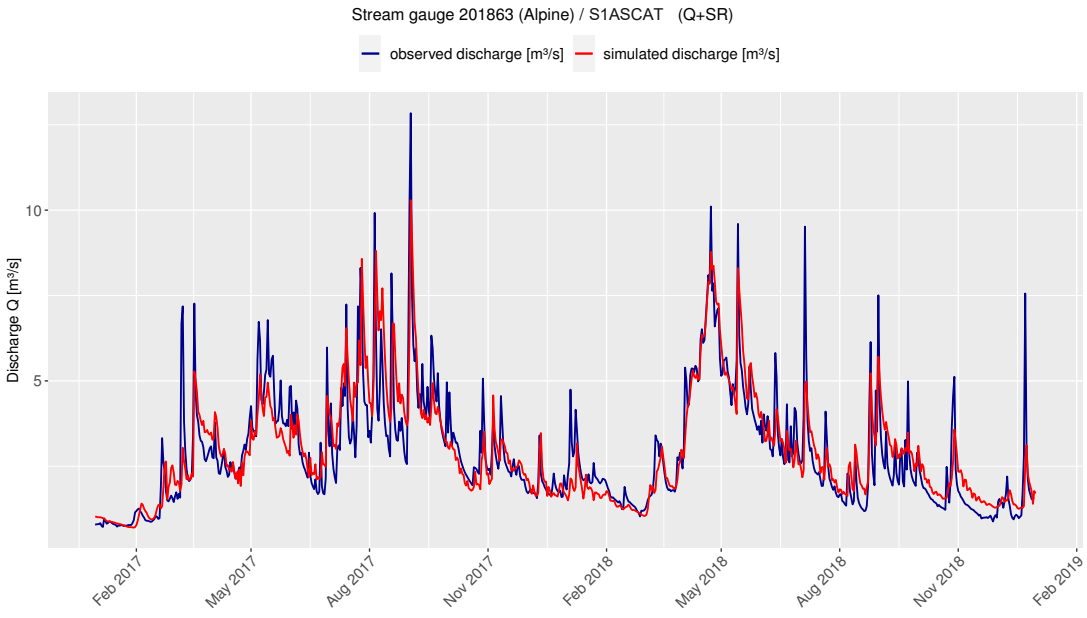

Fig. 7.3: Simulation results of the model calibrated to runoff and soil moisture in the root-zone layer (Q+SR) using the S1ASCAT satellite product for the Alpine catchment of stream gauge 201863, over the period from December 31, 2016, to December 31, 2018.

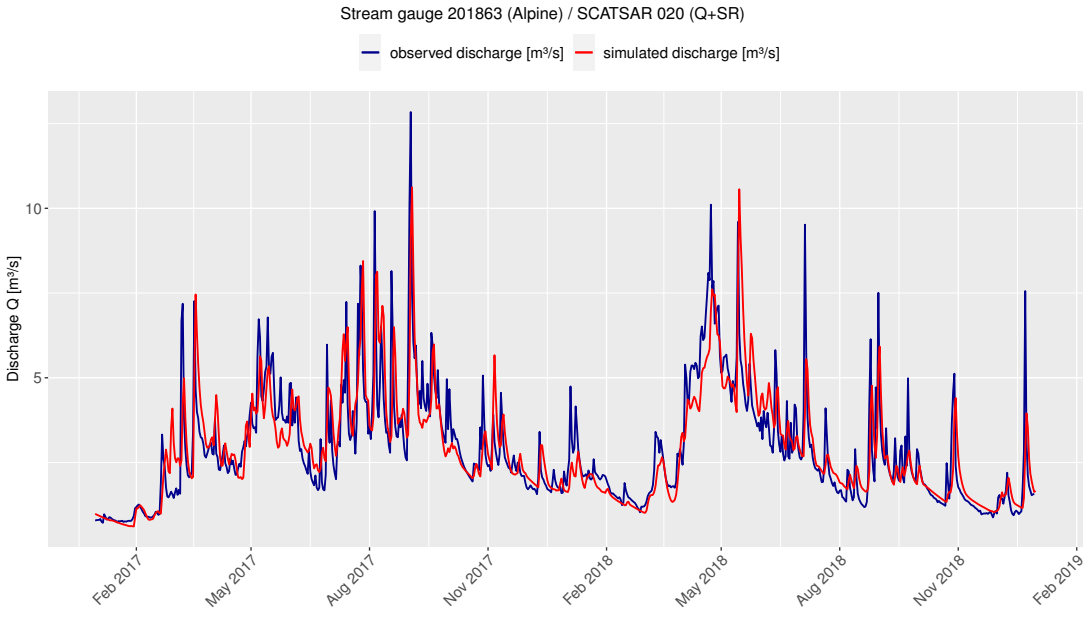

Fig. 7.4: Simulation results of the model calibrated to runoff and soil moisture in the root-zone layer (Q+SR) using the SCATSAR 020 satellite product for the Alpine catchment of stream gauge 201863, over the period from December 31, 2016, to December 31, 2018.

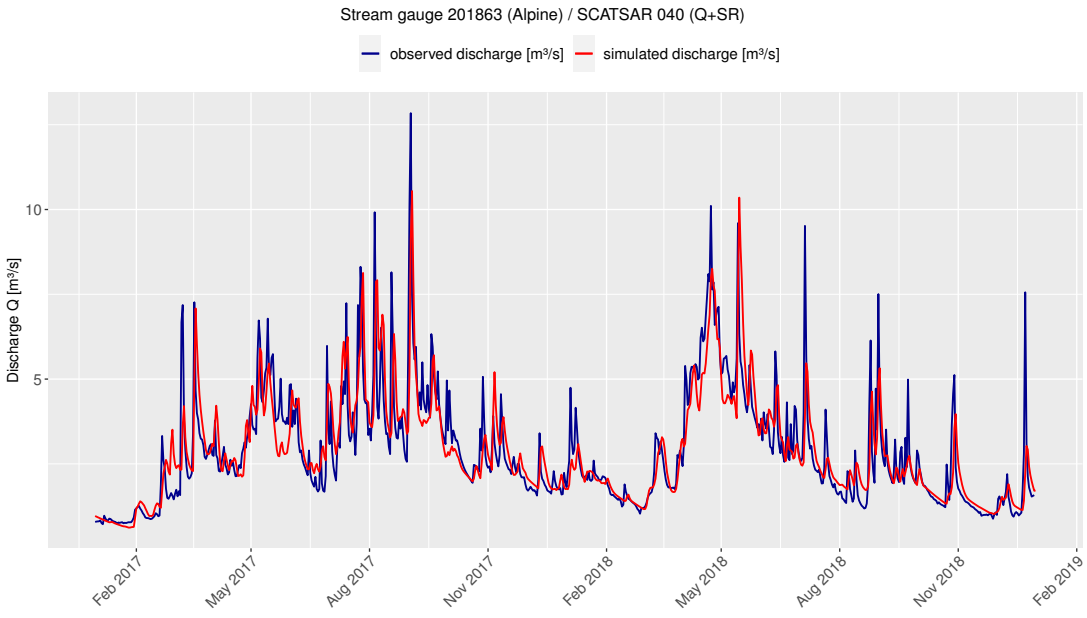

Fig. 7.5: Simulation results of the model calibrated to runoff and soil moisture in the root-zone layer (Q+SR) using the SCATSAR 040 satellite product for the Alpine catchment of stream gauge 201863, over the period from December 31, 2016, to December 31, 2018.

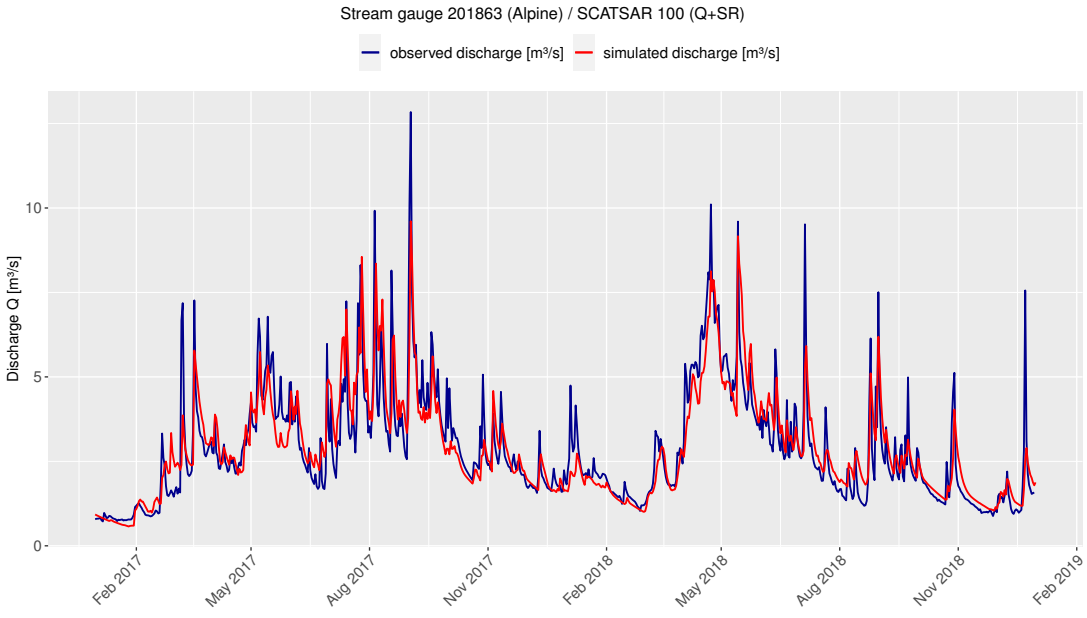

Fig. 7.6: Simulation results of the model calibrated to runoff and soil moisture in the root-zone layer (Q+SR) using the SCATSAR 100 satellite product for the Alpine catchment of stream gauge 201863, over the period from December 31, 2016, to December 31, 2018.

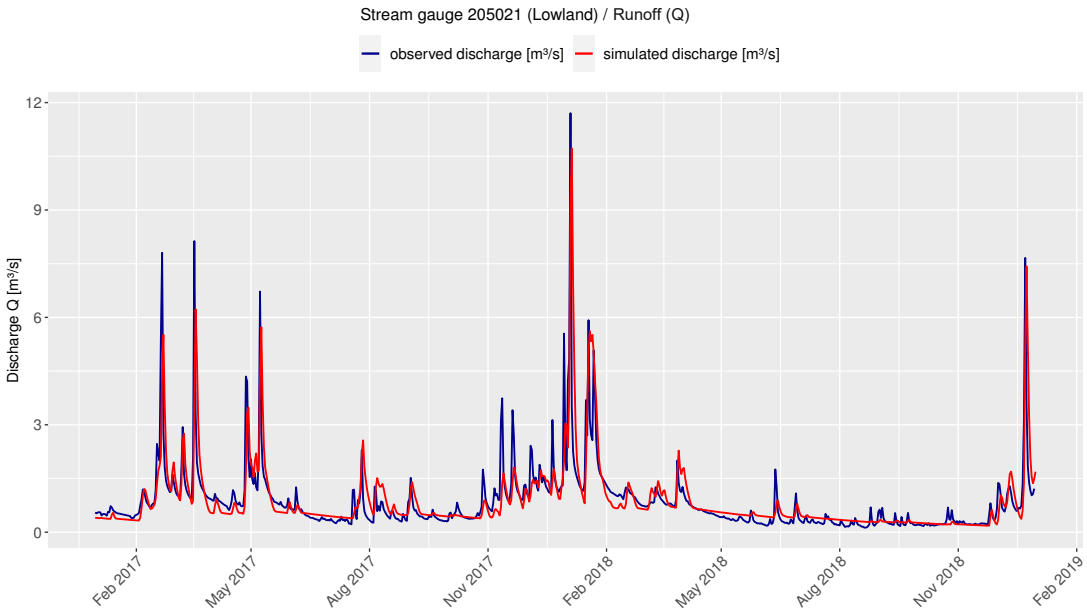

Fig. 7.7: Simulation results of the model calibrated to runoff only (Q) for the Lowland catchment of stream gauge 205021, over the period from December 31, 2016, to December 31, 2018.8

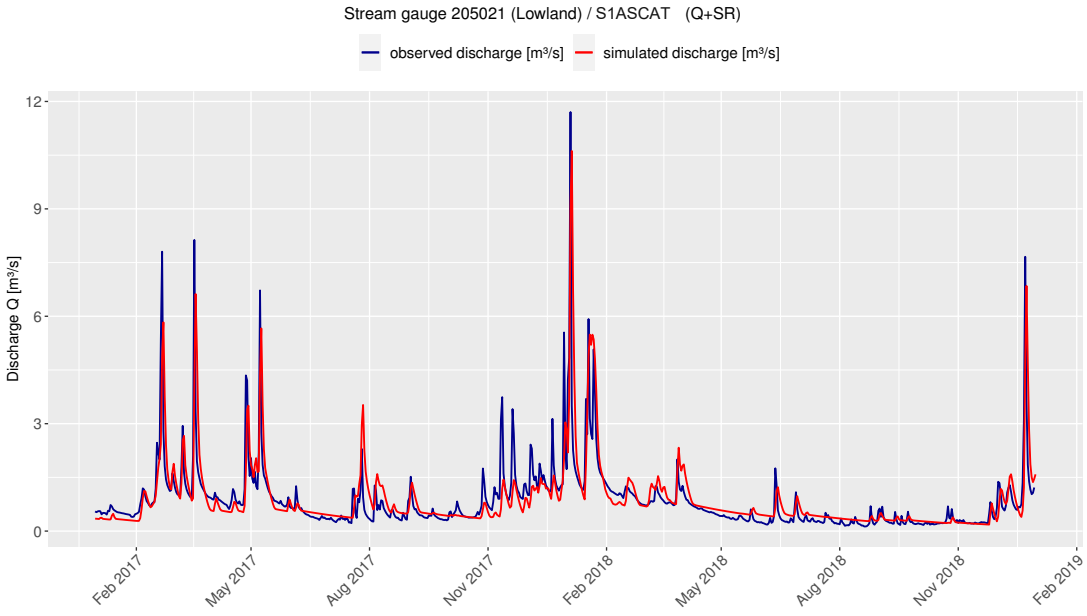

Fig. 7.8: Simulation results of the model calibrated to runoff and soil moisture in the root-zone layer (Q+SR) using the S1ASCAT satellite product for the Lowland catchment of stream gauge 205021, over the period from December 31, 2016, to December 31, 2018.

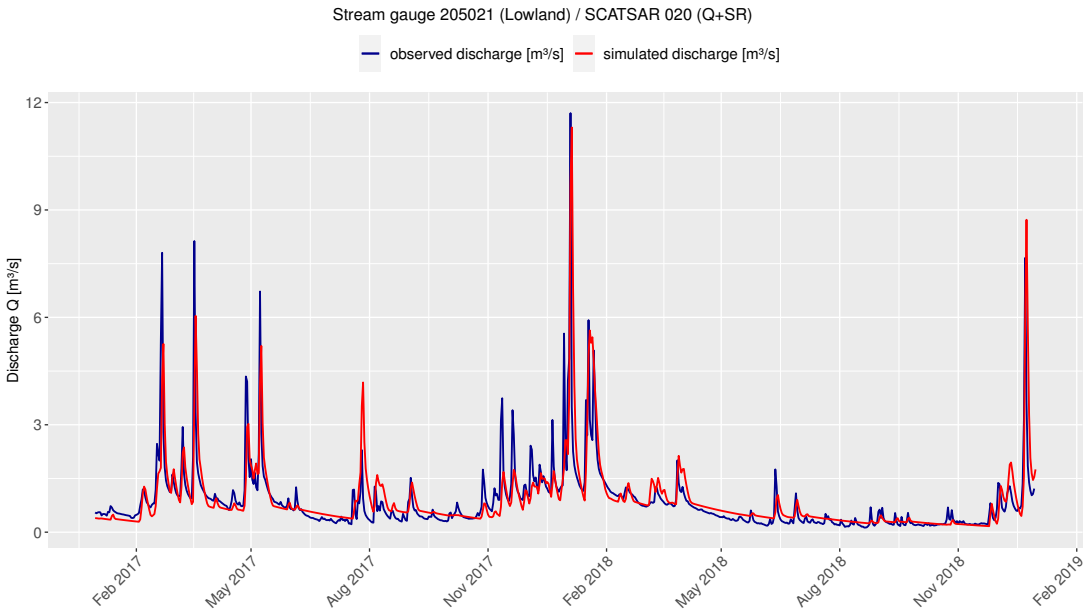

Fig. 7.9: Simulation results of the model calibrated to runoff and soil moisture in the root-zone layer (Q+SR) using the SCATSAR 020 satellite product for the Lowland catchment of stream gauge 205021, over the period from December 31, 2016, to December 31, 2018.

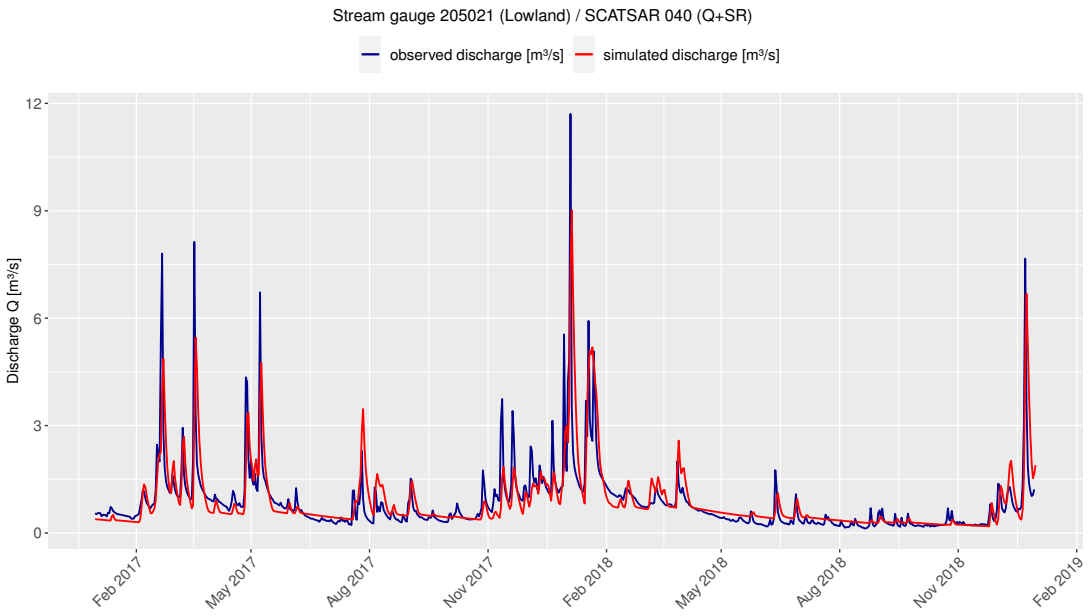

Fig. 7.10: Simulation results of the model calibrated to runoff and soil moisture in the root-zone layer (Q+SR) using the SCATSAR 040 satellite product for the Lowland catchment of stream gauge 205021, over the period from December 31, 2016, to December 31, 2018.

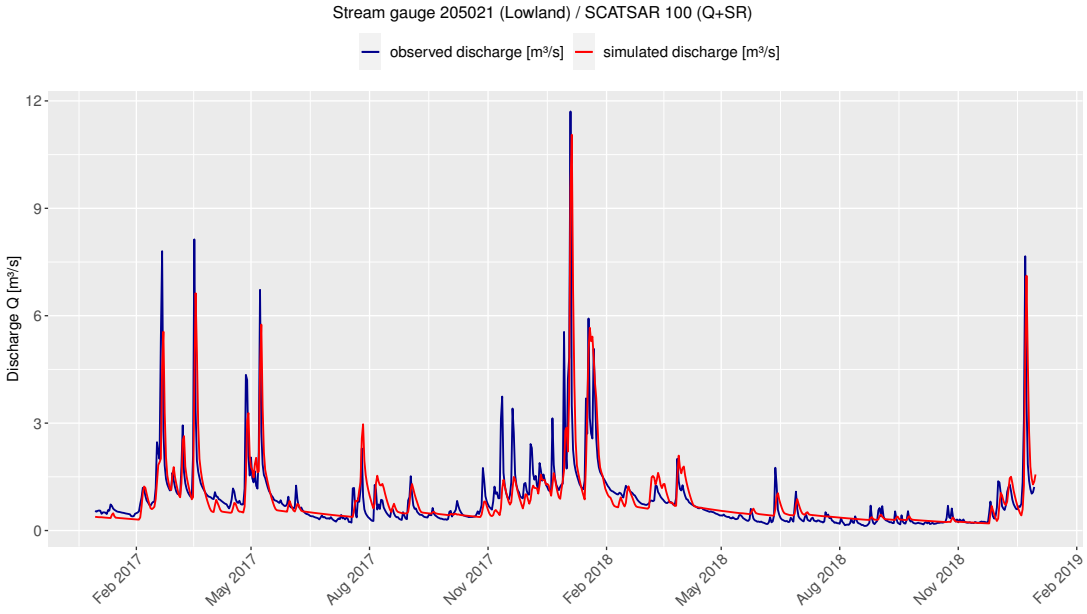

Fig. 7.11: Simulation results of the model calibrated to runoff and soil moisture in the root-zone layer (Q+SR) using the SCATSAR 100 satellite product for the Lowland catchment of stream gauge 205021, over the period from December 31, 2016, to December 31, 2018.

The NSE Values

The values of the Nash-Sutcliffe Efficiency Coefficient (NSE) calibrated to the runoff only (Q) and the runoff and soil moisture in the root-zone layer (Q+SR) using the four different satellite products (S1ASCAT, SCATSAR 020, SCATSAR 040, and SCATSAR 100) in the 196 Austrian catchments, during the calibration period from September 2014 to December 2020, are listed in the Table 7.11 to Table 7.15.

The KGE Values

The values of the Kling-Gupta Efficiency (KGE) calibrated to the runoff only (Q) and the runoff and soil moisture in the root-zone layer (Q+SR) using the four different satellite products (S1ASCAT, SCATSAR 020, SCATSAR 040, and SCATSAR 100) in the 196 Austrian catchments, during the calibration period from September 2014 to December 2020, are listed in the Table 7.16 to Table 7.20.

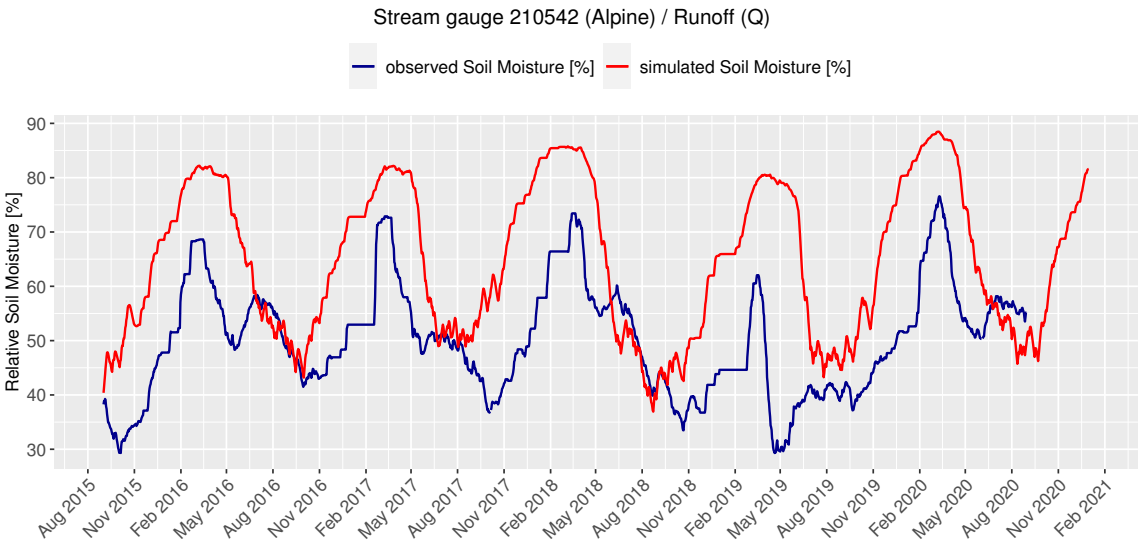

Fig. 7.12: Simulation results of the model calibrated to runoff only (Q) the Alpine catchment of stream gauge 210542, over the period from September 1, 2015, to December 31, 2020.

7.2.1.2 Soil Moisture Model Efficiency

In order to assess the model efficiency in simulating soil moisture during the calibration period one Alpine (210542 - Altaussee) and one Lowland (204925 - Hartmannsdorf) catchment were selected. The correlation coefficients (r_{SR}) in these chosen catchments indicate a better fit with S1ASCAT compared to SCATSAR 020/040/100.

Hydrographs - Alpine Stream Gauge 210542

Figures 7.12 to 7.16 depict the simulation results of the model calibration for the stream gauge 210542, situated in Alpine. Observed soil moisture hydrographs are shown in blue, with masked segments indicating unavailable data, and simulated soil moisture hydrographs are shown in red. The selected time series corresponds to the calibration period, i.e., from September 1, 2015, to December 31, 2020, excluding the 1-year warm-up period. The hydrographs are plotted for only one specific 200-meter hypsometrical elevation zone within the respective catchment.

Hydrographs - Lowland Stream Gauge 204925

Figures 7.17 to 7.21 depict the simulation results of the model calibration for the stream gauge 204925, situated in Lowland. Observed soil moisture hydrographs are shown in blue, with masked segments indicating unavailable data, and simulated soil moisture hydrographs are shown in red. The selected time series corresponds to the calibration period, i.e., from September 1, 2015, to December 31, 2020, excluding the 1-year warm-up period. The hydrographs are plotted for only one specific 200-meter hypsometrical elevation zone within the respective catchment.

Correlation Coefficient Values

The values of the correlation coefficient (r_{SR}) for the runoff only (Q) and the runoff and soil moisture in the root-zone layer (Q+SR) calibration variants using the four different satellite products (S1ASCAT, SCATSAR 020, SCATSAR 040, and SCATSAR 100) during the calibration period from September 2014 to December 2020, are listed in the Table 7.21 to Table 7.25.

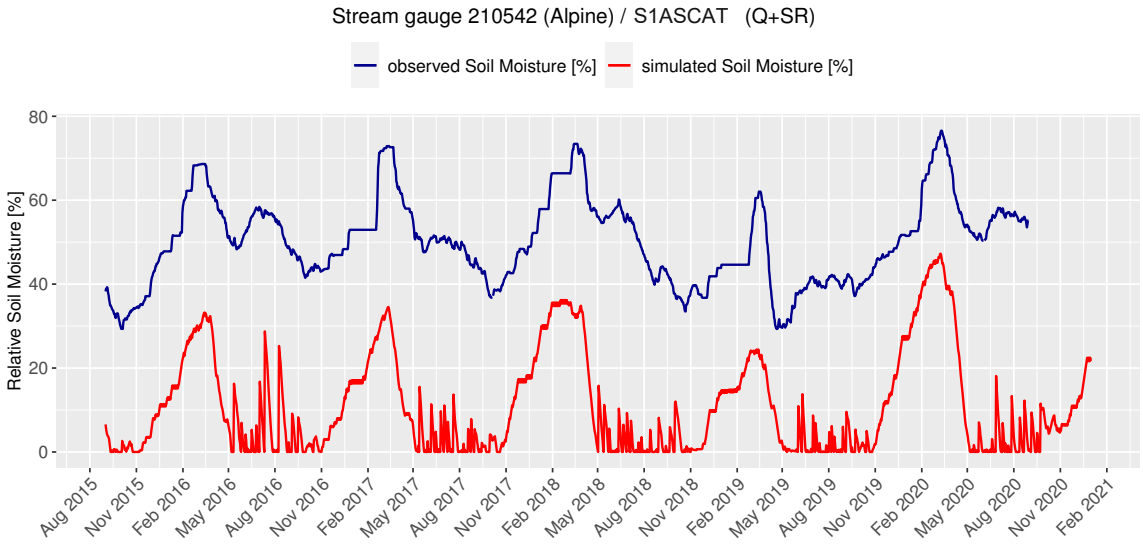

Fig. 7.13: Simulation results of the model calibrated to runoff and soil moisture in the root-zone layer (Q+SR) using the S1ASCAT satellite product for the Alpine catchment of stream gauge 210542, over the period from September 1, 2015, to December 31, 2020.

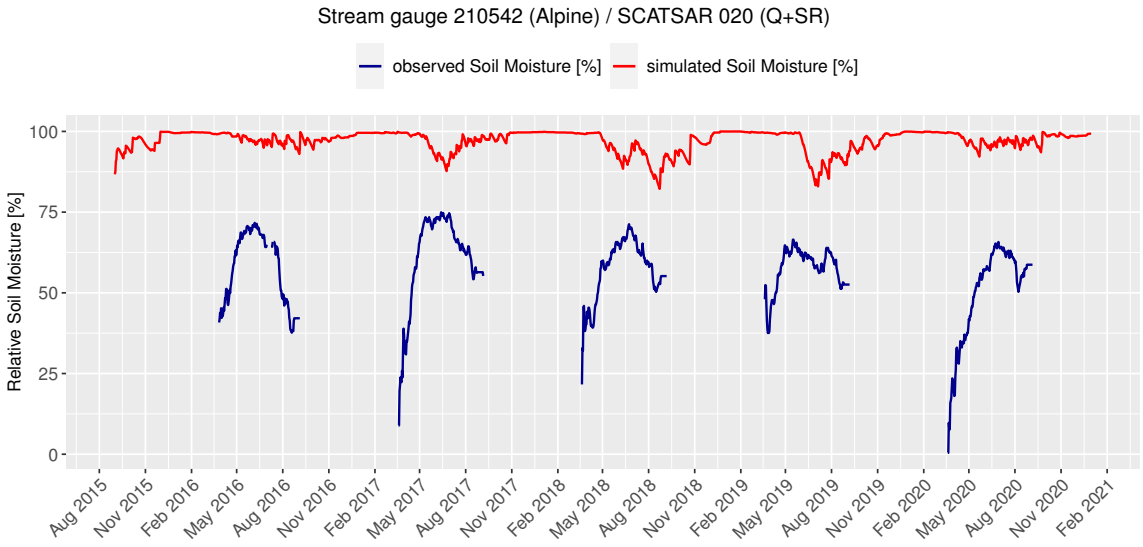

Fig. 7.14: Simulation results of the model calibrated to runoff and soil moisture in the root-zone layer (Q+SR) using the SCATSAR 020 satellite product for the Alpine catchment of stream gauge 210542, over the period from September 1, 2015, to December 31, 2020.

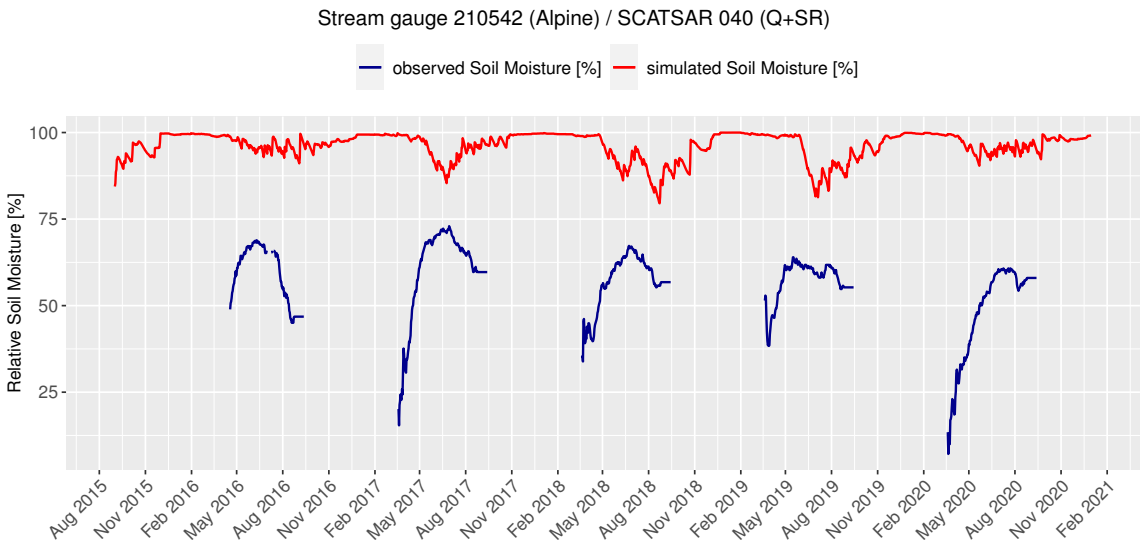

Fig. 7.15: Simulation results of the model calibrated to runoff and soil moisture in the root-zone layer (Q+SR) using the SCATSAR 040 satellite product for the Alpine catchment of stream gauge 210542, over the period from September 1, 2015, to December 31, 2020.

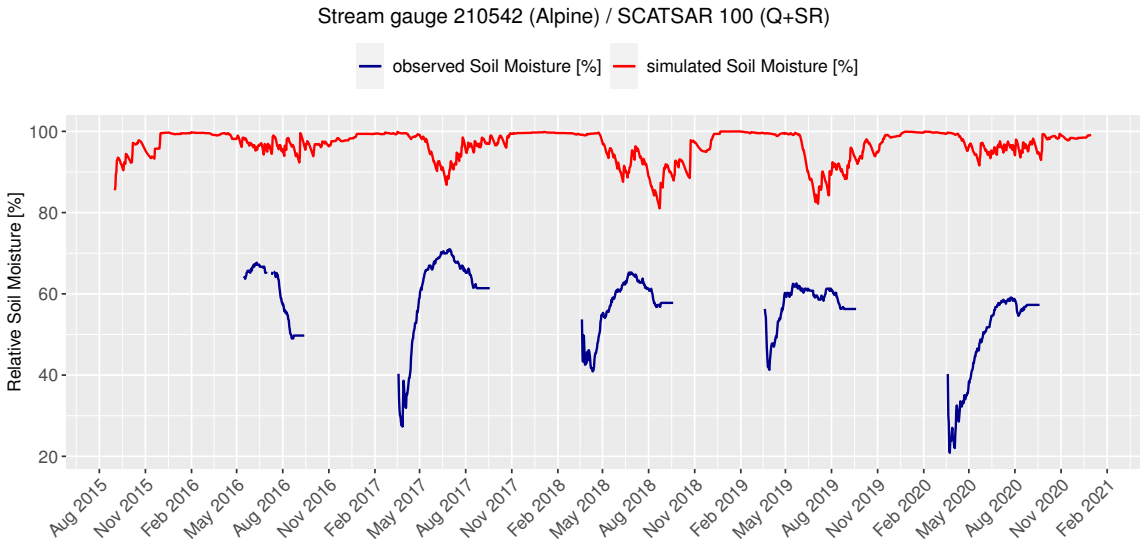

Fig. 7.16: Simulation results of the model calibrated to runoff and soil moisture in the root-zone layer (Q+SR) using the SCATSAR 100 satellite product for the Alpine catchment of stream gauge 210542, over the period from September 1, 2015, to December 31, 2020.

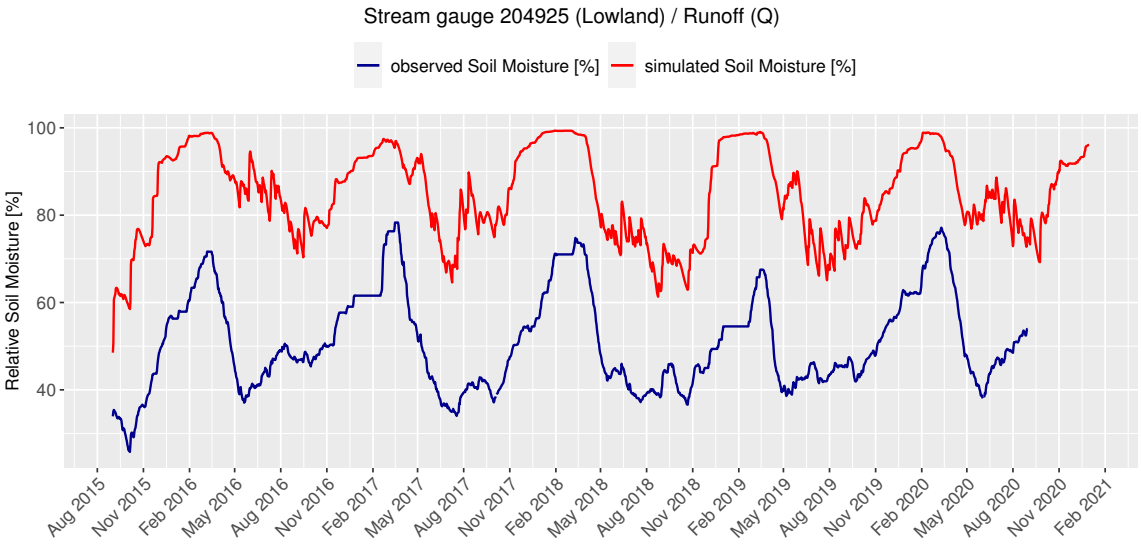

Fig. 7.17: Simulation results of the model calibrated to runoff only (Q) the Lowland catchment of stream gauge 20492, over the period from September 1, 2015, to December 31, 2020.

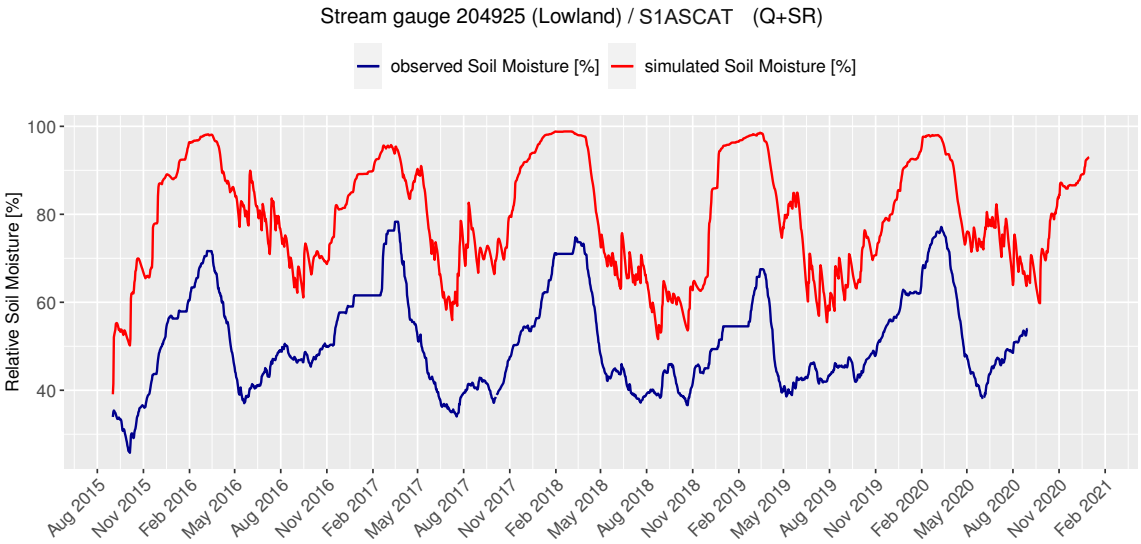

Fig. 7.18: Simulation results of the model calibrated to runoff and soil moisture in the root-zone layer (Q+SR) using the S1ASCAT satellite product for the Lowland catchment of stream gauge 20492, over the period from September 1, 2015, to December 31, 2020.

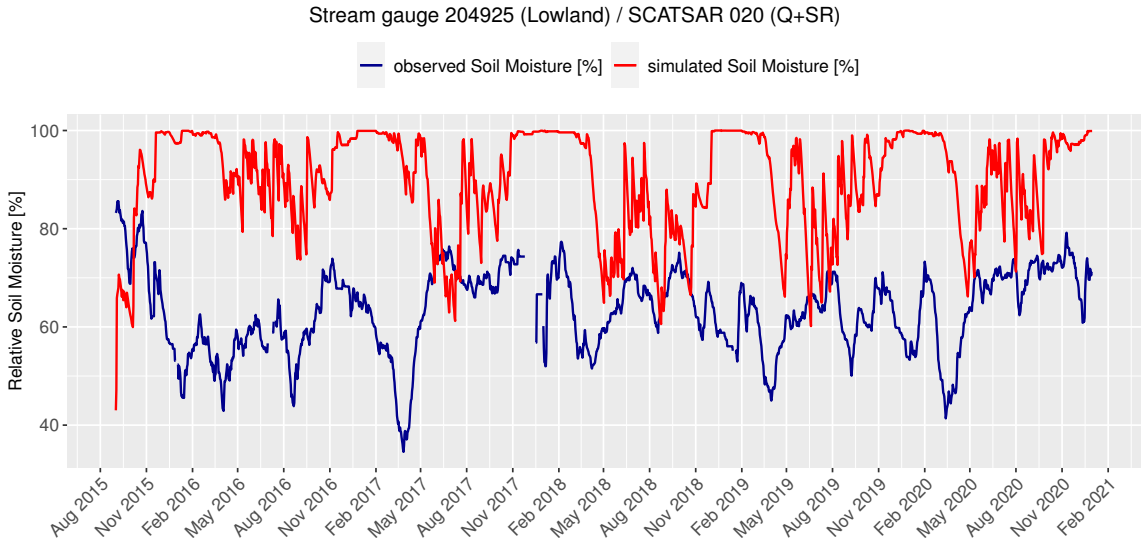

Fig. 7.19: Simulation results of the model calibrated to runoff and soil moisture in the root-zone layer (Q+SR) using the SCATSAR 020 satellite product for the Lowland catchment of stream gauge 20492, over the period from September 1, 2015, to December 31, 2020.

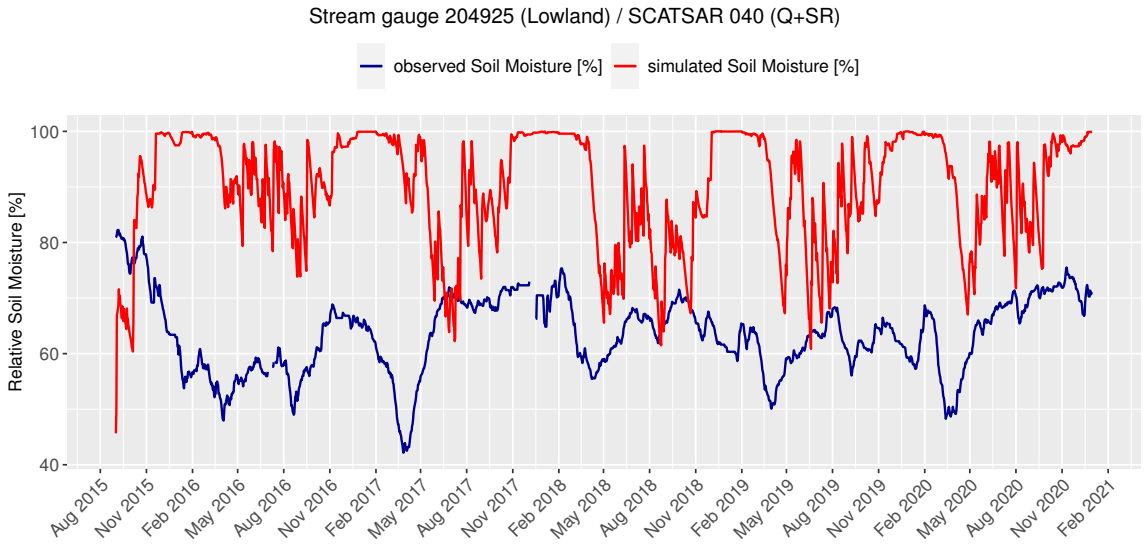

Fig. 7.20: Simulation results of the model calibrated to runoff and soil moisture in the root-zone layer (Q+SR) using the SCATSAR 020 satellite product for the Lowland catchment of stream gauge 20492, over the period from September 1, 2015, to December 31, 2020.

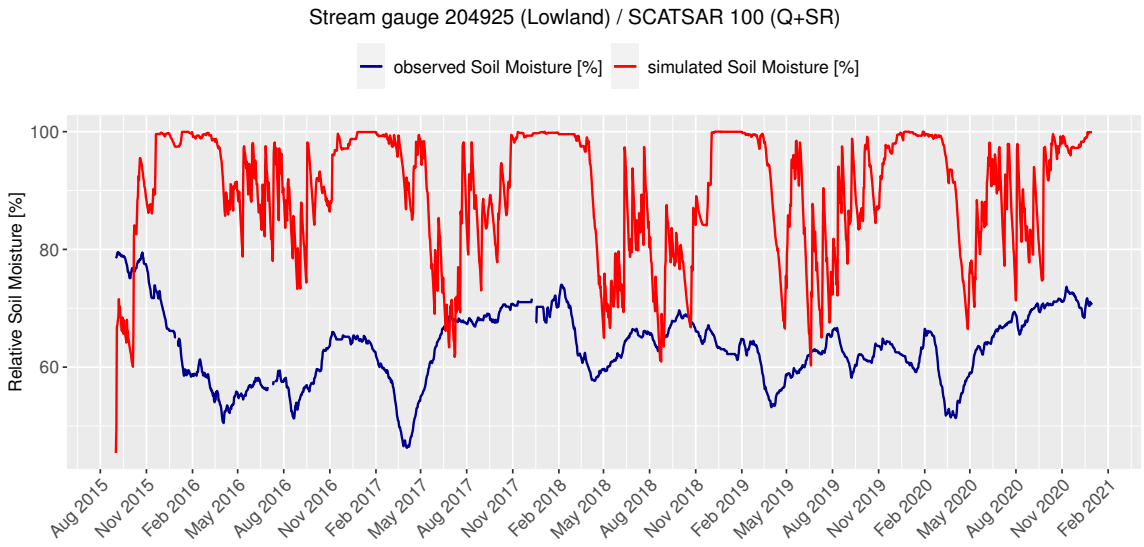

Fig. 7.21: Simulation results of the model calibrated to runoff and soil moisture in the root-zone layer (Q+SR) using the SCATSAR 020 satellite product for the Lowland catchment of stream gauge 20492, over the period from September 1, 2015, to December 31, 2020.

7.2.2 Validation Period

7.2.2.1 Runoff Model Efficiency

To visually assess the runoff model efficiency during the validation period, hydrographs of the same selected stream gauges in 7.2.1 were chosen for comparison.

Hydrographs - Alpine Stream Gauge 201863
Figures 7.22 to 7.26 depict the simulation results of the model validation for the stream gauge 201863, situated in Alpine. Observed discharge hydrographs are shown in blue, and simulated discharge hydrographs are shown in red. For better clarity of the hydrographs, a two-year period from August 31, 2012, to August 31, 2014, was selected.

Hydrographs - Lowland Stream Gauge 205021
Figures 7.27 to 7.31 depict the simulation results of the model validation for the stream gauge 205021, situated in Lowland. Observed discharge hydrographs are shown in blue, and simulated discharge hydrographs are shown in red. For better clarity of the hydrographs, a two-year period from August 31, 2012, to August 31, 2014, was selected.

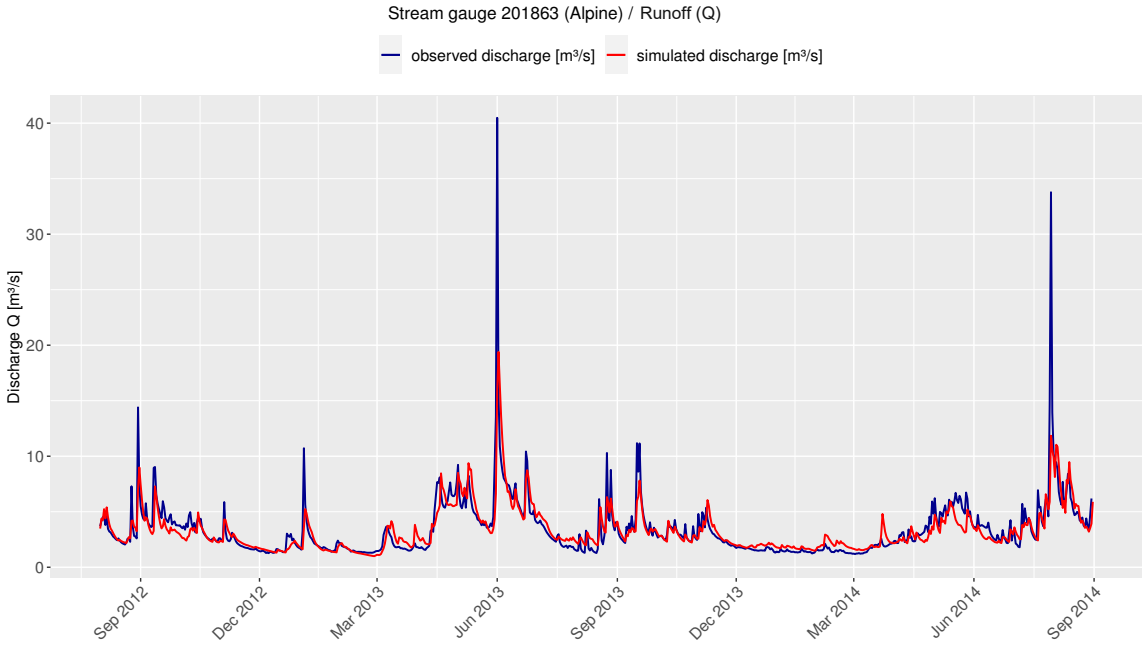

Fig. 7.22: Simulation results of the model validated with parameters calibrated to runoff only (Q) the Alpine catchment of stream gauge 201863, over the period from August 31, 2012, to August 31, 2014.

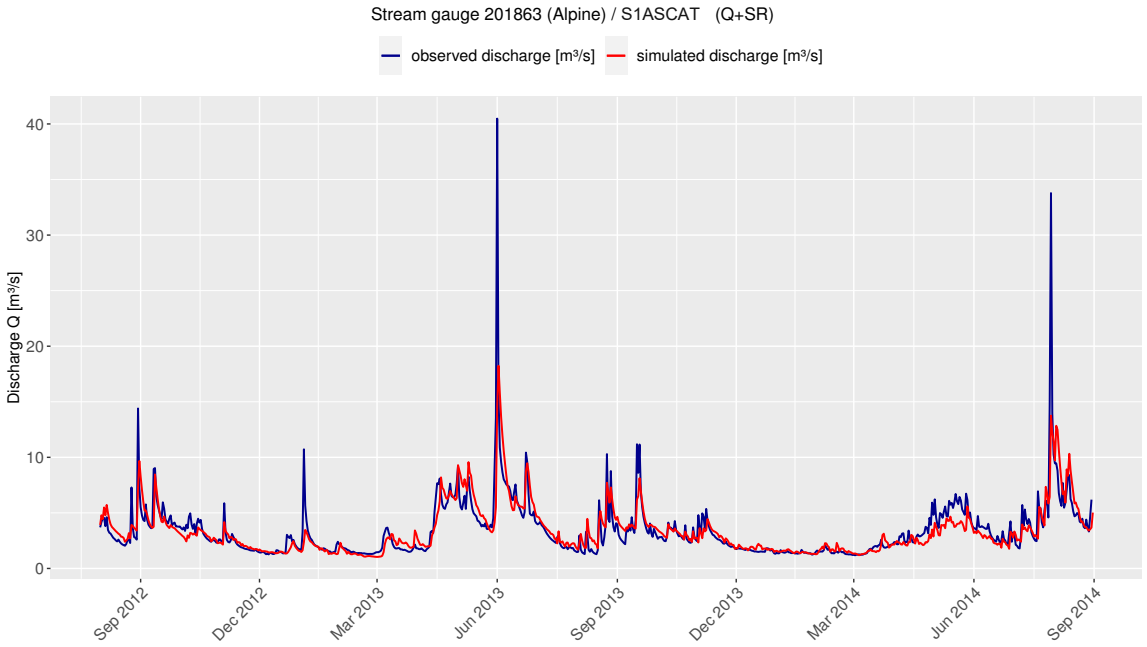

Fig. 7.23: Simulation results of the model validated with parameters calibrated to runoff and soil moisture in the root-zone layer (Q+SR) using the S1ASCAT satellite product for the Alpine catchment of stream gauge 201863, over the period from August 31, 2012, to August 31, 2014.

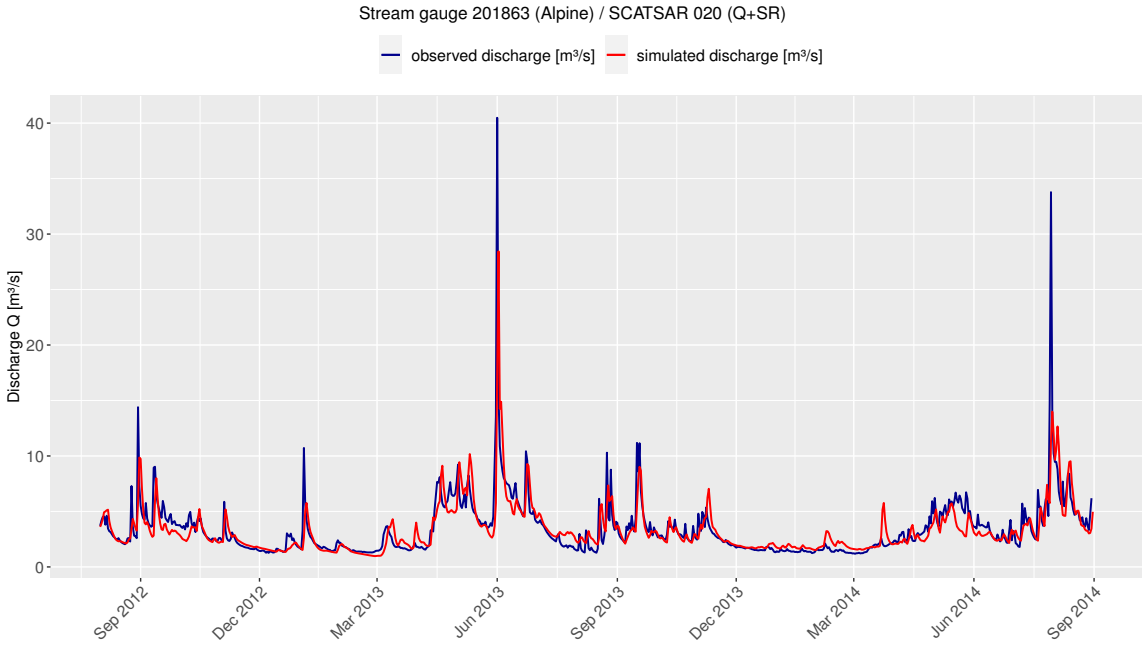

Fig. 7.24: Simulation results of the model validated with parameters calibrated to runoff and soil moisture in the root-zone layer (Q+SR) using the SCATSAR 020 satellite product for the Alpine catchment of stream gauge 201863, over the period from August 31, 2012, to August 31, 2014.

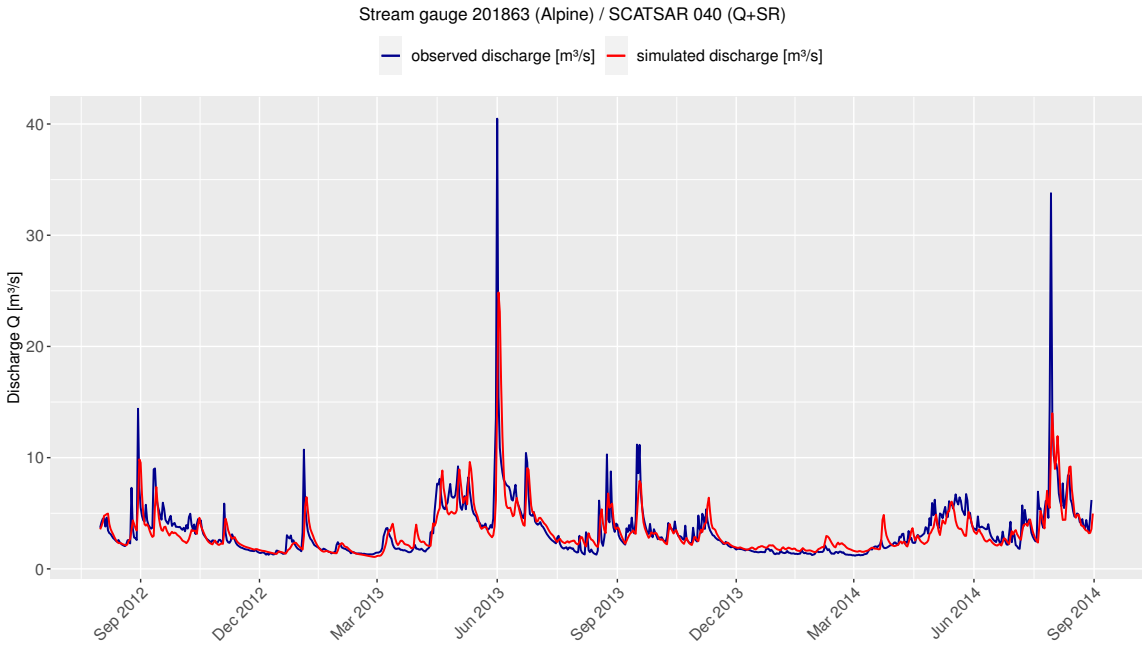

Fig. 7.25: Simulation results of the model validated with parameters calibrated to runoff and soil moisture in the root-zone layer (Q+SR) using the SCATSAR 040 satellite product for the Alpine catchment of stream gauge 201863, over the period from August 31, 2012, to August 31, 2014.

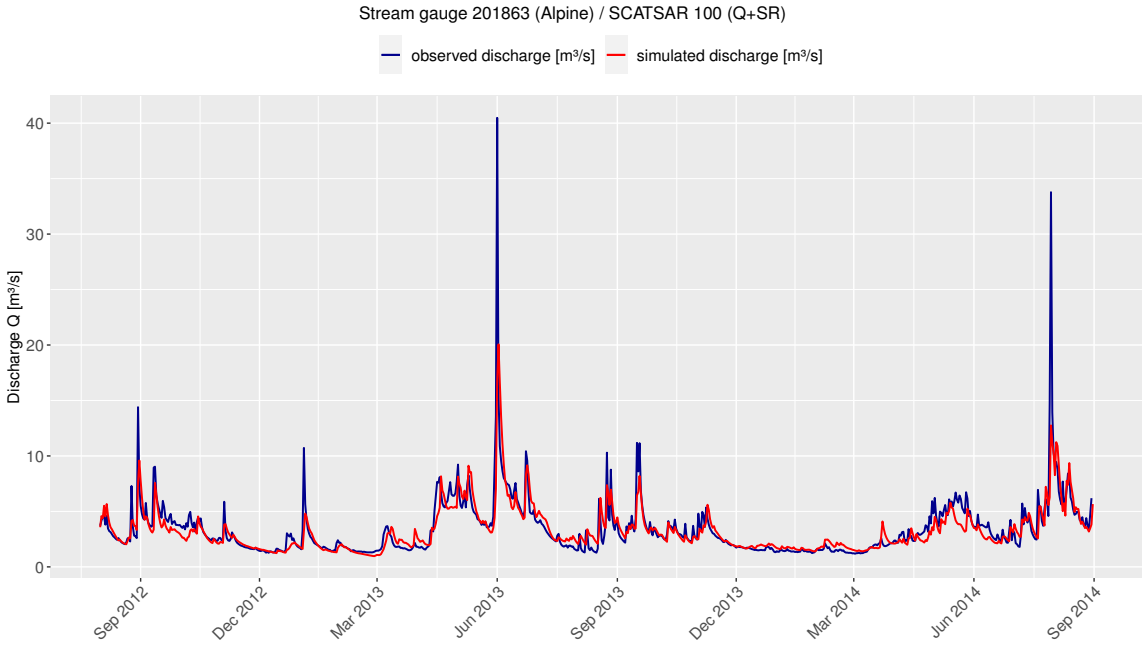

Fig. 7.26: Simulation results of the model validated with parameters calibrated to runoff and soil moisture in the root-zone layer (Q+SR) using the SCATSAR 100 satellite product for the Alpine catchment of stream gauge 201863, over the period from August 31, 2012, to August 31, 2014.

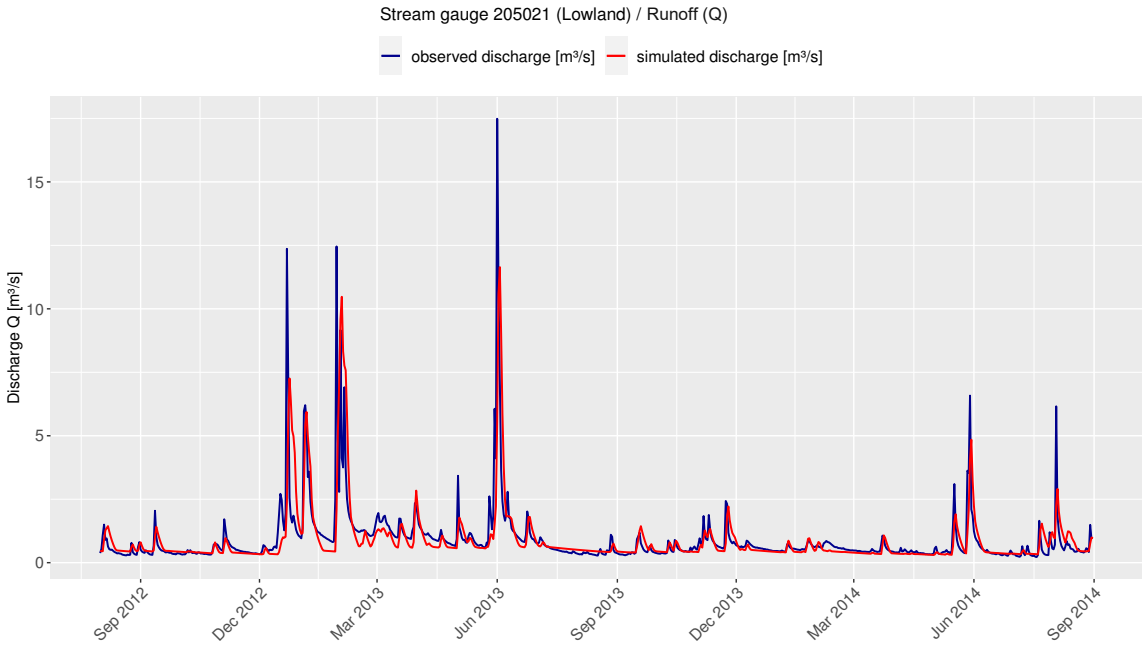

Fig. 7.27: Simulation results of the model validated with parameters calibrated to runoff only (Q) the Lowland catchment of stream gauge 205021, over the period from August 31, 2012, to August 31, 2014.

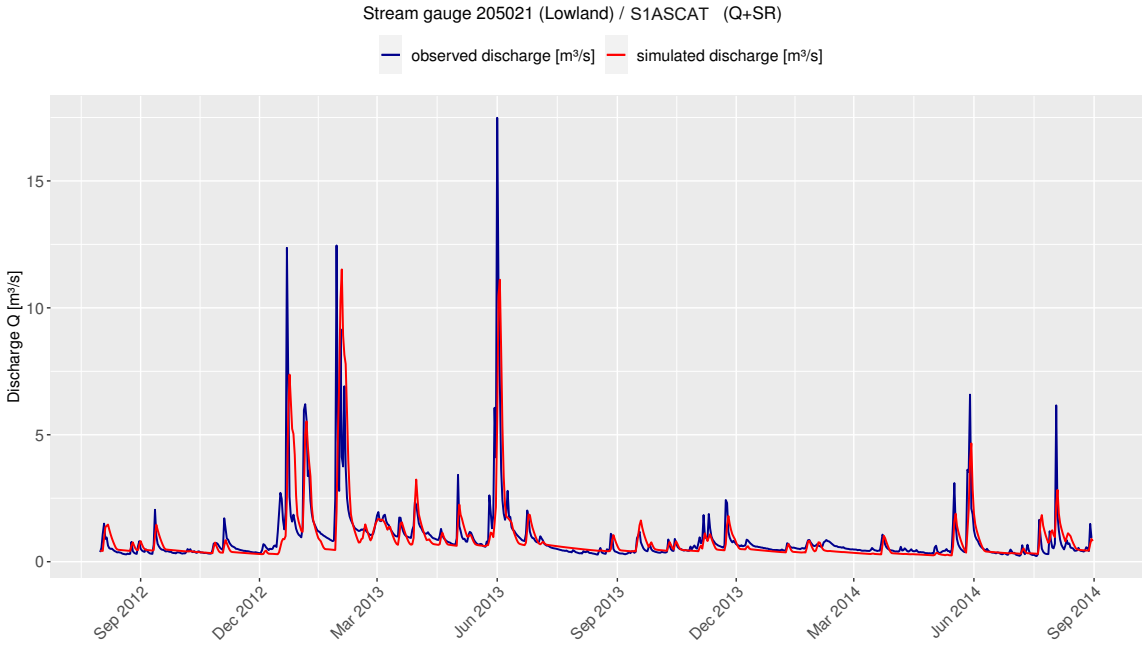

Fig. 7.28: Simulation results of the model validated with parameters calibrated to runoff and soil moisture in the root-zone layer (Q+SR) using the S1ASCAT satellite product for the Lowland catchment of stream gauge 205021, over the period from August 31, 2012, to August 31, 2014.

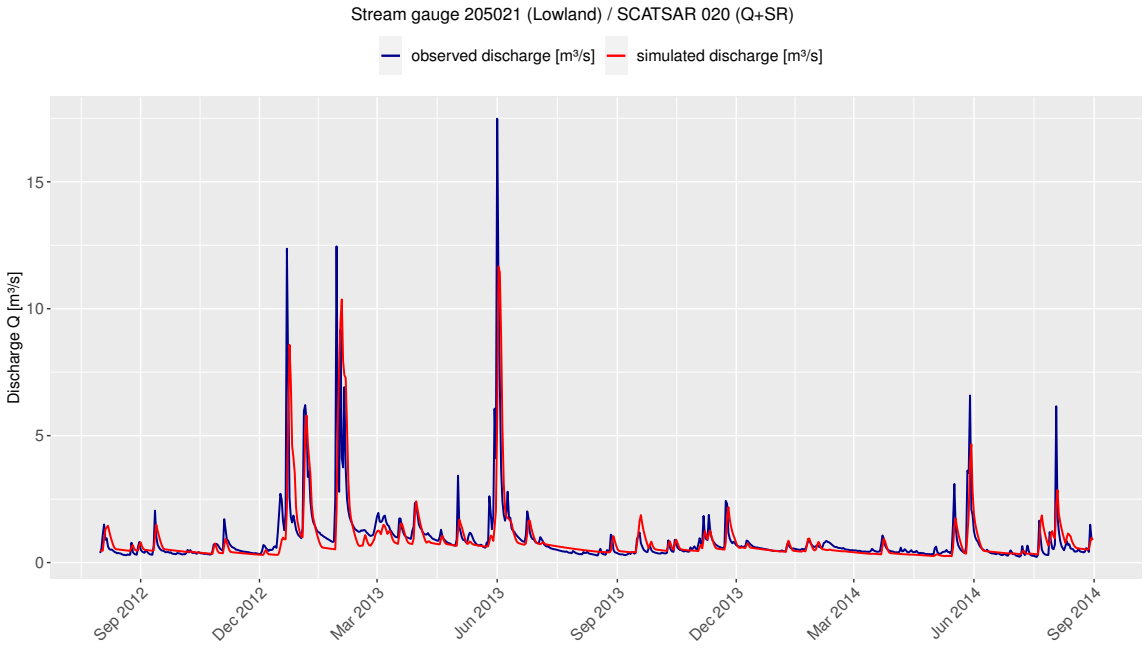

Fig. 7.29: Simulation results of the model validated with parameters calibrated to runoff and soil moisture in the root-zone layer (Q+SR) using the SCATSAR 020 satellite product for the Lowland catchment of stream gauge 205021, over the period from August 31, 2012, to August 31, 2014.

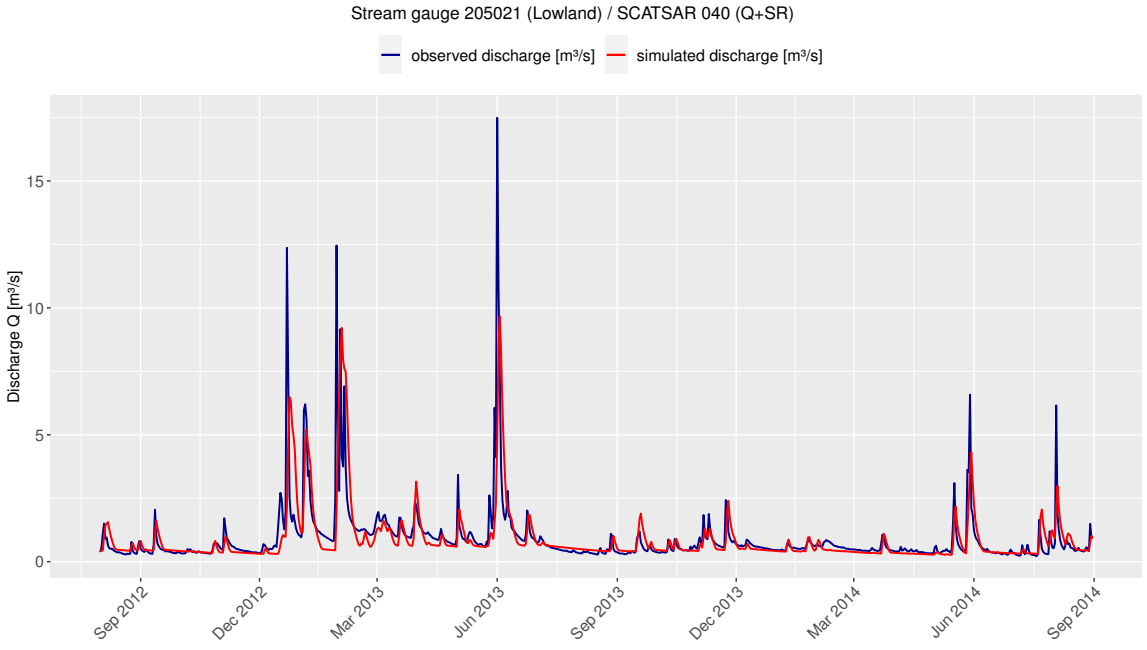

Fig. 7.30: Simulation results of the model validated with parameters calibrated to runoff and soil moisture in the root-zone layer (Q+SR) using the SCATSAR 040 satellite product for the Lowland catchment of stream gauge 205021, over the period from August 31, 2012, to August 31, 2014.

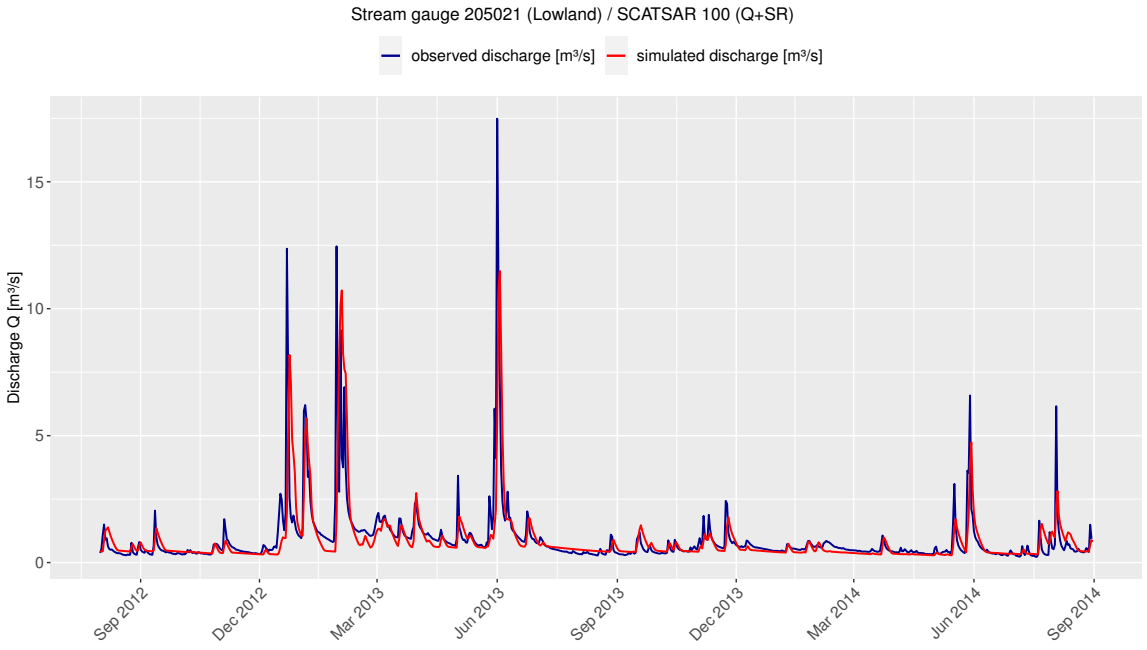

Fig. 7.31: Simulation results of the model validated with parameters calibrated to runoff and soil moisture in the root-zone layer (Q+SR) using the SCATSAR 100 satellite product for the Lowland catchment of stream gauge 205021, over the period from August 31, 2012, to August 31, 2014.

The Nash-Sutcliffe Efficiency Coefficient Values

The values of the Nash-Sutcliffe Efficiency Coefficient (NSE) calibrated to the runoff only (Q) and the runoff and soil moisture in the root-zone layer (Q+SR) using the four different satellite products (S1ASCAT, SCATSAR 020, SCATSAR 040, and SCATSAR 100) in the 196 Austrian catchments, during the validation period from September 2009 to August 2014, are listed in the Table 7.26 to Table 7.30.

The Kling-Gupta Efficiency Values

The values of the Kling-Gupta Efficiency (KGE) calibrated to the runoff only (Q) and the runoff and soil moisture in the root-zone layer (Q+SR) using the four different satellite products (S1ASCAT, SCATSAR 020, SCATSAR 040, and SCATSAR 100) during the validation period from September 2009 to August 2014, are listed in the Table 7.31 to Table 7.35.

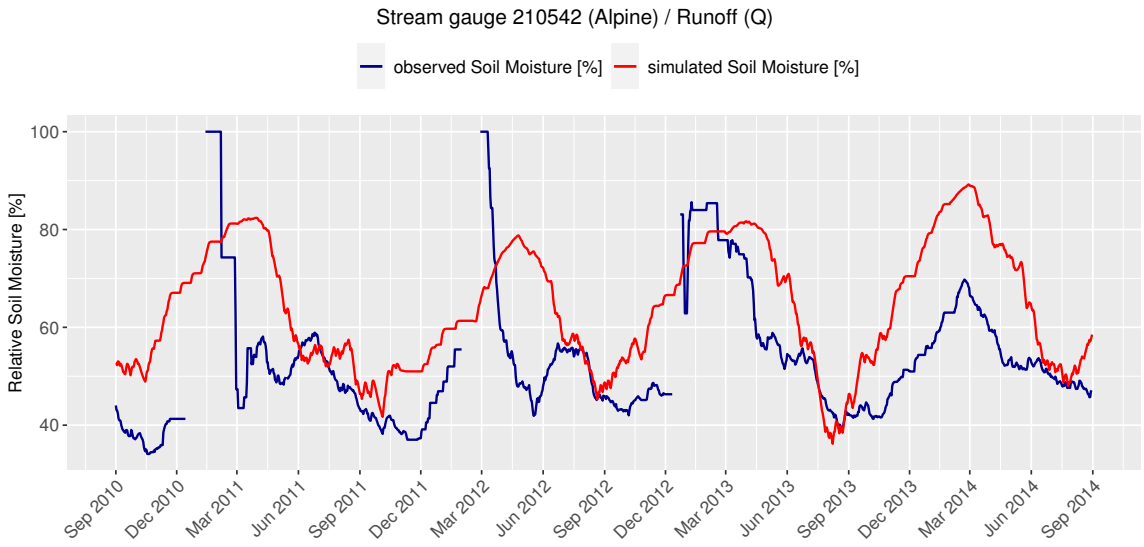

Fig. 7.32: Simulation results of the model validation, calibrated to runoff only (Q) the Alpine catchment of stream gauge 210542, over the period from September 1, 2010, to August 31, 2014.

7.2.2.2 Soil Moisture Model Efficiency

In order to assess the model efficiency in simulating soil moisture during the validation period, the same Alpine (210542 - Altaussee) and Lowland (204925 - Hartmannsdorf) catchment were from 7.2.1.2 selected. The correlation coefficients (r_{SR}) in these chosen catchments indicate a better fit with S1ASCAT compared to SCATSAR 020/040/100 .

Hydrographs - Alpine Stream Gauge 210542

Figures 7.32 to 7.36 depict the simulation results of the model validation for the stream gauge 210542, situated in Alpine. Observed soil moisture hydrographs are shown in blue, with masked segments indicating unavailable data, and simulated soil moisture hydrographs are shown in red. The selected time series corresponds to the calibration period, i.e., from September 1, 2010, to August 31, 2014, excluding the 1-year warm-up period. The hydrographs are plotted for only one specific 200-meter hypsometrical elevation zone within the respective catchment.

Hydrographs - Lowland Stream Gauge 204925

Figures 7.37 to 7.41 depict the simulation results of the model validation for the stream gauge 204925, situated in Lowland. Observed soil moisture hydrographs are shown in blue, with masked segments indicating unavailable data, and simulated soil moisture hydrographs are shown in red. The selected time series corresponds to the calibration period, i.e., from September 1, 2010, to August 31, 2014, excluding the 1-year warm-up period. The hydrographs are plotted for only one specific 200-meter hypsometrical elevation zone within the respective catchment.

Correlation Coefficient Values

The values of the correlation coefficient (r_{SR}) for the runoff only (Q) and the runoff and soil moisture in the root-zone layer (Q+SR) calibration vairants using the four different satellite products (S1ASCAT, SCATSAR 020, SCATSAR 040, and SCATSAR 100) during the validation period from September 2009 to August 2014, are listed in the Table 7.36 to Table 7.40.

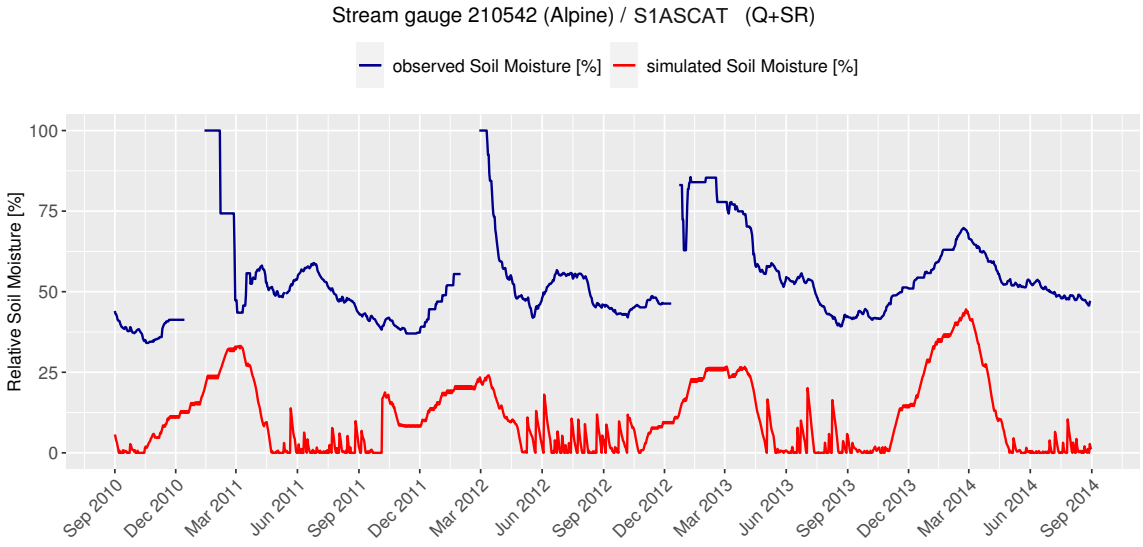

Fig. 7.33: Simulation results of the model validation, calibrated to runoff and soil moisture in the root-zone layer (Q+SR) using the S1ASCAT satellite product for the Alpine catchment of stream gauge 210542, over the period from September 1, 2010, to August 31, 2014.

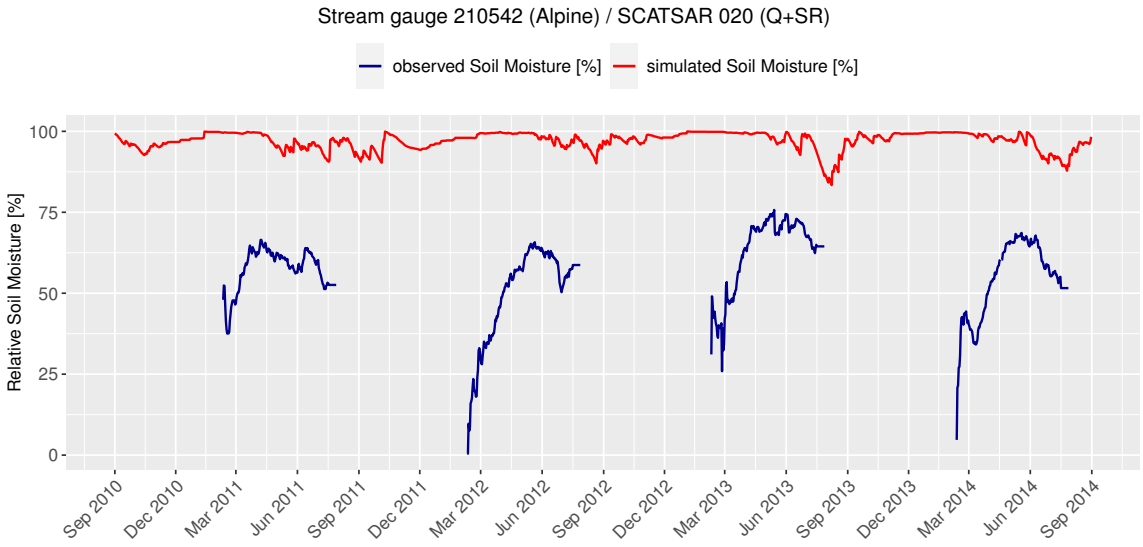

Fig. 7.34: Simulation results of the model validation, calibrated to runoff and soil moisture in the root-zone layer (Q+SR) using the SCATSAR 020 satellite product for the Alpine catchment of stream gauge 210542, over the period from September 1, 2010, to August 31, 2014.

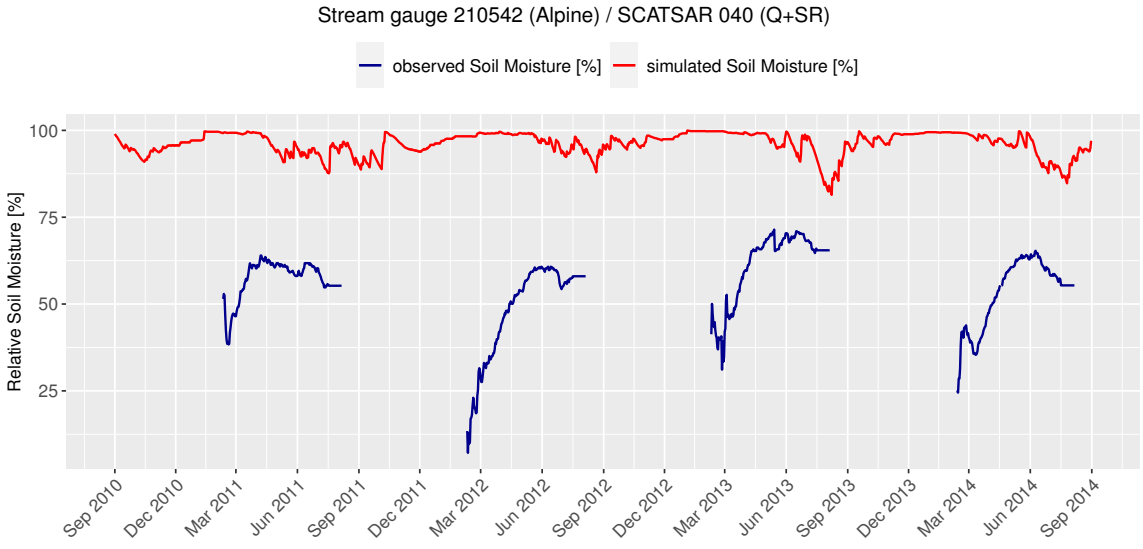

Fig. 7.35: Simulation results of the model validation, calibrated to runoff and soil moisture in the root-zone layer (Q+SR) using the S1ASCAT satellite product for the Alpine catchment of stream gauge 210542, over the period from September 1, 2010, to August 31, 2014.

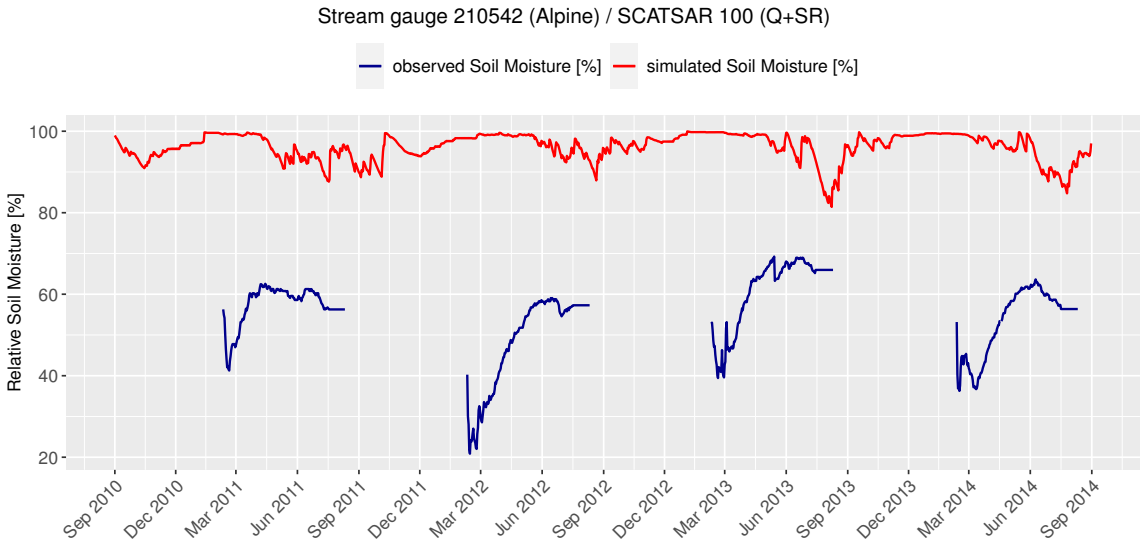

Fig. 7.36: Simulation results of the model validation, calibrated to runoff and soil moisture in the root-zone layer (Q+SR) using the S1ASCAT satellite product for the Alpine catchment of stream gauge 210542, over the period from September 1, 2010, to August 31, 2014.

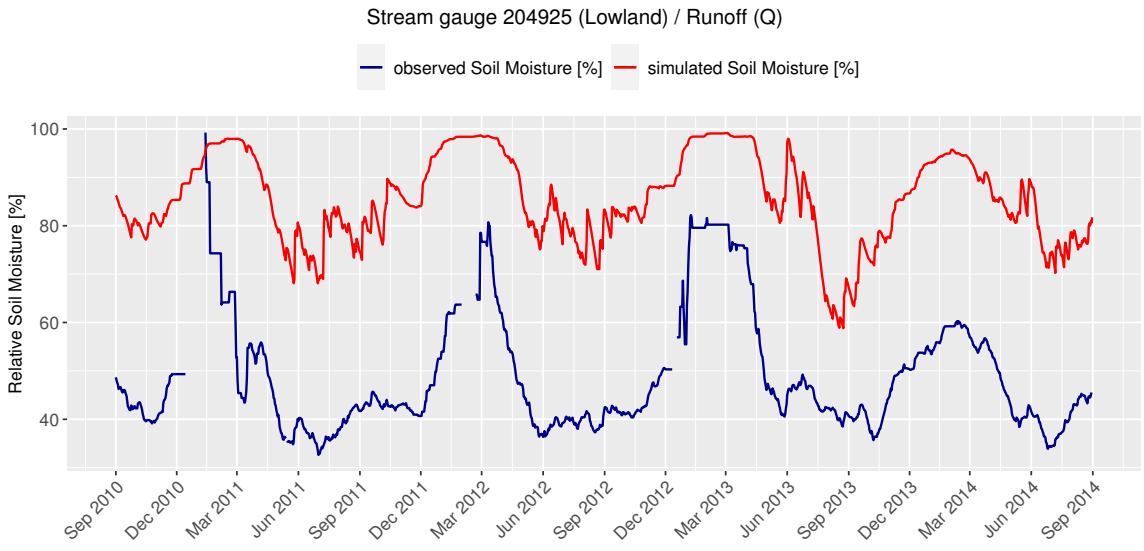

Fig. 7.37: Simulation results of the model validation, calibrated to runoff only (Q) the Lowland catchment of stream gauge 204925, over the period from September 1, 2010, to August 31, 2014.

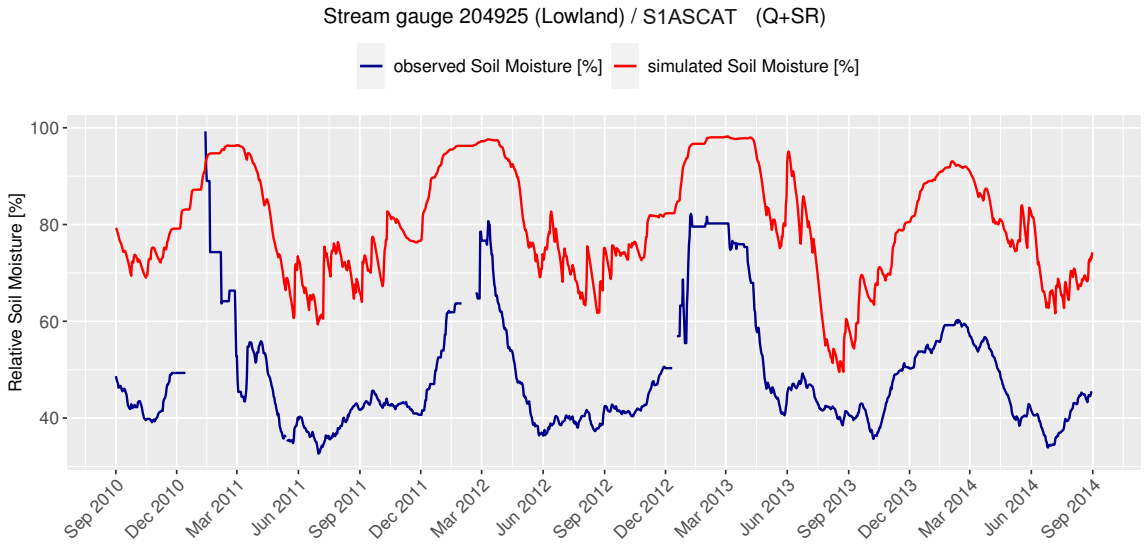

Fig. 7.38: Simulation results of the model validation, calibrated to runoff and soil moisture in the root-zone layer (Q+SR) using the S1ASCAT satellite product for the Lowland catchment of stream gauge 204925, over the period from September 1, 2010, to August 31, 2014.

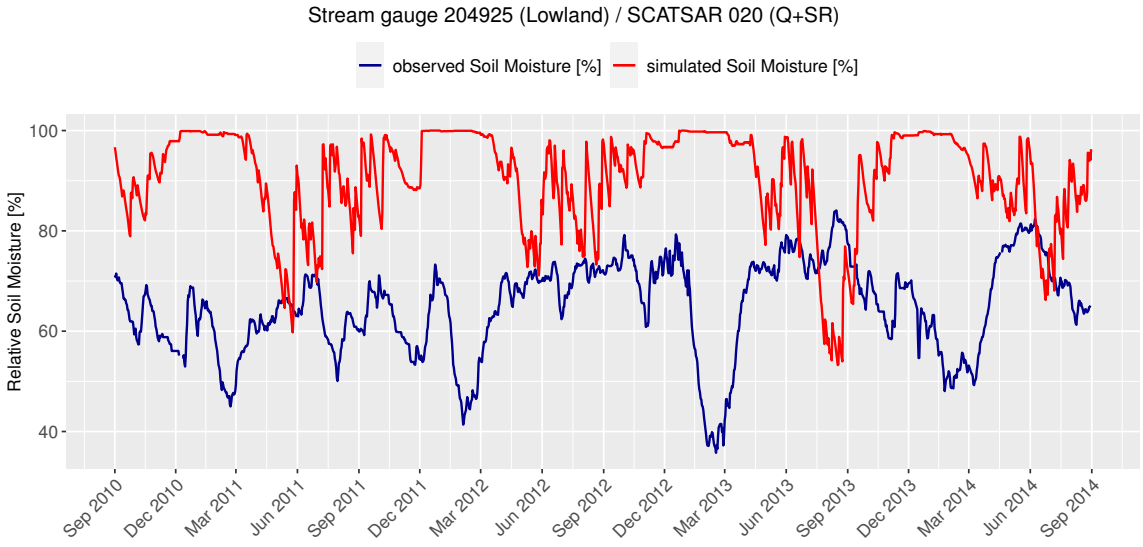

Fig. 7.39: Simulation results of the model validation, calibrated to runoff and soil moisture in the root-zone layer (Q+SR) using the SCATSAR 020 satellite product for the Lowland catchment of stream gauge 204925, over the period from September 1, 2010, to August 31, 2014.

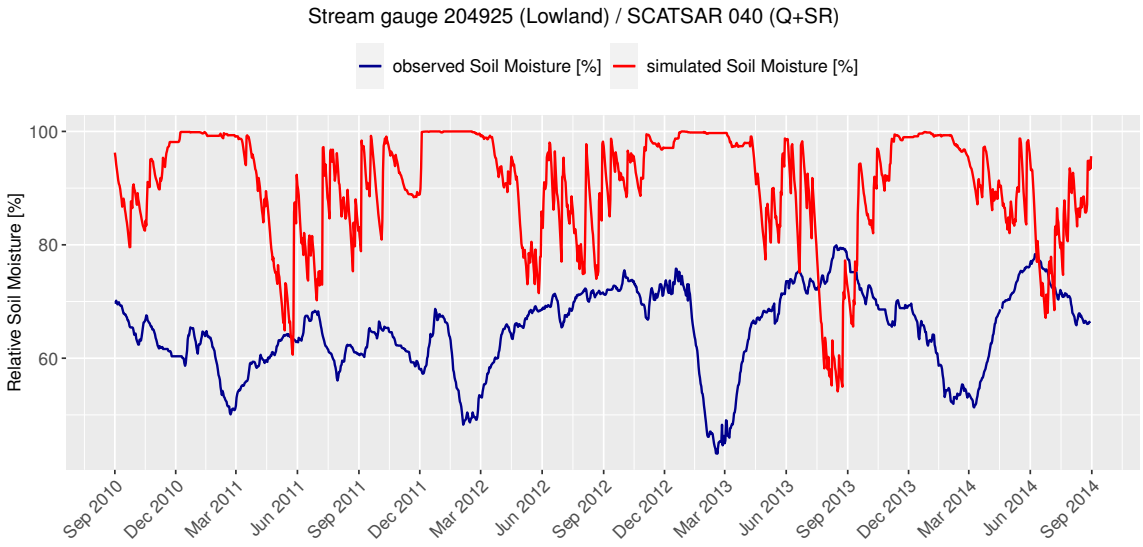

Fig. 7.40: Simulation results of the model validation, calibrated to runoff and soil moisture in the root-zone layer (Q+SR) using the S1ASCAT satellite product for the Lowland catchment of stream gauge 204925, over the period from September 1, 2010, to August 31, 2014.

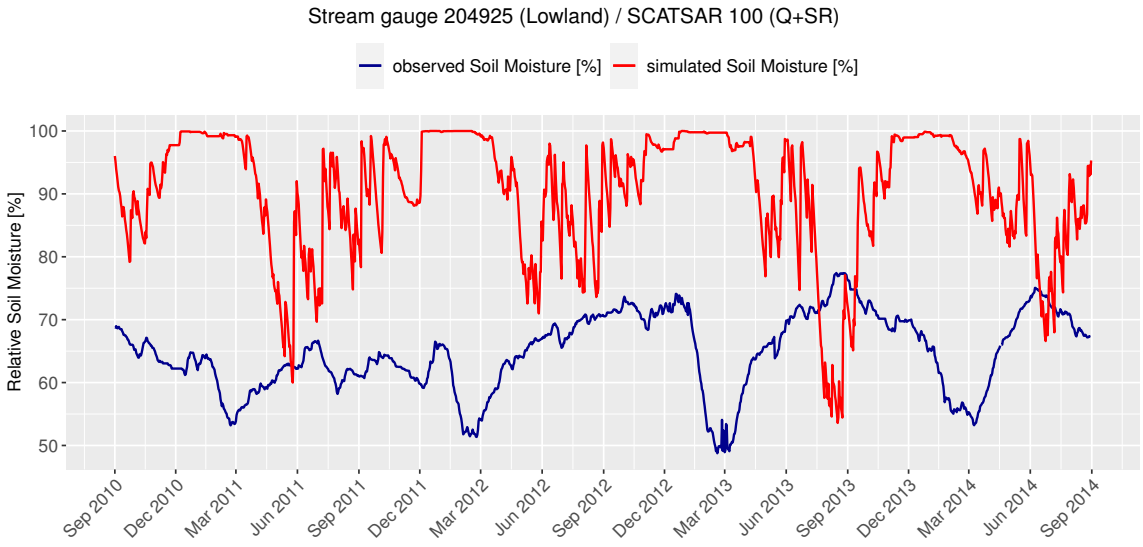

Fig. 7.41: Simulation results of the model validation, calibrated to runoff and soil moisture in the root-zone layer (Q+SR) using the S1ASCAT satellite product for the Lowland catchment of stream gauge 204925, over the period from September 1, 2010, to August 31, 2014.

Tab. 7.1: Catchments Characteristics (No.1 - 40); light gray rows = Alpine catchments, white rows = Lowland catchments.

Stream Gauge ID	Gauge No.	X Coordinates	Y Coordinates	Area [km²]	Mean Elevation [m.a.s.l.]	Mean Slope [%]
200105	1	138382	375463	95.5	1633.21	36.3
200147	2	116073	380278	1281	1655.19	32.7
200196	3	123222	400732	6110.1	1819.80	31.5
200204	4	130525	394710	51.1	1178.92	23.5
200212	5	126300	400757	112.9	940.01	17.5
200220	6	125935	399204	77.5	616.54	12.3
200246	7	151668	381484	41.7	1766.20	33.4
200253	8	146134	386543	149.3	1595.25	31.1
200261	9	139535	389744	228.6	1508.17	30.8
200287	10	151731	392500	31.1	1523.03	25.0
200311	11	139730	409024	90.1	805.56	8.2
200360	12	158336	372241	25.2	2114.78	30.2
200378	13	158351	372743	84.3	2046.72	29.4
201012	14	170036	375958	247.9	1994.35	31.7
201053	15	189034	389192	64	1759.35	42.3
201087	16	202596	403059	1012.2	1790.47	34.3
201111	17	198058	409370	198.1	1319.70	23.0
201533	18	259193	350058	58.3	1906.99	30.5
201574	19	257711	358725	341.8	1963.24	35.0
201723	20	284834	362283	129.2	2092.40	32.7
201822	21	289676	396073	272.6	1280.56	25.4
201863	22	307488	399763	322.3	1370.84	27.5
201913	23	329032	395533	153	1456.79	26.1
201921	24	330029	402524	147.4	1293.34	24.9
201939	25	331169	402585	332.4	1335.39	24.6
201947	26	332875	402658	165.3	1270.95	23.8
203034	27	317830	370767	80.7	2351.68	37.7
203042	28	319233	371278	40.5	2228.55	43.9
203075	29	335535	376339	582.6	1979.70	35.6
203141	30	361903	374854	161	1966.94	40.3
203166	31	374284	371426	242.2	1913.93	36.6
203208	32	383071	362732	220.7	1962.42	36.9
203224	33	389846	370878	144.6	1749.66	34.6
203307	34	388676	409707	394.5	1238.07	25.4
203315	35	386649	409641	65.5	1712.66	31.8
203463	36	354924	385288	150.8	1585.38	28.6
203471	37	362751	392208	119.5	1363.75	27.7
203505	38	352258	409698	107.4	1288.37	31.9
203539	39	369685	449099	6120	1386.11	28.2
203547	40	365933	455249	88.1	501.92	2.0

Tab. 7.2: Catchments Characteristics (No.41 - 80); light gray rows = Alpine catchments, white rows = Lowland catchments.

Stream Gauge ID	Gauge No.	X Coordinates	Y Coordinates	Area [km²]	Mean Elevation [m.a.s.l.]	Mean Slope [%]
203661	41	393356	435576	34.7	863.13	14.6
203711	42	406950	386944	134.5	1497.92	28.9
203760	43	426597	359325	102.1	1862.23	32.6
203778	44	428178	364168	75.2	1854.51	33.3
203786	45	435741	359552	377.9	1775.22	30.9
204545	46	370023	459271	69.9	506.20	2.0
204586	47	383940	455772	66.6	609.30	4.2
204685	48	406824	470502	24	659.61	4.6
204719	49	390261	486910	314.9	539.48	3.3
204735	50	411505	479775	69.3	572.25	3.3
204750	51	408717	485988	164.9	558.33	3.3
204768	52	408946	490430	68.6	486.12	3.1
204784	53	422167	489280	59.5	486.78	2.8
204826	54	421439	501348	64.1	546.47	5.5
204834	55	417862	500326	81.3	520.88	5.0
204867	56	409730	503622	340.9	467.11	3.4
204875	57	432290	517004	134.1	740.68	5.9
204883	58	443485	506641	199.2	642.40	6.7
204891	59	437486	533604	123.6	822.73	7.3
204917	60	450537	523003	253.3	804.33	8.3
204925	61	452906	519463	137.8	799.51	7.3
204933	62	451578	516278	452.2	795.21	7.8
204974	63	429735	480468	52	551.49	3.8
204990	64	426344	482108	19.4	476.84	2.2
205013	65	436649	481791	136.8	495.79	3.2
205021	66	443484	481077	183.8	479.41	3.4
205039	67	451636	487944	361.8	452.70	3.5
205047	68	430218	486103	26.1	456.96	1.7
205054	69	441707	497040	312.5	477.43	3.1
205088	70	459518	496803	227.4	744.48	6.2
205096	71	470975	496570	27.7	748.22	10.9
205104	72	429270	407230	334.4	1357.00	23.7
205120	73	422566	405620	41.6	1651.48	28.0
205179	74	411730	424729	124.9	952.95	22.3
205294	75	400306	436906	111.2	779.81	10.9
205377	76	408195	454184	100.3	688.54	5.3
205385	77	412619	458520	58.5	631.70	4.7
205393	78	420580	456167	331.3	637.69	4.7
205419	79	424181	456563	444.3	642.35	5.0
205435	80	430475	452894	81.6	752.22	13.9

Tab. 7.3: Catchments Characteristics (No.81 - 120); light gray rows = Alpine catchments, white rows = Lowland catchments.

Stream Gauge ID	Gauge No.	X Coordinates	Y Coordinates	Area [km²]	Mean Elevation [m.a.s.l.]	Mean Slope [%]
205450	81	437651	465239	1260.2	664.75	8.8
205500	82	448846	449993	315.2	993.18	24.8
205518	83	443998	461684	436.8	890.86	20.2
205633	84	457629	445793	37.1	689.42	16.8
205641	85	459553	461785	142.4	581.14	10.2
205658	86	469401	478246	363.5	489.48	5.7
205740	87	483781	443722	168.6	909.01	21.4
205765	88	458204	419085	25.2	1447.44	39.0
205799	89	462758	430096	184.9	1269.74	31.4
205807	90	475196	419292	40.2	1289.69	30.0
205815	91	474919	425195	69.5	1067.28	19.6
205823	92	472246	425856	148.6	1089.64	21.8
205831	93	465680	429982	232.8	1076.91	22.9
205856	94	460259	434166	72.4	1016.45	23.6
205880	95	475080	440914	99.6	989.95	25.5
205898	96	470811	444376	129.4	941.09	24.7
205914	97	476230	461793	898.1	984.63	23.8
205948	98	486654	512168	63.9	760.29	4.9
205971	99	491695	493917	266.1	811.95	6.5
205989	100	492431	488594	604.7	728.68	6.1
205997	101	511523	501777	80.4	881.23	5.3
206003	102	507123	505187	36.9	899.94	6.7
206029	103	500326	479657	303.1	723.72	6.0
206037	104	507352	480258	87.6	553.69	6.4
206151	105	434609	491830	55.2	458.27	2.5
206169	106	435397	491427	104	454.25	2.2
206185	107	409033	433698	247.2	741.12	12.9
207654	108	511820	444396	506.9	957.47	22.1
207688	109	515999	468993	1116.6	730.38	14.9
207704	110	546998	436786	29.7	1052.28	14.9
207712	111	545797	440652	36.1	1096.67	20.6
207720	112	548117	442257	23.2	1020.68	14.1
207746	113	532314	450569	51.5	773.77	17.5
207787	114	538577	454322	32.2	733.67	15.3
207795	115	534082	471270	167.5	557.72	10.8
207811	116	544940	484187	216.9	714.79	8.6
207829	117	548866	470554	37.6	502.47	9.3
207837	118	544666	479953	284.6	416.55	6.1
207845	119	552635	452911	42.2	891.95	18.5
207852	120	562342	468516	289.5	698.47	14.1

Tab. 7.4: Catchments Characteristics (No.121 - 160); light gray rows = Alpine catchments, white rows = Lowland catchments.

Stream Gauge ID	Gauge No.	X Coordinates	Y Coordinates	Area [km²]	Mean Elevation [m.a.s.l.]	Mean Slope [%]
207860	121	558287	478973	87.7	353.01	3.4
207894	122	568249	459508	333.4	813.24	18.5
207910	123	571529	474306	733.3	735.81	16.0
207936	124	534835	524662	269.1	749.60	3.6
207944	125	535730	524939	621.8	794.11	4.1
208009	126	591072	491050	268.3	392.75	5.7
208017	127	593428	487235	202.3	396.94	6.5
208090	128	611687	460980	181	522.88	7.7
208116	129	603902	456809	186	630.29	10.9
208124	130	612414	451643	287.3	590.27	10.1
208157	131	633679	476053	1119.39	436.29	6.2
208280	132	612850	444576	284.1	730.16	14.8
208413	133	636419	463350	417.3	578.93	10.1
208439	134	644041	472230	534.9	509.52	8.4
208462	135	519420	541044	267.6	743.52	6.1
208579	136	523118	542900	291.5	624.92	2.0
208611	137	541578	539816	175.5	624.54	1.9
208686	138	577711	437276	128.4	876.75	13.1
208702	139	580047	432975	252.3	987.28	19.7
208710	140	595599	422770	472.2	1012.23	21.4
208819	141	608188	412864	96.5	964.04	15.5
209197	142	543883	469047	95.2	447.98	6.8
210229	143	618368	379399	171.7	708.34	8.2
210526	144	437240	413524	125.1	1547.92	24.2
210542	145	432794	415137	54.5	1550.39	24.0
210583	146	437979	407524	57.4	1352.41	17.0
210625	147	428735	383923	65.2	1925.40	40.0
210641	148	427571	388689	648.8	1549.08	29.6
210773	149	461348	403657	161	1478.78	27.4
210815	150	473362	405405	368.7	1356.60	27.6
210864	151	547873	428701	280	1129.70	17.8
210880	152	538113	421269	54.1	1211.86	21.7
210898	153	524000	419664	592.3	1174.80	23.4
210989	154	594412	342861	689.4	619.39	7.7
211003	155	608821	371394	439.4	745.85	8.9
211102	156	488378	368326	2334.4	1597.90	26.4
211136	157	507588	365989	2957.5	1556.93	25.5
211169	158	518729	388864	265.6	1342.54	24.7
211193	159	528407	389635	167.3	1204.50	25.0
211227	160	568161	421417	231.5	1237.22	22.2

Tab. 7.5: Catchments Characteristics (No.161 - 196); light gray rows = Alpine catchments, white rows = Lowland catchments.

Stream Gauge ID	Gauge No.	X Coordinates	Y Coordinates	Area [km²]	Mean Elevation [m.a.s.l.]	Mean Slope [%]
211243	161	561023	405114	727.7	1133.88	19.3
211268	162	546307	394177	1364.5	1105.53	19.6
211292	163	547036	391882	6214	1344.46	22.6
211383	164	542962	319009	75.2	1278.21	18.1
211391	165	548275	315165	69.7	825.01	12.0
211458	166	567712	322351	1102.5	628.35	8.7
212027	167	334259	316585	374	1993.25	32.9
212068	168	333611	358720	39.3	2656.70	34.8
212076	169	336745	357817	59.9	2521.06	35.6
212092	170	340649	341941	518.4	2313.27	36.2
212126	171	347014	347578	14.2	2710.22	32.4
212183	172	338690	344303	285.3	2352.01	35.4
212316	173	358769	324857	1876.2	2082.05	35.4
212324	174	372528	316476	2112	2024.21	35.3
212357	175	401382	325283	2561.4	1920.98	34.6
212381	176	387939	342595	85.3	2092.61	42.7
212431	177	415586	333893	360.1	1756.12	26.9
212522	178	413355	323785	286.3	1390.73	26.9
212613	179	354718	311579	146.1	1843.91	30.3
212647	180	374520	307642	348.6	1691.39	31.8
212670	181	393964	302736	594.9	1522.06	31.4
212704	182	403125	302193	75.2	1101.95	24.7
212753	183	421727	298053	908.5	1385.03	29.4
212787	184	436975	296503	1304.9	1298.54	28.3
212860	185	445815	320897	201.4	1637.11	22.7
212886	186	466136	328009	431.8	1385.28	20.8
212894	187	484331	334105	469.4	1192.95	18.7
212928	188	492629	338301	130.3	1382.10	19.4
212936	189	491699	318244	315.6	1285.46	18.8
213025	190	474830	300472	220.064	628.08	8.4
213033	191	481910	301204	817.9	718.96	9.9
213082	192	516944	334045	380.2	1254.50	16.1
213090	193	523495	308480	954.5	1071.50	15.8
213157	194	487329	318344	1243.1	1177.27	17.7
213231	195	454560	310717	91.1	988.05	16.1
213256	196	480906	323319	106.5	940.22	13.2

Tab. 7.6: Catchments Characteristics (No.1 - 40)

Stream Gauge ID	Gauge No.	Forest Cover [%]	Elevation Range [m]	Mean Precip. [mm]	Mean Temp. [°C]	Mean Q/A [XX]
200105	1	29.12	1851	2003.4	4.66	1747.5
200147	2	37.35	2684	1544.0	4.43	1616.0
200196	3	29.59	2861	1520.6	3.46	1187.8
200204	4	75.00	1291	2126.0	6.98	1767.4
200212	5	54.91	1371	1971.9	8.07	1331.7
200220	6	33.97	1133	1478.3	9.81	778.7
200246	7	19.19	1463	2105.7	4.10	1926.9
200253	8	31.17	1699	2128.1	4.84	1720.0
200261	9	37.66	1792	2135.8	5.24	1793.6
200287	10	35.00	1047	2301.8	5.20	2036.2
200311	11	30.00	493	1828.4	8.32	1256.1
200360	12	7.61	1050	1631.7	2.16	1985.1
200378	13	11.18	1144	1850.4	2.46	1782.9
201012	14	13.84	1635	1717.2	2.67	1646.3
201053	15	23.05	1503	1769.1	3.81	1706.0
201087	16	26.83	2147	1597.9	3.61	1339.3
201111	17	47.72	1339	1773.8	5.94	1242.5
201533	18	36.21	1508	1325.6	3.40	798.7
201574	19	32.59	2376	1288.9	2.96	1032.9
201723	20	22.48	2180	1455.9	2.21	950.8
201822	21	80.75	1573	1627.8	6.63	1203.3
201863	22	47.13	1883	1504.6	6.17	1124.5
201913	23	40.22	1364	1520.1	5.75	1114.1
201921	24	46.33	1472	1531.5	6.58	1039.8
201939	25	42.94	1491	1513.5	6.34	1067.4
201947	26	51.67	1336	1713.6	6.56	1326.1
203034	27	17.59	2557	1656.4	0.75	2061.3
203042	28	22.37	2191	1560.9	1.50	1850.0
203075	29	28.62	2665	1543.1	2.84	1369.1
203141	30	26.52	2696	1470.1	2.95	1224.7
203166	31	27.18	2238	1419.4	3.25	1209.5
203208	32	26.12	2323	1475.2	2.93	1622.7
203224	33	37.85	1881	1351.2	4.17	1195.7
203307	34	60.79	1832	1721.1	6.47	1440.7
203315	35	35.87	1856	2054.2	4.34	1700.1
203463	36	45.56	1380	1572.2	5.08	1102.2
203471	37	45.30	1846	1476.6	5.96	1239.7
203505	38	66.04	1736	1887.2	6.52	1645.8
203539	39	45.53	3072	1560.5	5.79	1285.6
203547	40	24.43	180	1099.3	9.73	355.5

Tab. 7.7: Catchments Characteristics (No.41 - 80)

Stream Gauge ID	Gauge No.	Forest Cover [%]	Elevation Range [m]	Mean Precip. [mm]	Mean Temp. [°C]	Mean Q/A [XX]
203661	41	56.25	558	1817.6	8.26	1012.9
203711	42	54.32	1609	1315.4	5.31	951.0
203760	43	39.46	1507	1123.6	3.42	1176.6
203778	44	37.01	1427	1142.0	3.43	1116.6
203786	45	38.26	1625	1076.1	3.81	951.3
204545	46	24.65	144	1099.7	9.71	357.2
204586	47	14.34	238	1337.2	9.42	700.4
204685	48	44.57	198	1237.4	8.90	676.5
204719	49	26.11	415	1085.3	9.33	495.4
204735	50	14.64	260	1083.8	9.20	463.3
204750	51	14.72	324	1055.3	9.26	485.8
204768	52	5.36	173	998.2	9.47	429.4
204784	53	6.97	202	992.0	9.44	441.2
204826	54	30.38	384	1087.9	9.00	509.1
204834	55	26.23	395	1067.1	9.12	487.2
204867	56	12.13	419	998.5	9.42	432.4
204875	57	44.70	402	1217.5	8.17	704.1
204883	58	32.59	554	1024.4	8.60	516.2
204891	59	39.48	751	1224.4	7.70	741.6
204917	60	45.25	826	1129.4	7.79	698.8
204925	61	47.78	508	975.7	7.86	478.5
204933	62	46.88	860	1060.7	7.85	595.7
204974	63	20.28	367	968.7	9.31	428.9
204990	64	7.50	114	970.7	9.50	436.8
205013	65	12.22	419	947.5	9.45	403.7
205021	66	11.61	449	930.0	9.50	384.3
205039	67	9.79	487	897.4	9.62	367.9
205047	68	3.85	80	940.4	9.51	420.3
205054	69	12.46	297	953.5	9.33	424.6
205088	70	38.71	745	995.7	8.08	439.0
205096	71	50.93	445	1069.0	7.99	459.3
205104	72	47.41	1783	1863.5	5.96	1917.4
205120	73	46.88	1726	2046.6	4.55	2654.9
205179	74	67.20	1180	1767.1	7.84	1310.3
205294	75	43.81	722	1748.0	8.62	1051.4
205377	76	41.33	421	1362.3	8.96	846.6
205385	77	46.61	288	1154.0	9.12	634.1
205393	78	42.98	487	1210.4	9.16	632.2
205419	79	42.57	543	1237.5	9.16	607.4
205435	80	67.90	1190	1394.1	8.81	834.3

Tab. 7.8: Catchments Characteristics (No.81 - 120)

Stream Gauge ID	Gauge No.	Forest Cover [%]	Elevation Range [m]	Mean Precip. [mm]	Mean Temp. [°C]	Mean Q/A [XX]
205450	81	41.97	1357	1333.5	9.10	812.3
205500	82	73.95	2000	1817.7	7.62	1252.1
205518	83	64.90	2081	1661.4	8.10	1092.2
205633	84	47.09	964	1452.4	8.93	912.3
205641	85	26.76	1031	1251.2	9.39	627.0
205658	86	14.82	1107	1085.4	9.74	511.7
205740	87	94.59	1253	1673.3	7.61	1234.3
205765	88	46.30	1556	1718.9	5.32	1954.5
205799	89	58.33	1778	1636.8	6.13	1801.7
205807	90	71.34	1672	1591.7	6.05	1941.9
205815	91	63.06	1340	1641.3	7.01	862.9
205823	92	61.05	1747	1589.1	6.96	1203.8
205831	93	63.31	1817	1593.1	7.03	1415.3
205856	94	85.21	1638	1776.1	7.40	892.1
205880	95	88.54	1329	1805.3	7.42	910.4
205898	96	87.69	1356	1736.6	7.62	942.6
205914	97	66.40	2010	1593.3	7.45	1334.1
205948	98	35.32	363	833.2	7.84	322.7
205971	99	65.61	684	922.7	7.67	394.2
205989	100	47.69	759	870.5	8.04	349.2
205997	101	60.39	417	974.1	7.36	436.7
206003	102	46.53	398	975.5	7.26	425.2
206029	103	49.60	788	936.4	8.15	421.3
206037	104	37.93	512	925.4	9.07	341.7
206151	105	5.80	117	961.0	9.41	421.8
206169	106	5.64	120	949.3	9.45	410.4
206185	107	42.30	855	1662.7	8.77	1144.9
207654	108	82.17	1408	1759.9	7.05	1266.1
207688	109	53.76	1549	1414.7	8.28	926.0
207704	110	76.67	720	1459.2	6.68	886.7
207712	111	86.49	1066	1806.9	6.52	1257.9
207720	112	80.68	441	1603.4	6.79	1102.3
207746	113	72.60	800	1565.2	7.83	853.9
207787	114	73.53	670	1521.4	7.98	741.1
207795	115	33.68	816	1136.0	9.05	576.7
207811	116	51.95	774	768.2	8.32	227.1
207829	117	27.70	518	1014.4	9.45	427.6
207837	118	20.49	634	868.8	9.89	355.0
207845	119	88.07	781	1633.6	7.40	1258.3
207852	120	57.44	976	1343.2	8.32	691.3

Tab. 7.9: Catchments Characteristics (No.121 - 160)

Stream Gauge ID	Gauge No.	Forest Cover [%]	Elevation Range [m]	Mean Precip. [mm]	Mean Temp. [°C]	Mean Q/A [XX]
207860	121	12.78	373	805.5	10.30	262.2
207894	122	88.05	1194	1380.2	7.90	846.3
207910	123	75.48	1262	1221.9	8.29	647.4
207936	124	35.00	440	794.2	7.67	284.7
207944	125	46.57	496	833.3	7.52	317.3
208009	126	30.70	543	787.0	10.10	204.0
208017	127	37.63	676	782.5	10.04	216.9
208090	128	77.72	566	826.8	9.55	266.0
208116	129	72.69	622	915.4	8.87	337.2
208124	130	74.23	678	863.3	9.11	293.0
208157	131	49.34	810	746.7	10.09	232.2
208280	132	86.49	1006	1000.4	8.45	348.3
208413	133	60.86	1143	869.0	9.29	517.7
208439	134	49.62	1164	817.7	9.66	467.0
208462	135	52.80	547	838.0	7.90	302.6
208579	136	44.85	262	741.7	8.17	241.3
208611	137	25.58	193	728.1	8.10	215.2
208686	138	94.00	751	1311.7	7.85	594.5
208702	139	90.52	1333	1348.4	7.40	684.2
208710	140	80.66	1616	1244.4	7.36	606.4
208819	141	70.57	1244	1019.8	7.67	393.6
209197	142	14.52	596	917.9	9.71	483.1
210229	143	53.80	1201	859.6	9.20	207.8
210526	144	35.22	1603	1959.4	4.99	1540.6
210542	145	21.81	1224	2163.5	5.04	2212.3
210583	146	52.19	1190	1701.5	6.01	2068.1
210625	147	29.30	1770	1193.0	3.19	1411.8
210641	148	54.04	2055	1281.3	5.03	1053.7
210773	149	52.06	1517	1355.8	5.23	972.7
210815	150	57.69	1765	1306.4	5.76	898.3
210864	151	86.40	1210	1422.1	6.47	799.1
210880	152	87.96	1062	1777.5	6.04	1227.2
210898	153	78.41	1595	1565.1	6.25	1173.2
210989	154	43.31	1158	861.6	9.40	235.4
211003	155	47.67	1430	838.8	9.02	219.1
211102	156	53.57	2337	1014.3	4.86	652.0
211136	157	53.81	2392	1020.3	5.05	626.8
211169	158	67.57	1667	1308.2	5.76	756.8
211193	159	64.43	1520	1195.4	6.33	622.5
211227	160	79.42	1147	1444.6	6.17	1035.6

Tab. 7.10: Catchments Characteristics (No.161 - 196)

Stream Gauge ID	Gauge No.	Forest Cover [%]	Elevation Range [m]	Mean Precip. [mm]	Mean Temp. [°C]	Mean Q/A [XX]
211243	161	78.59	1423	1205.2	6.67	610.0
211268	162	75.63	1698	1170.3	6.80	535.6
211292	163	61.76	2571	1064.8	5.87	566.0
211383	164	75.69	1480	1261.3	6.38	724.5
211391	165	65.36	1192	1167.7	8.41	481.0
211458	166	53.80	1646	1023.3	9.36	385.7
212027	167	44.03	1885	1179.9	2.64	743.9
212068	168	0.00	1836	1806.1	-1.06	2724.6
212076	169	2.97	2036	1754.1	-0.30	2336.2
212092	170	18.75	2620	1414.9	0.74	1268.1
212126	171	3.33	1844	1318.3	-1.54	1210.9
212183	172	19.41	2610	1328.6	0.48	1193.4
212316	173	34.38	2877	1247.4	2.05	923.5
212324	174	36.17	2923	1250.5	2.38	934.3
212357	175	39.54	2982	1274.4	2.97	872.9
212381	176	27.30	1932	1377.3	2.11	1352.5
212431	177	48.96	2107	1044.0	4.09	585.8
212522	178	53.15	1752	1052.7	6.10	523.5
212613	179	50.87	1370	1382.5	3.54	918.1
212647	180	55.98	1787	1518.9	4.38	934.5
212670	181	58.40	2045	1618.0	5.26	992.0
212704	182	79.05	1401	1473.3	7.39	813.5
212753	183	61.18	2092	1606.3	5.95	1032.0
212787	184	63.73	2143	1593.7	6.39	1071.4
212860	185	55.93	1282	1102.4	5.03	575.5
212886	186	67.68	1579	1076.0	6.06	427.5
212894	187	69.15	1502	947.9	6.86	351.6
212928	188	70.54	1554	917.7	6.07	385.0
212936	189	70.16	1862	913.6	6.42	354.6
213025	190	45.69	566	1097.9	9.46	367.0
213033	191	48.35	908	981.7	8.92	349.5
213082	192	66.71	1613	986.5	6.47	402.5
213090	193	57.77	1839	959.6	7.23	375.6
213157	194	66.99	1770	970.9	6.88	364.1
213231	195	63.22	1217	1042.3	7.94	605.2
213256	196	75.00	803	938.3	7.79	284.0

Tab. 7.11: The NSE values for calibration variants Q and Q+SR using S1ASCAT and SCATSAR products during the calibration period in the 196 Austrian catchments (No.1 - 40).

Stream Gauge ID	Gauge No.	NSE Runoff Q	NSE S1ASCAT Q+SR	NSE SCATSAR 020 Q+SR	NSE SCATSAR 040 Q+SR	NSE SCATSAR 100 Q+SR
200105	1	0.81	0.79	0.79	0.79	0.79
200147	2	0.78	0.76	0.77	0.77	0.77
200196	3	0.84	0.83	0.82	0.82	0.82
200204	4	0.62	0.61	0.59	0.58	0.58
200212	5	0.68	0.67	0.66	0.66	0.71
200220	6	0.73	0.73	0.73	0.72	0.83
200246	7	0.78	0.74	0.77	0.77	0.77
200253	8	0.8	0.78	0.78	0.79	0.78
200261	9	0.76	0.75	0.74	0.74	0.74
200287	10	0.7	0.7	0.68	0.68	0.68
200311	11	0.7	0.69	0.68	0.65	0.65
200360	12	0.88	0.85	0.85	0.85	0.85
200378	13	0.88	0.86	0.87	0.87	0.86
201012	14	0.86	0.83	0.84	0.85	0.85
201053	15	0.77	0.76	0.74	0.74	0.74
201087	16	0.83	0.81	0.81	0.83	0.83
201111	17	0.73	0.71	0.71	0.72	0.72
201533	18	-10.95	-10.95	-10.95	-10.95	-10.95
201574	19	0.91	0.87	0.85	0.86	0.9
201723	20	0.87	0.83	0.86	0.86	0.86
201822	21	0.74	0.65	0.62	0.66	0.64
201863	22	0.85	0.83	0.86	0.86	0.84
201913	23	0.8	0.8	0.79	0.79	0.79
201921	24	0.81	0.74	0.74	0.73	0.77
201939	25	0.81	0.79	0.85	0.8	0.78
201947	26	0.69	0.69	0.75	0.75	0.75
203034	27	0.8	0.8	0.81	0.81	0.81
203042	28	0.82	0.82	0.82	0.82	0.82
203075	29	0.86	0.83	0.86	0.86	0.86
203141	30	0.88	0.86	0.88	0.88	0.88
203166	31	0.85	0.84	0.84	0.83	0.83
203208	32	0.76	0.73	0.73	0.71	0.71
203224	33	0.8	0.75	0.76	0.76	0.76
203307	34	0.62	0.61	0.58	0.59	0.58
203315	35	0.79	0.74	0.75	0.75	0.69
203463	36	0.77	0.74	0.73	0.73	0.73
203471	37	0.76	0.74	0.76	0.76	0.76
203505	38	0.73	0.7	0.76	0.7	0.71
203539	39	0.83	0.7	0.82	0.75	0.75
203547	40	0.71	0.83	0.81	0.7	0.84

Tab. 7.12: The NSE values for calibration variants Q and Q+SR using S1ASCAT and SCATSAR products during the calibration period in the 196 Austrian catchments (No.41 - 80).

Stream Gauge ID	Gauge No.	NSE Runoff Q	NSE S1ASCAT Q+SR	NSE SCATSAR 020 Q+SR	NSE SCATSAR 040 Q+SR	NSE SCATSAR 100 Q+SR
203661	41	0.85	0.84	0.85	0.83	0.83
203711	42	0.84	0.81	0.78	0.77	0.81
203760	43	0.84	0.77	0.79	0.79	0.79
203778	44	0.83	0.78	0.76	0.76	0.79
203786	45	0.88	0.82	0.81	0.81	0.85
204545	46	0.87	0.87	0.8	0.72	0.7
204586	47	0.94	0.9	0.94	0.94	0.94
204685	48	0.62	0.61	0.61	0.61	0.61
204719	49	0.7	0.72	0.73	0.67	0.72
204735	50	0.58	0.57	0.69	0.71	0.57
204750	51	0.64	0.62	0.73	0.63	0.71
204768	52	0.56	0.55	0.69	0.7	0.7
204784	53	0.78	0.79	0.8	0.65	0.82
204826	54	-156.42	-156.41	-156.42	-156.41	-156.41
204834	55	0.68	0.78	0.72	0.7	0.78
204867	56	0.8	0.79	0.76	0.79	0.8
204875	57	0.75	0.74	0.7	0.71	0.71
204883	58	0.81	0.82	0.75	0.78	0.79
204891	59	0.79	0.8	0.73	0.73	0.73
204917	60	0.81	0.82	0.76	0.79	0.78
204925	61	0.76	0.75	0.67	0.69	0.69
204933	62	0.81	0.83	0.76	0.76	0.77
204974	63	0.72	0.71	0.72	0.72	0.65
204990	64	-90.71	-90.71	-90.71	-90.71	-90.71
205013	65	0.66	0.65	0.64	0.79	0.78
205021	66	0.77	0.77	0.75	0.75	0.77
205039	67	-29.53	-29.54	-29.54	-29.53	-29.54
205047	68	0.75	0.57	0.7	0.57	0.57
205054	69	0.79	0.77	0.61	0.62	0.77
205088	70	0.81	0.8	0.77	0.78	0.78
205096	71	0.8	0.78	0.73	0.74	0.76
205104	72	0.83	0.8	0.8	0.75	0.8
205120	73	0.8	0.76	0.78	0.78	0.78
205179	74	0.88	0.84	0.81	0.81	0.8
205294	75	0.7	0.7	0.68	0.68	0.69
205377	76	0.71	0.64	0.64	0.64	0.64
205385	77	0.67	0.74	0.66	0.76	0.66
205393	78	0.67	0.74	0.76	0.64	0.65
205419	79	0.75	0.66	0.73	0.75	0.77
205435	80	0.59	0.59	0.62	0.57	0.57

Tab. 7.13: The NSE values for calibration variants Q and Q+SR using S1ASCAT and SCATSAR products during the calibration period in the 196 Austrian catchments (No.81 - 120).

Stream Gauge ID	Gauge No.	NSE Runoff Q	NSE S1ASCAT Q+SR	NSE SCATSAR 020 Q+SR	NSE SCATSAR 040 Q+SR	NSE SCATSAR 100 Q+SR
205450	81	0.84	0.82	0.79	0.82	0.83
205500	82	0.73	0.71	0.7	0.68	0.68
205518	83	0.82	0.77	0.68	0.71	0.74
205633	84	0.66	0.66	0.63	0.64	0.64
205641	85	0.63	0.73	0.68	0.59	0.61
205658	86	0.71	0.73	0.71	0.74	0.71
205740	87	0.64	0.6	0.65	0.57	0.58
205765	88	0.68	0.66	0.65	0.65	0.66
205799	89	0.69	0.7	0.65	0.66	0.67
205807	90	0.62	0.64	0.56	0.6	0.57
205815	91	0.74	0.73	0.71	0.71	0.71
205823	92	0.73	0.63	0.68	0.65	0.63
205831	93	0.67	0.66	0.65	0.65	0.72
205856	94	0.6	0.61	0.58	0.58	0.58
205880	95	-40.35	-40.36	-40.36	-40.36	-40.36
205898	96	0.68	0.62	0.61	0.61	0.61
205914	97	0.76	0.77	0.74	0.74	0.72
205948	98	0.42	0.42	0.25	0.27	0.29
205971	99	0.75	0.74	0.72	0.72	0.73
205989	100	0.7	0.68	0.62	0.63	0.64
205997	101	0.72	0.74	0.68	0.7	0.74
206003	102	0.72	0.71	0.72	0.69	0.72
206029	103	0.8	0.83	0.72	0.72	0.72
206037	104	0.75	0.75	0.71	0.71	0.72
206151	105	0.59	0.73	0.56	0.7	0.71
206169	106	0.61	0.59	0.58	0.59	0.59
206185	107	0.89	0.9	0.89	0.88	0.89
207654	108	0.82	0.7	0.79	0.77	0.78
207688	109	0.81	0.81	0.82	0.81	0.76
207704	110	0.78	0.62	0.7	0.7	0.75
207712	111	0.74	0.71	0.71	0.69	0.69
207720	112	0.74	0.71	0.71	0.68	0.66
207746	113	0.75	0.76	0.8	0.75	0.73
207787	114	0.64	0.65	0.66	0.62	0.68
207795	115	0.68	0.77	0.77	0.77	0.77
207811	116	0.6	0.6	0.58	0.59	0.6
207829	117	0.57	0.58	0.59	0.58	0.59
207837	118	0.66	0.7	0.66	0.71	0.71
207845	119	0.72	0.72	0.71	0.71	0.71
207852	120	0.68	0.74	0.7	0.72	0.71

Tab. 7.14: The NSE values for calibration variants Q and Q+SR using S1ASCAT and SCATSAR products during the calibration period in the 196 Austrian catchments (No.121 - 160).

Stream Gauge ID	Gauge No.	NSE Runoff Q	NSE S1ASCAT Q+SR	NSE SCATSAR 020 Q+SR	NSE SCATSAR 040 Q+SR	NSE SCATSAR 100 Q+SR
207860	121	0.56	0.58	0.5	0.51	0.57
207894	122	0.74	0.82	0.75	0.63	0.55
207910	123	0.77	0.82	0.65	0.65	0.65
207936	124	0.68	0.66	0.64	0.64	0.64
207944	125	0.74	0.71	0.7	0.69	0.7
208009	126	0.54	0.53	0.48	0.49	0.54
208017	127	0.6	0.58	0.55	0.57	0.63
208090	128	0.68	0.7	0.68	0.71	0.71
208116	129	0.66	0.65	0.62	0.65	0.64
208124	130	0.62	0.63	0.62	0.64	0.63
208157	131	0.63	0.68	0.64	0.65	0.67
208280	132	0.8	0.82	0.76	0.76	0.75
208413	133	-36.82	-36.83	-36.82	-36.82	-36.82
208439	134	0.66	0.66	0.62	0.59	0.59
208462	135	0.66	0.66	0.68	0.6	0.63
208579	136	0.72	0.7	0.67	0.65	0.66
208611	137	0.41	0.19	0.43	0.43	0.48
208686	138	0.71	0.71	0.66	0.62	0.62
208702	139	0.74	0.74	0.67	0.7	0.66
208710	140	0.76	0.76	0.7	0.57	0.57
208819	141	0.77	0.78	0.75	0.77	0.75
209197	142	0.63	0.62	0.62	0.62	0.62
210229	143	0.69	0.67	0.68	0.68	0.69
210526	144	0.88	0.85	0.85	0.84	0.84
210542	145	0.83	0.7	0.77	0.75	0.77
210583	146	0.66	0.64	0.62	0.54	0.58
210625	147	0.78	0.77	0.69	0.69	0.69
210641	148	0.83	0.81	0.81	0.81	0.83
210773	149	0.82	0.71	0.79	0.79	0.8
210815	150	0.78	0.75	0.79	0.69	0.77
210864	151	0.71	0.69	0.69	0.7	0.65
210880	152	0.62	0.53	0.51	0.62	0.61
210898	153	0.8	0.77	0.69	0.67	0.68
210989	154	0.78	0.77	0.61	0.69	0.72
211003	155	0.65	0.63	0.6	0.57	0.57
211102	156	0.91	0.82	0.81	0.75	0.74
211136	157	0.92	0.88	0.81	0.82	0.82
211169	158	0.8	0.73	0.8	0.76	0.8
211193	159	0.79	0.77	0.75	0.75	0.75
211227	160	0.71	0.73	0.64	0.69	0.69

Tab. 7.15: The NSE values for calibration variants Q and Q+SR using S1ASCAT and SCATSAR products during the calibration period in the 196 Austrian catchments (No.161 - 196).

Stream Gauge ID	Gauge No.	NSE Runoff Q	NSE S1ASCAT Q+SR	NSE SCATSAR 020 Q+SR	NSE SCATSAR 040 Q+SR	NSE SCATSAR 100 Q+SR
211243	161	0.79	0.73	0.77	0.77	0.77
211268	162	0.78	0.76	0.74	0.74	0.75
211292	163	0.93	0.92	0.87	0.93	0.92
211383	164	0.67	0.66	0.67	0.67	0.68
211391	165	0.65	0.57	0.61	0.61	0.61
211458	166	0.8	0.82	0.8	0.81	0.81
212027	167	0.9	0.85	0.85	0.84	0.85
212068	168	0.8	0.7	0.71	0.71	0.71
212076	169	0.85	0.73	0.8	0.8	0.8
212092	170	0.9	0.87	0.89	0.89	0.89
212126	171	0.89	0.86	0.88	0.88	0.88
212183	172	0.91	0.89	0.9	0.9	0.9
212316	173	0.93	0.9	0.89	0.9	0.9
212324	174	0.91	0.88	0.87	0.87	0.89
212357	175	0.92	0.9	0.87	0.87	0.89
212381	176	0.86	0.82	0.83	0.83	0.83
212431	177	0.87	0.83	0.8	0.8	0.79
212522	178	0.88	0.76	0.84	0.85	0.85
212613	179	0.88	0.82	0.84	0.85	0.85
212647	180	0.9	0.88	0.85	0.85	0.9
212670	181	0.88	0.85	0.83	0.87	0.86
212704	182	0.77	0.69	0.76	0.76	0.75
212753	183	0.87	0.82	0.83	0.88	0.88
212787	184	0.85	0.79	0.8	0.82	0.84
212860	185	0.87	0.82	0.8	0.8	0.81
212886	186	0.81	0.77	0.75	0.75	0.8
212894	187	0.76	0.72	0.71	0.71	0.72
212928	188	0.82	0.79	0.77	0.69	0.62
212936	189	0.82	0.8	0.77	0.78	0.78
213025	190	0.81	0.71	0.8	0.79	0.78
213033	191	0.9	0.83	0.84	0.84	0.82
213082	192	0.79	0.75	0.76	0.75	0.75
213090	193	0.81	0.79	0.75	0.74	0.75
213157	194	0.86	0.82	0.84	0.84	0.86
213231	195	0.78	0.76	0.77	0.77	0.76
213256	196	0.8	0.72	0.71	0.72	0.72

Tab. 7.16: The KGE values for calibration variants Q and Q+SR using S1ASCAT and SCATSAR products during the calibration period in the 196 Austrian catchments (No.1 - 40).

Stream Gauge ID	Gauge No.	KGE Runoff Q	KGE S1ASCAT Q+SR	KGE SCATSAR 020 Q+SR	KGE SCATSAR 040 Q+SR	KGE SCATSAR 100 Q+SR
200105	1	0.82	0.78	0.78	0.78	0.78
200147	2	0.85	0.86	0.85	0.84	0.85
200196	3	0.89	0.88	0.88	0.86	0.88
200204	4	0.63	0.62	0.57	0.55	0.54
200212	5	0.74	0.76	0.72	0.71	0.74
200220	6	0.76	0.81	0.77	0.74	0.83
200246	7	0.8	0.73	0.81	0.8	0.83
200253	8	0.85	0.85	0.86	0.85	0.83
200261	9	0.79	0.78	0.78	0.78	0.77
200287	10	0.71	0.69	0.7	0.7	0.7
200311	11	0.76	0.77	0.73	0.7	0.69
200360	12	0.89	0.8	0.8	0.8	0.8
200378	13	0.91	0.89	0.86	0.84	0.85
201012	14	0.91	0.85	0.89	0.92	0.92
201053	15	0.79	0.77	0.76	0.76	0.76
201087	16	0.88	0.85	0.85	0.88	0.89
201111	17	0.81	0.8	0.8	0.81	0.81
201533	18	-0.35	-0.34	-0.34	-0.34	-0.34
201574	19	0.95	0.93	0.84	0.85	0.95
201723	20	0.93	0.88	0.93	0.93	0.93
201822	21	0.79	0.73	0.71	0.7	0.7
201863	22	0.87	0.88	0.9	0.88	0.87
201913	23	0.82	0.87	0.77	0.79	0.84
201921	24	0.87	0.82	0.82	0.79	0.79
201939	25	0.84	0.85	0.87	0.8	0.83
201947	26	0.8	0.8	0.81	0.81	0.81
203034	27	0.7	0.7	0.79	0.79	0.79
203042	28	0.8	0.8	0.78	0.78	0.78
203075	29	0.89	0.91	0.89	0.89	0.89
203141	30	0.92	0.92	0.9	0.9	0.9
203166	31	0.88	0.89	0.86	0.85	0.83
203208	32	0.8	0.74	0.72	0.69	0.68
203224	33	0.84	0.76	0.82	0.82	0.82
203307	34	0.67	0.68	0.62	0.64	0.62
203315	35	0.85	0.83	0.82	0.82	0.73
203463	36	0.86	0.86	0.79	0.79	0.79
203471	37	0.8	0.82	0.78	0.79	0.79
203505	38	0.77	0.77	0.79	0.75	0.74
203539	39	0.86	0.83	0.87	0.8	0.79
203547	40	0.78	0.85	0.84	0.74	0.9

Tab. 7.17: The KGE values for calibration variants Q and Q+SR using S1ASCAT and SCATSAR products during the calibration period in the 196 Austrian catchments (No.41 - 80).

Stream Gauge ID	Gauge No.	KGE Runoff Q	KGE S1ASCAT Q+SR	KGE SCATSAR 020 Q+SR	KGE SCATSAR 040 Q+SR	KGE SCATSAR 100 Q+SR
203661	41	0.92	0.89	0.91	0.88	0.88
203711	42	0.89	0.89	0.83	0.82	0.84
203760	43	0.89	0.86	0.74	0.74	0.74
203778	44	0.91	0.88	0.84	0.83	0.89
203786	45	0.93	0.83	0.9	0.9	0.9
204545	46	0.89	0.91	0.86	0.83	0.82
204586	47	0.87	0.86	0.88	0.89	0.88
204685	48	0.76	0.72	0.74	0.75	0.75
204719	49	0.72	0.73	0.78	0.74	0.82
204735	50	0.67	0.66	0.77	0.8	0.66
204750	51	0.71	0.71	0.83	0.72	0.83
204768	52	0.59	0.56	0.69	0.67	0.68
204784	53	0.75	0.72	0.78	0.66	0.77
204826	54	-0.4	-0.4	-0.4	-0.4	-0.4
204834	55	0.8	0.88	0.85	0.8	0.88
204867	56	0.88	0.83	0.83	0.85	0.85
204875	57	0.83	0.84	0.8	0.79	0.83
204883	58	0.88	0.88	0.85	0.86	0.87
204891	59	0.83	0.84	0.79	0.79	0.79
204917	60	0.83	0.84	0.8	0.81	0.84
204925	61	0.81	0.81	0.7	0.72	0.71
204933	62	0.85	0.88	0.78	0.81	0.83
204974	63	0.84	0.85	0.86	0.86	0.79
204990	64	-0.58	-0.63	-0.58	-0.52	-0.53
205013	65	0.76	0.75	0.78	0.88	0.88
205021	66	0.89	0.88	0.87	0.87	0.89
205039	67	-0.4	-0.4	-0.4	-0.4	-0.4
205047	68	0.75	0.6	0.71	0.62	0.62
205054	69	0.87	0.81	0.71	0.7	0.82
205088	70	0.89	0.89	0.86	0.86	0.87
205096	71	0.89	0.88	0.83	0.84	0.85
205104	72	0.82	0.76	0.76	0.71	0.78
205120	73	0.76	0.7	0.7	0.71	0.72
205179	74	0.88	0.85	0.81	0.81	0.79
205294	75	0.79	0.79	0.79	0.78	0.79
205377	76	0.8	0.74	0.71	0.74	0.74
205385	77	0.76	0.8	0.76	0.84	0.75
205393	78	0.74	0.81	0.86	0.75	0.76
205419	79	0.86	0.75	0.83	0.84	0.85
205435	80	0.65	0.65	0.71	0.68	0.68

Tab. 7.18: The KGE values for calibration variants Q and Q+SR using S1ASCAT and SCATSAR products during the calibration period in the 196 Austrian catchments (No.81 - 120).

Stream Gauge ID	Gauge No.	KGE Runoff Q	KGE S1ASCAT Q+SR	KGE SCATSAR 020 Q+SR	KGE SCATSAR 040 Q+SR	KGE SCATSAR 100 Q+SR
205450	81	0.85	0.87	0.85	0.86	0.86
205500	82	0.78	0.8	0.77	0.77	0.77
205518	83	0.87	0.78	0.78	0.79	0.86
205633	84	0.74	0.75	0.77	0.75	0.77
205641	85	0.74	0.8	0.81	0.66	0.74
205658	86	0.79	0.82	0.81	0.86	0.81
205740	87	0.67	0.62	0.62	0.57	0.59
205765	88	0.71	0.69	0.76	0.71	0.67
205799	89	0.73	0.74	0.66	0.67	0.73
205807	90	0.64	0.66	0.55	0.63	0.61
205815	91	0.84	0.83	0.82	0.82	0.82
205823	92	0.79	0.74	0.74	0.7	0.68
205831	93	0.7	0.69	0.72	0.68	0.77
205856	94	0.67	0.66	0.68	0.67	0.67
205880	95	-0.33	-0.33	-0.33	-0.33	-0.33
205898	96	0.82	0.75	0.75	0.75	0.75
205914	97	0.81	0.83	0.77	0.79	0.75
205948	98	0.49	0.47	0.31	0.37	0.36
205971	99	0.82	0.79	0.75	0.75	0.77
205989	100	0.78	0.74	0.67	0.7	0.71
205997	101	0.81	0.83	0.71	0.75	0.79
206003	102	0.81	0.8	0.8	0.78	0.79
206029	103	0.85	0.84	0.76	0.76	0.76
206037	104	0.85	0.85	0.8	0.82	0.84
206151	105	0.61	0.69	0.6	0.68	0.69
206169	106	0.67	0.63	0.65	0.64	0.63
206185	107	0.88	0.9	0.91	0.85	0.89
207654	108	0.88	0.76	0.84	0.8	0.82
207688	109	0.86	0.85	0.86	0.85	0.79
207704	110	0.86	0.7	0.8	0.8	0.84
207712	111	0.81	0.77	0.76	0.77	0.76
207720	112	0.76	0.7	0.73	0.66	0.66
207746	113	0.81	0.81	0.87	0.8	0.8
207787	114	0.74	0.75	0.78	0.74	0.78
207795	115	0.74	0.81	0.81	0.81	0.81
207811	116	0.7	0.72	0.69	0.7	0.7
207829	117	0.64	0.63	0.65	0.65	0.64
207837	118	0.7	0.74	0.69	0.75	0.75
207845	119	0.75	0.75	0.72	0.71	0.71
207852	120	0.78	0.83	0.82	0.83	0.83

Tab. 7.19: The KGE values for calibration variants Q and Q+SR using S1ASCAT and SCATSAR products during the calibration period in the 196 Austrian catchments (No.121 - 160).

Stream Gauge ID	Gauge No.	KGE Runoff Q	KGE S1ASCAT Q+SR	KGE SCATSAR 020 Q+SR	KGE SCATSAR 040 Q+SR	KGE SCATSAR 100 Q+SR
207860	121	0.66	0.66	0.6	0.61	0.67
207894	122	0.77	0.85	0.8	0.66	0.6
207910	123	0.79	0.85	0.66	0.68	0.7
207936	124	0.75	0.76	0.74	0.74	0.74
207944	125	0.82	0.81	0.78	0.77	0.79
208009	126	0.64	0.66	0.59	0.64	0.64
208017	127	0.7	0.69	0.69	0.68	0.75
208090	128	0.71	0.8	0.74	0.74	0.76
208116	129	0.71	0.71	0.73	0.7	0.69
208124	130	0.68	0.68	0.73	0.68	0.69
208157	131	0.75	0.75	0.73	0.76	0.72
208280	132	0.87	0.9	0.81	0.82	0.82
208413	133	-0.3	-0.29	-0.3	-0.29	-0.3
208439	134	0.83	0.82	0.81	0.79	0.8
208462	135	0.75	0.79	0.81	0.73	0.77
208579	136	0.83	0.84	0.83	0.81	0.81
208611	137	0.55	0.13	0.61	0.6	0.65
208686	138	0.76	0.75	0.74	0.69	0.68
208702	139	0.81	0.79	0.77	0.76	0.75
208710	140	0.82	0.83	0.85	0.73	0.73
208819	141	0.86	0.84	0.84	0.84	0.82
209197	142	0.66	0.63	0.65	0.65	0.65
210229	143	0.74	0.75	0.78	0.8	0.79
210526	144	0.92	0.9	0.87	0.87	0.84
210542	145	0.78	0.66	0.71	0.68	0.71
210583	146	0.63	0.61	0.5	0.46	0.52
210625	147	0.76	0.73	0.62	0.62	0.62
210641	148	0.87	0.87	0.89	0.81	0.82
210773	149	0.9	0.85	0.88	0.86	0.89
210815	150	0.8	0.85	0.83	0.76	0.84
210864	151	0.75	0.74	0.75	0.78	0.69
210880	152	0.72	0.64	0.63	0.7	0.7
210898	153	0.85	0.81	0.8	0.73	0.75
210989	154	0.81	0.84	0.7	0.8	0.79
211003	155	0.71	0.7	0.72	0.68	0.66
211102	156	0.95	0.89	0.86	0.83	0.82
211136	157	0.96	0.92	0.88	0.88	0.88
211169	158	0.88	0.86	0.88	0.87	0.87
211193	159	0.87	0.87	0.86	0.86	0.86
211227	160	0.77	0.77	0.7	0.75	0.74

Tab. 7.20: The KGE values for calibration variants Q and Q+SR using S1ASCAT and SCATSAR products during the calibration period in the 196 Austrian catchments (No.161 - 196).

Stream Gauge ID	Gauge No.	KGE Runoff Q	KGE S1ASCAT Q+SR	KGE SCATSAR 020 Q+SR	KGE SCATSAR 040 Q+SR	KGE SCATSAR 100 Q+SR
211243	161	0.82	0.82	0.82	0.81	0.83
211268	162	0.84	0.86	0.81	0.8	0.81
211292	163	0.96	0.95	0.93	0.96	0.96
211383	164	0.71	0.69	0.68	0.69	0.69
211391	165	0.81	0.75	0.76	0.74	0.75
211458	166	0.83	0.85	0.81	0.84	0.84
212027	167	0.95	0.89	0.91	0.91	0.92
212068	168	0.65	0.51	0.55	0.55	0.55
212076	169	0.77	0.58	0.68	0.68	0.68
212092	170	0.95	0.92	0.94	0.93	0.93
212126	171	0.94	0.93	0.91	0.91	0.91
212183	172	0.95	0.93	0.95	0.95	0.95
212316	173	0.96	0.92	0.92	0.94	0.94
212324	174	0.96	0.92	0.92	0.92	0.93
212357	175	0.96	0.94	0.92	0.91	0.92
212381	176	0.86	0.8	0.75	0.75	0.75
212431	177	0.9	0.89	0.88	0.88	0.87
212522	178	0.93	0.85	0.91	0.91	0.91
212613	179	0.94	0.86	0.87	0.89	0.89
212647	180	0.94	0.92	0.85	0.9	0.95
212670	181	0.93	0.92	0.91	0.91	0.91
212704	182	0.83	0.79	0.82	0.81	0.82
212753	183	0.9	0.89	0.87	0.89	0.91
212787	184	0.87	0.87	0.8	0.85	0.86
212860	185	0.91	0.87	0.88	0.88	0.86
212886	186	0.83	0.8	0.85	0.84	0.81
212894	187	0.82	0.82	0.84	0.84	0.83
212928	188	0.87	0.84	0.85	0.82	0.79
212936	189	0.91	0.9	0.88	0.89	0.88
213025	190	0.89	0.81	0.88	0.86	0.86
213033	191	0.91	0.87	0.91	0.89	0.9
213082	192	0.87	0.84	0.84	0.83	0.83
213090	193	0.88	0.85	0.83	0.83	0.83
213157	194	0.89	0.87	0.88	0.88	0.89
213231	195	0.84	0.81	0.83	0.83	0.81
213256	196	0.87	0.82	0.82	0.83	0.85

Tab. 7.21: The r_{SR} values for calibration variants Q and Q+SR using S1ASCAT and SCATSAR products during the calibration period in the 196 Austrian catchments (No.1 - 40).

Stream Gauge ID	Gauge No.	r_{SR} Runoff Q	r_{SR} S1ASCAT Q+SR	r_{SR} SCATSAR 020 Q+SR	r_{SR} SCATSAR 040 Q+SR	r_{SR} SCATSAR 100 Q+SR
200105	1	N/A	N/A	N/A	N/A	N/A
200147	2	N/A	N/A	0.53	0.59	0.64
200196	3	N/A	N/A	0.43	0.47	0.54
200204	4	N/A	N/A	0.11	0.15	0.16
200212	5	N/A	N/A	0.22	0.26	0.27
200220	6	N/A	N/A	0.46	0.51	0.50
200246	7	N/A	N/A	0.68	0.68	0.67
200253	8	N/A	N/A	0.57	0.59	0.63
200261	9	N/A	N/A	0.48	0.50	0.53
200287	10	N/A	N/A	0.59	0.59	0.61
200311	11	N/A	N/A	0.40	0.47	0.48
200360	12	N/A	N/A	N/A	N/A	N/A
200378	13	N/A	N/A	0.75	0.74	0.67
201012	14	0.54	0.60	0.64	0.63	0.54
201053	15	0.35	0.51	N/A	N/A	N/A
201087	16	0.34	0.44	0.11	0.12	0.14
201111	17	0.55	0.63	0.34	0.30	0.27
201533	18	-0.11	0.11	0.01	0.03	0.13
201574	19	0.01	0.19	0.26	0.32	0.32
201723	20	0.07	0.25	N/A	N/A	N/A
201822	21	0.06	0.41	0.35	0.15	0.16
201863	22	0.38	0.52	0.48	0.47	0.49
201913	23	0.36	0.61	0.15	0.09	0.21
201921	24	0.24	0.58	0.21	0.20	0.16
201939	25	0.38	0.59	0.07	0.10	0.20
201947	26	0.53	0.53	0.10	0.13	0.15
203034	27	0.29	0.29	N/A	N/A	N/A
203042	28	0.20	0.20	N/A	N/A	N/A
203075	29	0.01	0.15	0.54	0.58	0.62
203141	30	-0.01	0.14	N/A	N/A	N/A
203166	31	-0.16	0.16	0.25	0.32	0.40
203208	32	0.01	0.13	0.49	0.54	0.61
203224	33	0.23	0.31	N/A	N/A	N/A
203307	34	-0.06	0.42	0.23	0.13	0.16
203315	35	0.28	0.37	0.23	0.23	0.26
203463	36	0.13	0.55	N/A	N/A	N/A
203471	37	0.28	0.38	0.13	0.17	0.22
203505	38	0.32	0.39	0.11	0.11	0.03
203539	39	-0.06	0.37	0.27	0.29	0.31
203547	40	0.58	0.88	0.71	0.72	0.72

Tab. 7.22: The r_{SR} values for calibration variants Q and Q+SR using S1ASCAT and SCATSAR products during the calibration period in the 196 Austrian catchments (No.41 - 80).

Stream Gauge ID	Gauge No.	r_{SR} Runoff Q	r_{SR} S1ASCAT Q+SR	r_{SR} SCATSAR 020 Q+SR	r_{SR} SCATSAR 040 Q+SR	r_{SR} SCATSAR 100 Q+SR
203661	41	0.55	0.74	0.47	0.48	0.46
203711	42	0.33	0.45	0.21	0.23	0.10
203760	43	0.32	0.51	N/A	N/A	N/A
203778	44	0.18	0.49	0.34	0.23	0.11
203786	45	0.30	0.50	0.29	0.22	0.25
204545	46	0.86	0.87	0.52	0.52	0.54
204586	47	0.75	0.85	0.67	0.72	0.72
204685	48	0.67	0.87	0.78	0.78	0.78
204719	49	0.53	0.88	0.78	0.82	0.82
204735	50	0.84	0.89	0.82	0.85	0.86
204750	51	0.80	0.90	0.82	0.86	0.85
204768	52	0.83	0.88	0.83	0.85	0.86
204784	53	0.81	0.88	0.82	0.85	0.84
204826	54	0.54	0.60	0.24	0.44	0.44
204834	55	0.87	0.89	0.77	0.81	0.82
204867	56	0.87	0.89	0.78	0.82	0.82
204875	57	0.87	0.88	0.49	0.56	0.58
204883	58	0.85	0.87	0.58	0.61	0.63
204891	59	0.78	0.80	0.00	0.05	0.10
204917	60	0.78	0.81	0.09	0.12	0.16
204925	61	0.83	0.85	0.27	0.32	0.36
204933	62	0.81	0.82	0.09	0.12	0.16
204974	63	0.78	0.87	0.81	0.84	0.84
204990	64	0.64	0.74	0.48	0.49	0.63
205013	65	0.82	0.88	0.81	0.84	0.84
205021	66	0.83	0.87	0.79	0.83	0.83
205039	67	0.54	0.89	0.73	0.77	0.83
205047	68	0.82	0.88	0.83	0.85	0.85
205054	69	0.83	0.88	0.76	0.81	0.81
205088	70	0.80	0.84	0.54	0.58	0.60
205096	71	0.79	0.83	0.45	0.45	0.46
205104	72	0.12	0.57	0.12	0.18	0.17
205120	73	0.09	0.31	0.50	0.48	0.50
205179	74	0.30	0.68	0.38	0.37	0.36
205294	75	0.77	0.79	0.49	0.53	0.52
205377	76	0.50	0.86	0.58	0.62	0.62
205385	77	0.75	0.89	0.71	0.71	0.73
205393	78	0.79	0.86	0.64	0.67	0.67
205419	79	0.80	0.83	0.57	0.62	0.63
205435	80	0.62	0.66	0.60	0.60	0.60

Tab. 7.23: The r_{SR} values for calibration variants Q and Q+SR using S1ASCAT and SCATSAR products during the calibration period in the 196 Austrian catchments (No.81 - 120).

Stream Gauge ID	Gauge No.	r_{SR} Runoff Q	r_{SR} S1ASCAT Q+SR	r_{SR} SCATSAR 020 Q+SR	r_{SR} SCATSAR 040 Q+SR	r_{SR} SCATSAR 100 Q+SR
205450	81	0.66	0.69	0.58	0.61	0.62
205500	82	0.55	0.64	0.51	0.58	0.61
205518	83	0.54	0.57	0.58	0.63	0.67
205633	84	0.71	0.73	0.59	0.59	0.59
205641	85	0.69	0.72	0.65	0.66	0.66
205658	86	0.70	0.73	0.69	0.71	0.71
205740	87	0.25	0.60	0.23	0.17	0.13
205765	88	0.18	0.69	0.06	0.04	0.10
205799	89	0.25	0.69	0.26	0.17	0.06
205807	90	0.59	0.65	0.26	0.15	0.17
205815	91	0.43	0.55	0.04	0.03	0.05
205823	92	0.36	0.69	-0.04	-0.04	0.00
205831	93	0.24	0.69	0.27	-0.01	-0.01
205856	94	0.54	0.61	0.13	0.16	0.19
205880	95	0.35	0.06	0.14	0.07	-0.01
205898	96	0.35	0.62	0.54	0.55	0.54
205914	97	0.52	0.62	0.43	0.48	0.53
205948	98	0.80	0.82	0.27	0.27	0.29
205971	99	0.81	0.83	0.29	0.34	0.38
205989	100	0.81	0.85	0.35	0.41	0.43
205997	101	0.84	0.86	-0.04	0.00	0.07
206003	102	0.84	0.88	0.02	0.07	0.13
206029	103	0.80	0.85	0.39	0.45	0.48
206037	104	0.83	0.84	0.54	0.57	0.57
206151	105	0.85	0.89	0.81	0.85	0.84
206169	106	0.85	0.89	0.81	0.85	0.85
206185	107	0.72	0.78	0.49	0.52	0.50
207654	108	0.17	0.56	0.09	0.04	0.06
207688	109	0.27	0.54	0.55	0.58	0.70
207704	110	0.09	0.52	0.01	-0.06	-0.09
207712	111	0.16	0.54	0.14	0.08	0.01
207720	112	0.30	0.63	0.19	0.14	0.09
207746	113	0.58	0.67	0.41	0.42	0.46
207787	114	0.73	0.74	0.55	0.57	0.58
207795	115	0.59	0.71	0.68	0.69	0.70
207811	116	0.80	0.82	0.38	0.43	0.47
207829	117	0.75	0.78	0.72	0.72	0.71
207837	118	0.75	0.79	0.75	0.75	0.74
207845	119	0.60	0.71	0.18	0.11	0.06
207852	120	0.65	0.66	0.58	0.62	0.65

Tab. 7.24: The r_{SR} values for calibration variants Q and Q+SR using S1ASCAT and SCATSAR products during the calibration period in the 196 Austrian catchments (No.121 - 160).

Stream Gauge ID	Gauge No.	r_{SR} Runoff Q	r_{SR} S1ASCAT Q+SR	r_{SR} SCATSAR 020 Q+SR	r_{SR} SCATSAR 040 Q+SR	r_{SR} SCATSAR 100 Q+SR
207860	121	0.80	0.85	0.77	0.79	0.77
207894	122	0.58	0.60	0.02	0.09	0.16
207910	123	0.60	0.62	0.55	0.60	0.65
207936	124	0.74	0.85	0.35	0.37	0.38
207944	125	0.70	0.84	0.25	0.28	0.31
208009	126	0.78	0.79	0.62	0.68	0.67
208017	127	0.70	0.79	0.54	0.60	0.61
208090	128	0.76	0.83	0.41	0.49	0.52
208116	129	0.72	0.76	0.29	0.36	0.38
208124	130	0.75	0.78	0.27	0.31	0.38
208157	131	0.80	0.80	0.32	0.43	0.45
208280	132	0.55	0.57	0.04	0.12	0.19
208413	133	0.29	0.64	-0.04	-0.02	0.03
208439	134	0.45	0.57	0.12	0.23	0.26
208462	135	0.69	0.82	-0.01	0.11	0.10
208579	136	0.86	0.88	0.44	0.50	0.52
208611	137	0.86	0.09	0.61	0.65	0.66
208686	138	0.50	0.52	-0.11	-0.15	-0.15
208702	139	0.30	0.35	-0.13	-0.16	-0.14
208710	140	0.34	0.38	-0.09	0.03	0.07
208819	141	0.48	0.50	-0.01	0.07	0.14
209197	142	0.74	0.78	0.68	0.67	0.67
210229	143	0.55	0.60	0.22	0.28	0.34
210526	144	0.41	0.57	0.14	0.22	0.30
210542	145	0.58	0.70	0.20	0.30	0.38
210583	146	-0.09	0.46	0.06	0.08	0.21
210625	147	-0.18	0.38	NA	NA	NA
210641	148	0.05	0.37	0.12	0.13	0.16
210773	149	-0.15	0.33	0.24	0.13	0.10
210815	150	-0.29	0.32	0.12	0.22	0.01
210864	151	0.25	0.35	-0.05	-0.12	-0.13
210880	152	0.05	0.55	0.03	-0.17	-0.15
210898	153	0.23	0.33	0.04	-0.04	-0.05
210989	154	0.51	0.53	0.20	0.20	0.25
211003	155	0.51	0.54	0.21	0.27	0.29
211102	156	0.14	0.40	0.06	0.09	0.19
211136	157	0.11	0.30	0.09	0.08	0.05
211169	158	-0.15	0.31	0.04	-0.02	-0.06
211193	159	-0.12	0.05	0.00	0.02	0.05
211227	160	-0.01	0.37	0.24	-0.04	-0.05

Tab. 7.25: The r_{SR} values for calibration variants Q and Q+SR using S1ASCAT and SCATSAR products during the calibration period in the 196 Austrian catchments (No.161 - 196).

Stream Gauge ID	Gauge No.	r_{SR} Runoff Q	r_{SR} S1ASCAT Q+SR	r_{SR} SCATSAR 020 Q+SR	r_{SR} SCATSAR 040 Q+SR	r_{SR} SCATSAR 100 Q+SR
211243	161	0.19	0.30	-0.29	-0.29	-0.26
211268	162	0.13	0.16	-0.18	-0.16	-0.13
211292	163	0.13	0.28	-0.19	-0.27	-0.23
211383	164	0.35	0.52	-0.12	-0.09	-0.04
211391	165	0.28	0.59	0.01	0.03	0.05
211458	166	0.34	0.49	0.02	0.06	0.09
212027	167	0.10	0.32	0.20	0.17	0.13
212068	168	-0.05	0.08	NA	NA	NA
212076	169	-0.31	0.06	NA	NA	NA
212092	170	0.02	0.17	0.70	0.70	0.71
212126	171	0.03	0.17	NA	NA	NA
212183	172	0.02	0.15	0.73	0.73	0.73
212316	173	-0.02	0.07	0.31	0.33	0.35
212324	174	-0.04	0.06	0.28	0.30	0.28
212357	175	-0.07	0.00	0.27	0.28	0.26
212381	176	0.19	0.30	NA	NA	NA
212431	177	0.01	0.25	0.07	0.03	0.01
212522	178	0.01	0.39	-0.02	0.00	0.03
212613	179	-0.17	0.36	0.32	0.30	0.27
212647	180	-0.02	0.23	0.27	0.24	0.11
212670	181	-0.20	0.11	0.16	0.00	-0.01
212704	182	-0.31	0.02	-0.07	-0.11	-0.10
212753	183	-0.29	0.08	0.04	-0.09	-0.10
212787	184	-0.34	0.11	0.00	-0.08	-0.07
212860	185	0.09	0.53	0.09	0.04	0.02
212886	186	0.08	0.42	-0.07	-0.13	-0.25
212894	187	0.23	0.33	-0.12	-0.11	-0.12
212928	188	0.15	0.21	-0.26	-0.14	0.03
212936	189	0.05	0.13	-0.20	-0.18	-0.13
213025	190	-0.06	0.18	-0.17	-0.08	-0.01
213033	191	0.11	0.21	-0.12	-0.05	0.02
213082	192	0.10	0.20	-0.25	-0.23	-0.19
213090	193	0.11	0.17	-0.16	-0.14	-0.12
213157	194	0.11	0.26	-0.19	-0.15	-0.11
213231	195	0.12	0.27	-0.24	-0.16	-0.08
213256	196	0.17	0.29	-0.07	-0.01	0.08

Tab. 7.26: The NSE values for calibration variants Q and Q+SR using S1ASCAT and SCATSAR products during the validation period in the 196 Austrian catchments (No.1 - 40).

Stream Gauge ID	Gauge No.	NSE Runoff Q	NSE S1ASCAT Q+SR	NSE SCATSAR 020 Q+SR	NSE SCATSAR 040 Q+SR	NSE SCATSAR 100 Q+SR
200105	1	0.73	0.74	0.74	0.74	0.74
200147	2	0.76	0.77	0.77	0.77	0.77
200196	3	0.78	0.8	0.78	0.79	0.79
200204	4	0.62	0.62	0.6	0.58	0.58
200212	5	0.7	0.7	0.68	0.68	0.73
200220	6	0.72	0.67	0.69	0.69	0.83
200246	7	0.74	0.7	0.73	0.73	0.73
200253	8	0.8	0.79	0.8	0.8	0.81
200261	9	0.77	0.76	0.77	0.77	0.76
200287	10	0.75	0.76	0.74	0.74	0.74
200311	11	0.71	0.69	0.71	0.7	0.69
200360	12	0.85	0.8	0.8	0.8	0.8
200378	13	0.85	0.81	0.84	0.84	0.84
201012	14	0.86	0.84	0.82	0.85	0.85
201053	15	0.76	0.79	0.75	0.75	0.75
201087	16	0.81	0.82	0.82	0.82	0.83
201111	17	0.75	0.77	0.76	0.76	0.76
201533	18	-14	-14	-14	-14.01	-14.01
201574	19	0.86	0.81	0.79	0.79	0.86
201723	20	0.82	0.8	0.82	0.82	0.82
201822	21	0.73	0.69	0.64	0.68	0.68
201863	22	0.76	0.74	0.8	0.79	0.77
201913	23	0.75	0.73	0.74	0.75	0.73
201921	24	0.77	0.74	0.74	0.74	0.78
201939	25	0.76	0.73	0.8	0.78	0.74
201947	26	0.71	0.71	0.76	0.76	0.76
203034	27	0.69	0.69	0.72	0.72	0.72
203042	28	0.55	0.55	0.57	0.57	0.57
203075	29	0.79	0.79	0.8	0.79	0.8
203141	30	0.81	0.79	0.78	0.78	0.78
203166	31	0.8	0.83	0.8	0.8	0.81
203208	32	0.71	0.66	0.64	0.63	0.63
203224	33	0.75	0.72	0.75	0.75	0.75
203307	34	0.65	0.66	0.61	0.61	0.62
203315	35	0.73	0.65	0.67	0.66	0.65
203463	36	0.68	0.68	0.62	0.62	0.62
203471	37	0.7	0.72	0.7	0.7	0.7
203505	38	0.75	0.74	0.75	0.74	0.74
203539	39	0.78	0.72	0.75	0.69	0.68
203547	40	0.77	0.87	0.49	0.78	0.83

Tab. 7.27: The NSE values for calibration variants Q and Q+SR using S1ASCAT and SCATSAR products during the validation period in the 196 Austrian catchments (No.41 - 80).

Stream Gauge ID	Gauge No.	NSE Runoff Q	NSE S1ASCAT Q+SR	NSE SCATSAR 020 Q+SR	NSE SCATSAR 040 Q+SR	NSE SCATSAR 100 Q+SR
203661	41	0.72	0.76	0.71	0.73	0.74
203711	42	0.82	0.8	0.79	0.78	0.8
203760	43	0.79	0.74	0.69	0.69	0.69
203778	44	0.86	0.8	0.77	0.77	0.8
203786	45	0.85	0.78	0.81	0.82	0.82
204545	46	0.75	0.81	0.72	0.73	0.7
204586	47	0.84	0.88	0.87	0.86	0.86
204685	48	0.62	0.61	0.6	0.6	0.6
204719	49	0.63	0.6	0.71	0.62	0.61
204735	50	0.65	0.61	0.67	0.67	0.63
204750	51	0.65	0.63	0.76	0.63	0.69
204768	52	0.59	0.54	0.73	0.66	0.64
204784	53	0.61	0.61	0.64	0.59	0.64
204826	54	-121.17	-121.17	-121.18	-121.17	-121.17
204834	55	0.65	0.65	0.57	0.68	0.67
204867	56	0.71	0.68	0.69	0.73	0.71
204875	57	0.65	0.64	0.7	0.68	0.66
204883	58	0.75	0.74	0.75	0.76	0.74
204891	59	0.61	0.62	0.58	0.63	0.64
204917	60	0.75	0.68	0.69	0.7	0.69
204925	61	0.73	0.72	0.72	0.7	0.7
204933	62	0.73	0.74	0.74	0.72	0.74
204974	63	0.69	0.69	0.71	0.7	0.64
204990	64	-88.53	-88.53	-88.53	-88.53	-88.53
205013	65	0.67	0.66	0.7	0.76	0.76
205021	66	0.7	0.69	0.74	0.67	0.7
205039	67	-25.03	-25.03	-25.03	-25.03	-25.03
205047	68	0.62	0.54	0.61	0.54	0.54
205054	69	0.77	0.71	0.67	0.66	0.81
205088	70	0.74	0.72	0.73	0.73	0.72
205096	71	0.74	0.73	0.71	0.7	0.71
205104	72	0.79	0.75	0.74	0.74	0.76
205120	73	0.76	0.77	0.76	0.75	0.76
205179	74	0.86	0.8	0.79	0.8	0.79
205294	75	0.76	0.77	0.76	0.75	0.76
205377	76	0.7	0.61	0.57	0.61	0.61
205385	77	0.67	0.65	0.67	0.7	0.66
205393	78	0.61	0.67	0.69	0.64	0.63
205419	79	0.7	0.65	0.73	0.71	0.71
205435	80	0.59	0.59	0.63	0.6	0.6

Tab. 7.28: The NSE values for calibration variants Q and Q+SR using S1ASCAT and SCATSAR products during the validation period in the 196 Austrian catchments (No.81 - 120).

Stream Gauge ID	Gauge No.	NSE Runoff Q	NSE S1ASCAT Q+SR	NSE SCATSAR 020 Q+SR	NSE SCATSAR 040 Q+SR	NSE SCATSAR 100 Q+SR
205450	81	0.82	0.83	0.81	0.82	0.83
205500	82	0.67	0.67	0.62	0.64	0.64
205518	83	0.81	0.71	0.68	0.7	0.71
205633	84	0.61	0.6	0.6	0.6	0.6
205641	85	0.64	0.67	0.64	0.63	0.63
205658	86	0.71	0.71	0.76	0.77	0.73
205740	87	0.68	0.65	0.66	0.66	0.67
205765	88	0.68	0.65	0.69	0.67	0.65
205799	89	0.74	0.77	0.7	0.72	0.74
205807	90	0.72	0.74	0.7	0.65	0.63
205815	91	0.6	0.55	0.44	0.47	0.48
205823	92	0.65	0.69	0.69	0.67	0.67
205831	93	0.66	0.69	0.66	0.67	0.75
205856	94	0.65	0.66	0.64	0.65	0.65
205880	95	-55.88	-55.89	-55.89	-55.89	-55.88
205898	96	0.42	0.63	0.63	0.64	0.64
205914	97	0.7	0.7	0.7	0.63	0.63
205948	98	0.6	0.59	0.35	0.57	0.52
205971	99	0.65	0.57	0.82	0.81	0.75
205989	100	0.78	0.69	0.76	0.76	0.75
205997	101	0.68	0.75	0.62	0.7	0.71
206003	102	0.55	0.61	0.7	0.67	0.7
206029	103	0.71	0.76	0.79	0.78	0.79
206037	104	0.75	0.76	0.79	0.75	0.8
206151	105	0.65	0.58	0.65	0.68	0.67
206169	106	0.66	0.63	0.65	0.65	0.63
206185	107	0.88	0.91	0.89	0.91	0.89
207654	108	0.79	0.63	0.8	0.7	0.77
207688	109	0.8	0.79	0.82	0.82	0.76
207704	110	0.79	0.71	0.76	0.77	0.8
207712	111	0.75	0.72	0.72	0.72	0.72
207720	112	0.76	0.73	0.74	0.72	0.7
207746	113	0.66	0.55	0.59	0.69	0.66
207787	114	0.69	0.7	0.7	0.7	0.71
207795	115	0.79	0.79	0.79	0.79	0.82
207811	116	0.53	0.54	0.44	0.52	0.54
207829	117	0.71	0.69	0.71	0.7	0.66
207837	118	0.74	0.62	0.68	0.71	0.69
207845	119	0.74	0.71	0.71	0.71	0.71
207852	120	0.78	0.84	0.82	0.8	0.82

Tab. 7.29: The NSE values for calibration variants Q and Q+SR using S1ASCAT and SCATSAR products during the validation period in the 196 Austrian catchments (No.121 - 160).

Stream Gauge ID	Gauge No.	NSE Runoff Q	NSE S1ASCAT Q+SR	NSE SCATSAR 020 Q+SR	NSE SCATSAR 040 Q+SR	NSE SCATSAR 100 Q+SR
207860	121	0.73	0.71	0.63	0.65	0.68
207894	122	0.68	0.76	0.72	0.66	0.67
207910	123	0.81	0.79	0.71	0.7	0.68
207936	124	0.69	0.72	0.75	0.75	0.75
207944	125	0.64	0.79	0.58	0.76	0.75
208009	126	0.68	0.61	0.71	0.71	0.7
208017	127	0.58	0.62	0.66	0.69	0.63
208090	128	0.53	0.6	0.58	0.62	0.61
208116	129	0.69	0.71	0.78	0.74	0.72
208124	130	0.68	0.67	0.67	0.69	0.71
208157	131	0.62	0.58	0.61	0.68	0.67
208280	132	0.72	0.74	0.77	0.42	0.43
208413	133	-20.5	-20.52	-20.49	-20.49	-20.49
208439	134	0.65	0.66	0.67	0.74	0.73
208462	135	0.66	0.78	0.79	0.72	0.78
208579	136	0.55	0.66	0.51	0.5	0.53
208611	137	0.49	0.25	0.46	0.41	0.42
208686	138	0.65	0.66	0.65	0.64	0.64
208702	139	0.66	0.67	0.61	0.68	0.6
208710	140	0.64	0.66	0.5	0.38	0.39
208819	141	0.72	0.76	0.38	0.4	0.39
209197	142	0.54	0.53	0.55	0.54	0.54
210229	143	0.46	0.45	0.22	0.27	0.28
210526	144	0.81	0.82	0.8	0.82	0.77
210542	145	0.78	0.61	0.75	0.69	0.74
210583	146	0.67	0.68	0.63	0.58	0.61
210625	147	0.78	0.78	0.65	0.65	0.65
210641	148	0.78	0.77	0.79	0.78	0.78
210773	149	0.69	0.59	0.7	0.68	0.7
210815	150	0.85	0.81	0.84	0.75	0.83
210864	151	0.63	0.58	0.63	0.67	0.64
210880	152	0.68	0.63	0.53	0.7	0.7
210898	153	0.77	0.77	0.68	0.73	0.75
210989	154	0.55	0.73	0.72	0.54	0.59
211003	155	0.46	0.51	0.27	0.29	0.39
211102	156	0.88	0.78	0.79	0.72	0.71
211136	157	0.81	0.79	0.78	0.79	0.78
211169	158	0.83	0.82	0.81	0.49	0.79
211193	159	0.62	0.67	0.61	0.61	0.62
211227	160	0.47	0.46	0.44	0.43	0.42

Tab. 7.30: The NSE values for calibration variants Q and Q+SR using S1ASCAT and SCATSAR products during the validation period in the 196 Austrian catchments (No.161 - 196).

Stream Gauge ID	Gauge No.	NSE Runoff Q	NSE S1ASCAT Q+SR	NSE SCATSAR 020 Q+SR	NSE SCATSAR 040 Q+SR	NSE SCATSAR 100 Q+SR
211243	161	0.56	0.55	0.59	0.6	0.58
211268	162	0.63	0.66	0.72	0.75	0.74
211292	163	0.85	0.78	0.76	0.83	0.83
211383	164	0.69	0.64	0.67	0.67	0.63
211391	165	0.58	0.54	0.57	0.6	0.58
211458	166	0.51	0.77	0.62	0.57	0.64
212027	167	0.86	0.76	0.76	0.77	0.79
212068	168	0.75	0.66	0.66	0.66	0.66
212076	169	0.79	0.7	0.75	0.75	0.75
212092	170	0.85	0.82	0.83	0.83	0.83
212126	171	0.86	0.86	0.87	0.87	0.87
212183	172	0.87	0.84	0.86	0.86	0.86
212316	173	0.88	0.81	0.83	0.82	0.83
212324	174	0.88	0.81	0.82	0.82	0.82
212357	175	0.86	0.79	0.78	0.77	0.78
212381	176	0.86	0.86	0.87	0.87	0.87
212431	177	0.63	0.58	0.6	0.62	0.63
212522	178	0.86	0.79	0.87	0.88	0.87
212613	179	0.53	0.49	0.4	0.26	0.25
212647	180	0.47	0.39	0.25	0.37	0.64
212670	181	0.69	0.56	0.58	0.71	0.71
212704	182	0.66	0.65	0.68	0.67	0.67
212753	183	0.71	0.69	0.7	0.73	0.72
212787	184	0.71	0.68	0.69	0.7	0.71
212860	185	0.78	0.75	0.69	0.68	0.73
212886	186	0.6	0.47	0.5	0.5	0.56
212894	187	0.7	0.61	0.3	0.23	0.47
212928	188	0.58	0.67	0.57	0.49	0.2
212936	189	0.78	0.75	0.72	0.72	0.72
213025	190	0.77	0.75	0.73	0.73	0.72
213033	191	0.8	0.71	0.79	0.75	0.82
213082	192	0.49	0.55	0.09	-0.02	0.03
213090	193	0.65	0.55	0.33	0.31	0.37
213157	194	0.81	0.78	0.72	0.72	0.78
213231	195	0.61	0.67	0.68	0.7	0.71
213256	196	0.46	0.56	0.33	0.31	0.3

Tab. 7.31: The KGE values for calibration variants Q and Q+SR using S1ASCAT and SCATSAR products during the validation period in the 196 Austrian catchments (No.1 - 40).

Stream Gauge ID	Gauge No.	KGE Runoff Q	KGE S1ASCAT Q+SR	KGE SCATSAR 020 Q+SR	KGE SCATSAR 040 Q+SR	KGE SCATSAR 100 Q+SR
200105	1	0.84	0.86	0.86	0.86	0.86
200147	2	0.86	0.88	0.86	0.87	0.87
200196	3	0.88	0.88	0.88	0.88	0.88
200204	4	0.56	0.56	0.51	0.49	0.49
200212	5	0.73	0.76	0.71	0.69	0.72
200220	6	0.81	0.82	0.81	0.79	0.87
200246	7	0.77	0.7	0.79	0.78	0.81
200253	8	0.83	0.84	0.87	0.86	0.83
200261	9	0.75	0.75	0.76	0.76	0.74
200287	10	0.78	0.76	0.77	0.78	0.77
200311	11	0.81	0.83	0.78	0.75	0.74
200360	12	0.79	0.68	0.68	0.68	0.68
200378	13	0.92	0.89	0.88	0.86	0.86
201012	14	0.86	0.81	0.82	0.88	0.89
201053	15	0.82	0.81	0.77	0.77	0.77
201087	16	0.84	0.82	0.82	0.85	0.85
201111	17	0.78	0.79	0.76	0.78	0.78
201533	18	-0.45	-0.45	-0.45	-0.45	-0.45
201574	19	0.93	0.9	0.83	0.85	0.93
201723	20	0.85	0.85	0.86	0.86	0.86
201822	21	0.77	0.73	0.72	0.65	0.71
201863	22	0.74	0.77	0.81	0.78	0.75
201913	23	0.76	0.81	0.76	0.75	0.78
201921	24	0.88	0.84	0.81	0.8	0.83
201939	25	0.78	0.8	0.86	0.78	0.79
201947	26	0.84	0.84	0.86	0.87	0.86
203034	27	0.58	0.58	0.67	0.67	0.67
203042	28	0.49	0.49	0.49	0.49	0.49
203075	29	0.75	0.78	0.75	0.74	0.75
203141	30	0.85	0.86	0.83	0.83	0.83
203166	31	0.83	0.87	0.82	0.83	0.81
203208	32	0.66	0.62	0.59	0.57	0.57
203224	33	0.77	0.73	0.76	0.76	0.76
203307	34	0.68	0.7	0.62	0.63	0.64
203315	35	0.78	0.74	0.74	0.73	0.69
203463	36	0.68	0.71	0.6	0.6	0.6
203471	37	0.65	0.69	0.64	0.65	0.65
203505	38	0.75	0.77	0.75	0.72	0.71
203539	39	0.81	0.78	0.83	0.75	0.75
203547	40	0.88	0.9	0.72	0.88	0.83

Tab. 7.32: The KGE values for calibration variants Q and Q+SR using S1ASCAT and SCATSAR products during the validation period in the 196 Austrian catchments (No.41 - 80).

Stream Gauge ID	Gauge No.	KGE Runoff Q	KGE S1ASCAT Q+SR	KGE SCATSAR 020 Q+SR	KGE SCATSAR 040 Q+SR	KGE SCATSAR 100 Q+SR
203661	41	0.7	0.76	0.68	0.73	0.74
203711	42	0.86	0.87	0.82	0.82	0.82
203760	43	0.76	0.71	0.62	0.62	0.62
203778	44	0.88	0.83	0.79	0.78	0.84
203786	45	0.86	0.75	0.84	0.87	0.84
204545	46	0.86	0.83	0.85	0.86	0.85
204586	47	0.91	0.88	0.93	0.86	0.92
204685	48	0.74	0.68	0.71	0.72	0.72
204719	49	0.81	0.79	0.81	0.81	0.81
204735	50	0.72	0.68	0.77	0.76	0.7
204750	51	0.77	0.75	0.87	0.74	0.84
204768	52	0.58	0.55	0.68	0.62	0.61
204784	53	0.79	0.77	0.82	0.72	0.8
204826	54	-0.41	-0.41	-0.41	-0.41	-0.41
204834	55	0.77	0.81	0.79	0.82	0.83
204867	56	0.79	0.73	0.76	0.77	0.77
204875	57	0.78	0.78	0.73	0.7	0.77
204883	58	0.8	0.8	0.76	0.79	0.76
204891	59	0.73	0.73	0.7	0.69	0.69
204917	60	0.75	0.77	0.74	0.76	0.77
204925	61	0.71	0.7	0.66	0.64	0.63
204933	62	0.78	0.84	0.74	0.74	0.76
204974	63	0.78	0.81	0.82	0.82	0.73
204990	64	-0.55	-0.63	-0.56	-0.5	-0.5
205013	65	0.69	0.68	0.73	0.79	0.78
205021	66	0.84	0.83	0.86	0.79	0.83
205039	67	-0.37	-0.37	-0.38	-0.38	-0.37
205047	68	0.69	0.58	0.65	0.6	0.6
205054	69	0.83	0.8	0.7	0.69	0.85
205088	70	0.87	0.86	0.85	0.84	0.85
205096	71	0.82	0.81	0.77	0.77	0.78
205104	72	0.78	0.73	0.72	0.67	0.74
205120	73	0.78	0.76	0.73	0.73	0.74
205179	74	0.92	0.89	0.86	0.87	0.85
205294	75	0.83	0.84	0.83	0.82	0.83
205377	76	0.72	0.6	0.54	0.6	0.59
205385	77	0.7	0.71	0.7	0.74	0.68
205393	78	0.71	0.81	0.84	0.76	0.76
205419	79	0.84	0.77	0.83	0.84	0.84
205435	80	0.51	0.5	0.56	0.53	0.53

Tab. 7.33: The KGE values for calibration variants Q and Q+SR using S1ASCAT and SCATSAR products during the validation period in the 196 Austrian catchments (No.81 - 120).

Stream Gauge ID	Gauge No.	KGE Runoff Q	KGE S1ASCAT Q+SR	KGE SCATSAR 020 Q+SR	KGE SCATSAR 040 Q+SR	KGE SCATSAR 100 Q+SR
205450	81	0.78	0.82	0.77	0.76	0.78
205500	82	0.69	0.69	0.69	0.7	0.7
205518	83	0.8	0.68	0.73	0.73	0.78
205633	84	0.74	0.71	0.72	0.71	0.72
205641	85	0.78	0.79	0.8	0.71	0.76
205658	86	0.74	0.77	0.81	0.85	0.78
205740	87	0.74	0.71	0.73	0.68	0.71
205765	88	0.65	0.62	0.68	0.66	0.61
205799	89	0.78	0.79	0.71	0.75	0.78
205807	90	0.74	0.76	0.68	0.71	0.69
205815	91	0.77	0.74	0.67	0.69	0.7
205823	92	0.79	0.8	0.78	0.76	0.76
205831	93	0.72	0.73	0.75	0.69	0.79
205856	94	0.63	0.65	0.67	0.66	0.66
205880	95	-0.31	-0.31	-0.31	-0.32	-0.31
205898	96	0.68	0.79	0.79	0.79	0.79
205914	97	0.77	0.8	0.79	0.76	0.74
205948	98	0.52	0.49	0.25	0.45	0.38
205971	99	0.63	0.57	0.81	0.84	0.85
205989	100	0.72	0.62	0.79	0.8	0.82
205997	101	0.82	0.83	0.76	0.77	0.8
206003	102	0.78	0.81	0.81	0.83	0.79
206029	103	0.77	0.8	0.79	0.79	0.79
206037	104	0.75	0.75	0.73	0.79	0.72
206151	105	0.68	0.67	0.65	0.69	0.69
206169	106	0.72	0.67	0.69	0.69	0.68
206185	107	0.79	0.83	0.84	0.78	0.82
207654	108	0.89	0.81	0.9	0.85	0.88
207688	109	0.86	0.85	0.83	0.83	0.82
207704	110	0.89	0.83	0.87	0.87	0.89
207712	111	0.83	0.83	0.82	0.83	0.82
207720	112	0.85	0.83	0.84	0.83	0.83
207746	113	0.71	0.65	0.58	0.72	0.72
207787	114	0.8	0.8	0.78	0.8	0.8
207795	115	0.78	0.79	0.83	0.82	0.83
207811	116	0.67	0.71	0.67	0.65	0.68
207829	117	0.82	0.83	0.85	0.85	0.83
207837	118	0.81	0.79	0.76	0.81	0.8
207845	119	0.86	0.86	0.86	0.86	0.86
207852	120	0.84	0.9	0.88	0.87	0.88

Tab. 7.34: The KGE values for calibration variants Q and Q+SR using S1ASCAT and SCATSAR products during the validation period in the 196 Austrian catchments (No.121 - 160).

Stream Gauge ID	Gauge No.	KGE Runoff Q	KGE S1ASCAT Q+SR	KGE SCATSAR 020 Q+SR	KGE SCATSAR 040 Q+SR	KGE SCATSAR 100 Q+SR
207860	121	0.77	0.73	0.63	0.64	0.72
207894	122	0.72	0.85	0.78	0.75	0.82
207910	123	0.86	0.88	0.85	0.83	0.84
207936	124	0.84	0.71	0.76	0.77	0.77
207944	125	0.81	0.84	0.79	0.83	0.87
208009	126	0.84	0.78	0.8	0.83	0.84
208017	127	0.77	0.72	0.7	0.78	0.79
208090	128	0.52	0.59	0.54	0.53	0.58
208116	129	0.69	0.69	0.87	0.8	0.74
208124	130	0.78	0.79	0.82	0.82	0.84
208157	131	0.8	0.78	0.77	0.83	0.82
208280	132	0.85	0.86	0.84	0.64	0.65
208413	133	-0.27	-0.28	-0.27	-0.27	-0.27
208439	134	0.73	0.76	0.76	0.82	0.82
208462	135	0.72	0.76	0.84	0.7	0.83
208579	136	0.47	0.61	0.46	0.44	0.46
208611	137	0.51	0.15	0.54	0.5	0.57
208686	138	0.8	0.78	0.75	0.77	0.77
208702	139	0.83	0.82	0.8	0.82	0.8
208710	140	0.81	0.82	0.63	0.69	0.7
208819	141	0.8	0.82	0.53	0.51	0.5
209197	142	0.48	0.45	0.49	0.49	0.49
210229	143	0.71	0.68	0.56	0.56	0.55
210526	144	0.84	0.86	0.83	0.83	0.8
210542	145	0.75	0.62	0.69	0.66	0.69
210583	146	0.65	0.65	0.54	0.5	0.57
210625	147	0.78	0.76	0.62	0.62	0.62
210641	148	0.89	0.88	0.89	0.88	0.89
210773	149	0.84	0.79	0.84	0.83	0.85
210815	150	0.9	0.87	0.91	0.81	0.89
210864	151	0.76	0.73	0.76	0.76	0.77
210880	152	0.79	0.68	0.62	0.79	0.79
210898	153	0.85	0.87	0.82	0.86	0.88
210989	154	0.75	0.81	0.77	0.75	0.79
211003	155	0.72	0.75	0.6	0.62	0.64
211102	156	0.91	0.88	0.88	0.85	0.84
211136	157	0.84	0.87	0.87	0.88	0.85
211169	158	0.91	0.9	0.88	0.69	0.87
211193	159	0.73	0.75	0.73	0.73	0.72
211227	160	0.7	0.69	0.68	0.66	0.67

Tab. 7.35: The KGE values for calibration variants Q and Q+SR using S1ASCAT and SCATSAR products during the validation period in the 196 Austrian catchments (No.161 - 196).

Stream Gauge ID	Gauge No.	KGE Runoff Q	KGE S1ASCAT Q+SR	KGE SCATSAR 020 Q+SR	KGE SCATSAR 040 Q+SR	KGE SCATSAR 100 Q+SR
211243	161	0.76	0.68	0.74	0.78	0.74
211268	162	0.79	0.79	0.84	0.86	0.85
211292	163	0.87	0.83	0.84	0.88	0.88
211383	164	0.84	0.81	0.83	0.82	0.81
211391	165	0.78	0.75	0.79	0.8	0.79
211458	166	0.73	0.84	0.8	0.75	0.79
212027	167	0.92	0.84	0.81	0.82	0.84
212068	168	0.65	0.52	0.54	0.54	0.54
212076	169	0.79	0.61	0.7	0.7	0.7
212092	170	0.92	0.89	0.91	0.91	0.91
212126	171	0.89	0.86	0.92	0.92	0.92
212183	172	0.93	0.91	0.93	0.93	0.93
212316	173	0.9	0.84	0.86	0.85	0.87
212324	174	0.93	0.86	0.88	0.88	0.87
212357	175	0.89	0.84	0.83	0.82	0.83
212381	176	0.92	0.9	0.89	0.89	0.89
212431	177	0.8	0.77	0.77	0.77	0.78
212522	178	0.81	0.79	0.82	0.82	0.83
212613	179	0.77	0.75	0.7	0.65	0.65
212647	180	0.68	0.61	0.54	0.64	0.8
212670	181	0.81	0.78	0.79	0.78	0.77
212704	182	0.76	0.76	0.76	0.75	0.77
212753	183	0.79	0.79	0.81	0.78	0.8
212787	184	0.76	0.72	0.76	0.74	0.76
212860	185	0.87	0.86	0.83	0.82	0.84
212886	186	0.71	0.68	0.73	0.73	0.68
212894	187	0.73	0.7	0.67	0.64	0.74
212928	188	0.73	0.8	0.7	0.76	0.63
212936	189	0.88	0.86	0.85	0.85	0.85
213025	190	0.83	0.87	0.79	0.81	0.81
213033	191	0.89	0.85	0.82	0.8	0.84
213082	192	0.65	0.73	0.46	0.42	0.44
213090	193	0.76	0.73	0.61	0.6	0.63
213157	194	0.82	0.8	0.79	0.8	0.82
213231	195	0.79	0.83	0.82	0.84	0.85
213256	196	0.73	0.76	0.67	0.66	0.66

Tab. 7.36: The r_{SR} values for calibration variants Q and Q+SR using S1ASCAT and SCATSAR products during the validation period in the 196 Austrian catchments (No.1 - 40).

Stream Gauge ID	Gauge No.	r_{SR} Runoff Q	r_{SR} S1ASCAT Q+SR	r_{SR} SCATSAR 020 Q+SR	r_{SR} SCATSAR 040 Q+SR	r_{SR} SCATSAR 100 Q+SR
200105	1	NA	NA	NA	NA	NA
200147	2	NA	NA	0.32	0.37	0.44
200196	3	NA	NA	-0.03	0.21	0.28
200204	4	NA	NA	-0.24	-0.24	-0.19
200212	5	NA	NA	-0.23	-0.22	-0.18
200220	6	NA	NA	-0.17	-0.12	-0.06
200246	7	NA	NA	-0.04	-0.06	-0.06
200253	8	NA	NA	0.21	0.23	0.29
200261	9	NA	NA	0.27	0.28	0.30
200287	10	NA	NA	0.43	0.46	0.52
200311	11	NA	NA	-0.22	-0.22	-0.16
200360	12	NA	NA	NA	NA	NA
200378	13	NA	NA	-0.20	-0.11	-0.06
201012	14	0.53	0.63	-0.07	-0.17	-0.01
201053	15	0.49	0.61	NA	NA	NA
201087	16	0.51	0.59	-0.10	-0.17	-0.21
201111	17	0.62	0.74	-0.14	-0.13	-0.11
201533	18	0.02	0.14	0.05	-0.06	-0.09
201574	19	0.08	0.06	0.02	-0.02	-0.09
201723	20	0.16	0.24	NA	NA	NA
201822	21	0.24	0.50	-0.32	-0.23	0.08
201863	22	0.41	0.61	-0.15	-0.18	-0.21
201913	23	0.45	0.67	0.23	-0.36	-0.41
201921	24	0.33	0.65	-0.45	-0.47	-0.45
201939	25	0.50	0.66	-0.26	-0.39	-0.43
201947	26	0.67	0.67	-0.33	-0.44	-0.47
203034	27	0.30	0.30	NA	NA	NA
203042	28	0.23	0.23	NA	NA	NA
203075	29	0.04	0.17	0.32	0.33	0.37
203141	30	-0.03	0.05	NA	NA	NA
203166	31	-0.11	0.18	-0.14	-0.12	-0.16
203208	32	0.13	0.15	0.36	0.23	0.14
203224	33	0.30	0.32	NA	NA	NA
203307	34	0.25	0.45	-0.35	-0.27	-0.23
203315	35	0.48	0.42	0.31	0.30	0.06
203463	36	0.36	0.58	NA	NA	NA
203471	37	0.43	0.45	-0.44	-0.55	-0.56
203505	38	0.50	0.44	-0.36	-0.40	-0.44
203539	39	0.24	0.48	-0.10	-0.09	-0.03
203547	40	0.54	0.88	NA	NA	NA

Tab. 7.37: The r_{SR} values for calibration variants Q and Q+SR using S1ASCAT and SCATSAR products during the validation period in the 196 Austrian catchments (No.41 - 80).

Stream Gauge ID	Gauge No.	r_{SR} Runoff Q	r_{SR} S1ASCAT Q+SR	r_{SR} SCATSAR 020 Q+SR	r_{SR} SCATSAR 040 Q+SR	r_{SR} SCATSAR 100 Q+SR
203661	41	0.61	0.75	-0.22	-0.21	-0.15
203711	42	0.39	0.49	-0.35	-0.40	-0.36
203760	43	0.50	0.56	NA	NA	NA
203778	44	0.37	0.56	0.45	0.47	0.30
203786	45	0.48	0.54	0.33	0.26	-0.02
204545	46	0.87	0.87	NA	NA	NA
204586	47	0.70	0.84	-0.24	-0.21	-0.15
204685	48	0.70	0.93	NA	NA	NA
204719	49	0.57	0.90	-0.17	-0.11	0.00
204735	50	0.84	0.90	NA	NA	NA
204750	51	0.80	0.92	NA	NA	NA
204768	52	0.82	0.90	NA	NA	NA
204784	53	0.80	0.90	NA	NA	NA
204826	54	0.35	0.41	NA	NA	NA
204834	55	0.90	0.92	-0.22	-0.17	-0.07
204867	56	0.89	0.91	-0.20	-0.10	-0.03
204875	57	0.89	0.90	-0.32	-0.30	-0.30
204883	58	0.85	0.89	-0.34	-0.37	-0.33
204891	59	0.83	0.84	-0.31	-0.36	-0.33
204917	60	0.81	0.84	-0.31	-0.34	-0.38
204925	61	0.83	0.86	-0.46	-0.46	-0.42
204933	62	0.84	0.85	-0.36	-0.42	-0.42
204974	63	0.78	0.90	NA	NA	NA
204990	64	0.49	0.63	NA	NA	NA
205013	65	0.82	0.90	-0.24	-0.12	-0.04
205021	66	0.84	0.90	-0.24	-0.14	-0.07
205039	67	0.34	0.86	-0.44	-0.21	-0.26
205047	68	0.83	0.91	NA	NA	NA
205054	69	0.84	0.91	NA	NA	NA
205088	70	0.77	0.83	-0.43	-0.39	-0.37
205096	71	0.76	0.81	-0.62	-0.63	-0.62
205104	72	0.31	0.46	-0.28	-0.30	-0.22
205120	73	0.08	0.27	-0.13	-0.18	-0.21
205179	74	0.41	0.66	-0.07	-0.05	0.00
205294	75	0.78	0.78	-0.26	-0.26	-0.21
205377	76	0.49	0.87	-0.22	-0.22	-0.18
205385	77	0.76	0.90	NA	NA	NA
205393	78	0.82	0.87	-0.21	-0.18	-0.13
205419	79	0.82	0.84	-0.25	-0.21	-0.15
205435	80	0.68	0.72	-0.22	-0.20	-0.17

Tab. 7.38: The r_{SR} for calibration variants Q and Q+SR using S1ASCAT and SCATSAR products during the validation period in the 196 Austrian catchments (No.81 - 120).

Stream Gauge ID	Gauge No.	r_{SR} Runoff Q	r_{SR} S1ASCAT Q+SR	r_{SR} SCATSAR 020 Q+SR	r_{SR} SCATSAR 040 Q+SR	r_{SR} SCATSAR 100 Q+SR
205450	81	0.70	0.73	-0.21	-0.18	-0.11
205500	82	0.55	0.63	-0.06	0.01	0.08
205518	83	0.54	0.57	-0.05	0.00	0.04
205633	84	0.76	0.78	-0.22	-0.21	-0.17
205641	85	0.71	0.76	-0.22	-0.18	-0.16
205658	86	0.73	0.76	-0.17	-0.14	-0.07
205740	87	0.30	0.62	0.05	-0.01	-0.05
205765	88	0.37	0.55	0.19	-0.37	-0.43
205799	89	0.37	0.56	0.06	-0.06	-0.30
205807	90	0.36	0.46	-0.10	0.25	0.31
205815	91	0.48	0.57	-0.18	-0.21	-0.22
205823	92	0.44	0.56	-0.17	-0.18	-0.21
205831	93	0.37	0.54	-0.10	-0.03	0.00
205856	94	0.55	0.59	-0.09	-0.13	-0.14
205880	95	0.08	0.26	-0.19	-0.24	-0.05
205898	96	0.30	0.61	0.07	0.07	0.10
205914	97	0.54	0.58	-0.05	-0.02	0.03
205948	98	0.72	0.75	-0.47	-0.51	-0.51
205971	99	0.73	0.76	-0.40	-0.42	-0.39
205989	100	0.74	0.79	-0.39	-0.40	-0.39
205997	101	0.76	0.77	-0.43	-0.55	-0.61
206003	102	0.76	0.81	-0.47	-0.59	-0.61
206029	103	0.76	0.80	-0.35	-0.34	-0.32
206037	104	0.78	0.79	-0.18	-0.15	-0.21
206151	105	0.88	0.92	NA	NA	NA
206169	106	0.87	0.92	NA	NA	NA
206185	107	0.77	0.79	-0.24	-0.22	-0.18
207654	108	0.32	0.49	-0.04	0.13	-0.13
207688	109	0.33	0.58	0.04	0.09	0.16
207704	110	0.26	0.46	0.02	-0.04	-0.09
207712	111	0.32	0.52	0.29	0.31	0.32
207720	112	0.43	0.59	0.11	0.24	0.28
207746	113	0.59	0.62	-0.08	-0.09	-0.08
207787	114	0.69	0.69	-0.07	-0.07	-0.06
207795	115	0.57	0.69	-0.10	-0.10	-0.09
207811	116	0.70	0.71	-0.35	-0.38	-0.34
207829	117	0.63	0.67	-0.29	-0.32	-0.31
207837	118	0.66	0.70	-0.28	-0.26	-0.27
207845	119	0.69	0.71	0.08	0.05	0.04
207852	120	0.61	0.61	-0.08	-0.05	-0.02

Tab. 7.39: The r_{SR} for calibration variants Q and Q+SR using S1ASCAT and SCATSAR products during the validation period in the 196 Austrian catchments (No.121 - 160).

Stream Gauge ID	Gauge No.	r_{SR} Runoff Q	r_{SR} S1ASCAT Q+SR	r_{SR} SCATSAR 020 Q+SR	r_{SR} SCATSAR 040 Q+SR	r_{SR} SCATSAR 100 Q+SR
207860	121	0.67	0.71	NA	NA	NA
207894	122	0.64	0.61	0.20	0.27	0.05
207910	123	0.61	0.61	0.06	0.11	0.16
207936	124	0.76	0.80	-0.36	-0.35	-0.31
207944	125	0.66	0.71	-0.37	-0.39	-0.36
208009	126	0.64	0.66	-0.46	-0.38	-0.34
208017	127	0.52	0.66	-0.35	-0.37	-0.36
208090	128	0.60	0.68	-0.14	-0.16	-0.16
208116	129	0.59	0.64	-0.11	-0.18	-0.17
208124	130	0.63	0.66	-0.17	-0.34	-0.33
208157	131	0.68	0.68	-0.35	-0.35	-0.35
208280	132	0.56	0.59	-0.27	-0.33	-0.32
208413	133	0.23	0.63	0.02	-0.02	-0.06
208439	134	0.59	0.63	-0.30	-0.28	-0.23
208462	135	0.67	0.75	-0.38	-0.47	-0.57
208579	136	0.70	0.68	NA	NA	NA
208611	137	0.72	0.08	NA	NA	NA
208686	138	0.50	0.50	-0.04	-0.15	-0.19
208702	139	0.45	0.44	-0.02	-0.11	-0.15
208710	140	0.45	0.51	0.20	-0.19	-0.21
208819	141	0.64	0.71	-0.39	-0.41	-0.41
209197	142	0.71	0.74	-0.31	-0.36	-0.35
210229	143	0.69	0.68	-0.19	-0.16	-0.10
210526	144	0.44	0.48	-0.07	-0.07	-0.04
210542	145	0.57	0.52	0.00	-0.03	-0.01
210583	146	0.08	0.41	-0.28	-0.33	-0.39
210625	147	-0.12	0.44	NA	NA	NA
210641	148	0.32	0.41	0.29	-0.03	-0.06
210773	149	0.22	0.53	-0.10	-0.23	-0.26
210815	150	0.18	0.48	0.05	-0.09	0.04
210864	151	0.48	0.50	0.02	-0.05	-0.10
210880	152	0.18	0.53	-0.25	-0.10	-0.14
210898	153	0.45	0.40	-0.32	0.04	0.06
210989	154	0.63	0.64	-0.29	-0.38	-0.39
211003	155	0.65	0.64	-0.24	-0.22	-0.21
211102	156	0.39	0.49	0.01	0.04	-0.02
211136	157	0.36	0.49	0.02	0.05	0.05
211169	158	0.15	0.42	-0.05	-0.12	-0.24
211193	159	0.04	0.11	-0.05	-0.18	-0.25
211227	160	0.30	0.47	0.00	0.14	0.14

Tab. 7.40: The r_{SR} for calibration variants Q and Q+SR using S1ASCAT and SCATSAR products during the validation period in the 196 Austrian catchments (No.161 - 196).

Stream Gauge ID	Gauge No.	r_{SR} Runoff Q	r_{SR} S1ASCAT Q+SR	r_{SR} SCATSAR 020 Q+SR	r_{SR} SCATSAR 040 Q+SR	r_{SR} SCATSAR 100 Q+SR
211243	161	0.45	0.47	-0.09	-0.19	-0.24
211268	162	0.36	0.34	-0.16	-0.25	-0.29
211292	163	0.31	0.47	-0.13	-0.26	-0.30
211383	164	0.46	0.70	-0.13	-0.24	-0.29
211391	165	0.36	0.73	-0.30	-0.33	-0.37
211458	166	0.38	0.68	-0.23	-0.27	-0.28
212027	167	0.13	0.20	0.34	0.34	0.34
212068	168	-0.10	0.01	NA	NA	NA
212076	169	-0.11	0.11	NA	NA	NA
212092	170	0.03	0.06	0.07	0.03	0.01
212126	171	0.10	0.09	NA	NA	NA
212183	172	0.00	0.03	0.01	-0.02	-0.03
212316	173	0.01	0.12	0.41	0.47	0.50
212324	174	0.01	0.10	0.30	0.35	0.38
212357	175	-0.01	0.05	0.27	0.33	0.37
212381	176	0.28	0.28	NA	NA	NA
212431	177	0.10	0.39	0.16	0.15	0.11
212522	178	0.14	0.40	-0.14	-0.26	-0.34
212613	179	-0.13	0.15	0.36	0.33	0.34
212647	180	-0.03	0.08	0.35	0.38	-0.11
212670	181	-0.10	-0.01	0.22	-0.15	-0.21
212704	182	-0.16	-0.04	-0.14	-0.27	-0.33
212753	183	-0.19	-0.03	0.15	-0.21	-0.27
212787	184	-0.19	0.03	0.07	-0.25	-0.30
212860	185	0.18	0.52	0.33	0.34	0.33
212886	186	0.20	0.47	0.20	0.14	-0.39
212894	187	0.38	0.46	-0.29	-0.38	-0.46
212928	188	0.31	0.35	-0.28	-0.41	-0.38
212936	189	0.34	0.39	-0.33	-0.44	-0.47
213025	190	0.08	0.30	-0.40	-0.52	-0.57
213033	191	0.30	0.38	-0.47	-0.54	-0.63
213082	192	0.33	0.48	-0.27	-0.37	-0.43
213090	193	0.38	0.44	-0.26	-0.35	-0.38
213157	194	0.31	0.47	-0.27	-0.37	-0.42
213231	195	0.29	0.39	-0.46	-0.57	-0.61
213256	196	0.35	0.44	-0.49	-0.60	-0.60